DEVELOPMENT OF CALCIUM-BASED HETEROGENEOUS CATALYST FOR DEOXYGENATION OF TRIGLYCERIDES INTO GREEN FUEL

NURUL ASIKIN BT MIJAN

INSTITUTE OF GRADUATE STUDIES
UNIVERSITY OF MALAYA
KUALA LUMPUR

2018

DEVELOPMENT OF CALCIUM-BASED HETEROGENEOUS CATALYST FOR DEOXYGENATION OF TRIGLYCERIDES INTO GREEN FUEL

NURUL ASIKIN BT MIJAN

THESIS SUBMITTED IN FULFILMENT OF THE REQUIREMENTS FOR THE DEGREE OF DOCTOR OF PHILOSOPHY

INSTITUTE OF GRADUATE STUDIES
UNIVERSITY OF MALAYA
KUALA LUMPUR

2018

UNIVERSITY OF MALAYA

ORIGINAL LITERARY WORK DECLARATION

Name of Candidate: NURUL ASIKIN BT MIJAN

Matric No: HHC 140016

Name of Degree: DOCTOR OF PHILOSOPHY

Title of Thesis ("this Work"): DEVELOPMENT OF CALCIUM-BASED HETEROGENEOUS CATALYST FOR DEOXYGENATION OF TRIGLYCERIDES INTO GREEN FUEL

Field of Study: CHEMISTRY

I do solemnly and sincerely declare that:

(1) I am the sole author/writer of this Work;
(2) This Work is original;
(3) Any use of any work in which copyright exists was done by way of fair dealing and for permitted purposes and any excerpt or extract from, or reference to or reproduction of any copyright work has been disclosed expressly and sufficiently and the title of the Work and its authorship have been acknowledged in this Work;
(4) I do not have any actual knowledge nor do I ought reasonably to know that the making of this work constitutes an infringement of any copyright work;
(5) I hereby assign all and every rights in the copyright to this Work to the University of Malaya ("UM"), who henceforth shall be owner of the copyright in this Work and that any reproduction or use in any form or by any means whatsoever is prohibited without the written consent of UM having been first had and obtained;
(6) I am fully aware that if in the course of making this Work I have infringed any copyright whether intentionally or otherwise, I may be subject to legal action or any other action as may be determined by UM.

Candidate's Signature Date:

Subscribed and solemnly declared before,

Witness's Signature Date:

Name: Dr. Lee Hwei Voon

Designation: Doctor/Supervisor

DEVELOPMENT OF CALCIUM-BASED HETEROGENEOUS CATALYST FOR DEOXYGENATION OF TRIGLYCERIDES INTO GREEN FUEL

ABSTRACT

The utilization of green fuel derived from biomass in industries and transportation has improved energy security by reducing the dependency on the non-renewable fossil petroleum. Deoxygenation process is one of the alternative pathways to produce green fuel via decarboxylation/decarbonylation (deCOx) reaction. Bonded oxygen molecules in the feedstock were removed in the form of CO_2/CO gas in deCOx reaction. Acid catalyst is generally used for promoting deoxygenation reaction, however, the high acidity of the catalyst will promote coke formation at the end of the reaction. As a result, researchers have moved forward with the utilization of basic catalysts in deoxygenation reaction. Since, the study on implementation of basic catalyst in defying coke formation during the deoxygenation reaction still maintain unknown or limited. Hence, chapter 3 was focused on the development of high basic catalysts via surfactant assisted sonochemical method and the catalyst further explored in deoxygenation process. Due to the low deoxygenation activity shown by pure basic catalyst, the prospects of utilizing acid-base catalysts over transition metals (Ni, Zn, Fe, Co and W) supported CaO catalysts were further investigated and reported in chapter 4 and 5 with Co and Ni metals promoted catalyst found to be the most effective in catalyzing the deoxygenation reaction. Furthermore, the degree of coke formation also was found to be minimal at < 8.2 wt.%. With the effort to overcome low activity by TMO-CaO catalyst due low surface area and low desired acidic sites, extensive studies were focused on the utilization of mesoporous acidic support (SiO_2-Al_2O_3) promoted NiO-CaO and Co_3O_4-CaO in chapter 6 to 8. The impact of Ca, Ni and Co metals oxides on the deoxygenation routes via deCOx was investigated. Ni-promoted catalyst exhibited highest deoxygenation activity and remarkable enhancement of deCOx reaction which is

achieved due to the large existence of mildly acidic sites than strong acid and basic sites. Instead of using basic metal promoter, the use of neutral support (carbon-based support) was found to be effective in suppressing the coke formation (chapter 9). The coke was found to be < 4.2 wt.% after 4 consecutive deoxygenation runs. Overall studies, it can be concluded that the implementation of basic metal promoter and carbon-based catalyst in deoxygenation process will inhibit the growth of coke and would enhance catalyst stability.

Keywords: Green diesel, deoxygenation, calcium, metal oxides, coke

PEMBANGUNAN MANGKIN HETEROGENUS BERASASKAN KALSIUM UNTUK PENYAHOKSIDAAN TRIGLESERIDA KEPADA BAHAN API HIJAU

ABSTRAK

Penggunaan bahan api hijau yang dihasilkan daripada biojisim dalam industri dan pengangkutan telah meningkatkan keselamatan tenaga dengan mengurangkan kebergantungan terhadap petroleum. Proses Penyahoksigenan adalah salah satu cabang yang penting untuk menghasilkan bahan api hijau melalui tindak balas penyahkarbosilan/penyahkarbonilan (deCOx), yang mana molekul oksigen dalam bahan mentah akan disingkirkan dalam bentuk gas CO_2/CO. Mangkin asid secara amnya digunakan untuk meningkatkan tindak balas penyahoksigenan, walaubagaimanapun, keasidan mangkin yang tinggi juga mampu meningkatkan pembentukan cok. Sehubungan dengan itu, penyelidikan telah beralih kearah penggunaan mangkin bes dalam tindak balas penyahoksigenan. Memandangkan kajian implimentasi mangkin bes dalam menghalang pembentukan cok semasa tindak balas penyahdeoxygenan masih tidak diketahui atau terbatas. Dalam 3, difokuskan kepada pembangunan mangkin bes tinggi melalui kaedah surfaktan berbantu sono-kimia dan penerokaan lanjut dalam proses penyahoksigenan. Disebabkan oleh aktiviti penyahoksigenan yang rendah terhadap mangkin bes tulen, prospek penggunaan mangkin asid-bes terhadap logam peralihan (Ni, Zn, Fe, Co and W) berpenyokong mangkin CaO telah dikaji dan dilaporkan dalam bab 4 dan 5. Logam Co dan Ni telah dikenalpasti menjadi efektif dalam membantu proses penyahoksigenan. Tambahan pula, darjah pembentukan cok juga dikenalpasti menjadi minimum sehingga <8.2 wt.%. Disamping itu, aktiviti mangkin TMO-CaO yang rendah disebabkan oleh luas permukaan dan tapak asid yang rendah, kajian lanjutan telah memfokuskan kepada penggunaan penyokong mesoporous asid (SiO_2-Al_2O_3) berpenggalak NiO-CaO dan Co_3O_4-CaO (bab 6-8). Kesan

penggunaan logam Ca, Ni dan Co terhadap kaedah penyahoksidaan terhadap deCOx telah dikaji. Mangkin Ni berpenggalak menunjukkan aktiviti penyahoksigenan yang tertinggi dan pencapaian yang luar biasa bagi tindak balas deCOx terutamanya dikenalpasti disebabkan oleh kehadiran tapak asid sederhana yang banyak berbanding tapak asid kuat dan bes. Selain menggunakan penggalak logam bes, penggunaan penyokong semulajadi (penyokong berasaskan carbon) didapati sangat effektif dalam menghalang pembentukan cok (Bab 9). Didapati 4.2 wt.% cok selepas 4 kali penyakoksidaan dijalankan secara berturut-turut. Secara keseluruhannya, kajian ini boleh dirumuskan sebagai implimentasi penggalak logam bes dan mangkin berasaskan karbon dalam proses penyahoksigenan akan menghalang pertumbuhan cok dan seterusnya meningkatkan sestabilan mangkin.

Kata kunci: bahan api hijau, penyahoksigenan, kalsium, logam oksida, cok

ACKNOWLEDGEMENTS

Bismillah Ar-Rahman Ar-Rahim. Alhamdullilah, my gratitude to Allah S.W.T the Almighty for giving me the strength, patience and faith to pursue my dream and also for His blessings which have led me through the journey of completing this research.

First of all, I would like to express my warmest sense of thanks and also my appreciation to my honorable project supervisor, Dr. Lee Hwei Voon, Prof. Dr. Juan Joon Ching and Prof. Dr. Noorsaadah Binti Abd Rahman for giving me the motivation, inspiration, constructive criticism and encouragement throughout the duration of completing this project. Moreover, I would like to express my sincere gratitude to my co-supervisor Professor Taufiq Yap Yun Hin from Universiti Putra Malaysia. My warmest regards go to my co-authors, especially Associate Prof. Dr. Ong Hwai Chuan, Abdul Kareem Al-Ghassan Al-Sultan, Mahashanoon Arumugam, Sufri Mastuli, Dr. Sharifah Marliza and Mohd Razali for the helps rendered during the research. My appreciation also goes to my colleagues at NanoCAT and PutraCAT centre.

I saved the last part of my acknowledgement to my family because they are my greatest assets. To my mother, Saniah binti Amri for showering me with lots of love which keeps people wondering of my never-ending source of happiness and smiles during the period of my research. Furthermore, a big thank you to financial sponsorship from MyPhd program initiated by Ministry of Higher Learning (MOHE). Last but not least, my appreciation to the most Merciful and Beneficent, Allah S.W.T for every challenge and favor that He showered upon me during the research. Thank you.

TABLE OF CONTENTS

LIST OF FIGURES

LIST OF TABLES

LIST OF SYMBOLS AND ABBREVIATIONS

DO	:	Deoxygenation
HDO	:	Hydrodeoxygenation
DeCOx	:	Decarboxylation/Decarbonylation
FAME	:	Fatty Acid Methyl Ester
WCO	:	Waste Cooking Oil
PFAD	:	Palm Fatty Acid Distilled
JCO	:	Jatropha Curcas Oil
MWCNT	:	Multi-Wall Carbon Nanorode
AN	:	Acid Value
TAN	:	Total Acid Value
FFA	:	Free Fatty Acid
TMO	:	Transition metal oxide
XRD	:	X-Ray Diffraction
XRF	:	X-ray fluorescence
SEM	:	Scanning electron microscope
TEM	:	Transmission Electron Microscopy
BET	:	Brunauer–Emmet–Teller Surface Area Measurement
FESEM-EDX	:	Field Emission Scanning Electron Microscopy
TPD-NH_3	:	Temperature Programme Desorption Ammonia
TPD-CO_2	:	Temperature Programme Desorption Carbon Dioxide
FTIR	:	Fourier Transform Infrared Spectrometer
GC-FID	:	Gas Chromatography Flame Ionization Detection
GC-MS	:	Gas Chromatography Mass Spectrometer
TGA	:	Thermogravimetric

ICP-AES	:	Inductively Coupled Plasma-Atomic Emission Spectroscopy
EN	:	European Standard
ASTM	:	American Society for Testing and Materials
NIST	:	National Institute of Standards and Testing
ULSD	:	Standard Ultra-Low Sulphur Diesel
RSM	:	Response Surface Methodology
EG	:	Ethylene Glycol
PTFE	:	Polytetrafluoroethylene
CTAB	:	N-Cetyl-N,N,N-trimethylammonium bromide
$H_{26}N_6O_{40}W_{12}.xH_2O$	:	Ammonium Metatungstate Hydrate,
$Ni(NO_3)_2.6H_2O$	:	Nickel (II) Nitrate Hexahydrate
$Fe(NO_3)_3.9H_2O$	:	Iron (III) Nitrate Nanohydrate
$Zn(NO_3)_2.6H_2O$	:	Zinc (II) Nitrate Hexahydrate
$Co(NO_3)_2.6H2O$	:	Cobalt (II) Nitrate Hexahydrate
$Ca(NO_3)_2.4H_2O$	:	Calcium Nitrate Tetrahydrate
CHBr	:	1-Bromo Hexane
	:	

LIST OF APPENDICES

CHAPTER 1: INTRODUCTION

1.1 Overview of renewable energy, biofuel, green fuel

Interest in renewable energy has sharply risen in last decade as countries and the world community associated with progressive depletion of conventional fossil fuels and oscillating petroleum fuel prices. In addition, the continues usage of fossil fuels will results in several carcinogenic influences on ecosystem, such as large greenhouse gas emissions, acid rain, and also global warming (Avhad and Marchetti, 2015). Therefore, it have triggered numerous research interest in necessity to find an alternate "green" sources of energy which are sustainable, environmentally tolerable, economically competitive and easily available. There are several modes of renewable energy resources which were anticipated to play vital role in resolving the world's entire dependency on the use of fossil fuels such as solar energy, wind energy, hydro-energy, and biofuels. Biofuel is an alternative cleaner burning fuel that has been commercialized by the nation to replace conventional fuels. Biofuels referred to liquid or gaseous fuel which are renewable and sustainable as it derived from biomass such as sugarcane, oleaginous plants, forest biomass and other sources of organic matter (Demirbas, 2007). Growing interest in biofuel is driven by the following facts among others: (1) biofuels largely available from common biomass sources, (2) they are representing a carbon dioxide-cycle in combustion, (3) it contributes many benefit on the environment, economical and consumers in utilization of biofuels and (4) biofuel are biodegradable and contribute to sustainability.

Green fuel is one of the categories of biofuels. Green fuel including short chain hydrocarbon fractions (green gasoline) within the range of C_6-C_{12} and long chain hydrocarbon fractions (green diesel) within range C_{13}-C_{20} is generally free of oxygen,

sulphur, and aromatics. The green fuel contains *n*-alkanes and *n*-alkenes that are hydrocarbons, similar to those found in gasoline and diesel fuel obtained by refining crude oil in petroleum refineries. As the green fuel is entirely fungible with petroleum derived fuel, its properties are vastly close to petrodiesel. However, green fuel is completely different from current well-established commercialized biofuel; biodiesel (FAMEs). Another advantage of green fuel process is that it can be produced in large volumes at existing centralized petroleum refineries. Biodiesel, on the other hand, is more suited for smaller scale production plants in rural areas close to the source of oil used in the process.

Table 1.1 shows the fuel properties of biodiesel, petroleum ULSD and green fuel at diesel range compared with European standard EN-14214 and American standard ASTM-D6751. It could be seen that green diesel possesses high cetane number (70-90) than biodiesel and diesel standards which indicate it has a competitive petrodiesel substitute. Cetane number of a fuel is a measure of its susceptibility for auto-ignition. The higher the cetane number, the shorter the ignition delay period is. Therefore, the cetane number is preferably high. In the case of heating value, green diesel has net heating value of 44 MJ/kg, which is exactly similar to that of conventional diesel and higher than biodiesel (Aatola et al., 2008;Kalnes et al., 2014). The density and viscosity of green diesel ranges from 0.78–0.85 g/ml and 2.5-4.15 Cst, which meets the diesel requirement standard and has even better properties than biodiesel (Guzman et al., 2010). The fuel density must be controlled in a specific range since it optimizes the engine performance and exhaust emission of vehicles while low viscosity is important for lowering the resistance of a fluid to flow. For low-temperature applications of biodiesel the cloud point (CP) is a decisive parameter. It is the temperature at which the first visible crystals form upon cooling a fuel and at which problems such as fuel filter

plugging could result. It may be noted that in connection with low-temperature properties, often the pour point (PP) is reported. The PP is the temperature at which the fuel can no longer be poured freely or the temperature at which it becomes semi solid and loses its flow characteristics.

Another test related to cold flow properties is the cold filter plugging point (CFPP) which is a filterability test and is linearly related to the CP. Concerning its cold flow properties, the presence of higher amounts of saturated fatty esters in the biodiesel results in higher cloud point temperature within range of -5 to +15 ^{o}C than that of green fuel which is from -30 to -5 °C. Additionally, the green diesel showed higher pour point ranging from -3 to 29 °C than biodiesel (-15 to 16 ^{o}C). Thus, biodiesel would easily lose its flow characteristic as compared to green diesel, similar to CFPP. Thus, utilization of green diesel could avoid cold filter plugging during cold climate together with increase of performance in cold weather.

Moreover, green diesel and petrodiesel have a flash point lower than biodiesel. The branched and lower molecular weight component in green diesel and petrodiesel possess lower boiling points, leading to a reduction of the flash point. It was reported that biodiesel such as methyl palmitate possesses higher boiling point (417 ^{o}C) and 224 ^{o}C for methyl decanoate while hexadecane is 287 ^{o}C and decane is 174 ^{o}C (Knothe, 2010). Finally, as catalytic hydroprocessing technology includes desulphurization reactions, green diesel is a low sulphur fuel in comparison with petrodiesel with concentration of <1 ppm/wt, indicating that it is a very low greenhouse gas emissions fuel (Šimáček et al., 2011).

Table 1.1: Comparison between biodiesel, petroleum ULSD and green diesel

Fuel Properties	EN-14214	ASTM-D6751	Petrodiesel	FAME Biodiesel	Green Diesel	Syndiesel
Oxygen/%	-	-	0	11	0	0
Density (g/mL)	0.86-0.90	-	0.84	0.88	0.78-0.85	0.77-0.82
Sulphur (ppm)	10	15	<10	<1	<1	<1
Heating Value (MJ/kg)	-	-	43	38	44	44
Cetane Number	51	47	40-55	45-72	70-90	>75
Viscosity (40°C) CSt	3.5-5.0	1.9-6.0	2.7	3.8-7.9	2.5-4.1	2.1-3.5
CFPP/°C	-	-	-6	(-13)-15	>20	(-22)-0
Cloud Point /°C	-		-23-+4	-5-+15	-30-(-5)	-18-+2
Flash Point/°C	120 min	130 min	52-136	96-188	68-120	55-78
Pour Point/°C	-	-	-21	(-15)-16	(-3)-29	-
Acid value mg KOH/g	0.5	0.8	-	-	-	-

Based on the above arguments, green diesel seemed to be a superior product over biodiesel and better than petrodiesel.

1.2 Problem statement

The utilization of green fuel has been established in many countries but majority of the industry preferred hydrodeoxygenation (HDO) reaction as it produces large quantity of green fuel. Hydrodeoxygenation reaction involves C-O breakage via hydrogenolysis reaction of oxygenated compound which produces hydrocarbons of the same carbon number as the fatty acids in triglycerides with H_2 consumption under the presence of high pressure (Zhang et al., 2014). Unfortunately, this approach required high pressure H_2 and it was low in cost efficiency. An alternative pathway lies in the deoxygenation (DO) of triglycerides via decarboxylation ($-CO_2$)/decarbonylation($-CO,H_2O$) (deCOx) reaction which produces hydrocarbons with one carbon number less than their corresponding fatty acids. This approach has a significant advantage of proceeding under considerably lower H_2 pressures compared to hydrodeoxygenation

(HDO). It is also made possible to conduct deCOx in the complete absence of H_2 gas and thus lowered the production cost of green fuel.

Generally, the catalyst selected by default for deoxygenation was Pd (Mäki-Arvela et al., 2008) or Pt (Payormhorm et al., 2013). The noble metal-based catalysts displayed the most promising catalytic deoxygenation performance but the cost of the metal may be prohibitive to the potential user. Therefore, the development of a more affordable catalyst which displayed similar performance to noble metal catalyst is necessary. Due to the higher price of noble metal catalyst, the sulphide-, phosphate- and carbide-based catalysts were commonly use in cracking process for production of green fuel. However, due to the sulphur leaching, tedious and rigorous preparation method for phosphate- and carbide-based catalysts have initiated a research to search for an alternative catalyst which is simple to be prepared, sulphur-free which could produce high quality green fuel (Liu et al., 2014). Recent studies had shown that transition metal oxide (TMO) with acidic sites were highly active for the removal of oxygenates via deCOx reaction (Loe et al., 2016;Junming et al., 2009;He and Wang, 2014). However, those acidic sites were susceptible to deactivation by the accumulation of carbonaceous deposits on their surface and reduce the catalytic activity. Therefore, the utilization of base catalyst has gained remarkable attention in the green fuel industry as a coke resistant catalyst for the conversion of triglycerides into fuel-like hydrocarbons via deCOx reaction.

In general, renewable raw material derived from 1st generation feedstock (edible oil) and 2nd generation feedstock (non-edible oil) could be industrially deoxygenated for the production of green fuel. With the concern of edible oil rivalry between food and fuel purposes, the use of edible oil as a feedstock for production of green fuel may not

be viable. Therefore, the transition of green fuel feedstock from edible sources to non-edible sources is imminent. Several listed non-edible oils contained high FFA level and some contained low FFA level. However, majority of the non-edible oil was found to be rich in unsaturated fatty acids. The chemical nature of the feedstock plays a crucial role in determining both the pathway and the outcome of deoxygenation (Mäki-Arvela et al., 2007). Feedstock that has high content of FFA generally results in higher conversion and product selectivity compared to ester. However, it will result in extensive catalyst deactivation (Mäki-Arvela et al., 2008). High degree of unsaturated of fatty acids in the feedstock would also contribute towards catalyst deactivation which was caused by the formation of oligomers and aromatics during the reaction (Immer et al., 2010). As a conclusion, the use of pure acid catalyst (coke stimulator) in conversion of feedstocks with high content of unsaturated fatty acid is highly undesirable. The inferiority of pure acid catalyst in green fuel production has stimulated the search on the utilization of basic catalyst for green fuel production via deCOx reaction.

Recently, nano-sized basic catalyst has received considerable attentions as it could provide high surface area to volume ratio in nano-crystalline structure, which is five times more in the number of active sites per unit area (Dorozhkin, 2009). Thus, offering higher basicity in catalyst shall has positive effects on various reactions. However, previous researches barely focused on the utilization of nano-sized basic catalyst in the conversion of triglycerides into green fuel. Therefore, our research also focuses on development of a new nano dimension base catalyst which is to be utilized in the production of green fuel.

1.3 Scope of study

In the present study, the single Ca-based oxides in nano-size will be synthesized via sono- assisted surfactant method and the catalyst was further tested in catalytic deoxygenation of triglycerides under free-H_2 (without H_2) condition. The deoxygenation study will be further extended using acid-base catalyst derived Ca-based binary oxide catalyst (Co-CaO and W-CaO). The mixed metal oxides are believed to consist of more superior physicochemical properties than individual oxide, which are able to improve the deoxygenation activity and product selectivity. In order to reduce internal diffusion limitation of bulk mixed metal oxides and optimizes the deoxygenation to the greatest reaction rate, the introduction of mesoporous support such as SiO_2-Al_2O_3 and MWCNT are included in the study. The optimum conditions of the deoxygenation processes will be further optimized using "one-variable-at-a-time technique" or response surface methodology (RSM). The most effective catalyst in deoxygenation reaction in each study will be selected and tested for recyclability and catalyst stability. The efficiency of the catalysts will then be investigated by deoxygenizing different type of non-edible oils such as jatropha curcas oil (JCO), waste cooking oil (WCO) and palm fatty acid distillate (PFAD). The deoxygenation performances of base and acid-base catalysts are then compared side-by-side with the deoxygenation performance of pure acid catalyst for further understanding.

1.4 Objectives

The objective of this study are to:

1. To synthesize nano-size Ca-based and modified Ca-based catalysts.
2. To synthesize catalyst with different support (activated carbon, SiO_2-Al_2O_3)
3. To characterize the physicochemical properties of the catalysts for green fuel production.
4. To investigate the effect of different deoxygenation variables on green fuel yield and optimization condition in deoxygenation process.
5. To study the reusability and catalyst stability of the synthesized catalysts.

CHAPTER 2: LITERATURE REVIEW

2.1 Current scenario of conventional energy

Interest in renewable energy had seen a steady rise since the last decade, with countries and the world community associating it with several main reasons. The first reason is an increment in the transportation sector which is currently steering the demand for conventional petroleum-derived fuel. It was estimated that the world demand would continue growing, resulting in a higher production level compared to refined petroleum product (Figure 2.1) (Hermida, Abdullah, & Mohamed, 2015). It was also predicted that the demand for diesel fuel would increase to 35 million barrels per day in 2035 from just 26 million barrels per day in 2012. Meanwhile, demand for gasoline would increase to 27 million barrels in 2035 from 23 million barrels in 2012. Similar projection was projected with the other products such as ethane/LPG, naphtha, bitumen, lubricant waxes, coke and direct use of crude oil. These results are in contrast with demand for residual fuel whereby it was estimated to be reduced in the coming years.

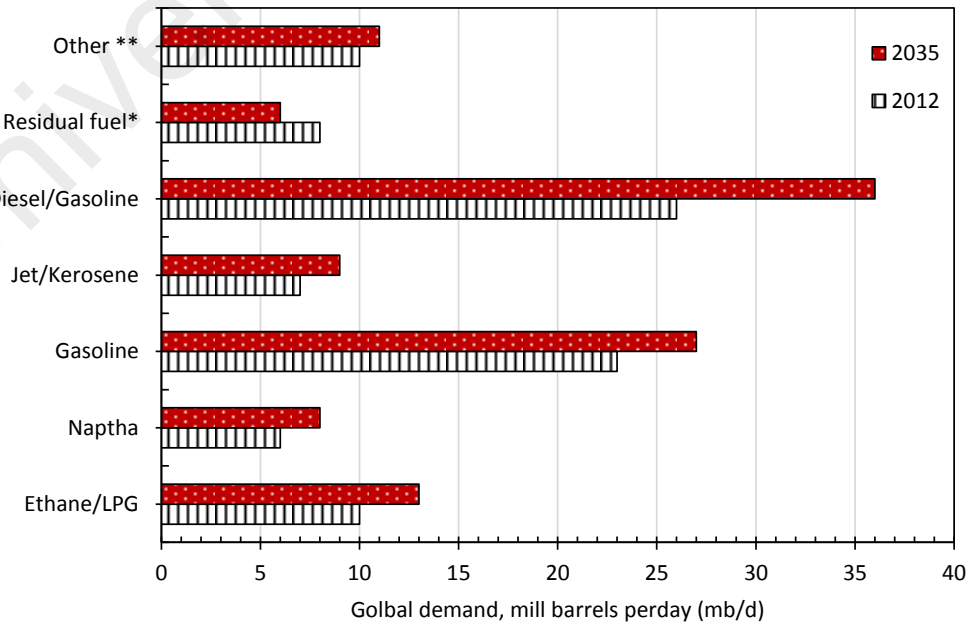

Figure 2.1: Global demands for diesel fuel in 2012 and forecast in 2035 compared to other refined oil products

Universally, the outlook and motivation toward finding an alternative renewable fuel (biofuel) are due to the increase of crude oil prices, diminishing of non-renewable fossil-fuel resources and environmental health hazards which is associated with fossil fuel emissions. The fossil-fuel resources are non-renewable and it was predicted that they would be exhausted in the near future. It was also supported by (BP Statistical Review of World Energy) whose claim that current oil and gas reserves will be depleted in 41 and 63 years, would come true, if the consumption pace remained constant. In the current availability of such sources; fossil fuels are being consumed without replacement. This in turn would create a volatile market with constantly increasing prices. Prior to past research, it had been known that 80% of primary energy were covered by fossil fuels and 57.7% of it were largely consumed by the transportation sector (Escobar et al., 2009). Therefore, it can be concluded that fossil fuels are responsible for the emission of a significant amount of pollutants in the atmosphere, including greenhouse gases (GHGs) (Avhad and Marchetti, 2015). The increment of greenhouse gases in the atmosphere produce a positive radiation in the climate system and a consequent rise of Earth's average temperature. The rise of sea level is also caused by thermal expansion of the warmer seawater (Aziz et al., 2015). Additionally, the increase of earth temperature would also contribute to the melting of glaciers and ice sheets which would threaten millions of people with flood, water shortage, risk of hunger and diseases such as malaria. Due to all these factors, extensive research in developing long-term strategies for biofuel production was initiated. This was to produce renewable feedstock which are sustainable, environment-friendly, economically competitive and easily available in order to substitute the declining fossil fuel production. There are several modes of renewable energy resources which were anticipated to play a vital role in resolving the entire world's dependency on the use of fossil fuel such as solar energy, wind energy, hydro-energy, and biofuel. Among the

listed renewable energies, biofuel can be considered as a relevant technology by both developing and industrialized countries (Demirbas, 2008). Biofuel is a clearer alternative of burning fuel that had been commercialized by the nation to replace conventional fuel.

2.2 Green fuel production cost

The production of green fuel is not yet produced commercially, but a considerable number of research in small lab scale production have been reported or set up in recent years. This was because the major obstacle in commercialization of green fuel is the cost production which involves raw material cost and the production cost. The analysis of the economic evaluation by U.S. Energy Information Administration (2016) drives to the conclusion that the cost of raw material is a dominant part of the overall cost of green diesel production, covering up to >57% of the total production cost (Diesel Prices and Outlook – Basics, 2016). Thus, to optimally enhance the economic point of view, utilization of sustainable, non-expensive and non-value added feedstock is extremely important. There are more than 350 oil-bearing crops recognized world-wide which could be used as a feedstock for the production of green fuel. However, in order to sustain the green fuel market continuously and in a large scale, several characteristics of the feedstock need to be considered (Silitonga et al., 2013); High yield of oil content, controllable growth and harvesting season (stable supply of raw material), consistent seed saturity rate, favorable fatty acid composition, low agriculture input (water, fertilizer, soils and pesticides), economically profitable for agriculture and reduction of carbon footprint from the usage of liquid fuel. By following preceding feedstock characteristics, lower and reasonable cost could be achieved and sustained in terms of supplies. The choice of feedstock also depends on the location at which the

crops are grown. Moreover, proper choice of feedstock can also aid in reduction of tariffs and transportation cost.

2.3 Feedstock for green fuel

As an alternative to renewable raw material, the triglycerides present in fats and vegetables oil can be industrially deoxygenated at petroleum refineries. General potential feedstocks for green fuel production could be categorized into the following; bio-oil, edible oil, non-edible oil, animal fats and yellow grease.

2.3.1 Pyrolysis oil (Bio-oil)

Bio-oil had gained considerable attention as potential feedstock for production of hydrocarbon by catalytic upgrading. Generally, bio-oil is produced via pyrolysis reaction. Pyrolysis is the thermal decomposition of biomass, which occurs in the absence of oxygen or when significantly less oxygen is supplied than needed for complete combustion (Han et al., 2010). Bio-oil is typically dark brown in color while some can be black or green, viscous, corrosive, and an unstable mixture of a large number of oxygenated molecules, depending on the pyrolysis process and biomass feedstock. The oxygen content in bio-oil is typically 35–40 % and contains hundreds of organic compounds that belong to acids, alcohols, ketones, aldehydes, phenols, ethers, esters, sugars, furans, nitrogen compounds and multifunctional compounds (Demirbas, 2011). Until now, over 300 organic compounds had been identified in different bio-oils with lower concentration. Thus, this could affect the homogeneity, polarity, heating value (HV), viscosity and acidity of oil. Bio-oil also contains 15–30 wt% water, although up to 60 % is reported (Rout et al., 2009;Jacobson et al., 2013), which is derived from the original moisture in the feedstock and is formed via dehydration during the pyrolysis reaction as well as during storage. Therefore, high water content

will reduce the immiscibility of the bio-oil with crude oil. High water content and oxygenated species will further result in reduction of HV oil which is 50% lower than crude oil. The pH of bio-oil is commonly within the range of 2 to 4, which is primarily related to the content of acetic acid and formic acid. The acidic nature of bio-oil might give further problems related to corrosion of the equipment used for storage, transport and processing (Oasmaa et al., 2012). Due to the vast differences of bio-oil and crude oil as tabulated in Table 2.1(Mortensen et al., 2011;Venderbosch and Prins, 2010;Lu et al., 2009), it would pose significant issues as it is not similar to crude oil. Even though bio-oil is CO_2/GHG neutral, cleaner and cause less pollution as the bio-oil usage emit no NOx and less Sox (Xiu and Shahbazi, 2012), the potential of substituting bio-oil for petroleum fuel and chemical feedstock is limited due to its high viscosity, high water and ash content, low heating value, instability and high corrosiveness (Jacobson et al., 2013). Thus, upgrading of bio-oil is essential in order to produce high quality liquid fuel or chemical feedstock. Owing to presence of high concentration of oxygenates and organic acids, the upgrading of the bio-oil is quite challenging and involve complex reaction network due to the high diversity of compound in the feed. Numerous research on upgrading the bio-oil via cracking, deoxygenation and hydrodeoxygenation reactions had been reported elsewhere (Wildschut et al., 2009;Karnjanakom et al., 2016;Iliopoulou et al., 2012). Although significant hydrocarbons were successfully produced, the high diversity compound in bio-oil and span of potential reaction resulted in difficulties of evaluation for bio-oil upgrading. Therefore, finding other alternative renewable feedstock which composed of narrow range diversity compound is paramount in order to manufacture a perfect type of bio-oil.

Table 2.1: Comparison properties of bio-oil and crude oil

Properties	**Bio-oil**	**Crude-oil**
Density at 15 °C (g/mL)	1.05-1.25	0.86
Viscosity at 50 °C (cP)	40-100	180
Water content (wt %)	15-30	0.1
pH	2.8-3.8	-
Heating value (MJ/kg)	16-19	40
Elemental composition (wt.%)		
C	54-58	85
H	5.5-7.0	11
O	35-40	1
N	0-0.2	0.3
Ash	0-0.2	0.1
Solids (wt.%	0.2-1	1

2.3.2 Triglycerides- and fatty acid-derived feedstock

The use of low diversity molecular compound, mainly triglycerides and/or fatty acid derived from edible and non-edible oil, waste oil and animal fat as an alternative food based-feedstock, could overcome the limitations of upgrading bio-oil, which simultaneously enhance the oxygenates species removal along with production of high quality green fuel. Triglycerides make up the structure of all vegetable oil including edible and non-edible oil. Chemically, triglyceride contains three fatty acids bound to single propane unit through ester bond as shown in Figure 2.2(a). Fatty acids account for 95% of the total weight of triglycerides and their content defines the characteristics of each vegetable oil. The fatty acids vary in their carbon chains and number of unsaturated chains (Lestari et al., 2009). The chemical structures of some frequently studied fatty acids are summarized in Figure 2.2(b). The fatty acids of triglycerides are either saturated, monounsaturated or polyunsaturated. Fully saturated triglycerides are solid at room temperature.

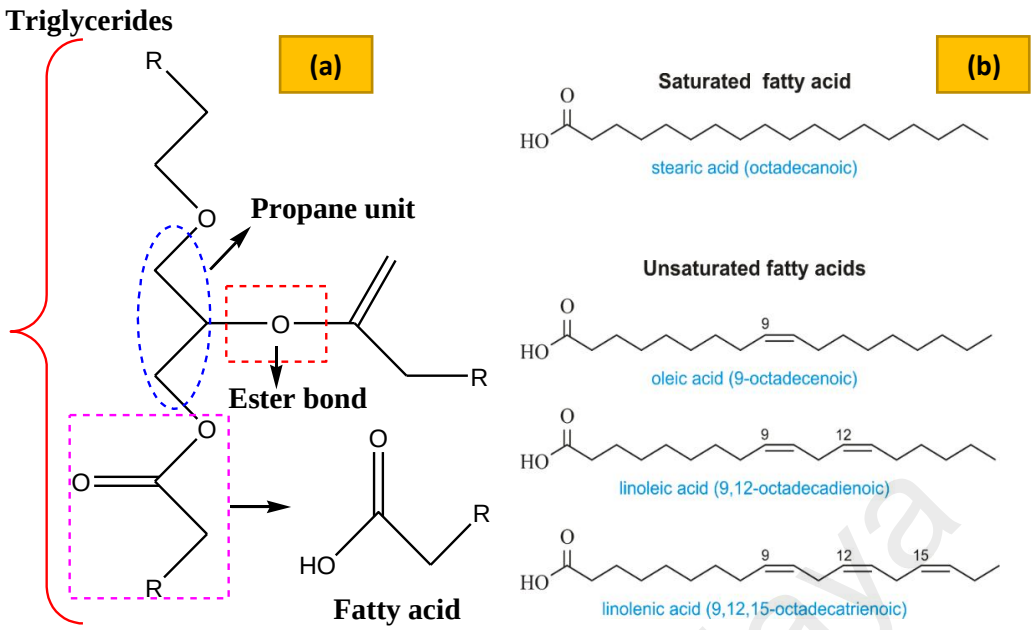

Figure 2.2: (a) Basic triglyceride and fatty acid structure in feedstock, (b) Fatty acids structure

2.3.2.1 Edible plant oil

Several types of edible oil could be potentially converted to green fuel via deoxygenation reaction. Table 2.2 presents the various types of well-known edible oil derived from plants around the world (Avhad & Marchetti, 2015;Al-Sabawi et al., 2012;Sotelo-Boyas et al., 2012;Gunstone, 1996). Due to geographical factor, every country has a preferred crop of choice. Therefore, the choice of feedstock for every country depends on regional preferences. Based on the Statisca portal, the global vegetable oil production volume of major vegetable oil worldwide from 2012/2013 to 2015/2016 increased from 156.38 to 182.33 million tonnes (an increase of 26 %). Due to increasing vegetable oil production for each feedstock per year, these oils have a great potential to be used as feedstock for green fuel production. Based on Table 2.2, among all the feedstocks, palm oil is the most pertinent feedstock followed by corn oil for continuous supply in production of green fuel process. Total global production of palm is estimated at over 65.5 million metric tonnes, with Indonesia and Malaysia as the majority world producers and exporters (Colchester et al., 2011). Based on commodity

prices, corn, canola and palm oil have the lowest prices with 300 USD, 470 USD and 688 USD per metric tonnes with majority of the oil content in the seed or kernel yielding > 40%. Even though >70% of olive could be converted to oil, its usage might be limited due to low availability (2.2 per metric tons per year) and high cost. Furthermore, large quantities of unsaturated fatty acid compounds were detected in most of the vegetable based oil except for coconut oil which would reduce the product selectivity to saturated hydrocarbon after undergoing deoxygenation reaction. Based on the fatty acid composition of the feedstock containing high unsaturated fatty acid (Figure 2.3) (Avhad and Marchetti, 2015;Al-Sabawi et al., 2012;Sotelo-Boyas et al., 2012;Lestari et al., 2009), the primary fatty acid constituent in canola, corn, peanut and olive oil, is oleic acid (C18:1). Meanwhile, linoleic acid (C18:2) was found significantly higher in soybean and sunflower seed oils. In case of saturated acid, palm oil also showed siginificant amount of palmitic acid (C16:0) with 46.3%. All of these feedstocks are expected to generate long diesel mainly *n*-C_{15} and *n*-C_{17} fractions via selective deoxygenation reaction as one carbon will be removed from the parent fatty acid chain of the feedstock. Meanwhile, coconut oil was dominated by lauric acid (C12:0)(48 %) and myristic acid (C14:0)(16 %). Thus, the deoxygenation of coconut oil is expected to generate the formation of straign chain alkanes of *n*-C_{11} and *n*-C_{13}. Although, it was proven that various types of edible oil are promising as feedstocks in deoxygenation reaction, but continuous usage of edible oil might result in rivalry of food and green fuel purposes. Therefore, the use of edible oil as a fuel source for production of green fuel may not be viable and not worthy. Thus, it stipulates more research for relatively non-food based feedstocks that are cheap and economically viable.

Table 2.2: Types of potential vegetable oil to be used in deoxygenation reaction

Feedstock	**Palm**	**Canola**	**Soybean**	**Sunflower**	**Corn**	**Peanut**	**Olive**	**Coconut**
Primary sources	Malaysia & Indonesia	Canada	U.S.A	Europe	U.S.A	China	Spain	Philippine
Availability (mill metric tonnes)	65.5	>16	53.7	16.6	60	29	2.2	61.4
Price (USD)* (Nov 2017) (per metric ton)	688	470	772	1,000	300	1,525	3,776	1523
Oil in seed or kernel (%)	30-60	44	15-20	25-37	48	45-55	45-70	65-72
Saturated fatty acid	48	6	14	11	16	16	12	90
Unsaturated fatty acid	50	92	81	89	84	79	79	9
Acid value ($mgKOHg_{-1}$)	0.5	0.071	0.6	<1.1	0.223	<4	6.6	<3

* http://www.indexmundi.com/commodities

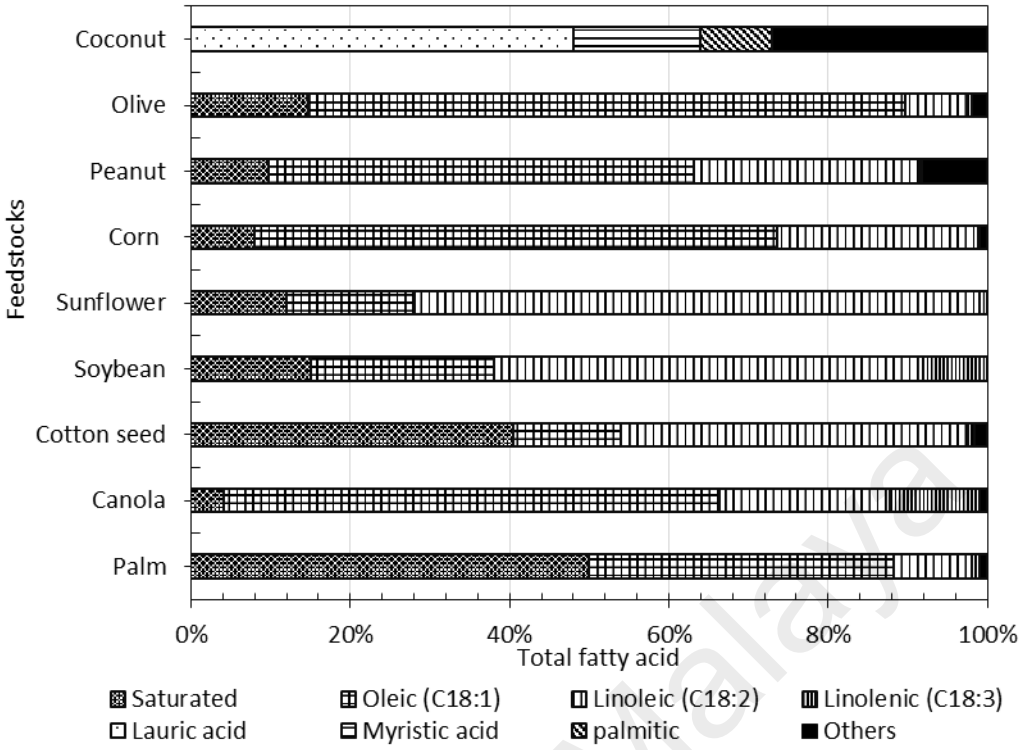

Figure 2.3: Fatty acid composition of vegetable oils

2.3.2.2 Non-edible oil

Global food or fuel debate on utilization of edible oil as green fuel feedstock is being seriously reviewed for their long-term impact. The use of non-edible plant oil had garnered enormous attention as a new generation feedstock due to their high oil content, availability and survival in abandoned land and climatic zones. Their growth is also not reliable with regional weather conditions. Thus, they could be grown with less intensive attention reducing the cost of cultivation. Additionally, several types of the non-edible plant trees also have longer life expectancy as high as 100 years which is promising in term of continuous feed supply (Silitonga et al., 2011;Ong et al., 2013). There are several types of well-known non-edible plant oil used in production of liquid biofuel especially in biodiesel production such as jatropha curcas oil (JCO) (Lee et al., 2014), jojoba oil (Al-Hamamre and Al-Salaymeh, 2014), karanja oil (Sharma and Singh, 2008),linseed oil (Varma and Madras, 2007), cottonseed oil (Avhad and Marchetti,

2015), ceiba oil, sterculia oil (Ong et al., 2013) and more as reported in Table 2.3 (Avhad and Marchetti, 2015;Lee et al., 2013;Asikin-mijan et al., 2016;Lianhua et al., 2010;G and Gopal, VKaviarasan, 2012;Pasias et al., 2009**;**Salimon et al., 2010;Ahmad et al., 2014;Evans et al., 1926;Moser, 2009). It was found that the raw materials derived non-edible plant seed or kernel have high oil content but lower than edible raw sources. JCO showed the highest oil content within the range of 50 to 60 % and the lowest was Tung oil and cotton seed oil, respectively with oil content within the range of 16-20 %. A majority of the oils were classified as non-edible oil due to free fatty acid (FFA) value with the lowest having 1 $mgKOHg^{-1}$ for jojoba oil while rubber oil, tobacco seed oil and JCO oil having the highest acid value of 45, >35 and 30.8 $mgKOHg^{-1}$, respectively. The fatty acid composition of non-edible oil showed that majority of the oils contain higher degree of unsaturated fatty acid than saturated carbon chain which deoxygenation of those feedstock might result in formation of product mainly composed of unsaturated hydrocarbon fractions (Santillan-Jimenez and Crocker, 2012a). Eventhough, the use of non-edible oil is highly promising but the major concerns on the use of non-edible oil are the high price of the feedstock compared to edible oil. However, there are a number of non-edible oil, such as jatropha oil, cotton seed oil, linseed oil, ceiba oil, sterculia oil, rubber seed oil and tobacco oil that were even lower and competitively priced (<USD500) per tons than edible oil.

Table 2.3: Types of non-edible oils and their free fatty acid value

Feedstock	JCO	Tung	Cotton seed	Lin seed	Jojoba	Ceiba	Sterculia	Castor	Rubber seed	Polanga	Tobacco seed
Price USD per metric ton/ml	400/t	1800/t	330/t	421/t	2000/t	360/t	250/t	1100/t	329/t	-	500/t
Oil in seed or kernel	50-60	16-18	18-20	35-45	45-50	25-28	34	45-50	40-60	65	30-43
Acid value ($mgKOHg^{-1}$)	30.8	9.5	19.6	4.9	1	5.1	12.0	5	45	44	>35
Lauric (C12:0)	-	-	-	-	-	0.1	0.1	-	-	-	-
Myristic (C14:0)	-	-	1.0	-	-	0.1	0.2	-	-	-	0.2
Palmitic(C16:0)	15.2	5.5	25.8	5.1	1.2	19.2	18.4	1.0	10.2	12.0	8.4
Palmitoleic(C16:1)	0.7	-	0.6	0.3	-	0.3	0.3	-	-	-	-
Stearic(C18:0)	6.8	-	2.5	2.5	-	2.6	7.6	-	8.7	12.9	3.4
Oleic(C18:1)	44.6	4.0	17.2	18.9	10.7	17.4	4.0	3.0	24.6	34.0	11.2
Linoleic(C18:2)	32.2	8.5	51.5	18.1	-	39.6	11.1	5.0	39.6	38.3	75.6
α-Eleosteari (C18:2)	-	89.0	-	-	-	-	-	-	-	-	-
Linolenic(C18:3)	-	-	0.2	55.1	-	1.5	2.3	1.0	16.3	0.3	1.0
Arachidic(C20:0)	0.2	-	0.3	-	9.1	0.56	-	-	-	-	-
Gondoic (C20:1)	-	-	-	-	59.5	-	-	-	-	-	-
Behenic(C22:0)	-	-	0.2	-	-	-	-	-	-	-	-
Erucic(C22:1)	-	-	-	-	12.3	-	-	-	-	-	-
Nervonic	-	-	-	-	1.7	-	-	-	-	-	-
Riconoleic	-	-	-	-	-	-	11.1	89.0	-	-	-
Malvaloyl18:*CE)	-	-	-	-	-	-	44.1	-	-	-	-
Sterculoyl(19:*CE)	-	-	-	-	-	18.5	-	-	-	-	-
Others	-	-	0.70	-	-	-	-	-	-	-	-
Saturated	22.2	5.5	29.8	7.6	10.3	22.6	26.3	1.0	18.9	24.9	12.0
Unsaturated	77.8	94.5	70.2	92.4	89.7	77.4	73.7	99.0	81.1	75.1	88.0

2.3.2.3 Waste oil and animal fat

Waste oil is the food waste that would be obtained after using the oil for cooking purposes, classified as invaluable and would always be discarded without further usage. The utilization of non-edible oil from recycled waste oil is extremely sustainable, capable of eliminating food rivalry debate, economical and environmentally friendly. Waste oil is divided into two types of grease; yellow grease (FFA<15%, acid value <30 $mgKOHg^{-1}$) and brown grease (FFA>15%, acid value > 30 $mgKOHg^{-1}$). Waste oil is the second most abundant waste residue, which is generated, in enormous amount by restaurants, food processing industries and fast food outlets every day. The worldwide demand for edible vegetable oil keeps growing. WCOs are highly viscous and generally contain high oxygen content, which is not compatible with the design of motor engines. To be used in engines, waste oil is required to be converted into suitable fuel by some advanced processes that can lower their viscosity and oxygen content, and improve their atomization and lubricity (De and Luque, 2014). The study focused on upgrading waste oil via deoxygenation reaction under zero-H_2 environment had been reported by (Romero et al., 2015a)., which yielded >80% of hydrocarbon fraction with majority of the product composed of unsaturated hydrocarbons. More studies on converting waste oil to valuable green fuel were further reported by (Li et al., 2013;Hanafi et al., 2015) and (Chang et al., 2016).

Animal fat is derived from the rendering process that uses animal tissues as raw materials. Several types of animal fat had been found such as beef tallow, duck tallow, chicken fat and fish fat (Avhad and Marchetti, 2015). Chicken fat contains a high level of linoleic acid, ranging between 17.9 and 22.8% (Nutter et al., 1943). Meanwhile, beef tallow contains a significant amount of oleic acid (between 47 and 50%) and also possesses a moderate combination of saturated fatty acids (~40%), namely, palmitic and

stearic acids (Al-Sabawi et al., 2012). The use of animal fat instead of vegetable oil to produce alternative diesel is an effective way to reduce the cost of raw materials, which is estimated to be about half the price of edible plant oil. In a recent study reported by (Kaewmeesri et al., 2015), It was found that the deoxygenation of waste chicken fat to green diesel over Ni/Al_2O_3 catalyst at a temperature of 330 ^oC under the presence of water resulted in a major reaction; deCOx, whereas hydrodeoxygenation was minor. The major fraction of *n*-alkanes in the liquid product consisted of *n*-C_{15} to *n*-C_{17} hydrocarbon fractions. Based on previous discussions, a great number of non-edible feedstock had been identified in recent years. The non-edible feedstock would not compete with food, thus providing more resources for green fuel production. However, it can be noted that only a few researchers studied the catalytic upgrading process for non-edible feedstocks under zero-H_2 environment condition.

2.4 Catalytic upgrading process

2.4.1 Cracking

The cracking process had become viable as the reaction might eliminate the oxygenated species in the fatty acid counterparts. Generally, cracking involves thermal cleavage or catalytic decomposition of triglycerides. The product possesses lighter alkanes, alkenes and fatty acid (Gosselink et al., 2013;Snåre et al., 2009). Cracking activity would also result in scission of C−C bonds in the intermediate fatty acids, and yield shorter chain of fatty acid and C-C bonds in the longer fraction of hydrocarbons (Figure 2.4a). Both reactions would yield light hydrocarbon fraction. Thermal cracking of vegetable oil is gaining worldwide attention as it is a low-cost process.

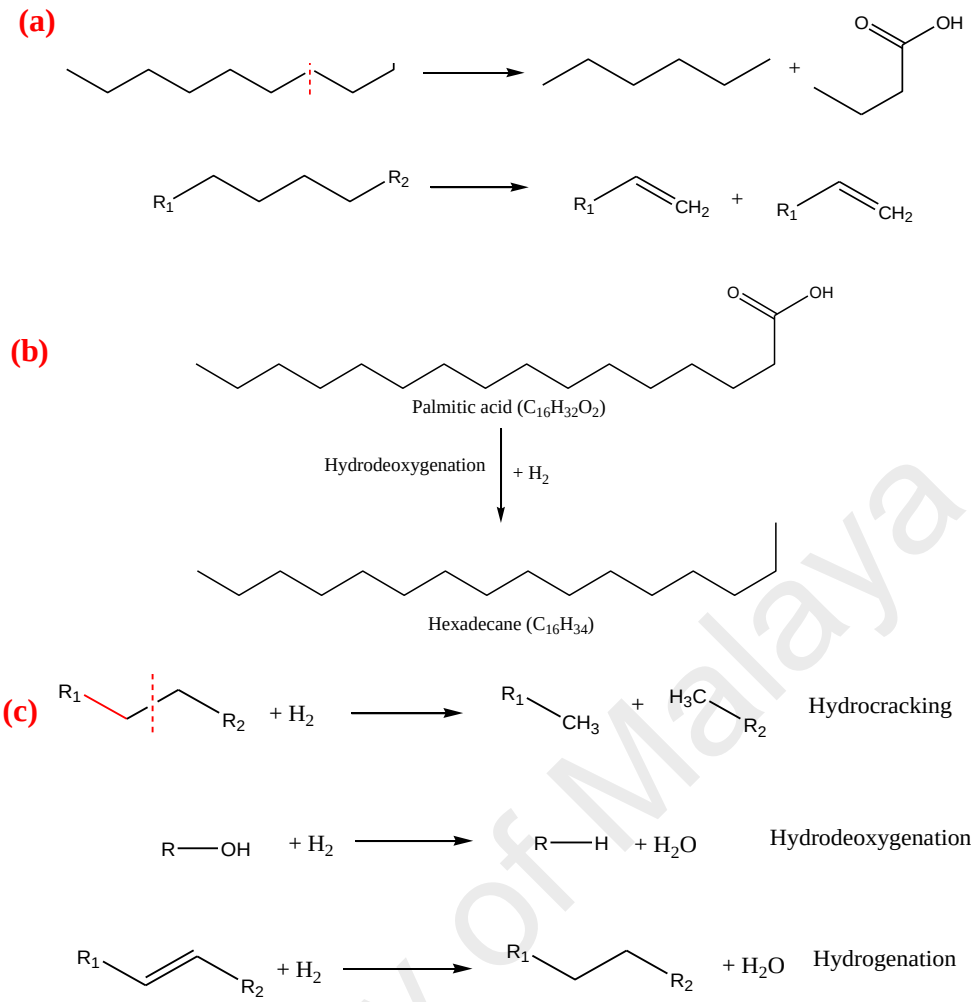

Figure 2.4: Reaction pathway of (a) cracking, (b) hydrodeoxygenation, (c) all reactions occur in hydrodeoxygenation reaction

Based on previous literatures dealing with catalytic cracking of vegetable oil via different catalytic systems, it was reported that majority of the occurrences of significant cracking reaction were promoted by the use of solid acid catalyst-zeolite and mesoporous silica-alumina (SiO_2-Al_2O_3) (Kubatova et al., 2012;Idem et al., 1996). Zeolite is an acid catalyst which possesses a large number of βronsted and lewis acid sites, coupled with its high selectivity (related to a network of internal canals with well-defined diameters), could lead to the formation of short-chain linear hydrocarbons, cyclic, aliphatic and aromatic compounds, such as benzene, toluene and xylene. Meanwhile, SiO_2-Al_2O_3 is an amorphous and high surface area acid catalyst with most of them containing lewis acid sites. This would lead to the formation of short-chain

hydrocarbons with a greater proportion of aliphatic hydrocarbons, to the detriment of aromatic hydrocarbons (Idem et al., 1997;Prado and Antoniosi Filho, 2009). The major weakness of the cracking reaction are the formation of unselective and wide range of hydrocarbon and oxygenates formed. Thus, the implementing of cracking process is not an optimal upgrading technology of converting vegetable oil for production of high quality biodiesel fuel.

2.4.2 Hydrodeoxygenation (HDO)

Currently, the technology to upgrade the process of vegetable oil-based via hydrodeoxygenation is focused. Theoretically, catalytic hydrodeoxygenation reaction involving C-O breakage via hydrogenolysis reaction of oxygenated compound produces hydrocarbons of the same carbon number as the fatty acids in triglycerides (Zhang et al., 2014) and water as by-products (Figure 2.4b) under large consumption of H_2 gas and at elevated pressure condition. Water is formed in the conceptual reaction, therefore at least two liquid phases would be observed as a product: one organic phase and one aqueous phase. The appearance of the two organic phases had also been reported due to the production of organic compounds with densities less than that of water. Therefore, light oil would be at the top of water and heavy oil at the bottom. The formation of two phases indicated high degree of fractionation in the feedstock (Venderbosch et al., 2010;Mortensen et al., 2011). There are three general reactions that occur during hydrodeoxygenation; hydrocracking, hydrodeoxygenation and hydrogenation. All these reactions occurred in hydrodeoxygenation reaction as shown in Figure 2.4c. Although high pressure hydrodeoxygenation consumes considerable amounts of hydrogen during the reactions, its ability to remove oxygen from oxygenated compound by hydrodeoxygenation is much better than that of reaction under zero-H_2 environment (deoxygenation). Hydrodeoxygenation had attracted considerable attention because

the product quality is even better than conventional transportation fuel (Lee et al., 2016). Hydrodeoxygenation of the vegetable oil-based oil produces diesel-like deoxygenated hydrocarbons, which is purportedly superior to both biodiesel and fossil diesel in terms of performance, cold flow properties, storability, reduced emission and compatibility with petrodiesel engines. Indeed, hydrodeoxygenation process forms the basis of a number of processes – including Neste Oil's NExBTL, UOP/Eni's Ecofining, Petrobras' HBio and Dynamic Fuels' Bio-Synfining. Unfortunately, hydrodeoxygenation process has the drawback of a high cost related mainly to the high amount of hydrogen used in the process (Romero et al., 2015b). Therefore, researching a new cracking technology for the production of selective diesel fractions under free hydrogen environment had been widely investigated.

2.4.3 Deoxygenation (DO)

Based on the preceding section, due to the economic standpoint of the deoxygenation process from triglycerides and fatty acid, it is more preferred as it allows for the removal of oxygen under H_2-free environment, simultaneously producing the hydrocarbon mainly composed of alkane and alkenes which is fungible to petro-diesel. Deoxygenation involves the removal of oxygen in form of carboxyl and carbonyl groups from fatty acid as CO_2 and/or CO via decarboxylation and/or decarbonylation (deCOx) and water as by-product. The deoxygenation reaction scheme is shown in Figure 2.5a. Generally, deoxygenation of triglycerides and fatty acid results in producing hydrocarbons with one carbon number less than their corresponding fatty acids. Figure 2.5b shows an example of reaction scheme for the deoxygenation of dodecanoic acid to undecane and undecene which had been reported by Bernas et al., (2010). The main reaction is the decarboxylation of dodecanoic (lauric) and the side reaction is the decarbonylation to undecene (different isomers). Undeniably, the

deoxygenation process could be implemented at a small scale as the feedstock would not have to be centralized at a large hydrogen gas supply facilities. Therefore, the 'stand-alone' processing of renewable feeds via deCOx pathways is now considered propitious by some workers compared to the co-processing of feedstock (Santillan-Jimenez and Crocker, 2012a). The deoxygenation process had been studied by numerous researchers (Hermida et al., 2015b;Asomaning et al., 2014) and found that the reactions were proceeded under limited or considerably lower H_2 pressures and over simple metal catalysts (Santillan-Jimenez et al., 2013). Thus, deoxygenation process is more convenient and cost effective as compared to hydrodeoxygenation process, producing similar diesel-like characteristics.

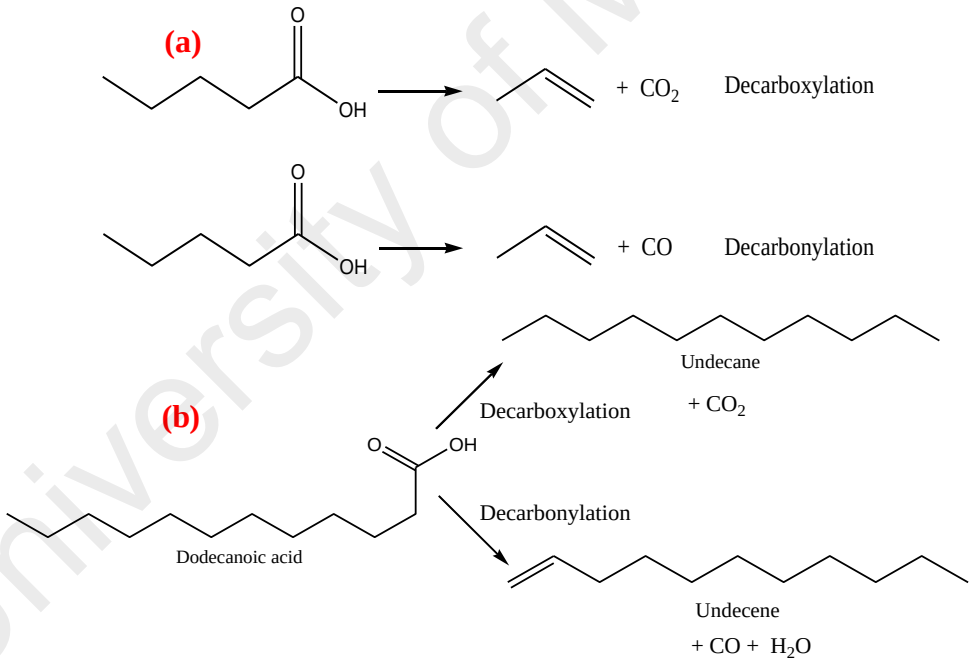

Figure 2.5: (a) Deoxygenation pathways via deCOx reactions
(b) reaction scheme for the deoxygenation of dodecanoic acid to undecane and undecene

2.5 Historical perspective on deoxygenation catalysts

Production of green fuel is relied on acid heterogeneous catalyst. High acid catalyst is preferred for oxygen removal via C-O cleavage from fatty acid via

deoxygenation reaction (Table 2.4). It has been established that the catalyst loaded with a noble metal (Pt, Pd or Rh) were considered to be the most active metal catalysts for deoxygenation, with respect to those containing non-noble transition metals (Kaewmeesri et al., 2015). It was proven by Snåre's study which tested various metals such as Ni, NiMo, Ru, Pd, Pd/Pt, Pt, Ir, Os and Rh on different supports (metal oxides and charcoal) in liquid phase reactions in order to determine their deoxygenation performance. It was found that the Pd/C resulted in a significant improvement in deoxygenation of fatty acid via hydrogenolysis of C-O-C bond (Mäki-Arvela et al., 2008;Snare et al., 2006). Even though the usage of noble-based catalyst showed high selectivity toward oxygen removal reaction and had shown quite selective propensity to formation of hydrocarbons, the high cost and rarity of noble metals limit large scale green fuel production.

Thus, for those reasons sulfided catalyst was chosen. From the investigation of conventional hydrodesulfurization catalyst such as CoMo, NiMo and NiW supported alumina, it was revealed that complete conversion of triglycerides occurred and it was found that the sulphide forms of CoMo and NiMo systems yield the best activity in oxygen removal (Kubička and Kaluža, 2010;Boullosa-Eiras et al., 2014). It was also reported that these catalysts resulted in hydrocarbon formation via hydrodeoxygenation and deoxygenation reaction through decarboxylation pathways. The removal of oxygen was done principally via C-O cleavage through the absorption of the vacancy site of metal-sulfided surface (Mortensen et al., 2011;Romero et al., 2010). Even though sulfided metal catalyst have a potential of removing the oxygenates species but there were several critical issues that needed to be considered such result in wide variety of products and sulphur contamination by catalyst which simultaneously affect the quality of oil. Moreover, a stringent legislation which enforces severe requirements to reduce

the sulphur content of diesel fuel to ultra-low levels (10 ppm) was triggered, aiming to lower the diesel engine's harmful exhaust emissions (US Environmental Protection Agency). In this connection, it is necessary to develop alternative, more economical free-sulphur catalysts such as (1) metal phosphide (Chen et al., 2014a;Yang et al., 2013), (2): carbide (Barrón et al., 2011;Sullivan et al., 2016) and (3): metal catalyst in reduced state (Kumar et al., 2014a). Eventhough it was proven that these types catalysts would successfully remove high amount of oxygen content via selective deoxygenation reaction (Zhang et al., 2016c)(Table 6), however due to the limitation of tedious, rigorous preparation method and alteration catalyst phase during reaction had produced limited lifetimes for these kind of catalysts (Liu et al., 2014).

Particularly, zeolite-based catalyst is well known as an efficient catalyst for petroleum-based fuel refinery due to its crystallinity, well-defined micropores, large surface area, interconnected network of channels, strong acidity and high thermal stability. All of these characteristics permit them to be used at high temperature, which often results in higher product yield and easier heat recovery. Even though zeolite is an excellent cracking catalyst, the use of zeolite-based catalyst on deoxygenation of vegetable oil, the reaction would be prone to unselective deoxygenation reaction and resulting in wide range of hydrocarbon fractions (Table 2.4). The light fractions of products would be theoretically caused by secondary reaction (cracking) via C-C scission due to high acidity of the zeolite-based catalyst and chemical characteristics of triglycerides-based oil. Large molecular structure of triglycerides led to diffusional limitation for the triglycerides to access narrow channel of zeolite-based catalyst (Botas et al., 2012). The reaction pathways of zeolite-cracking had been studied by Benson et al., (2009) and Kloprogge et al., (2005). The cracking reaction had been found to be stimulated by protonation of fatty acid of which proton charge subsequently migrate

along fatty acid chain followed by cracking of the fatty acid. The narrow channel of zeolite limited the protonation to the pore mouth of the zeolite catalyst and the resulting species were sufficiently small to enter the catalyst pores, and cause consequent cyclization and aromatization (Zhao et al., 2013). The formation of polyaromatic compound might cause pore blockage and deactivate the catalyst. It had been proved by Huang's research study, which investigated the performance of commercial zeolite H-Y with two different SiO_2/Al_2O_3 ratios (5.2 and 30) on deoxygenation of cyclopentanone. It was observed that both H-Y catalysts resulted in formation of coke which suggested that it was due to the formation of significant poly (aromatics) compounds (Huang et al., 2009). It can be suggested that, product yields and distribution obtained from the catalytic cracking of triglycerides based oil would be highly dependent on the catalyst type. Based on the catalytic limitations from the criteria listed by preceding literatures, the research for an alternative catalyst which is low cost, sulphur free catalyst, easily prepared and capable of producing high quality oil via selective deoxygenation reaction is needed.

Table 2.4: Performance of representative catalysts in the deoxygenation of triglycerides and fatty acid derivative via deCOx reaction

Type catalyst	Catalyst	Feed	Reaction condition	Reactor mode	[a]Con. (%)	Selectivity (%)	Properties	References
Noble metal	5% Ru/C	Stearic acid	6h;300 °C; atm; He 6Mpa	Semi-batch	13.2	65 (C_{17})	High selectivity Expensive	(Snare et al., 2006)
	5%Pd/C				100	99 (C_{17})		
	5%Pt/C				86	95 (C_{17})		
	1% Rh/C				19.9	85 (C_{17})		
	5%Os/C				6.9	53 (C_{17})		
	1%Pt/C	Tristearin	4h;350 °C;atm;N_2 6.8MPa	Batch	42	83 (C_8–C_{17})		(Morgan et al., 2010)
	5%Pd/C				29	93 (C_8-C_{17})		
	0.5%Pd/Al_2O_3	Stearic acid	3h;350 °C,atm;H_2	Batch	100	90.3 (C_{17})		(Berenblyum et al., 2011)
	5%Pd/ Al_2O_3				100	91 (C_{17})		
	5%Pd/C	Oleic acid	6h,360, 15%H_2/Ar		98			(Snåre et al., 2008)
Sulfided metal	NiMo/Al_2O_3	Rapeseed oil	4h^{-1},280°C, H_2=3.5MPa	Fixed-bed	100	85 (C_{15}-C_{18})	High selectivity Poor quality oil due sulphur leaching	(Kubička and Kaluža, 2010)
	Mo/Al_2O_3 Ni/Al_2O_3				100	78 (C_{15}-C_{18})		
					100	60 (C_{15}-C_{18})		
	CoMo/γ-Al_2O_3	PRO-primary refined rapeseed oil	2h^{-1},310°C, H_2=3.5 Mpa	Fixed-bed	90	80 (C_{17}-C_{18})		(Kubička and Horáček, 2011)
	NiMo/SiO_2	Rapeseed oil	2–8h^{-1},260–300◦C ,H_2=3.5MPa	Fixed-bed	100	80 (C_{17}-C_{18})		(Kubička et al., 2014)
	NiMo/Al_2O_3				100	85 (C_{17}-C_{18})		
	NiMo/TiO_2				100	>60 (C_{17}-C_{18})		
Phosphide and Carbide metal	Ni_2P/SiO_2	Methyl laurate	14h^{-1},340°C,H_2= MPa	Fixed-bed	~96	~94 (C_{11}-C_{12})	High selectivity Tedious and complex synthesis catalyst method	(Chen et al., 2014b)
	MoP/SiO_2				~90	~87 (C_{11}-C_{12})		
	b-Mo_2C/CNF	Stearic acid	3h,350°C,H_2=30 bar	Batch	65	41(C_{17}-C_{18})		(Stellwagen and Bitter, 2015)
	b-W_2C/CNF				>96	91(C_{17}-C_{18})		
Zeolite	ZSM-5	Sunflower oil	500 °C; atm;N_2	Fixed-bed	32.2	63 (C_{18}-C_{43})	Expensive Poor product selectivity	(Zhao et al., 2015)
	1% Pt/HZSM-5 (23)	Jatropha oil	2h,270°C,6.5MPa of H_2/N_2 gas	Batch	100	91(C_5-C_{21})		(Murata et al., 2010)
	1% Pt/USY (6.3)				31	88 (C_5-C_{21})		(Zhao et al., 2013)

2.5.1 Monometallic and mixed metal oxides

As alternatives to the catalysts limitation mentioned in the preceding section, the process of investigating transition metal catalysts in deoxygenation reaction had been performed (Zhang et al., 2014;Pstrowska et al., 2014). These metal oxide catalysts were not only sulphur free catalyst but also possessed high catalytic activity at mild temperature and the price was significantly cheaper. Common transition metal oxide which has been used in deoxygenation process include Ni, Co, W (Rezgui and Guemini, 2005),Mo, Cu, Fe and Zn (Chen et al., 2014a). Among these metals Ni and Co metal showed high deoxygenation activity via decarboxylation and/or decarbonylation pathways (Zhang et al., 2014). In deoxygenation reaction under free-H_2 environment, Ni-promoted catalyst gave predomination toward decarbonylation and mild hydrodeoxygenation degree. Meanwhile, Co-promoted catalyst was favoured toward both decarbonylation and decarboxylation reaction (Srifa et al., 2014). Ni metal was also proven to offer similar promotional effect as noble catalyst in deoxygenation activity. It was in agreement with Crocker and co-workers' finding in catalytic deoxygenation of tristearin using carbon-supported Ni, Pd and Pt catalysts. Where, high dosage of Ni metal (20 wt% Ni) afford similar performance with those obtained over 5 wt.% Pd and 1wt % Pt-promoted catalyst (Morgan et al., 2010). This finding is important due to the fact that the cost of Ni is ~1750 and ~3450 times lower than that of Pd and Pt, respectively. Even though Ni- promoted catalyst showed high deoxygenation activity and shown similar promotional effect like noble metal catalyst but Ni- promoted catalyst were easily deactivated due to metal sintering, metal leaching and coke formation (Reddy Yenumala et al., 2016). Thus, several studies on the implementation of coke inhibitor species derived alkaline earth metal such as beryllium(Be), magnesium(Mg), calcium(Ca), strontium (Sr), barium(Ba) and radium(Ra) had been investigated. such as beryllium(Be), magnesium(Mg), calcium(Ca), strontium (Sr),

barium(Ba) and radium(Ra). Among these metals, Ca and Mg metals were widely investigated in deoxygenation reaction (Dos Anjos et al., 1983). This is due to their strong basic sites which allow the removal of oxygenates species via deCOx of triglycerides and fatty acid derivatives (Sannita et al., 2012).

Even though the use of non-noble monometallic had already been investigated in deoxygenation studies but the monometallic catalyst easily to deactivate due to coke deposition. Thus, more attention have been focused toward the usage of bimetallic catalyst in recent years. There had been research indicating that the usage of bimetallic catalyst for green fuel production such as NiCo, NiMo, NiCu, NiW, and CoMo catalysts (Toba et al., 2011;Krár et al., 2010;Kim et al., 2013a) is favorable. Generally, the bimetallic formation would pose an extra benefit over monometallic. It was in agreement with Tagusagawa et al., (2010) findings which showed that the addition of W-oxide on Nb_3 oxide would form Nb_3W_7, offering a higher rate with mesoporous structure and multiple strong acid sites than W- and Nb-containing catalysts. Similar trend reported by Huynh et al., (2015) on NiCo alloy, where the result showed that the NiCo alloy catalyst contain capable to remove more oxygenates species due to a synergistic interaction of NiCo alloy from the support and greater dispersion of the metals. All of these criteria of bimetallic of NiCo alloy enabled it to perform all individual steps in the reaction network toward desired products at a high rate. Even though monometallic or bimetallic metal oxides were claimed to be effective in deoxygenation reaction for production of green fuel, however those catalyst commonly have small surface areas and limit the absorption and concentration of reactants around the active sites. For this reason, the synthesis of supported catalyst had been investigated and validating it as an efficient way to make up for the referred deficiency.

2.5.2 Support

The choice of support is an important aspect of catalyst formulation, significantly affecting the deoxygenation reaction. Metal support could not only enhance the active metal dispersion but might also contribute in the alteration of chemical properties of synthesized catalyst and tune the catalytic reaction activity (Dhar et al., 2003). It was reported Centeno et al., (1995) who investigated the effects of different support catalyst that their acidity could enhance the formation of active sites for both decarboxylation and hydrogenation of carboxyl groups. Generally, Al_2O_3 and zeolite were used as catalyst support, as they were conventional supports used in the hydro processing of petroleum fuel. Undeniably, the usage of acidic support was important in the cracking activity as it provided additional reaction sites for H_2 dissociation or absorption of oxygenated compounds. γ-Al_2O_3 and zeolite were considered as acidic support, zeolite contain an abundance of Brønsted acid sites, while Al_2O_3 was dominated by Lewis acid sites. Brønsted acid support was favourable toward hydrogenation–dehydration–hydrogenation reaction routes, which would favor hydrodeoxygenation reaction pathways. Meanwhile, lewis acid sites favoured deCOx pathways. The usage of strong acidic support catalyst such as zeolite was not preferable, strong acid catalyst would result in severe catalyst deactivation due to the coke formation and unselective cracking reaction. Therefore, the usage of moderate acidic support like Al_2O_3 was essential in order to breaking the carboxylic group in the vegetable-based oil. Even though Al_2O_3 resulted in high catalytic activity, this support also suffered toward catalyst deactivation due to coke formation but lesser than strong acidic support. It had been proven by Centeno et al. who studied hydrodeoxygenation process over Al_2O_3-supported CoMo and NiMo catalysts using various oxygen-containing phenolic model compounds such as guaiacol, catechol, phenol, 4-methyl acetophenone and para-cresol, in para-xylene medium. Large extent of coke formation

were observed on the surface of Al_2O_3 which became prominent especially when it reacted with oxygenate model compound such as guaiacols or catechols (Centeno et al., 1995). The coke formation produced by Al_2O_3 catalyst was generally resulted by large polymerization products. Therefore, a support less active than Al_2O_3 is required.

In this sense, the use of activated carbon (AC) as support could be a good option. The neutral nature of carbon is advantageous, as this would give a lower tendency for carbon formation compared to Al_2O_3. However, this neutral carbon support has no catalytic function and favors the direct deCOx route of carboxylic acid functional groups on metal sites. Therefore, some modification and treatment are necessary for improving the acidity of the carbon support. Moreover, high degree of deoxygenation by carbon supported catalysts is also attributed by the excellent catalyst structure, i.e., the higher specific surface areas compared to SiO_2 and Al_2O_3 supports, thus minimizing the influence of catalyst deactivation caused by sintering and/or coking (Zhao et al., 2013). SiO_2 had also been indicated as a prospective support for hydrotreating reaction as it, like carbon, has a neutral nature and therefore has a relatively low affinity for carbon formation. Popov et al., (2010) showed that the concentration of absorbed phenol species on SiO_2 was only 12% relative to the concentration found on Al_2O_3 at 400 ^oC. SiO_2 only interacted with phenol through hydrogen bonds, but on Al_2O_3, dissociation of phenol to more strongly adsorbed surface species on the acid sites was observed. More study on utilization of SiO_2 in deoxygenation of rapeseed oil over NiMo supported SiO_2, TiO_2 and Al_2O_3 were reported by Kubička et al., (2014). It was found at the same degree of deoxygenation, that the highest yield of hydrocarbons was obtained over SiO_2-supported catalyst and the lowest was over TiO_2-supported catalyst. Moreover, the SiO_2-supported catalyst also yielded *n*-heptadecane as the main deoxygenation product, while Al_2O_3- and particularly TiO_2-supported catalysts afforded

n-octadecane as the main deoxygenation product. It could be observed that the product selectivity depends on the nature of the support material. TiO_2 supported favoured an occurrence of hydrodeoxygenation as compared to the other supports. From the catalyst characterization analysis, it was revealed that the active phase was not dispersed completely and larger cluster phase had occurred. Meanwhile, active phase on SiO_2 rendered better dispersion in comparison to TiO_2 and Al_2O_3. In this study, the degree of dispersion of active phase was reported to be the main reason of the preference toward decarboxylation. It could also be concluded that the metal-support interaction and the support properties play important role in the tuning of reaction route and product selectivity. Due to the limitation of Al_2O_3 support and advantages of SiO_2 support, a mildly acidic silica–alumina support derived SiO_2-Al_2O_3 (low silicon/aluminum ratio) had started to gain interest (Castaño et al., 2007;Regali et al., 2013;Roussel et al., 2005). The mild acidity of the support gives a good balance between cracking and isomerization and limits secondary cracking. It was found that the rate of deactivation over CoMo/SiO_2-Al_2O_3 catalyst lessened as compared to CoMo/Al_2O_3 catalyst (Maity et al., 2012). From this finding, it was suggested that the acidic sites in SiO_2-Al_2O_3 support catalyst was the reason for formation of coke on the bare support surface. Supports such as CeO_2 and ZrO_2 had gained large interest owing to their high thermal stability, better dispersion of metal and ability to store oxygen and redox properties. ZrO_2 also had some acidic character, but significantly less than Al_2O_3 (Bui et al., 2011). On the other hand, deoxygenation activity also could be assisted over basic support catalyst such as CaO and MgO (Romero et al., 2015a). The usage of basic supported catalyst is interesting as it is resistant to formation of carbonaceous compound unfortunely, their usage still lack in cracking ability. This study had been examined by Idem et al., (1996) on the deoxygenation of rapeseed oil at 400 ^oC on MgO and CaO catalysts under atmospheric pressure. According to these authors, basic catalysts

resulted in a lower conversion when compared to acid catalysts, and they produced a limited amount of gases and a high yield of liquid. Similar case was also reported by Gómez et al., (2013) and Morgan et al., (2012). Thus, generally utilization high basic support requiring the co-existence of acid sites to optimize deoxygenation activity to be comparable with acidic catalyzed reaction. Owing to the decent performance of base catalyzed in suppressing the coke formation, it would be interesting to further study the deoxygenation reaction over acid-base catalyst.

2.5.3 Deoxygenation of triglycerides and fatty acid derivatives over base and acid-base catalyst

Extensive works had been published in the past on deoxygenation reaction over acid and base catalyst on a variety of fatty acid and triglycerides from edible, non-edible vegetable oil and model oil compound. They were widely discussed in these literatures (Kumar et al., 2014b;Tani et al., 2011;Asikin-mijan et al., 2016;Hermida et al., 2015a;Dawes et al., 2015). A majority of the reaction condition was active at temperatures within the range of 230-375^{o}C under zero hydrogen environment and H_2-modest environment (10-110 bar: 1bar=0.1 MPa). The H_2-modest environment, is defined as having a severely reduced external supply of H_2 gas with pressure near atmospheric pressure or below than minimum H_2 pressure required for hydrodeoxygenation process. Even though numerous deoxygenation studies were carried out under H_2-modest environment within the past decade over acid catalyzed reaction, studies toward the development of base and acid-base catalyst for selective deoxygenation under zero H_2 environment are still limited. Herein, the deoxygenation mechanism under the zero H_2 environment over base and acid-base catalyst were focused. Due to limited study on the utilization base and acid-base catalyst in deoxygenation under zero-H_2 environment, thus only few study only reported on the

usage of pure basic catalyst in deoxygenation reaction. It was suggested base catalyzed deoxygenation favored triglycerides cleavage forming intermediate fatty acid via C-O cleavage through hydrolysis reaction (Tani et al., 2011;Romero et al., 2015a;Morgan et al., 2012)(Figure 2.6). It was proposed by Santillan-Jimenez and Crocker (2012a) from the correspond glycerol formation via C-O cleavage in deoxygenation study. It was strongly supported by Tani et al., (2011), which studied the MgO catalyzed deoxygenation system on various bio-based feedstocks under complete mixed type (CSTR) reaction and proposed that the occurrence of the initial cleavage of C-O from triglycerides was triggered via hydrolysis reaction with the assistance of water existed in the feed forming glycerol and free of fatty acid. The water was continuously generated by the dehydration of glycerol, releasing gaseous hydrocarbon (propane) and the free fatty acid was produced further under decarboxylated/decarbonylation reaction. This also were agreement with Romero et al., (2015a). For acid-base catalyzed deoxygenation reaction suggested that the triglycerides cleavage facilitate via ß-elimination process (Figure 2.6). It was revealed due to significant detection of the ester carbonyl carbons characteristic in deoxygenation of soybean oil over Ni-Mg-Al LDH at 300^{o}C. It was suggested that by an action of acid-base neutralization, Ni-Mg-Al LDH would favor the development of these reaction under the given conditions.

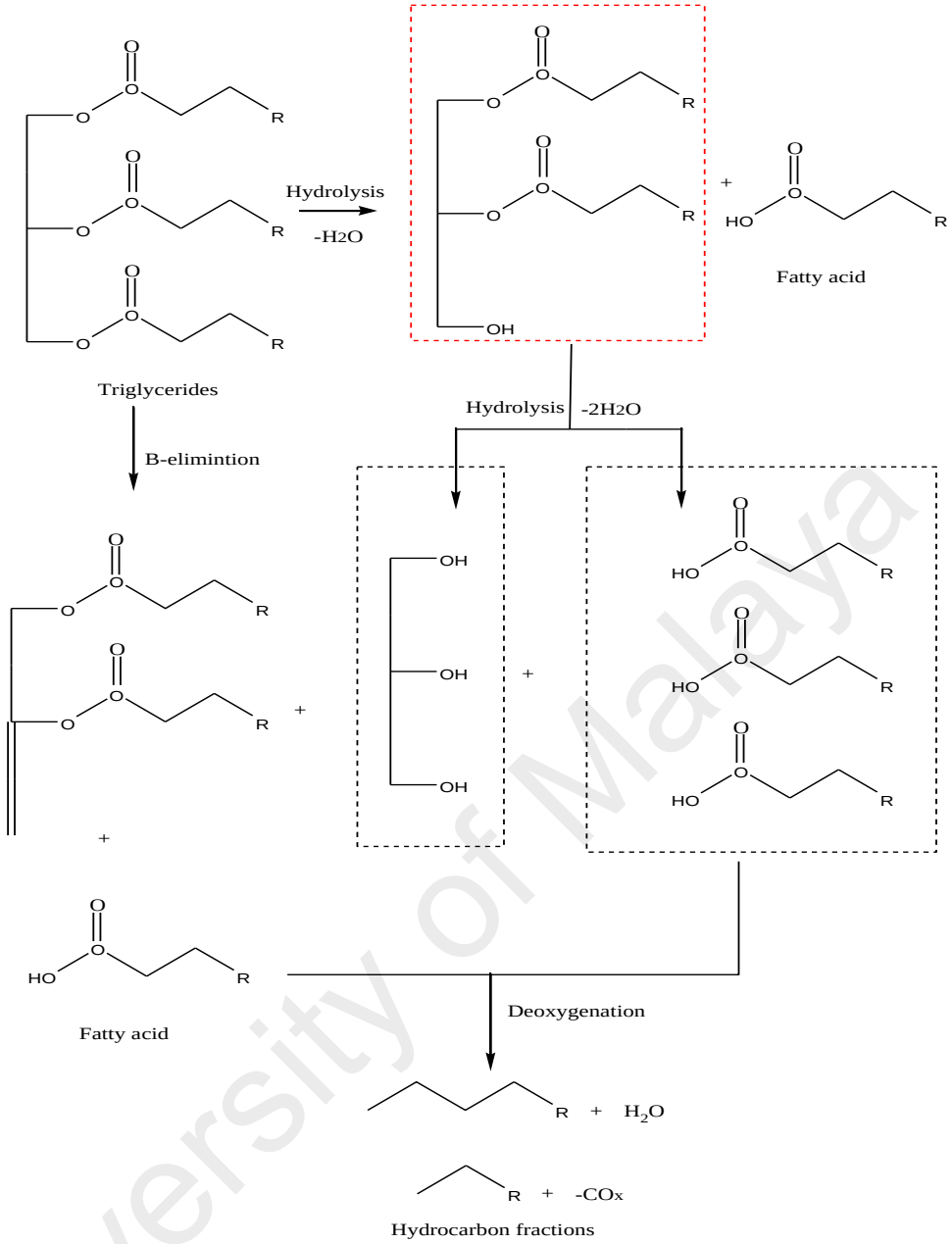

Figure 2.6: (a) ß-elimination and (b) hydrolysis reaction

The intermediate fatty acids thus formed are expected to subsequently undergo decarboxylation or decarbonylation to give respectively an alkane or an alkene containing one carbon less than the acid. Majority of the majority of the research reported that basic catalyzed deoxygenation was found to be favoured toward decarboxylation (removal of oxygen in the form of CO_2) (Tani et al., 2011;Na et al., 2010;Veses et al., 2016). These observations are consistent with findings previously reported by us concerning the deoxygenation of triolein oil nanosize-$Ca(OH)_2$ and

micron size CaO catalyst, where >90% of decarboxylated product (mono-unsaturated *n*-C_{17}) was achieved (Asikin-Mijan et al., 2015a). Again Tani et al., (2011) reported on the dominancy of decarboxylation reaction in deoxygenation of palm oil over MgO-promoted catalyst under free-H_2 environment by the large formation of decarboxylated products (*n*-C_{15} + CO_2). Similar trend were observed for the acid-base catalyzed deoxygenation reaction, deoxygenation of triglycerides was found to proceed via removal of carboxyl group in the fatty acid structures as CO_2 (major) and CO (Morgan et al., 2012). The dominancy of occurrence of both decarboxylation and decarbonylation reactions over acid-base catalyst was in agreement with Morgan's studies on deoxygenation of triglycerides over Ni-Al LDH (Santillan-Jimenez et al., 2013). All finding discussed above contradicted with acidic catalyzed deoxygenation, in which the acid sites appeared to facilitate decarbonylation to remove oxygen as CO and H_2O. Liu et al found that acidic catalysts derived Co/SiO_2 and Co/Hβ would preferentially result in C-O bond cleavage parallel with decarbonylation due to the transformation of heptanoic acid to more than 90% C_6/C_7 alkanes (Liu et al., 2014). For instance, Morgan's and co-workers had reported the results of detailed studies dealing with the acid catalyzed deoxygenation of tristearin over 1%Pt/C, 5%Pd/C and 20%Ni/C catalysts, where the oxygen was rejected from the triglycerides preferentially in the form of decarbonylated by product (CO) (Morgan et al., 2010). Similar case reported by former studies (John et al., 2016;Meller et al., 2014;Peng et al., 2013). The outcome of this comparison depicted that base and acid-base catalyzed favored decarboxylation, while acid sites favored decarbonylation reaction. However, it still controversial since several studies also discovered acid catalyst capable in rendering the occurrence of decarboxylation process (Bernas et al., 2010;Snare et al., 2006). During triglyceride deoxygenation over base and acid-base catalyst, formation of light hydrocarbons is observe (Romero et al., 2015a;Li et al., 2013;Gosselink et al., 2013;Tani et al.,

2011;Asikin-Mijan et al., 2016d), thereby providing additional pathways for hydrocarbon formation. The formation of light hydrocarbon fraction by basic catalyst was in line with a recent report by Romero et al. (2015a), a significant formation of light fraction within range of C_8 to C_{11} during deoxygenation of WCO and JCO over CaO. Meanwhile, cracking activity over acid-base catalyst have been proven in our recent study on deoxygenation of triolein over Co-CaO catalyst (Asikin-Mijan et al., 2016d). The result showed >80% of the hydrocarbon composed of light fraction within range of C_{11} to C_{12}, implying that C-C bond cleavage occurred tremendously.

2.5.4 Deoxygenation side reactions over base and acid catalyst

Apart from deoxygenation reaction under zero H_2 environment, utilization of base and acid-base catalyst also offers the occurrence of other reactions such as oligomerization/polymerization, cyclization, aromatization, ketonization and aldol condensation. Oligomerization reaction is a process which transforms lighter hydrocarbon by-products (C_3-C_6 olefin containing fractions) or lighter compounds to longer chain molecule (Figure 2.7a). Generally, acidic sites promote oligomerization (Krivan et al., 2016). Instead of acidic properties, it was found that the transition metals such as V, Ti, Zr and Ni could promote the occurrence of oligomerization due to their electropositive properties (Jiang et al., 2016). In contrast, the use of heterogenous basic catalyst in oligomerization reaction resulted in diminished activity. It was revealed by Di Cosimo and Apesteguía, (1998) which studied alkali-promoted MgO, resulting in extensive catalyst deactivation due to a blockage of basic sites by a carbonaceous residue created during oligomerization side reactions. Generally, aromatization occurs on the acidic sites of catalyst via carbocation intermediates starting with cracking of long chain olefins into smaller alkenes, condensation of carbenium ions and alkene molecules, ring enlargement via protonated cyclopentenyl ions and then the

dehydrocyclization (Taguchi and Schüth, 2005;Lou et al., 2016). Chang's study revealed that the acidic catalyst pellets ($Al_2(SO_4)_3$) and the related acidic zeolite based catalysts such as ZSM-5, MCM-41, and Y zeolite produced a pyrolysis oil with a high acid value and content of aromatic hydrocarbons (Chang et al., 2016). Meanwhile, a very low aromatic hydrocarbon content was obtained using the base catalyst. Other than the acidity of catalyst, higher content of unsaturated alkyl chains in fatty acid compound also possessed a strong tendency to undergo a very fast aromatization process (via sequential cyclization, dehydrogenation and condensation reactions) to form (poly)aromatic bodies with alkyl branches using acidic catalysts (Chang et al., 2016;Dupain et al., 2007). Particularly, aromatization was also promoted at a temperature region of 400-600 ^{o}C under atmospheric pressure (Wang et al., 2016). This is similar to cyclization. Generally, the occurrence of aromatization was exhibited after the formation of cyclic compound (Figure 2.7b). Recent study by Lou et al., (2016) found that the total selectivity of the aforementioned cycloalkane products was up to 91.3% when acid catalyst derived Pd/ZSM-5 were used. The utilization of base catalyst in deoxygenation reaction might also facilitate the formation of cyclic as it was reported in recent study (Mijan et al., 2016). Aldol condensation is a reaction combining two carbonyls containing molecules together to form a new carbon-carbon bond followed by a subsequent dehydration forming aldehyde compound (Figure 2.7c). This class of reaction, could generally be catalyzed by basic sites from supported alkaline or alkaline earth metals (Sundararaman and Song, 2013;Frey et al., 2013), supported metal oxides (Ji et al., 1997) and calcium hydroxyapatities (Rodrigues et al., 2014), hydrotalcites (Abelló et al., 2005) and alkaline-activated high-silica zeolite (Keller et al., 2014). It also was in agreement with recent finding, where under significant formation of aldehyde such as 9-hexadecanal was detected in the deoxygenated product catalyzed by W-CaO catalyst (Asikin-Mijan et al., 2016d).

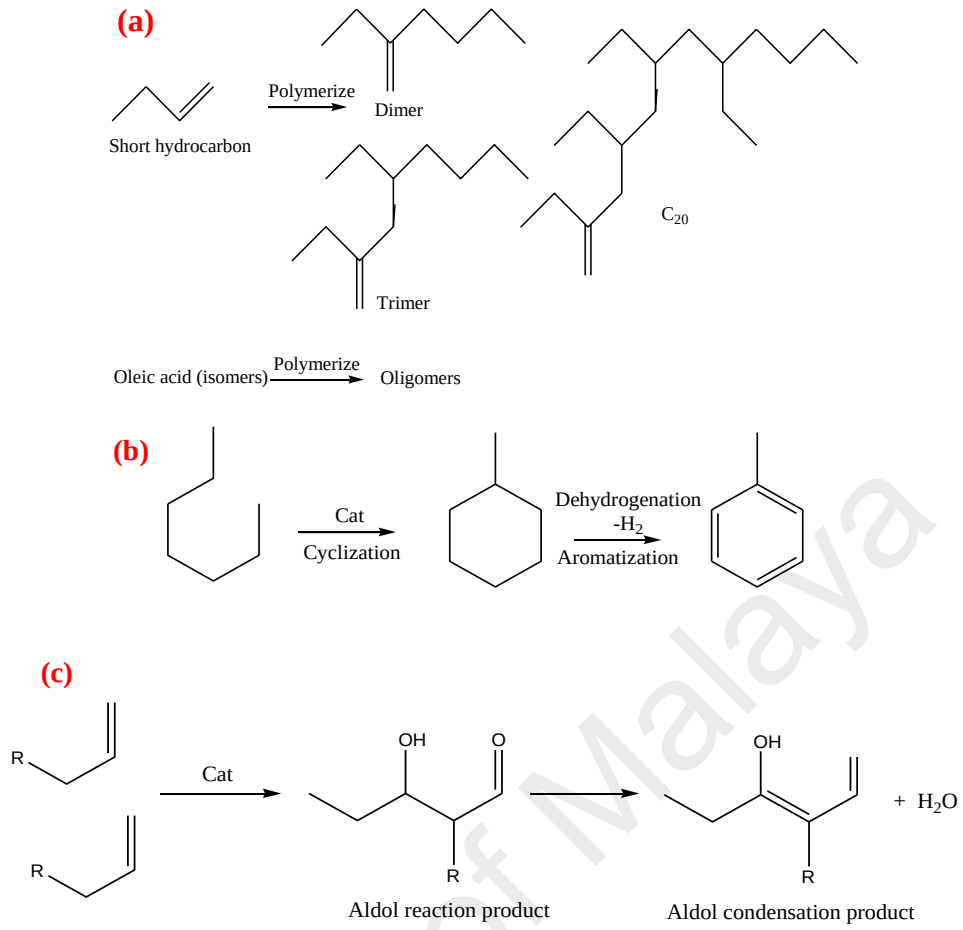

Figure 2.7: (a) Polymerization pathaways (b) cyclization and aromatization pathways. (c) aldol condensation pathway

Ketonization generally occurred in high availability of reactive oxygenates compound. Through ketonization, two carboxylic acids were condensed into a larger ketone with the release of stoichiometric amounts of water and CO_2 (Figure 2.8a). The ketonic decarboxylation could be described as the attack of a carbanion, formed by decarboxylation from a carboxylate, onto a carboxylic group. It had been demonstrated by former studies that made use of traditional strong solid bases such as alkaline earth metal oxides and activated hydrotalcites, which promoted ketonization rather than acid catalyzed deoxygenation (Asikin-Mijan et al., 2016d). This was in agreement with previous reports in upgrading of the bio-oil (Figure 2.8b). The results showed that MgO catalyst is favourable toward ketonization reaction due to the stronger basicity than acidic catalyst such as USY-P, USY-Na-CT0.02 and CS-X catalyst. Additionally,

Parida's group reported high ketonization degree (86.5%) of acetic acid to acetone catalyzed by basic catalyst derived Mg/Al hydrotalcite at 350 ^{o}C (Parida and Das, 2000). Again, pronounce ketonization rate also detected in deoxygenated product catalyzed by strong acid-strong basic catalyst of Co-CaO. The result showed Co-CaO rendered four times higher formation of ketone compound than strong acid-mild basic derived W-CaO catalyst. Thus, from this finding conclude that the ketonization would favored over strong basic sites than milder basic sites catalyst. It can be summarized that in deoxygenation reaction, basic sites promote more formation oxygenates compound than acid sites (Chang et al., 2016). From former finding, it can be suggested that main contributor for the rapid deactivation on the basic sites is due to the strong absorption of the oxygenates compound (Puértolas et al., 2016). Meanwhile, prompted deactivation due to the coke formation was prominent over acid catalyst deoxygenation reaction. Thus, it worth to notice that the occurrence of side reactions in deoxygenation under zero H_2 environment could be suppressed by the utilization of catalyst with co-existence of acid-base sites.

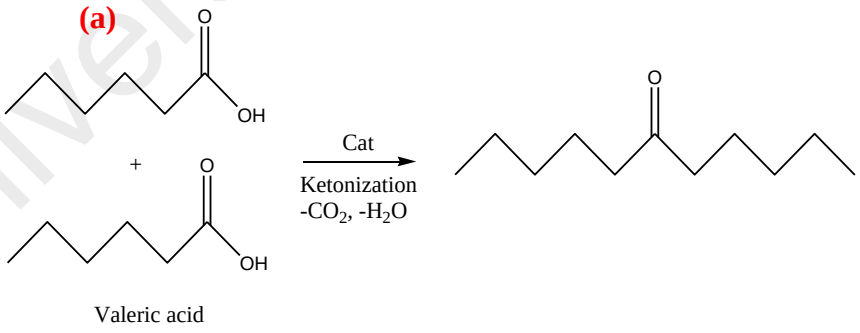

Figure 2.8: (a) Ketonization pathway, (b) product yields in the ketonization of propionic acid at 400 ^{o}C over USY zeolites and traditional base catalysts after 2 h on stream

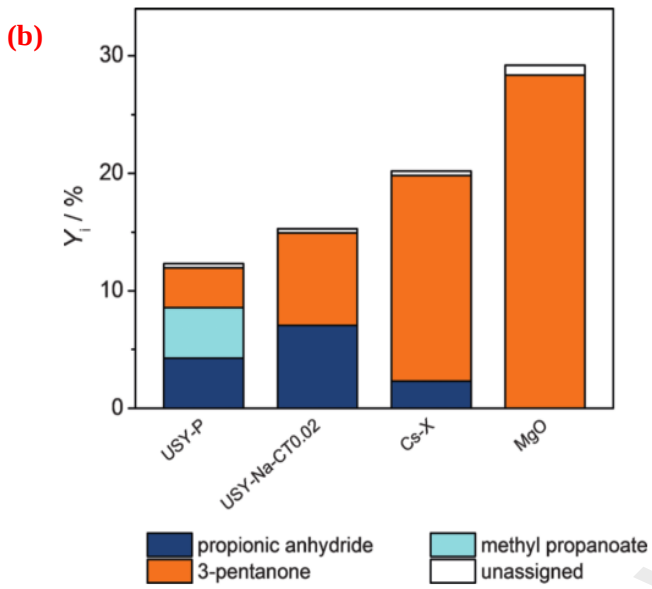

Figure 2.8, continued: (a) Ketonization pathway, (b) product yields in the ketonization of propionic acid at 400 ^{o}C over USY zeolites and traditional base catalysts after 2 h on stream

2.5.5 Factors influencing deactivation of basic and acid catalyst

Deactivation might be temporary or permanent and permanent deactivation needs the replacement of catalyst. Based on numerous studies, all catalyst involved in cracking- deoxygenation reaction would undergo reversible/irreversible deactivation but it depends on the type of catalyst (Arun et al., 2015). Properly designed catalyst would represent minimum deactivation. Typically, formation of irreversible deactivation resulted by formation of coke, which gradually accumulates on the catalyst surface. This carbon will continue to be deposited and leads to the mask or blockage of active sites, simultaneously decreasing the catalyst activity. This was in agreement with Bernas et al., finding on deoxygenation of dodecanoic acid over 1% Pd/Sibunit catalyst under inert environment which had claimed that coking was the most probable reason for catalyst deactivation as the surface area was decreased during the reaction and no leaching or sintering had taken place (Bernas et al., 2010). Formation of coke was known to be strongly related with the chemical properties of the catalyst (acid and base).

Based on recent finding showed that coke deposit would increase when strong acidic catalyst was used (Botas et al., 2014). Since the strong acid catalysed reaction would promote the occurrence of aromatization, polymerization and polycondensation reactions, which lead to the formation of large polyaromatic species (coke precursor). Thus, utilization of strong acid catalyst will enhance the affinity toward coke formation and simultaneously results in blockage of the active sites (Huang et al., 2009;Absi-Halabi et al., 1991;Nagy, 1996). It was in agreement with Guo et al., (2009) finding which investigated on the coke formation during bio-oil processing over strong acid catalyst (HZSM-5) catalyst. The result showed that the catalyst was prone to deactivate due to the initial build-up of high molecular weight compound, primarily having aromatic structures. A similar study was reported by Botas et al. that about 43 wt.% and 22 wt.% of coke deposited from nanocrystalline ZSM-5 zeolite and hierarchical zeolite in deoxygenation of rapeseed oil at 550 ^{o}C for 3 h in a fixed-bed down flow reactor (Botas et al., 2014). According to this research finding, the coke was derived mainly from the polymerization/condensation of aromatic hydrocarbons, which was consistent with the decrease in the yield of aromatic hydrocarbons as the reaction progresses. These compounds were not desorbed from the catalyst due to their low volatility or because they were trapped in interior cavities. It also found that, lewis acid type catalyst also lead to formation of via the presence of oxygenated aromatic compound. It was in agreement with Sooknoi's finding in the catalytic deoxygenation of methyl octanoate over CsNaX catalyst at 425 ^{o}C under He flow and reported that coke deposited was not caused by formation of polynuclear aromatic compound but due to the formation of oxygenated aromatic compounds over the weak acid sites of NaX (Sooknoi et al., 2008).

To date, implementation of high basic catalyst either as a support or active metals in deoxygenation catalyst also result in formation of coke. It was reported by

Zhang et al., (2016b) in deoxygenation of methylglyoxal at 500 ^{o}C which observed an enhancement of coke deposited after basic metal derived MgO incorporated with mild acidic supports (SiO_2-Al_2O_3, sulphated ZrO_2). However, this finding was contradicted with recent finding Asikin-Mijan et al., (2016d) whose found reduction of coke when basicity of the catalyst were increased. Thus, the issue of role basic sites in inhibiting formation of coke still under debate. Based on former studies, high degree coke formation is an inevitable phenomenon, however it can slowed or prevented and some of its consequences can be avoided, if the exact cause of deactivation is known (Rana et al., 2014).

2.5.6 Alternative pathways for coke inhibitor

Apparently, the major contribution for coke formation in deoxygenation under zero-H_2 environment are driven the presence of acid sites on the catalyst which led to formation of coke promoter species (poly-aromatic) and oxygenated aromatic compound. Herein, we discussed an overview on the alternative pathways in reducing the coke formation over acid and or basic catalysed deoxygenation. One of the alternatives is by using solvent such as water, methanol, nonane as sources of H_2. The solvent not only could reduce the coke formation but also might improve the catalytic activity. Zhu et al., showed addition of water was added to anisole feed treated with acid catalyst (HZSM-5) at 400 ^{o}C, the catalytic activity reach increased 2.5 times than reaction without water, which simultaneously suppressed the coke formation. Albeit addition of water can have beneficial effect on catalytic reaction but deoxygenated product with high moisture content should be avoided and some of the study report in the decrease of catalytic activity. It was found by former study, that deactivation of the catalyst could not be overcome by the addition of water and reported by the addition water will cover surface of the catalyst and hence blocked the active sites for further

reactions. Moreover, water content is reported to reduce the dispersion of active metal and also inhibition of intermediate reaction pathways (Arun et al., 2015). Thus, influence of water in supressing the coke formation during deoxygenation activity is still under debate. Meanwhile, Sooknoi's reported in using of methanol and nonane as solvent in deoxygenation of methyl octanoate over CsNaX reported coke formed within the range of 3.5-7.9 wt.% (Sooknoi et al., 2008). It was known utilization of strong acid and mild acidic support catalyst such as TiO_2, SiO_2-Al_2O_3 (Castaño et al., 2007;Regali et al., 2013;Roussel et al., 2005) prone to deactivated easily, thus utilization of neutral support like carbon and SiO_2 are preferable as it showed a low activity toward coke formation (Oi et al., 2016;Kubička et al., 2014). It was revealed by former study in deoxygenation of JCO over carbon-based catalyst (NiCo/MWCNT) which observed insignificant coke formation after reaction, thus giving insignificant effect on the further cycles of deoxygenation reaction activity. This result strongly suggested that NiCo/MWCNT catalyst has showed excellent resistance to coking (Asikin-mijan et al., 2016). Moreover, implementing basic metal with acid catalyst might lower the coke affinity. It was proven by Gómez et al., (2013) that the implementation of Na on zeolite (NaX1.4) resulted in reduction of coke formation. Meanwhile, Danuthai's reported that the increase of Cs lewis base sites from 2% to 20% resulted in reducing the coke formation from 4.4 wt.% to 3.5 wt.% (Danuthai et al., 2011). Similar case was reported by our former study, Asikin-Mijan et al., (2016d) which observe significant reduction of coke deposited from 14 wt.% to 8.2 wt.% when basicity of the Co-CaO were improve by cobalt loading 10% to 40%. However, as mentioned above, this method is still controversial as some of the study found by implementation of basic catalyst also promote the coke formation (Zhang et al., 2016b).

Additionally, lowering the reaction temperature could also reduce the degree of coke. At lower temperature, the dehydrogenation occurred can be subdued. Thus, formation of aromatic compound during deoxygenation reaction via dehydrogenation of hydrocarbon leading to cyclization could be prevented, simultaneously forcing the degree of coke formation to a minimum. In order to reduce high degree coke on early stages of hydrotreating reaction, a progressive heating could be achieved using fixed bed reactor. A progressive heating could also be supplied by microwave energy as the heat source (Lam et al., 2010;Lam et al., 2012). Microwave radiation provides a rapid and energy efficient heating process compared to conventional technologies (Fernández et al., 2010;Fernández et al., 2009). The application of this technology on deoxygenation reaction might fasten the heating process and facilitate a more efficient transfer to the feedstock, thus reducing the formation of undesirable species which was the reason for coke formation.

CHAPTER 3: PYROLYTIC-DEOXYGENATION OF TRIGLYCERIDES VIA NATURAL WASTE SHELL DERIVED $Ca(OH)_2$ NANOCATALYST

This chapter addressed the general objective of objective number 1: To synthesize nano-size Ca-based from clamshell via advanced sonochemical method assisted CTAB and EG surfactants. All the catalysts were further tested in deoxygenation reaction of triolein (vegetable oil model compound). The study is currently under *Journal of analytical and applied pyrolysis* publication with title ***Pyrolytic-deoxygenation of triglycerides via natural waste shell derived $Ca(OH)_2$ nanocatalyst***, volume 117 at pages 46-45. The authors including Asikin-mijan, N, Lee, H.V., Juan, J.C. and Rahman, N.A.

3.1 Introduction

Recently, concern of climate change had triggered the development of economical friendly and sustainable biofuel for the future of energy and fuel production (Shim et al., 2014). Biodiesel had attracted much attention by many researchers (Leung et al., 2010). However, this first generation biofuel energy has several disadvantages. In December 2014, the world's first Boeing flight (ecoDemonstrator 787) using "green diesel" took off, however, it showed that pure biodiesel (B100) was not suitable to be used as aviation fuel as it contained high oxygen content (less stable), which could cause serious damage to the engine plug, filter, and corrosion to the metal parts in long term operation (Karp, 2014;Vyas et al., 2010;Roh et al., 2011). Other incompatibility included poor storability, immiscibility with gasoline (Zhang et al., 2013), high cloud point and other engine compatibility issues. Hence, reduction of of oxygenated compound is a key factor in improving fuel stability. Numerous technologies for hydrocarbon biofuel production have been developed such as hydrodeoxygenation

(Kleinert et al., 2009;Srifa et al., 2014;Mu et al., 2014) and deoxygenation process (Snåre et al., 2008;Meller et al., 2014;Shi et al., 2014). Hydrodeoxygenation (HDO) is a hydrogenolysis reaction to remove oxygen from oxygenated compounds (ester and carbonyl groups) with the presence of H_2 gas and resulting in by-product (H_2O) formation. In contrast to the hydrodeoxygenation process, deoxygenation (DO) reaction involved the removal of oxygen via cracking-decarboxylation pathway by release of CO and CO_2 gaseous without H_2 consumption (Prado and Antoniosi Filho, 2009). Even though hydrodeoxygenation process is the most efficient method for high quality liquid hydrocarbon production. However, the inflated production cost due to hydrogen consumption is a sustainability issue. Therefore, many researchers focused on deoxygenation technique which requires no hydrogen gas.

Selective catalytic deoxygenation of triglyceride via base-catalyze cracking-decarboxylation mechanism has been an active area of recent research in order to reduce the production cost. The CaO and $Ca(OH)_2$ are highly basic catalyst that generally used many type of reactions. Nevertheless, there is no literature report pertaining nano-sizes of $Ca(OH)_2$ derived from waste shell for hydrocarbon biofuel production. Thus, in the present study, we have investigated the feasibility of nano-$Ca(OH)_2$ derived from waste clamshell (*Meretrix meretrix* sp.) for deoxygenation of triglyceride via decarboxylation and decarbonylation (deCOx) mechanism. Waste clamshell-derived $Ca(OH)_2$ nanoparticles was prepared by using sonochemical assisted wet surfactant treatment, where different type of surfactant (ionic and non-ionic surfactant) was tested. The physiochemical properties of prepared catalysts were characterized by using XRF, XRD, BET, TPD-CO_2, SEM and TEM analysis. Furthermore, the effect of deoxygenation efficiency from $Ca(OH)_2$ nanoparticles catalyzed reaction was investigated. The final deoxygenized liquid product was analyzed by using FTIR and

GC–MS for chemical composition study. Besides, CHNOS analysis was used to determine the oxygen composition in final deoxygenized liquid product.

3.2 Literature Review

According to literature study, heterogeneous basic catalysts can be employed for the production of liquid hydrocarbon fuel by means of deoxygenation of low quality biomass feedstock oil (oxygenated oil). Gómez et al., (2013) showed that the catalytic deoxygenation of methyl octanoate has successfully conducted with high activity (85%) and selectivity to the desired hydrocarbon products (80%) in the presence of high basic strength of K-zeolite and Cs-zeolite catalysts. Besides, it was found that MgO–supported catalyst promoted the decarboxyl-cracking of palm oil and other triglyceride to make middle-distillate range hydrocarbons (mixture of olefins and paraffin) at 430 ^{o}C. The basicity of supported MgO is capable to reduce the acid value and iodine value, which is suitable to be used for the diesel engine (Tani et al., 2011). Ding's research group (2009) has successfully converted organic acid (napthenic acid), which are naturally occurring compounds in petroleum into hydrocarbon chain products by using CaO catalyst. With the presence of CaO, multiple pathways (catalytic decarboxylation, neutralization, and thermal cracking) were responsible for the napthenic acid (NA) conversion (Ding et al., 2009). Furthermore, Lin et al. claimed that CaO catalyst could absorb more CO_2 either in gas phase or liquid phase, which simultaneously remove the oxygen molecule via decarboxylation/decarbonylation (deCOx) mechanism (Lin et al., 2010). Therefore, CaO is a potential catalyst for catalytic deoxygenation reaction. Equation below showed CaO catalysed deoxygenation of acid compound (Mu et al., 2014):

$$R - COOH \rightarrow RH + CO_2 \quad (3.1)$$

$$R - COOH + R' - COR' + CO_2 + H_2O \quad (3.2)$$

Several studies had reported that calcium hydroxide ($Ca(OH)_2$) is capable of rendering better reactivity and product selectivity compared to CaO catalyst (Yoosuk et al., 2011;Yoosuk et al., 2010). It is due to the presence of enhanced superior properties such as basicity and textural properties (surface area, pore volume, pore diameter) of $Ca(OH)_2$ especially in nanoparticles sizes (Asikin-Mijan et al., 2015c;Asikin-Mijan et al., 2015b). $Ca(OH)_2$ can be derived from waste natural shell, which is the common sources of calcium carbonate (Viriya-empikul et al., 2010). The waste shell can be easily converted into $Ca(OH)_2$ phases by using water hydroxylation treatment. Natural waste shell derived $Ca(OH)_2$ can be considered as a low cost green solid base catalyst which was enhanced for deoxygenation reaction.

3.3 Material and methods

3.3.1 Material

Washed natural waste clamshell (*Meretrix meretrix* sp.) was used as described in (Asikin-Mijan et al., 2015c). Triolein was obtained from Sigma Aldrich. Ethylene glycol (99.8%, Merck) and N-Cetyl-N,N,N-trimethylammonium bromide (98%, R&M chemical) was used as surfactant. Commercial $Ca(OH)_2$ nano-powder (>99.8%, Sigma Aldrich), and commerical CaO powder (99.9%, R&M chemical) was used for comparison study. Gas Chromatography (GC) grade *n*-Hexane for GC–MS analysis with purity > 98% was purchased from Merck.

3.3.2 Catalyst synthesis

Waste clamshell powder (~300 μ) was thermally activated at 800 ^{o}C for 2 h under atmosphere conditions and denoted as CaO. Clamshell-derived CaO was then underwent sonochemical assisted wet surfactant treatment, where the combusted clamshell was added into ethylene glycol (EG) solution (1 M) and N-Cetyl-N,N,N-

trimethylammonium bromide (CTAB) solution (1 M), respectively under 60 Hz to achieve uniform size of nanoparticles followed by aging for 5 h in room temperature. The medium was filtered with PTFE membrane filters and washed with mixture of distilled water and ethanol (1:1 ratio) for several times (1000 ml of solution) before it was dried in the oven overnight at 100 ^{o}C. Lastly, the precursors were calcined at 400 ^{o}C for 2 h for final catalyst activation. The calcined samples that treated with EG, CTAB and water are denoted as as $Ca(OH)_2$–EG, $Ca(OH)_2$–CTAB and $Ca(OH)_2$–H_2O, respectively.

3.3.3 Catalyst characterization

Elemental analysis of the samples was analyzed by using X-ray fluorescence (XRF) spectrometry (Philips PWI404) equipped with a scandium anode tube. The crystalline phases of calcined samples were analyzed by X-ray diffractometer (Shimadzu diffractometer model XRD-6000). The surface area and pore volume of the samples were determined by Brunauer–Emmet–Teller (BET) model by using Thermo–Finnigan Sorpmatic 1990 series. The samples were degassed overnight at 150 ^{o}C in vacuum. The chemical properties of catalysts was evaluated using temperature programme desorption CO_2 (Thermo Finnigan TPD/R/O 1100) equipped with a thermal conductivity detector (TCD). Approximately, 0.05 g of catalyst was treated under N_2 gas flow for 30 min at 250 ^{o}C. Then, the catalyst was exposed to CO_2 gas for 60 min at ambient temperature to allow adsorption of CO_2 on the surfaces. The excess of CO_2 were subsequently flushed out by flowing N_2 gas prior to the analysis. Desorption of the CO_2 from the basic sites of the catalyst were identified by TCD under helium gas (30 ml/min) ranging from 50 ^{o}C to 900 ^{o}C. Morphological and particle size of the catalyst was investigated by scanning electron microscopy (SEM) (SEM JOEL 6400) and

transmission electron microscopy (TEM) (Hitachi H-7100 TEM) with accelerating voltage of 10 mV.

3.3.4 Catalytic cracking-deoxygenation of triolein

The deoxygenation reaction of triolein were carried out at temperature of 350 ºC under partial vacuum condition (10 mbar) for 30 min (Botas et al., 2012). Approximately 10 g of triolein and clamshell derived catalyst (5 wt.%) was added into 250 ml of batch reactor equipped with distillation and vacuum system (Figure 3.1). Cold water flow in distillation system was used to promote condensation of deoxygenized species into liquid form. The fractions of deoxygenated product was further analysed by using FTIR, GC–MS and CHNOS analyser. All the reaction was repeated for three times in order to achieve precise and accurate readings.

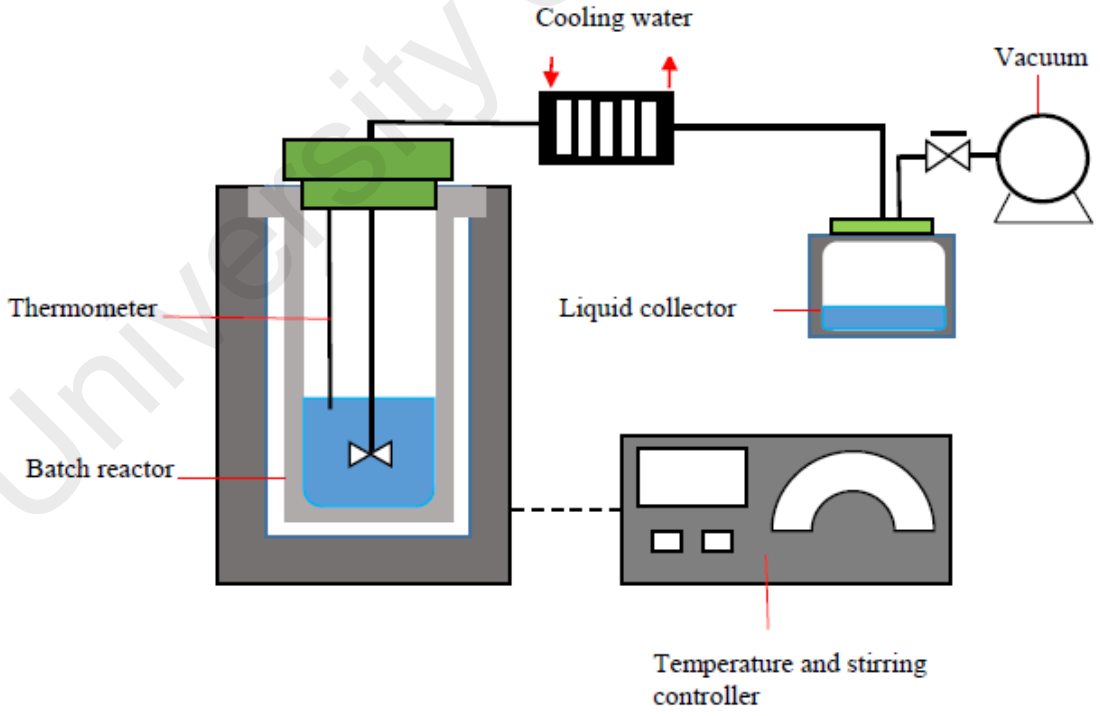

Figure 3.1: Schematic diagram of deoxygenation system for cracking-deCOx process

3.3.5 Analysis of deoxygenized products

FTIR analysis was performed using Perkin-Elmer Spectrum (PS)100 FT–IR spectrometer with resolution of 4 cm^{-1} operating in the range of 300-4000 cm^{-1}. This analysis helps to determine the chemical functional group of the liquid product. The distribution of deoxygenized products were further qualitatively and quantitatively determined using GC–MS (SHIMADZU QP2010) equipped with non-polar BPX-5 column (12 m × 0.53 mm I.D µm film thickness) in split mode. The fraction peaks obtained from mass spectra were identified using the National Institute of Standards and Testing (NIST) library. Furthermore, catalytic activity of different catalysts towards deoxygenation (Total product yield and product selectivity) was determined by comparing the peak area % of obtained spectra. It is known that the GC–MS analysis does not provide exact quantitative analytic result of compounds. However, it is possible to compare the product yield and product selectivity by comparing the peak areas as the chromatographic peak area of compounds is proportional to its quantity and the relative content of the product (Eq. (3.3) and Eq. (3.4) (Lu et al., 2010;Jeon et al., 2012;Romero et al., 2014). In order to confirm the reproducibility of the results, the experiments were conducted for three times, with the average of the peak area and peak area % was calculated. Besides, degree of oxygen to carbon molar ratio and degree of hydrogen to carbon molar ratio are shown in Eq. 3.5 and Eq. (3.6) (Duan et al., 2013), respectively.

$$Product\ Yield\ (\%) = \frac{Area\ of\ C_{6-}\ C_{24}}{Total\ area\ of\ the\ product} \times 100 \tag{3.3}$$

$$Product\ Selectivity\ (\%) = \frac{Area\ of\ the\ desired\ product}{Total\ area\ of\ the\ product} \times 100\ \% \tag{3.4}$$

Degree of oxygen to carbon molar ratio:

$$Oxygen\ to\ carbon\ \left(\frac{O}{C}\right) = \frac{Oxygen\ content}{Carbon\ content} \tag{3.5}$$

Degree of hydrogen to carbon molar ratio:

$$Hydrogen\ to\ carbon\ \left(\frac{H}{C}\right) = \frac{Hydrogen\ content}{Carbon\ content} \tag{3.6}$$

3.4 Results and discussion

3.4.1 X-ray fluorescence (XRF)

The elemental compositions of the clamshell, combusted clamshell and surfactant treated products are shown in Figure 3.2. CaO derived from waste clamshell showed high calcium content (98.81%), which indicated that the clamshell is a potential calcium resource for CaO catalyst preparation. The Ca content for surfactant treated samples $Ca(OH)_2$–EG, $Ca(OH)_2$–CTAB, and $Ca(OH)_2$–H_2O are maintained after calcined at 400 ^oC. This implies that the sonochemical method coupled with surfactant did not digest the calcium species from clamshell. It is also clear that there is no interfacial reaction occurred between the calcium species and surfactant during ultrasonication process, which could drastically change the composition of treated samples.

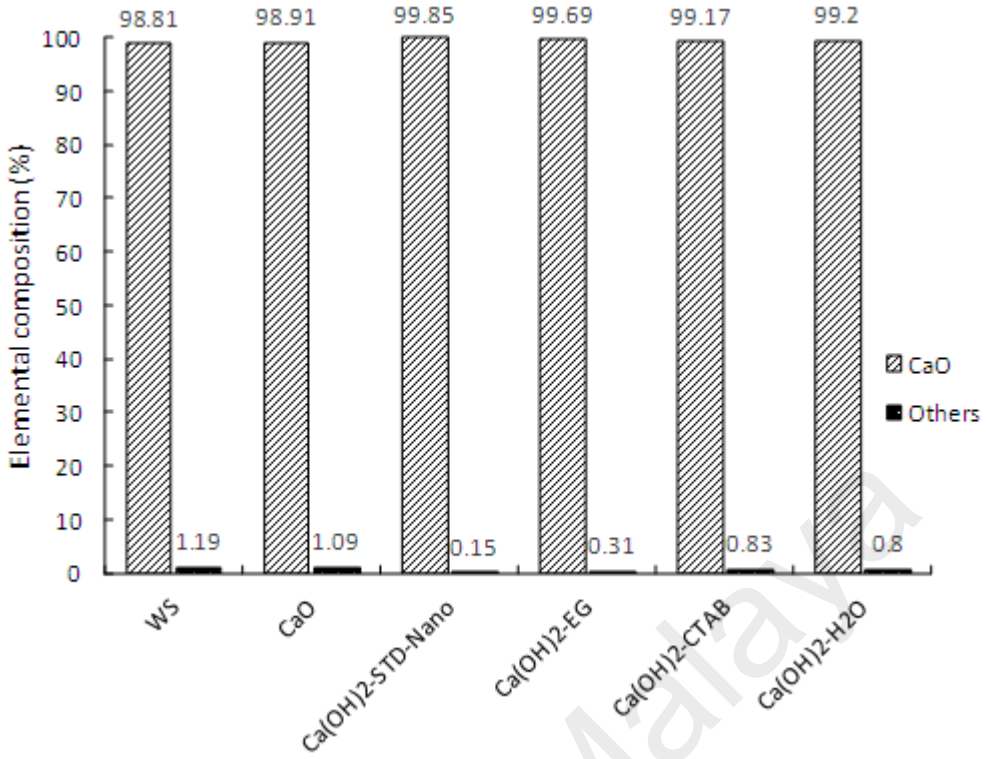

Figure 3.2: Elemental composition of fresh clamshell, CaO, $Ca(OH)_2$-STD-Nano, $Ca(OH)_2$-EG, $Ca(OH)_2$-CTAB and $Ca(OH)_2$-H_2O

3.4.2 X-ray diffraction (XRD)

Figure 3.3 shows the typical calcium carbonate ($CaCO_3$) phases at 2θ = 26.2º, 29.5º, 33.1º, 45.8º and 48.3º (JCPDS card No. 00-001-1033) from waste clamshell. The carbonate phases were successfully converted to oxide phases at temperature of 900 ºC as reported in previous study (Asikin-Mijan et al., 2015c). Minor peak of $CaCO_3$ at 29.4º were observed in all $Ca(OH)_2$ samples indicated the adsorption of CO_2 gas from the atmosphere to the active sites of catalyst. The ultrasonic wet surfactant treated samples ($Ca(OH)_2$–EG, $Ca(OH)_2$–CTAB) and non-surfactant treated $Ca(OH)_2$–H_2O exhibited $Ca(OH)_2$ phases at 2θ = 18.14º, 28.7º, 34.2º, and 50.8º (Portlandite, JCPDS card no. 00-002-0968), which indicated the hydroxylation reaction occurred in between water and CaO phases and showed that $Ca(OH)_2$ catalysts was successfully synthesized from clamshell materials. From the XRD patterns, it was observed that the crystallinity of nano-$Ca(OH)_2$ treated with ethylene glycol (EG) was lower compared to CTAB and water treated catalyst. This demonstrated that wet sonochemical with non-ionic

surfactant of ethylene glycol has the tendency to reduce the growth of crystallite size compared to cationic surfactant (CTAB). The EG surfactant was efficiently coated on the surface of $Ca(OH)_2$ particles and thus prevented aggregation during calcination (Jacob et al., 2007;Nam et al., 2011). Furthermore, the presence of ultrasonic effect has further enhanced the dispersibility between sample's particles and surfactant.

Crystallite size profile of clamshell derived CaO and $Ca(OH)_2$ with different wet surfactant treatment are shown in Table 3.1. The treated catalysts rendered significant reduction of crystallite sizes compared to clamshell derived CaO, which reduces in the order of $Ca(OH)_2$–EG < $Ca(OH)_2$–CTAB < $Ca(OH)_2$–H_2O. This implied thatsonochemical method coupled with surfactant and wet-sonication treatment has efficiently controlled the crystallite size of $Ca(OH)_2$.

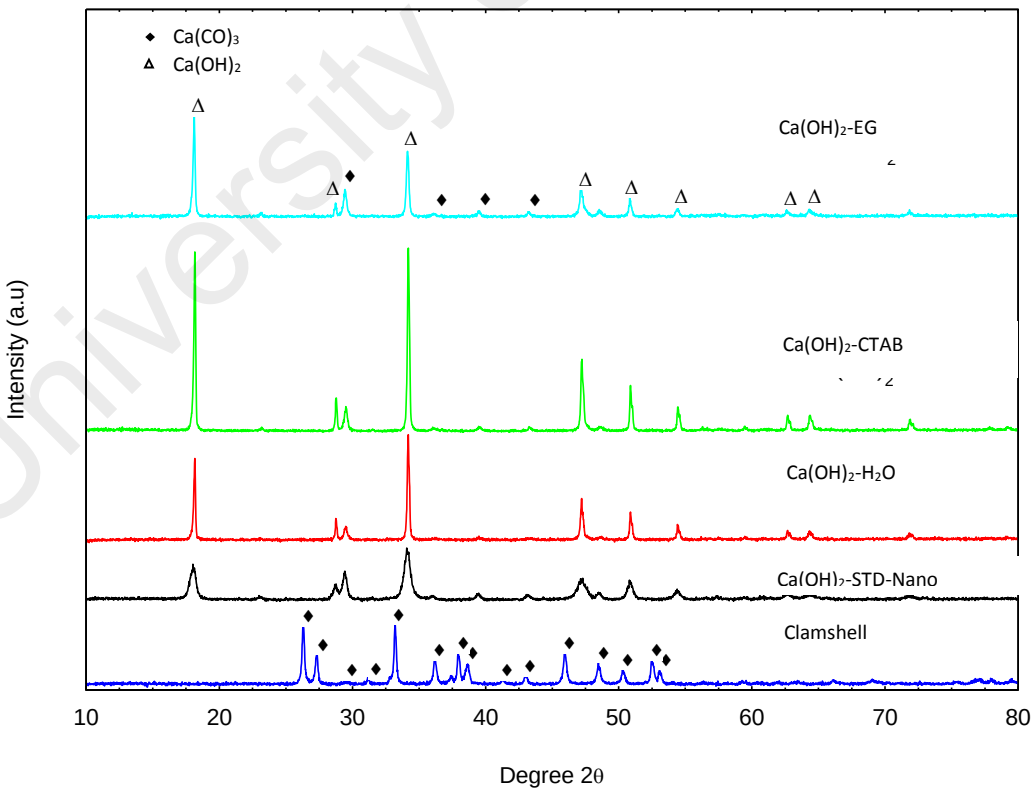

Figure 3.3: XRD analysis for clamshell, CaO, $Ca(OH)_2$-STD-Nano, $Ca(OH)_2$-EG, $Ca(OH)_2$-CTAB and $Ca(OH)_2$-H_2O

Table 3.1 Crystallite sizes and textural properties profile of CaO, $Ca(OH)_2$-STD-Nano, $Ca(OH)_2$-H_2O, $Ca(OH)_2$-EG, $Ca(OH)_2$-CTAB

Catalyst	[a]Crystallite size (nm)	[b]Surface area (m^2/g)	[b]Pore size diameter range (nm)
CaO	68.2	11	0.2
$Ca(OH)_2$-STD-Nano	17.3	84	0.3
$Ca(OH)_2$-H_2O	47.8	80	18.4
$Ca(OH)_2$-EG	39.6	130	18.3
$Ca(OH)_2$-CTAB	57.2	124	18.6

[a]Measured by using Scherer equation from XRD data (repeated twice)
[b] Determined by BET analysis (repeated twice)

3.4.3 Brunauer–Emmet–Teller surface area measurement (BET)

Table 3.1 shows the BET surface area of CaO (10.90 m^2g^{-1}) was drastically increased up to 130 m^2g^{-1}, 124 m^2g^{-1} and 80 m^2g^{-1} for $Ca(OH)_2$-EG, $Ca(OH)_2$-CTAB and $Ca(OH)_2$-H_2O, respectively, after being treated with surfactant-sonochemical process. The integration of surfactants (EG or CTAB) coupled with wet-sonochemical method was capable of increasing the surface area of $Ca(OH)_2$ by 55–62%. Furthermore, the presence of ultrasonic effectively dispersed the large aggregates of $Ca(OH)_2$, while adding of surfactant has avoided the formation of big aggregates during drying and calcination process. The collapse of the cavitational bubbles generated during sonication has led to the pitting and erosion on the newly formed of $Ca(OH)_2$ catalyst surface (Javidan et al., 2014) and thus high porosity was formed on the catalyst.

3.4.4 Temperature programme desorption-carbon dioxide (TPD–CO_2)

The basicity profile of catalysts was investigated by using TPD–CO_2 analysis (Figure 3.4 and Table 3.2). The basic strength distribution from catalyst's active sites is expressed in terms of CO_2 desorption temperature. The TPD–CO_2 desorption patterns (Figure 3.4) showed different desorption peaks at different temperature, where CO_2 desorption at 100–500 ^oC assigned as interaction of CO_2 with sites of weak and medium basic strengths (Lee et al., 2014). Whereas, the CO_2 desorbed at temperature of ~600 ^oC can be attributed an involvement of the stronger basic sites (National Biodiesel Board

(NBB), 2009;Lee et al., 2013). Based on the results, the sonochemically assisted surfactant treated catalysts exhibit stronger of basic strength and higher amount of basicity than the waste shell derived CaO and standard nano-$Ca(OH)_2$. The trend of the basicity was as follow $Ca(OH)_2$–CTAB > $Ca(OH)_2$–EG > $Ca(OH)_2$–STD-Nano > $Ca(OH)_2$–H_2O > CaO. The increased basicity of treated catalysts was due to the presence of Lewis and ßronsted basic sites after going through the hydration-dehydration pathway. Furthermore, the presence of high surface area of basic active sites has indicated the increment of active basic sites of treated catalysts.

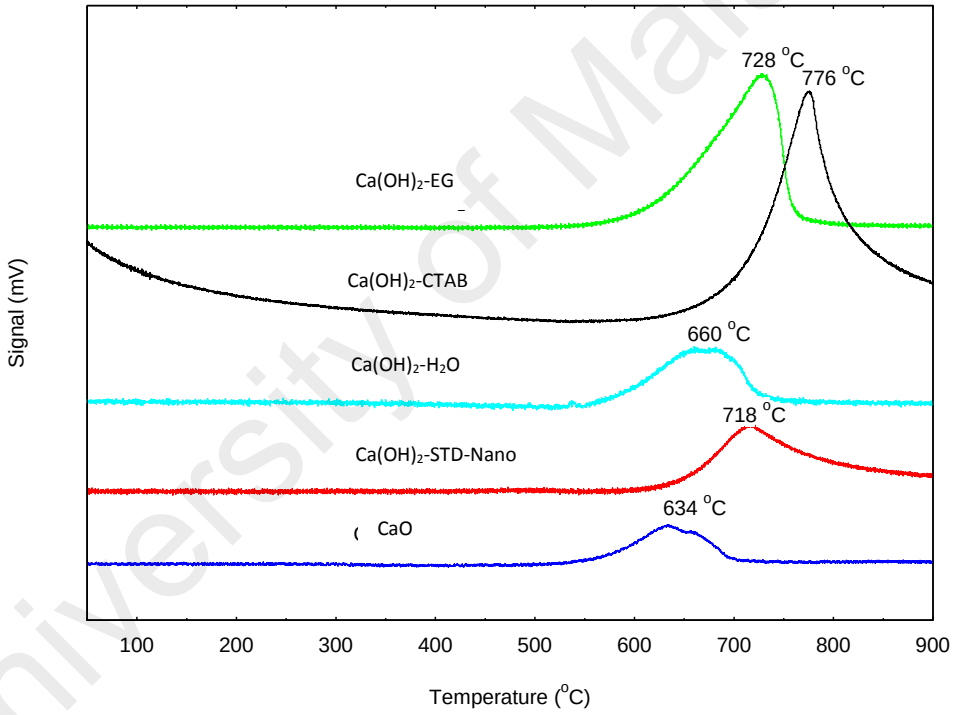

Figure 3.4: TPD-CO_2 analysis for CaO, $Ca(OH)_2$-STD-Nano, $Ca(OH)_2$-EG, $Ca(OH)_2$-CTAB and $Ca(OH)_2$-H_2O

Table 3.2: Temperature programme-carbon dioxide (TPD–CO_2) profile of catalysts

Catalyst	CO_2 desorption temperature (°C)	Amount of CO_2 desorbed (µmol/g)
CaO	634	554.87
$Ca(OH)_2$-STD-Nano	718	3335.82
$Ca(OH)_2$-H_2O	660	1133.41
$Ca(OH)_2$-EG	728	4658.77
$Ca(OH)_2$-CTAB	776	7556.38

3.4.5 Scanning electron microscopy (SEM)

SEM images for all catalysts are shown in Figure 3.5. The surface morphology and the microstructure of the starting material, CaO derived from clamshell, $Ca(OH)_2$–STD–Nano, treated surfactant catalysts ($Ca(OH)_2$–EG, $Ca(OH)_2$–CTAB) and water treated sample ($Ca(OH)_2$–H_2O) was found to be varied. CaO (Figure 3.5a) rendered large and irregular shape of particles compared to standard nano-$Ca(OH)_2$ (Figure 3.5b) and treated catalysts (Figures 3.5c and d). SEM images showed that the structure and particle shapes were different based on the nature of surfactant used. EG treated catalyst showed the presence of rod crystal particles while CTAB treated catalyst has round crystal structures. Furthermore, it is significantly observed that the particle sizes of treated catalysts were significantly smaller compared to catalyst without treatment.

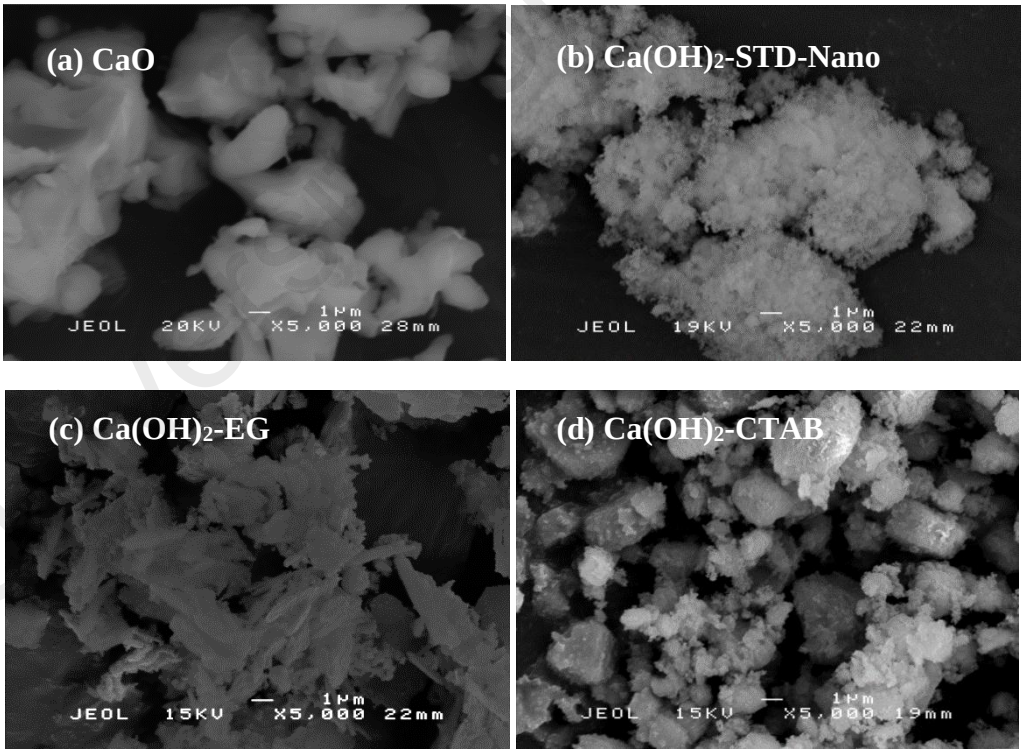

Figure 3.5: SEM images of (a) CaO, (b) $Ca(OH)_2$-STD-Nano, (c) CS-$Ca(OH)_2$-EG, (d) $Ca(OH)_2$-CTAB and (e) $Ca(OH)_2$-H_2O

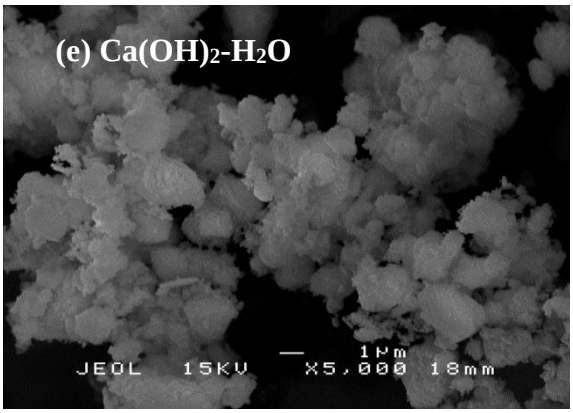

Figure 3.5, continued: SEM images of (a) CaO, (b) $Ca(OH)_2$-STD-Nano, (c) CS-$Ca(OH)_2$-EG, (d) $Ca(OH)_2$-CTAB and (e) $Ca(OH)_2$-H_2O

3.4.6 Transmission electron microscopy (TEM)

TEM images showed that initial shape of waste shell-derived CaO appeared in irregular aggregates forms had changed to cubic-like nanostructures after being treated with surfactants in the presence of sonication effect (Figure 3.6). Results showed that the treated catalysts ($Ca(OH)_2$–EG and $Ca(OH)_2$–CTAB) rendered comparable of particle sizes to standard nano–$Ca(OH)_2$. It was anticipated that the treated nano-catalysts with high textural properties and highly amount of active sites are capable of performing more efficiently in cracking-decarboxylation reaction.

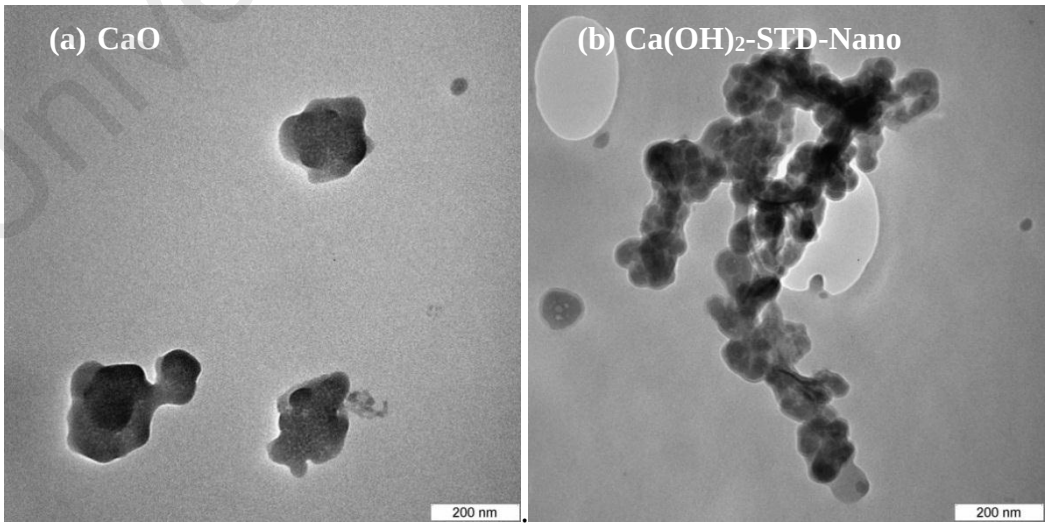

Figure 3.6: TEM images of (a) CaO and (b) $Ca(OH)_2$-STD-Nano, (c) $Ca(OH)_2$-EG (d) $Ca(OH)_2$-CTAB and (e) $Ca(OH)_2$-H_2O

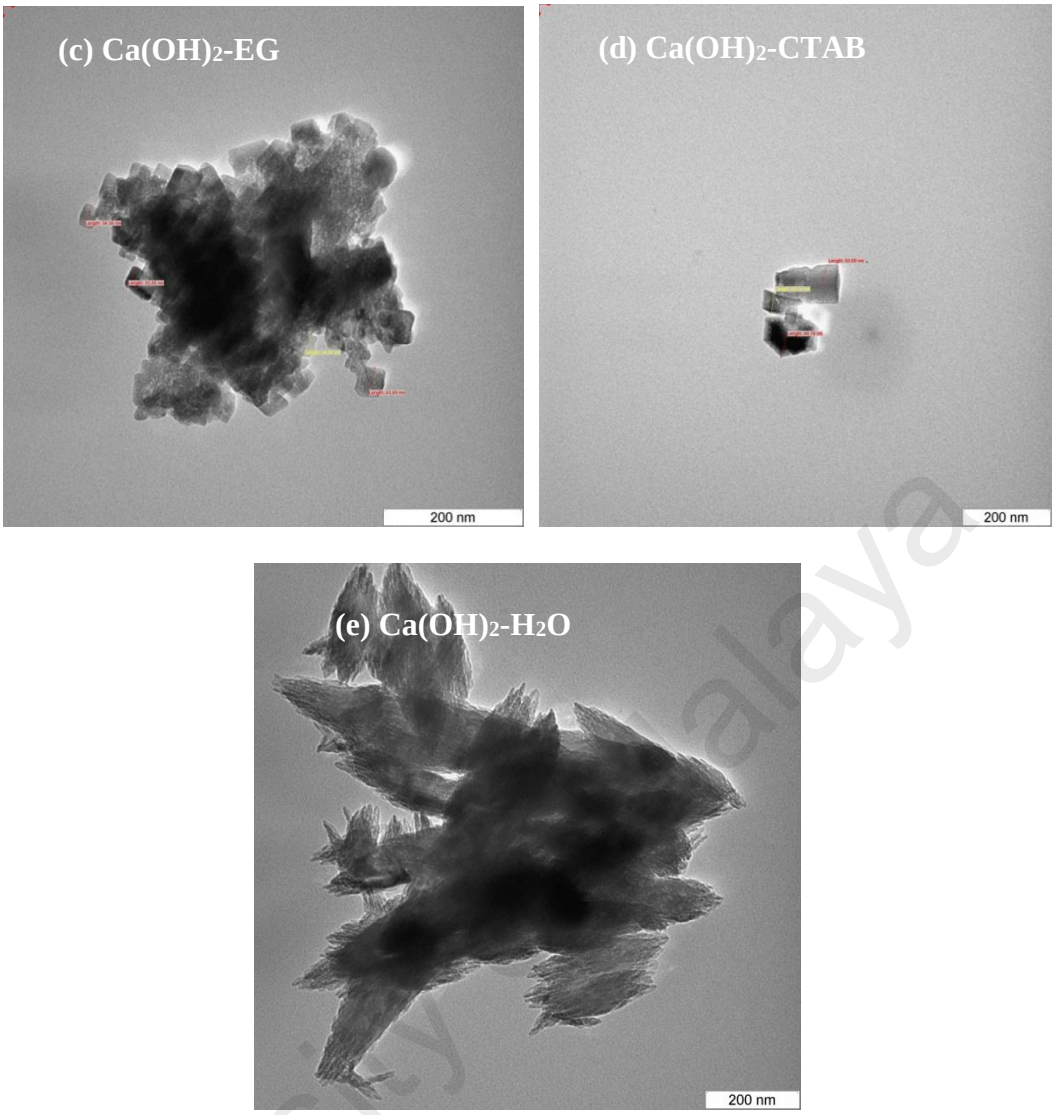

Figure 3.6, continued: TEM images of (a) CaO and (b) $Ca(OH)_2$-STD-Nano, (c) $Ca(OH)_2$-EG (d) $Ca(OH)_2$-CTAB and (e) $Ca(OH)_2$-H_2O

3.5 Catalytic activity study

3.5.1 Chemical composition profile of deoxygenized product

FTIR analysis was performed in order to study the chemical functional group exhibited in deoxygenized product (Figure 3.7). The FTIR spectra for triolein showed three main absorption band at 2950, 1741 and 1150 cm^{-1}, which attributed to stretching absorption of the C-H bond attached to the cis-carbon atom in the oleic acid moieties, absorption of glyceride carbonyl group (-C-O) and C-O-C group from ester bond, respectively. Results showed that reacted products rendered a new peak at ~2919 cm^{-1},

which indicated merging of two -CH_2 absorption bands of triolein. This resulted in shifting of -CH_2 (symmetrical stretching) in triolein into -CH_2 of asymmetrical stretching. Furthermore, slight shift of FTIR peaks (~1710 cm^{-1}) of deoxygenized product has indicated –C-O of carboxylic acid group (Salimon et al., 2011). Similar case occurred at absorption bands of -CH_2 (~1455 cm^{-1}) and -CH_3 (~1372 cm^{-1}) from triolein, where a new peak was appeared at 1448 cm^{-1} (-CH_2 bending in aliphatic) after deoxygenation reaction. This was in agreement with the formation of C-C bond of alkyl chain in hydrocarbon compounds that observed at 1265–1281 cm^{-1}, which agreed to the occurrence of deoxygenation reaction.

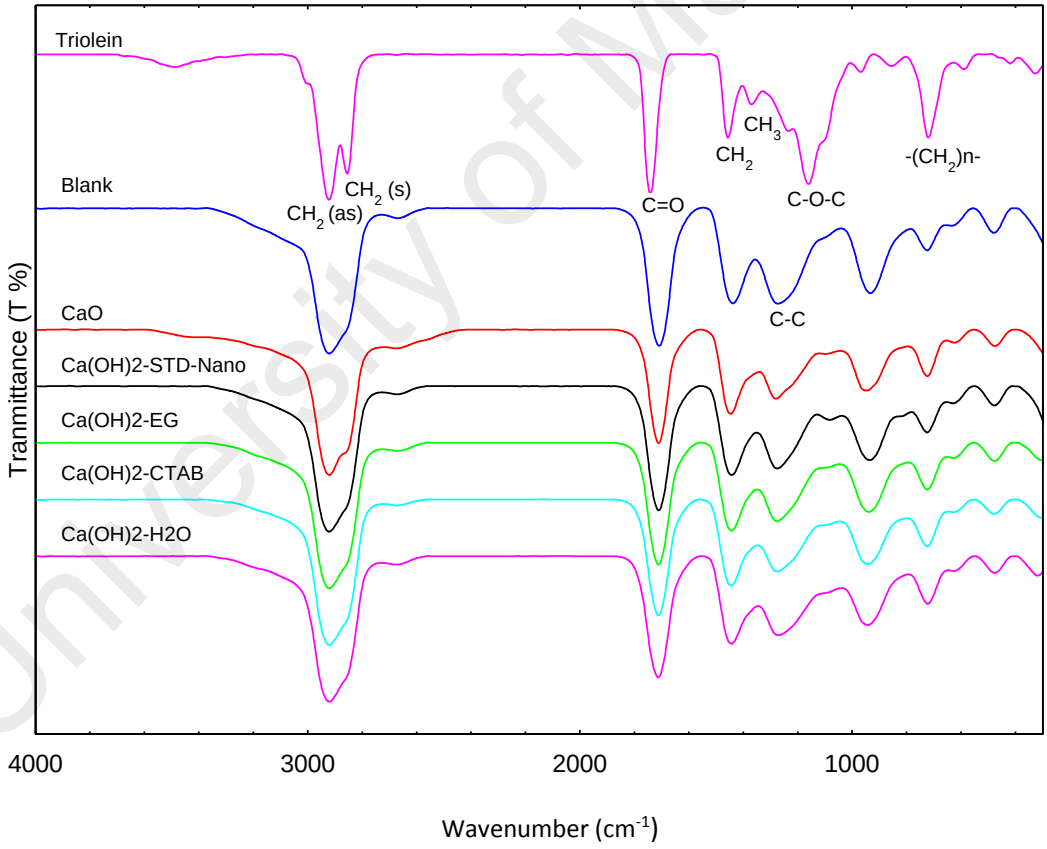

Figure 3.7: FTIR results for triolein and deoxygenated products

3.5.2 Oxygen removal rate

Elemental analysis for oxygen, carbon and hydrogen content of deoxygenized product was determined via CHNOS analyser. The results were depicted in terms of H/C and O/C ratio in Krevelen diagram (Figure 3.8). The H/C and O/C ratio of triolein was 0.1801 and 0.3139, respectively, which consisted highest amount of oxygen content. Interestingly, all the products from deoxygenation reaction rendered reduction of O/C ratio, which indicated oxygen compounds were removed via deCOx process. Although deoxygenized product from blank experiment (without catalyst) showed reduction of oxygen content, however the reaction prone to high cracking effect that caused the formation of shorter carbon chain compounds with low saturated chain (H/C ratio = 0.159). Similar case with CaO catalysed deoxygenation reaction, where low H/C ratio (0.157) resulted in undesired light hydrocarbon products. Alternatively, the treated catalysts ($Ca(OH)_2$–EG and $Ca(OH)_2$–CTAB) and standard nano-$Ca(OH)_2$ rendered decrement in oxygen content, while maintained H/C ratio as triolein. In the absence of H_2 condition, oxygen tends to be removed in the form of CO_2 or CO gases without addition of hydrogen atom, which might yield most of alkene compounds. This is in agreement with Lin's research study where the oxygen content significantly decreased in the presence of Ca-based catalyst. Moreover, Ca-based catalyst are capable of absorbing CO_2 efficiently from the feeds and enhancing the oxygen removal (Lin et al., 2010). Kim's group reported that the presence of H_2 gas in hydrodeoxygenation process would reduce unsaturated bond of alkene compounds into alkanes products, and thus increase the hydrogen content (H/C) of final product (Kim et al., 2013b).

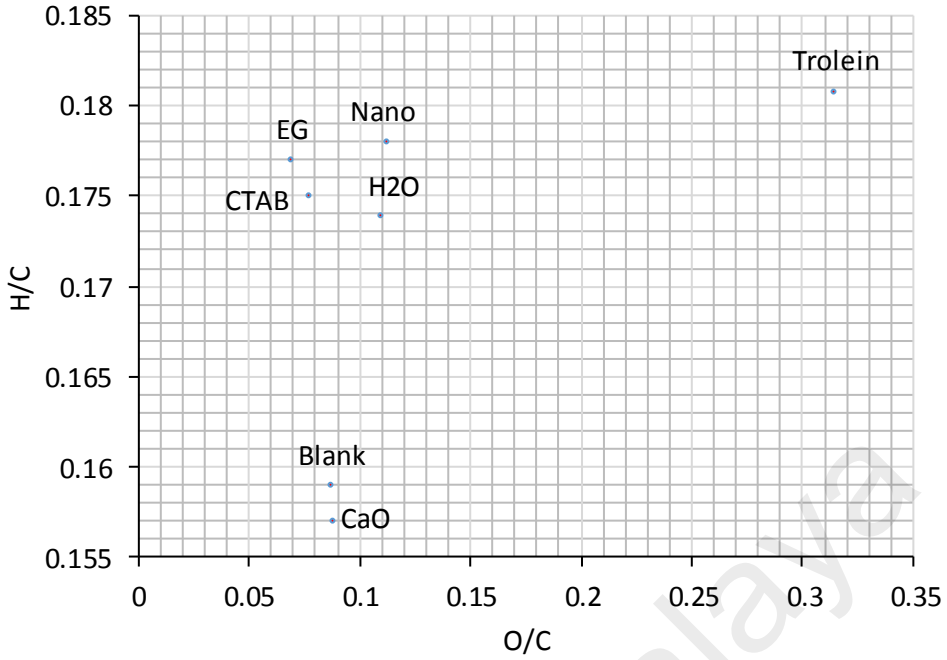

Figure 3.8: H/C and O/C ratio for deoxygenized liquid product (Van Krevelen diagram)

3.5.3 Chemical composition study of deoxygenized liquid

The degree of selectivity for each catalyst toward n-alkane and n-alkene obtained from the deoxygenation reaction was determined by using GC–MS analysis. Table 3.3 showed the total composition of *n*-alkane and *n*-alkene products, which mainly focus on the hydrocarbon chain length from C_6–C_{24}. Based on the results, it was indicated that the produced liquid was mostly in alkene form rather than alkane. Under hydrogen-deficiency atmosphere, the reaction tends to remove the oxygen content via cracking (the C-C bond scission), decarboxylation (CO_2), decarbonylation (CO) and also dehydration (H_2O), which shall then lead to rearrangement of molecular compounds to a more stable alkenes form (Snåre et al., 2008). Results showed that catalyst-free product (blank experiment) rendered considerable amount *n*-alkanes (12.51%) and *n*-alkenes (28.45%) of C_6-C_{16} range. This shows that blank reaction system possess high cracking reaction but low tendency to undergo deCOx reaction due to the low formation of C_{17} both saturated and unsaturated compounds (Kim et al., 2013b). In contrast, Ca-based catalysts (CaO, standard nano-$Ca(OH)_2$ and surfactant-

treated $Ca(OH)_2$) gave significant formation of saturated C_{17} and unsaturated C_{17} hydrocarbon chain. The *n*-C_{17} selectivity was followed the order of $Ca(OH)_2$–CTAB ≈ $Ca(OH)_2$- EG > $Ca(OH)_2$-H_2O > CaO > $Ca(OH)_2$-STD-nano > free-catalyst reaction. Surfactant treated $Ca(OH)_2$ nano-catalyst is prone to decarboyxlation/decarbonylation and rendered the highest selectivity due to the presence of larger amount of surface area with large porosity, which provided a bigger sites for large molecular triolein to react. Furthermore, higher basicity of active sites from surfactant-treated $Ca(OH)_2$ has made the absorption of the released of CO_2 gas during deoxygenation reaction more effective and hence avoided the formation of by-product (coke). In additional, the superior properties of surfactant treated catalysts ($Ca(OH)_2$–CTAB and $Ca(OH)_2$–EG) have higher reactivity with higher yield of deoxygenated product (liquid hydrocarbon C_6–C_{24}), 47.37% and 44.50%, respectively as compared to other catalysts.

The relative activities indicator for deCOx reactions were determined by calculating the ratio of *n*-alkanes ($C_{oddnumber}$) to *n*-alkanes ($C_{evennumber}$) of the deoxygenized product. As triolein composed mainly of C_{18} fatty acid, thus the ratio used for calculation was *n*-C_{17}/(*n*-C_{17} + *n*-C_{18}). Based on the results, the C_{17}/(*n*-C_{17} + *n*-C_{18}) ratio was increased in the order of $Ca(OH)_2$-EG) (0.88) > $Ca(OH)_2$-STD-Nano(0.85) > $Ca(OH)_2$–CTAB(0.75) > $Ca(OH)_2$–H_2O(0.68) > CaO(0.52) > free-catalyst reaction (0.42). Surfactant treated $Ca(OH)_2$ nanocatalyst rendered high ratio at 0.75–0.88, suggesting that triolein were deoxygenated efficiently via deCOx. In contrast, low ratio of C_{17}/(*n*-C_{17} + *n*-C_{18}) indicated that the generated product were mostly in light hydrocarbon (*n*-C_8 to *n*-C_{16}). This is in agreement with selectivity study where blank reaction or CaO catalysed reaction rendered large fraction of light hydrocarbon in range of *n*-C_8 to *n*-C_{16}.

Under hydrogen deficiency condition, the decarboxylation of unsaturated oleic acid (from triolein) tends to form *n*-heptadecenes (mono-unsaturated; $C_{17}H_{34}$) via scission of C-C bond of fatty acid (oleic acid), which leads to the oxygen removal in the form of CO_2 gas as by products. For decarbonylation reaction, di-unsaturated *n*-heptadecene ($C_{17}H_{32}$) was produced by removing oxygen in the form of CO gas and water as a by-product (Figure 3.9) (Snare et al., 2006). Thus, the efficiency of deCOx using different type of catalysts can be determined by comparing the GC–MS peak area% of mono-unsaturated and di-unsaturated C_{17} hydrocarbon fractions that obtained from the deoxygenated product. Based on the GC–MS results (Table 3.3 and Figure 3.10), the higher content of $C_{17}H_{34}$ suggested that the decarboxylation reaction was preferred instead to the decarbonylation reaction during Ca-based catalysed reaction pathways.

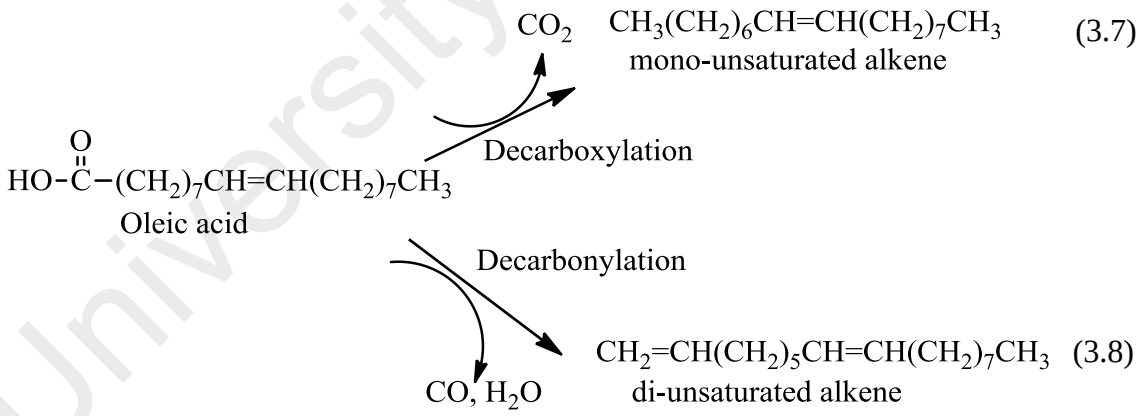

Figure 3.9: Proposed mechanism for decarboxylation and decarbonylation of oleic acid

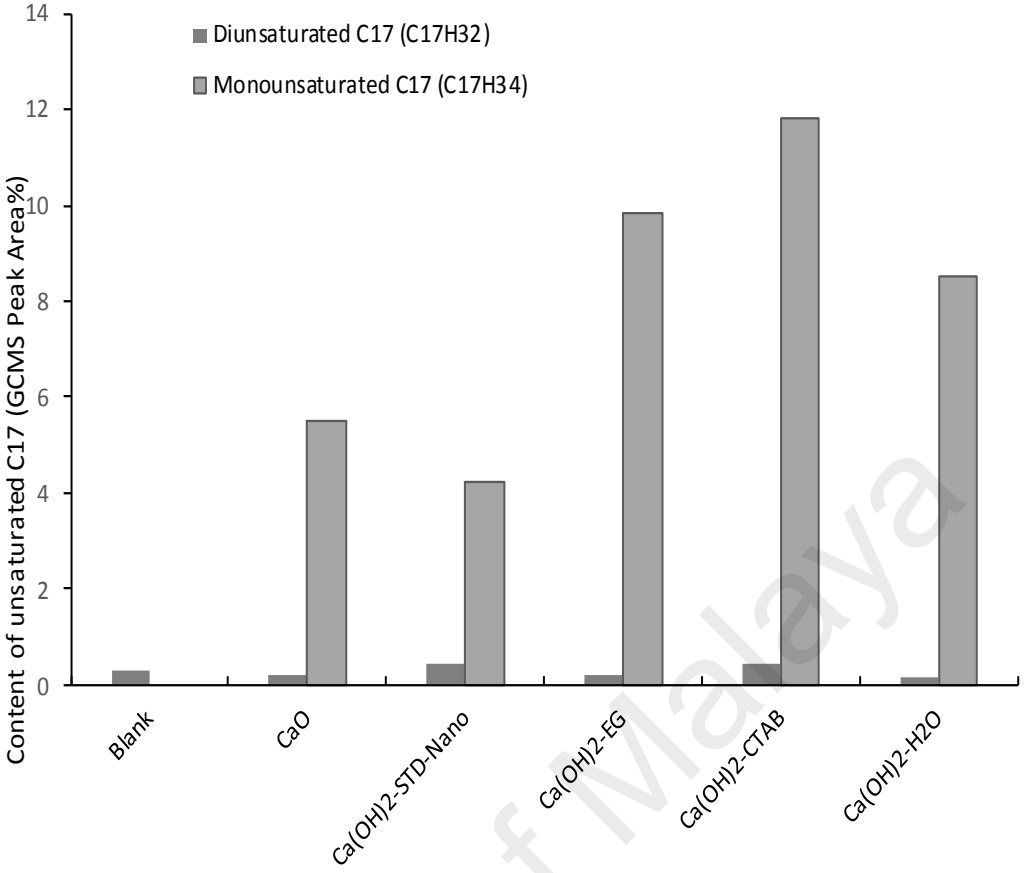

Figure 3.10: Decarboxylation and decarbonylation profile for different types of Ca-based catalysed reaction

Table 3.3: Composition profile of deoxygenized product (liquid hydrocarbon)

Catalyst	Total deoxygenated product (Peak area%)	*n*-alkane (Peak Area%)	*n*-alkene (Peak Area%)	Selectivity of the product obtained (Peak area%)						
				n-C_6-*n*-C_{16}	*n*-$C^{=}_{17}{}^{a}$	*n*-$C^{=}_{17}{}^{b}$	*n*-C^{-}_{17}	*n*-C_{18}	*n*-C_{19}-*n*-C_{24}	*n*-C_{17}/(*n*-C_{17}+*n*-C_{18})
Blank (without catalyst)	41.13	12.51	28.62	39.96	-	0.17	0.29	0.4	0.31	0.42
CaO	35.86	5.28	30.58	14.26	5.50	0.2	0.70	5.83	3.34	0.52
$Ca(OH)_2$-STD-Nano	34.71	16.33	18.38	28.17	4.22	0.42	0.74	0.92	1.39	0.85
$Ca(OH)_2$-EG	47.37	12.89	34.48	29.01	9.84	0.2	-	1.34	6.34	0.88
$Ca(OH)_2$-CTAB	44.55	13.77	30.78	23.6	11.84	0.42	1.43	4.36	2.9	0.75
$Ca(OH)_2$-H_2O	35.70	6.85	28.85	18.01	8.52	0.16	-	3.94	3.94	0.68

*Reaction parameter; reaction time : 30 min; Temperature : 350 ºC; Pressure : 10 mbar
Total deoxygenated product: liquid hydrocarbon (n-C_6-n-C_{24})
$C^{=}_{17}{}^{a}$: mono-unsaturated C_{17} alkene ($C_{17}H_{34}$)
$C^{=}_{17}{}^{b}$: di-unsaturated C_{17} alkene ($C_{17}H_{32}$)
C^{-}_{17}: alkane C_{17} ($C_{17}H_{36}$)

3.6 Conclusion

The clamshell-derived catalysts (CaO and nano–$Ca(OH)_2$) are potential deoxygenation catalysts for the biofuel production via cracking-deCOx pathways. The $Ca(OH)_2$ nanocatalyst that prepared via sonochemically assisted wet surfactant method has successfully increased of catalyst's textural properties and surface basicity. The presence of superior properties from surfactant treated catalysts has been proven to have high selectivity of alkane and alkene in chain length of *n*-C_{17} (high value of C_{17}/(*n*-C_{17} + *n*-C_{18}) ratio). Both $Ca(OH)_2$–EG and $Ca(OH)_2$–CTAB are capable of producing higher content of liquid hydrocarbon (*n*-C_6-*n*-C_{24}) with the yield of 47.37% and 44.5%, respectively.

CHAPTER 4: WASTE CLAMSHELL-DERIVED CaO SUPPORTED Co AND W CATALYST FOR RENEWABLE FUELS PRODUCTION VIA CRACKING-DEOXYGENATION OF TRIOLEIN

In the chapter 3, it was showed that nanosize of $Ca(OH)_2$ treated EG resulted in excellent cracking-deCOx activity with total of hydrocarbon fraction 47% and micron size of CaO resulted in ~37%. The performance of the CaO and $Ca(OH_2)$-based catalysts were not significantly vary anyway and it also found the nano-$Ca(OH)_2$ treated EG also promote the formation of longer chain hydrocarbon which might resulted from polymerization reaction. Therefore, in order to solve undesirable polymerization reaction by high basic $Ca(OH)_2$-based catalyst, introduction of active metals derived transition metals is necessary. Chapter 4 introduced a published work focused on the utilization of CaO supported transition metals (Co and W) in deoxygenation reaction under partial vacuum condition. This study entitles of "***Waste clamshell-derived CaO supported Co and W catalyst for renewable fuels production via cracking-deoxygenation of triolein***" have been published by the international *Journal of Analytical and Applied Pyrolysis on 2016, volume 120, page 110-120.* The list of authors including N. Asikin-Mijan, H.V. Lee, J.C. Juan, A.R. Noorsaadah, G. Abdulkareem-Alsultan, M. Arumugam, and Y.H. Taufiq-Yap.

4.1 Introduction

The development of alternative fuels from plant-derived oils (such as sunflower, palm, rapeseed, algal oil and their derivatives) as a substitute for fossil fuels has attracted much attention due to the increase of energy demand, environmental concerns and the depletion of fossil fuel resources (Prado and Antoniosi Filho, 2009). Fatty acid methyl ester (FAME) or biodiesel has emerged as potential fossil fuel substitute through

many mature and proven technologies (Tubino et al., 2016). However, FAME composed of highly oxygenated compounds which lead to many inevitable disadvantages such as high viscosity, pour point, acid number, low heating value and oxidation stability (Yang et al., 2013b). Thus, greener alternative route has been developed in order to produce biofuel with higher oxidative stability from plant oil. Recently, conversion of renewable oil into liquid hydrocarbons via hydrodeoxygenation (HDO), deoxygenation (DO) and hydrocracking was getting immersive attentions. Generally, hydrodeoxygenation reaction would have been deemed a more preferable route to high-quality hydrocarbon fuel via hydrogenolysis process by removing oxygen from the triglycerides in the form of H_2O. However, hydrodeoxygenation process is not economical since it consumes a large amount of hydrogen during the hydrogenation of the triglyceride (Huber et al., 2007). In contrast, deoxygenation process capable to convert oxygenates oil into hydrocarbon-based biofuel via decarboxylation/decarbonylation (deCOx) under hydrogen-free atmosphere and produced CO_2/CO as by products (Santillan-Jimenez et al., 2013;Asomaning et al., 2014).

Nowadays, various type of catalysts has been studied for the production of hydrocarbon-based biofuel via deoxygenation process. Majority of the studies focused on the use of catalysts comprising of high acidity such as noble metal-, metal sulphide-, metal phosphide- and metal carbide-based catalysts. However, due to several limitations such as cost, metal leaching by sulfur species and complexity of the synthesis methodr had triggered more research on the utilization of simple catalyst such as mixed metal oxides. In this study, transition metal oxides (TMO) supported with waste shell-derived CaO (TMO-CaO) such as Co-CaO and W-CaO were prepared for the deoxygenation of triolein. The physicochemical properties of the synthesized catalysts were characterized

by X-ray fluorescence (XRF), X-ray diffractometer (XRD), Brunauer-Emmet-Teller (BET), temperature programmed desorption NH_3 (TPD-NH_3), temperature programmed desorption CO_2 (TPD-CO_2) and scanning electron microscopy (SEM) analyses. The role of active Co_2O_4 and WO_3 with the presence of CaO support towards the triolein conversion and hydrocarbon selectivity was further investigated. The chemical composition of the liquid product was determined by Fourier transform infrared spectroscopy (FTIR), gas chromatography flame ionization detector (GC-FID) and gas chromatography mass spectrometry (GCMS) analyses. Moreover, the physicochemical properties of the spent Ca-based catalyst were further studied by XRD and thermogravimetric (TGA) analyses.

4.2 Literature Review

The usage of noble metal-based catalysts had been known to be actively used in oxygen removal reactions, but these types of catalyst are very costly, especially the Pd- and Pt-based catalysts. In addition, the presence of sulphur in metal easily contaminates the product, while other catalysts such as carbide, nitride, phosphide and oxide catalysts show fast deactivation and coking problem (Boullosa-Eiras et al., 2014;Mu et al., 2014;Wang et al., 2014). Mesoporous-based catalysts such as zeolite, SBA-15, HMS, KIT-6 and MCM-41 are also commonly used for the deoxygenation reaction, however they having the complexity in preparation process (Boullosa-Eiras et al., 2014;Zhao et al., 2016;Jiang et al., 2015;Arun et al., 2015;Wang et al., 2010). Therefore, the limitations of above mentioned catalysts has triggered the exploration of alternative catalysts in terms of low cost, simple and sulphur free for higher quality fuel production. Recently, application of transition metal oxides either in mono-metallic (Mo-, Ni-, Co-, Zn-) or bi-metallic (Ni/Mo-, Co/W) forms was reported by researchers for the deoxygenation process (Yigezu and Muthukumar, 2014). Furthermore, some studies had

shown that the solid base catalysts such as CaO and MgO are capable of deoxygenating the vegetable oil via decarboxylation (removal of CO_2) and decarbonylation (removal of CO) pathways (Romero et al., 2015). This is due to the basicity of the catalyst whereby it capable to absorb the released CO_2 during the deoxygenation process as well as reduce the coking problem of catalyst (Romero et al., 2015c;Morgan et al., 2012;Santillan-Jimenez et al., 2014a).

4.3 Experimental

4.3.1 Material

The CaO was synthesized from the waste clamshell according to our previous study (Asikin-Mijan et al., 2015c). Cobalt (II) nitrate hexahydrate ($Co(NO_3)_2 \cdot 6H_2O$) with purity > 99.9% was purchased from Sigma Aldrich. While, ammonium metatungstate hydrate, $H_{26}N_6O40W_{12}.xH_2O$ with purity ≥99% was purchased from Fluka. Ethyl alcohol with purity 99.7% was obtained from R&M Company and sulphuric acid with purity 95-95% was purchased from J.T. Baker. The model compound triolein (65%, Sigma Aldrich) wasused as feedstock for deoxygenation reaction. Standard solution for gas chromatograph (GC) analysis such as alkane ranging from C_8-C_{20} standard solution and internal standard 1-bromohexane were bought from Sigma Aldrich. GC grade n-hexane with purity > 98% from Merck was used as solvent for GC analysis.

4.3.2 Catalyst development

Calcium-based catalysts (Co-CaO and W-CaO) were synthesized by using wet impregnation method. 5 g of calcium oxide (CaO) that derived from waste clamshell was impregnated with a cobalt salt solution (20 wt.%) and the mixture was stirred for 6 h. The mix- ture was then dried in the oven at temperature of 100◦C for 24 h and

thermally activated at temperature 900 °C for 2 h under the atmospheric condition (Taufiq-Yap et al., 2012). The above mentioned procedures were repeated using 20 wt.% of tungsten salt solution. The both samples were denoted as Co-CaO and W-CaO catalysts. Furthermore, similar wet impregnation technique was applied to Co-CaO catalyst with different cobalt loading (10–40 wt.%) for optimization study.

4.3.3 Catalyst characterization

X-ray fluorescence (XRF) spectrometry is widely used for major and trace elemental composition analyses of many materials, including catalyst. In this study, the x-ray fluorescence spectrometer (XRF) (Philips PWI404) equipped with a scandium anode tube was used. A 2 g of catalyst was added into the sample cup (31 mm Double Open End X-Ray Cell with Collar). Later, it was transferred into the XRF chamber and the elemental composition of the catalyst was accurately quantified. The powder X-ray diffraction (XRD) analysis was carried out to identify the crystallography of the mixed metal oxide catalysts. The XRD analysis was performed using Shimadzu diffractometer model XRD-6000. The specific surface area and pore distribution of the catalysts were determined by Brunauer-Emmet-Teller (BET) method with N_2 adsorption/desorption analyser using Thermo-Finnigan Sorpmatic 1990 series. The catalyst was degassed overnight at 150 °C to remove moisture and foreign gases on the surfaces of the catalyst. Adsorption and desorption processes of N_2 on the catalyst surfaces were analysed in a vacuum chamber at −196 °C. The basicity and acidity of the catalysts were studied using temperature programmed desorption (TPD-CO_2) and (TPD-NH_3) with CO_2 and NH_3 as probe molecules, respectively. The analysis was carried out by using Thermo Finnigan TPD/R/O 1100 instrument equipped with thermal conductivity detector (TCD). The catalyst (~0.05 g) was pre-treated with N_2 gas flow for 30 min at 250 °C, followed by exposed with CO_2 gas for an hour at ambient temperature to allow

adsorption of CO_2 onto the surfaces. The excess CO_2 was subsequently flushed with N_2 gas flow at rate 20 mL/min for 30 min. The desorption of CO_2 from the basic sites of the catalyst was detected by TCD under helium gas flow (30 mL/min) from 50 ^oC to 900 ^oC and held for 30 min. The adsorption and desorption of NH_3 was similar to TPD-CO_2 method. Morphological of the catalysts was investigated using scanning electron microscopy (SEM) (SEM JOEL 6400). The coking tendency of catalyst was evaluated using thermogravimetric analysis (TGA) with simultaneous thermal analyser (TGA, Mettler Toledo 990). The experiments were conducted in the present of nitrogen gas flow at the rate of 10 ml/min with heating rate 10 ^oC/min. The oven temperature was ramped till it reached a maximum temperature of 1000 ^oC.

4.3.4 Catalytic deoxygenation of triolein

The deoxygenation of triolein was performed in a mechanically stirred 250 mL of semi-batch reactor (Figure 4.1). In a typical experiment, approximately 10 g of triolein and 5 wt.% of catalyst were added to the reactor. The deoxygenation reaction temperature was performed at temperature of 350 ^oC, 45 min under 10 mbar of partial vacuum condition. The released vapour/volatile species during cracking-deoxygenation reaction was condensed into liquid product using external water cooling circulator under temperature of 16 ^oC. It was observed that majority of vapour was condensed completely when longer condenser tube was used. In order to reduce the error of experimental results, the experiment was repeated for 3 times to obtained and average range of results.

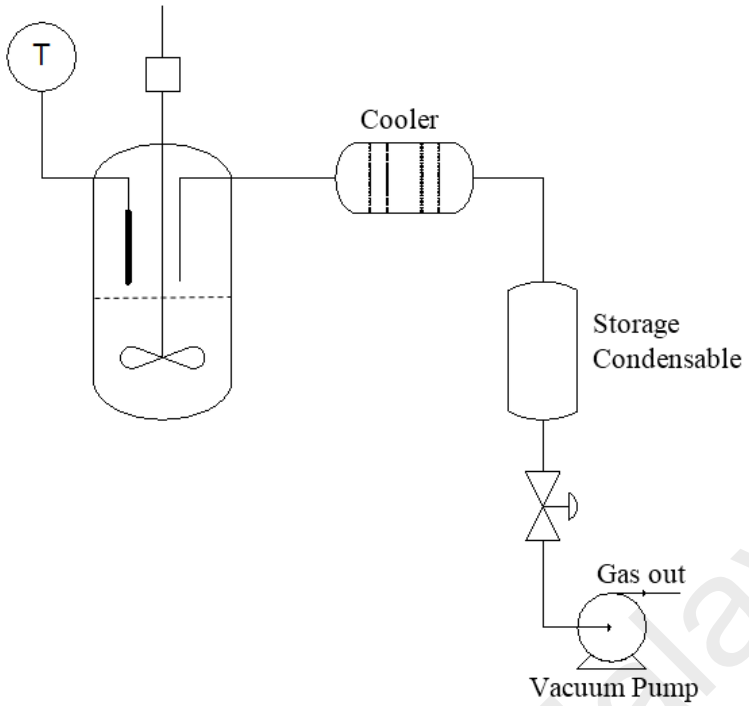

Figure 4.1: Schematic diagram for semi-batch reactor

During deoxygenation reaction of triolein, deCOx reaction lead to the released of CO_2/CO gases, where the waste gases were further collected via absorption column filled with soda lime granules (mixtures of $Ca(OH)_2$ or KOH and NaOH) for lab-scale study (Grace, W.R.C., 1993;Keith and Wong, 2006;Johnson et al., 2008). Moreover, the CO_2/CO gases emitted during deoxygenation reaction also partially absorbed by Ca-CaO catalyst, which active CaO phases was converted into inactive $CaCO_3$ phase for spent Ca-CaO catalyst (Figure 4.9). For industrial scale, larger amount of CO_2/CO release from the deoxygenation reaction can use as feed gas for the conventional steam reforming process into valuable gases and chemical such as methane (CH_4) and methanol (CH_3OH) (Oyama et al., 2012;Aasberg-Petersen et al., 2008).

The liquid products was then analysed with acid number (AN) test, Fourier transform infrared spectroscopy (FTIR), gas chromatography flame ionization detector

(GC-FID) and gas chro- matography flame ionization detector (GCMS). The liquid product was also tested according to ASTM method for estimating its density.

4.3.5 Product analysis

The deoxygenated liquid products were identified using alkane standards (C_8-C_{20}), which procured from Sigma Aldrich. The liquid products were quantified using a gas chromatography (Shimadzu GC-14B) equipped with a HP-5 capillary column (length:30 m × inner diameter: 0.32 mm × film thickness: 0.25 µm) with a flame ionization detector (FID) operating at 300 ^{o}C. The liquid product was diluted with GC grade n-hexane prior to the yield analysis. The 1-bromohexane was used as an internal standard for the quantitative analysis. An aliquot of 1 µL of sample was injected with into GC column. The injection temperature was operated at 250 ^{o}C. Nitrogen gas served as a carrier gas. The initial temperature of the oven was set at 40 ^{o}C and held for 6 min, then ramped to 270 ^{o}C at heating rate of 7 ^{o}C/min. The feedstock and deoxygenated liquid products was qualitatively characterized using gas chromatography mass spectrometer (GC–MS) (model SHIMADZU QP5050A) equipped with a non-polar DB-5HT column (length:30 m × inner diameter: 0.32 mm × film thickness: 0.25 µm) with splitless inlet. The feedstock was diluted with GC grade n-hexane (purity >98%) to 100 ppm. The fraction peaks from GC–MS spectrum were identified via National Institute of Standards and Testing (NIST) library. The identification of the major products was based on a probability match equal or higher than 95%. Furthermore, (Fourier Transform–Infrared Spectrometer (FT-IR) analysis was performed using Perkin Elmer (PC) Spectrum 100 FTIR with a resolution of 4 cm^{-1} and operating in the IR range of 300–4000 cm^{-1}. This analysis help to determine the relevant chemical functional groups found in the liquid product. The acid values of the feedstock and product were

determined by using the classical titration method by referring to the standard method of AOCS Cd 3d-63 (Eq. 4.1).

$$Acid\ Number\ (AN): (V_f - V_i)N\frac{56}{W_{oil}} \quad (4.1)$$

The quantity of base is expressed in terms of milligrams of potassium hydroxide that is required to neutralize the (0.1 M) acidic constituents in 0.2 g of sample. The catalytic activity of catalysts towards deoxygenation (Total product yield and product selectivity) was determined by comparing the peak area% of obtained spectra. It is known that the GCMS analysis does not provide exact quantitative analytic result of compounds. However, it is possible to compare the product yield and product selectivity by comparing the peak areas as the chromatographic peak area of compounds is proportional to its quantity and the relative content of the product (Eq. (4.2), Eq. (4.3) and Eq. (4.4) (Asikin-Mijan et al., 2015a)Romero et al., 2014). In order to confirm the reproducibility of the results, the experiments were conducted for three times, with the average of the peak area and peak area% was calculated.

$$= \frac{Total\ area\ of\ the\ parafinic\ hydrocarbon\ (C_8 - C_{17})}{Total\ area\ of\ the\ product} \times 100\ \% \quad (4.2)$$

Gasoline selectivity (%)

$$= \frac{Total\ area\ of\ the\ parafinic\ hydrocarbon\ (C_8 - C_{12})}{Total\ area\ of\ the\ parafinic\ hydrocarbon\ (C_8 - C_{17})} \times 100\ \% \quad (4.3)$$

Diesel selectivity (%)

$$= \frac{Total\ area\ of\ the\ parafinic\ hydrocarbon\ (C_{13} - C_{17})}{Total\ area\ of\ the\ parafinic\ hydrocarbon\ (C_8 - C_{17})} \times 100\ \% \quad (4.4)$$

4.4 Result and discussion

4.4.1 Catalyst characterization

The elemental compositions for the raw clamshell, clamshell-derived CaO, TMO-CaO (Co-CaO and W-CaO) were studied by using XRF analysis (Table 4.1). Result shows that raw clamshell and com- busted clamshell rendered comparable calcium content of > 98 atomic%. From the data obtained, each catalyst (Co-CaO and W-CaO) shows the presence of transition metal oxide (Co and W) at range of 16 − 19 atomic% and their Ca contains were > 80 atomic%. This was in agreement with the theoretical ratio of the synthesized range of 16 − 19 atomic% and their Ca contains were > 80 atomic%. This was in agreement with the theoretical ratio of the synthesized catalyst TMO:CaO (2:8), where 20 wt.% of the catalyst corresponded to active TMO and 80 wt.% was CaO.

Table 4.1: Elemental composition of fresh clamshell, combusted clamshell, CaO, Co-CaO and W-CaO catalysts

Catalyst	Ca	Co	W	Other*
Clamshell	98.81	-	-	1.19
CaO	98.91	-	-	1.09
Co-CaO	80.29	19.37	-	0.34
W-CaO	83.04	-	16.24	0.72

*Other representing minor element: S, Sr, Cu, Br, K and Fe

XRD patterns of the raw clamshell, CaO and TMO-CaO were shown in Figure 4.2. Raw clamshell shows major phases of $CaCO_3$ (2θ = 26.2°, 33.2°, 45.8° and 48.4°) (JCPDS File No. 1-0628). However, the thermally activated clamshell rendered intense peaks of cubic CaO phases at 2θ = 32.21°, 37.21°, 54.34°, 64.62° and 67.76° (JCPDS card no. 00-037-1497). This indicating that the majority of the carbonate phases of clamshell were successfully transformed into oxide phases at high temperature of 800 °C. For Co-CaO, the diffraction pattern clearly observed at 2θ of 33.76° (JCPDS card

no. 00-042-1467), representing the existent of Co_2O_4 species. Whereas, W-CaO catalyst showed diffraction peak of WO_3 at 2θ of 23.45º (JCPDS card no. 01-072-1465). The low intensities of Co_2O_4 and WO_3 peaks suggesting that the metal oxide dispersed well on the clamshell-derived CaO support. This is also in accordance to other studies, where CaO intensity peaks has reduced after impregnated with active metal (Wu et al., 2014;Qian et al., 2014). The average crystallite size of clamshell-derived CaO was 64.29 nm. Nevertheless, crystallite size of Co-CaO and W-CaO was reduced after the impregnation of cobalt and tungsten metal oxides, which were 57.54 nm and 58.41 nm, respectively.

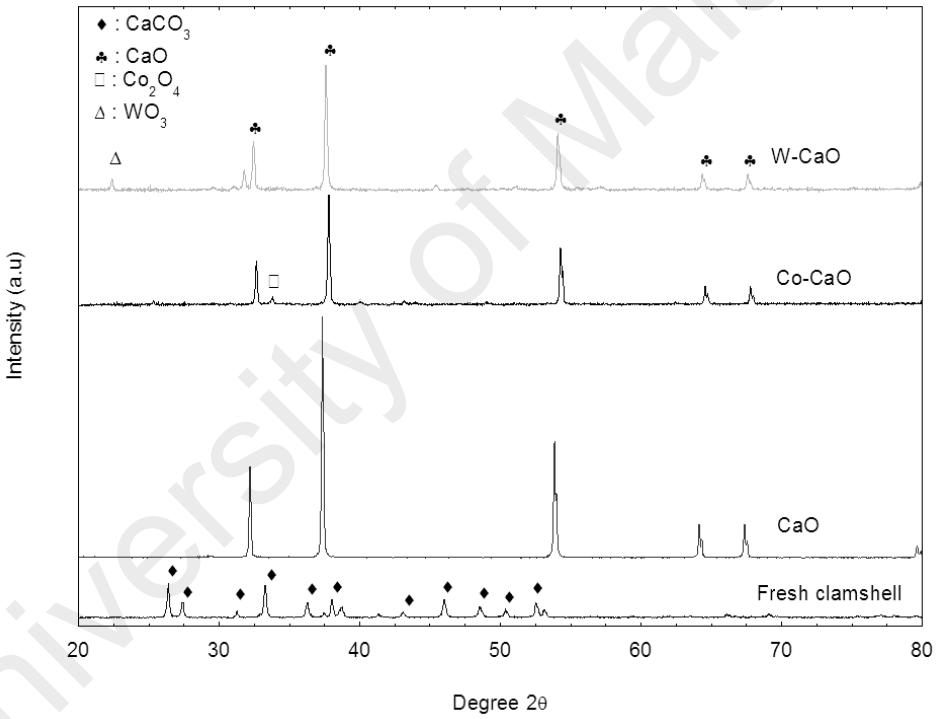

Figure 4.2: XRD diffraction peak for raw clamshell, CaO, Co-CaO and W-CaO catalysts.

The textural properties of combusted clamshell, Co-CaO and W-CaO are summarized in Table 4.2. All the prepared catalysts showed low surface areas as the majority content was attributed to CaO support. The bulk CaO rendered 9.80 m^2/g of surface area with low porous structure and pore size diameter at range of 2.86-78.32

nm. Surface areas for Co-CaO and W-CaO were 7.46 m^2/g and 7.48 m^2/g, respectively. Reduction of the surface area indicates that Co_2O_4 and WO_3 were successfully impregnated on the surface of CaO support. Moreover, low surface area of catalysts may also due to the sintering effect of the catalyst where further re-calcination after impregnation step at temperature of 900 ^oC for 2h created severe agglomeration of particles. It was observed that the pore size diameter of both Co-CaO and W-CaO catalysts were increased after impregnation, which were accordance with 2.96-116.50 nm and 2.98-152.88 nm, respectively. The enlargement of pore size was due to the collapse of pore walls during impregnation and led to surface modification. The large pore is beneficial to the diffusion of the reactants into active sites of catalysts. Therefore, it is estimated that Co-CaO and W-CaO catalysts consisted of high catalytic activity for the deoxygenation reaction.

Basicity and acidity profile of synthesized catalysts were evaluated by using temperature programmed desorption of CO_2 and NH_3, respectively. The amount of basicity and basic strength distribution of the catalysts were displayed in Table 4.2. TPD patterns of the catalysts shows CO_2 desorption peaks at the temperature higher than 600 ^oC, indicating all the catalysts derived from clamshell exhibit strong basic strength (Wu et al., 2014). It was observed that the amount of basicity for WO_3, Co_2O_4, CaO and W-CaO was lower as compared to that of Co-CaO. The basicity density of the catalyst increase in the order of Co_2O_4> Co-CaO> CaO > W-CaO> WO_3. Co-CaO catalyst rendered highest amount of basicity of 568.56 µmol/g at strong active basic sites of 603 ^oC and 826 ^oC. Based on the acidity profile (Table 4.2), the acid density follows the order of W-CaO > Co-CaO > WO_3 > Co_2O_4 > CaO. Co-CaO and W-CaO catalysts rendered higher acidity with strong acid strength introduction of selective active metal into CaO has capable to increase the acidic property of catalyst. WO_3 with strong

acidity capable to enhanced the acidity of W-CaO catalyst with highest amount of acid density of 10417.71 µmol/g at temperature of 734 ^{o}C.

SEM micrographs for all synthesized catalysts were shown in Figure 4.3. The combusted clamshell (CaO) showed irregular shapes with agglomeration structure of particles demonstrating sintering effect of the CaO at high calcination temperature (900 ^{o}C) (Figure 4.3a). The SEM morphology for all active metals-doped CaO catalysts show significantly change of particle structure. In the case of Co-CaO, aggregated particles consisted of interconnected sheet-like structure with rough catalyst surface was formed (Figure 4.3b). Meanwhile, W-CaO shows formation of smaller aggregates with cluster agglom- eration (Figure 4.3c). Both Co-CaO and W-CaO catalysts were sintered and changed to larger cluster upon calcination at 900 ^{o}C. This was in agreement with the surface area analysis that the surface area of the catalyst decreased markedly after calcination (Table 4.2).

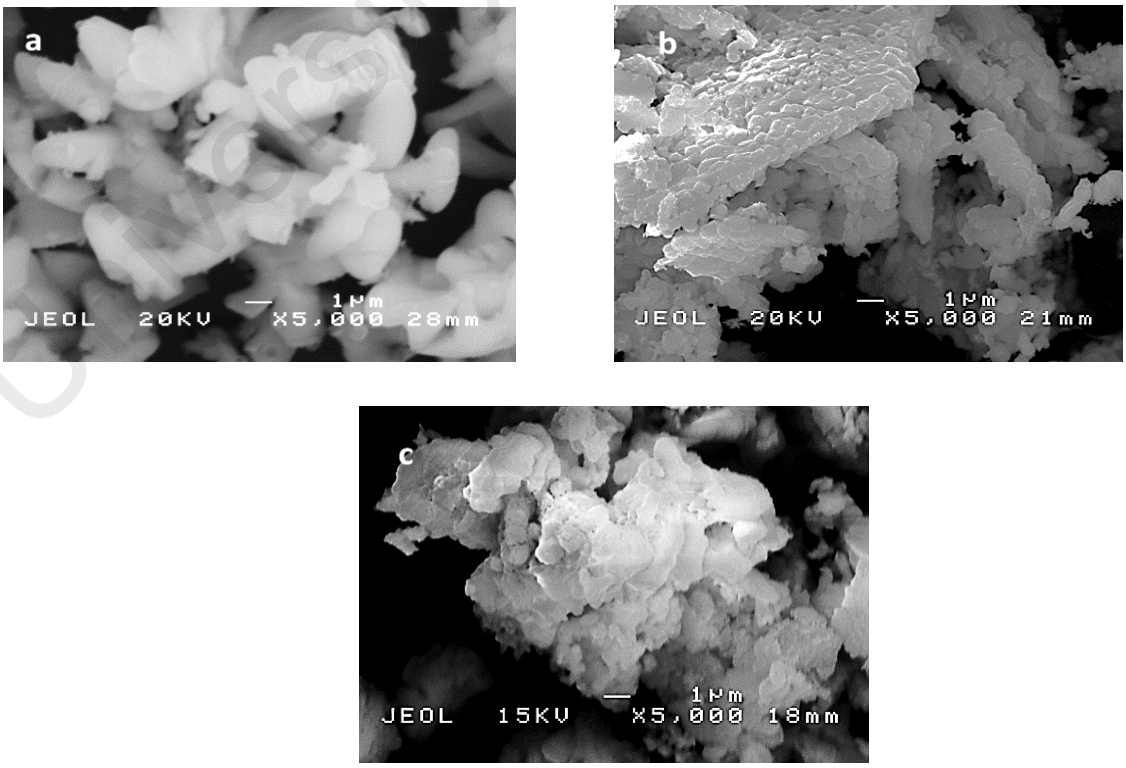

Figure 4.3: SEM Micrograph for (a) CaO,(b) Co-CaO and (c) W-CaO catalysts

Table 4.2: Physicochemical properties of CaO, Co_2O_4, WO_3, Co-CaO and W-CaO catalysts

Catalyst	**XRD**	**BET**		**TPD**			
	[a]Crystallite size(nm)	[b]Surface area (m^2/g)	[b]Pore size diameter range (nm)	[c]Temperature (^oC)	[c]Basic sites (µmol/g)	[d]Temperature (^oC)	[d]Acid sites (µmol/g)
CaO	64.29±0.21	9.80	2.86-78.32	636	548.52	-	-
Co_2O_4	-	-	-	660	1030.00	878	3001.73
WO_3	-	-	-	-	-	457	576.68
Co-CaO	57.54±0.13	7.46	2.96-116.50	603,826	260.79, 307.77	488,840	257,486.91
W-CaO	58.41±0.22	7.48	2.98-152.88	638	450.55	505,734	77.22, 10340.49

[a] measured by using Scherer equation from XRD data (repeat twice)
[b] Determined by BET analysis
[c] Determined by TPD-CO_2 analysis
[d] Determined by TPD-NH_3 analysis

4.4.2 Catalytic deoxygenation activity

Catalytic activity profile of deoxygenation reaction was shown in Figure 4.4. Based on the results, the catalytic deoxygenized liquid products were composed of both gasoline fraction (C_8-C_{12} hydrocarbon chain) and diesel fraction (C_{13}-C_{17} hydrocarbon chain). The catalyst free (blank) deoxygenation reaction rendered low yield of liquid hydrocarbon (13.4 %), which indicated low deoxygenation rate of triglycerides in the absence of catalyst. As compared to TMO-CaO catalysed deoxygenating reaction, the yields of liquid hydrocarbon were significantly increased in the order of Co-CaO > W-CaO > Co_2O_4 > WO_3 > CaO > blank.

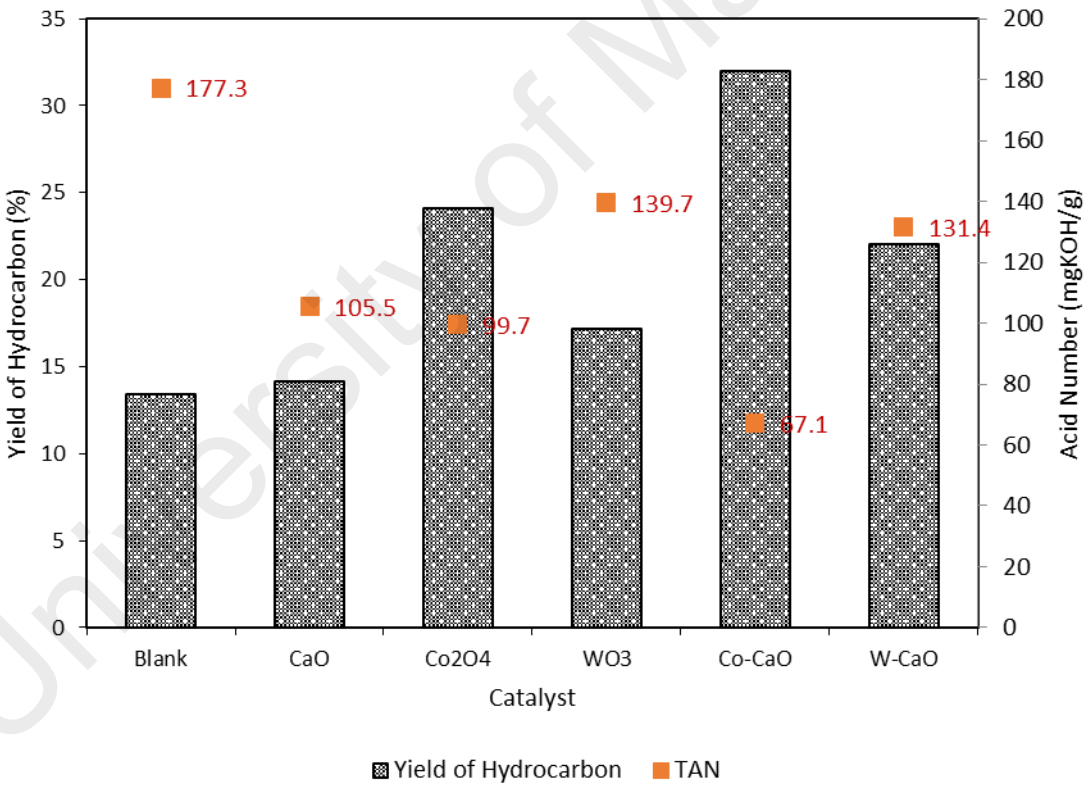

Figure 4.4: Hydrocarbon yields and TAN for free catalyst, TMOs and TMO-CaO catalysed deoxygenations reaction

According to the findings from Figure 4.5, TMO-CaO catalysed reaction capable to produce high selectivity of gasoline-ranged product as compared to that of bulk metal oxides (Co_2O_4 and WO_3). This was due to the presence of acid-base interaction between

binary metal oxide system (Co_2O_4-CaO and WO_3-CaO), which rendered a synergistic effect for both triglyceride cracking (cleavage of C-C bond) and deCOx of free fatty acid chain(Arun et al., 2015;De Lange et al., 2001). It was found that basicity of catalyst playing an important role in cracking and favour for the formation of light alkanes (gasoline fractions) (Romero et al., 2015a;Santillan-Jimenez et al., 2014b;Roh et al., 2011;Na et al., 2012a;Tani et al., 2011;Na et al., 2012b).

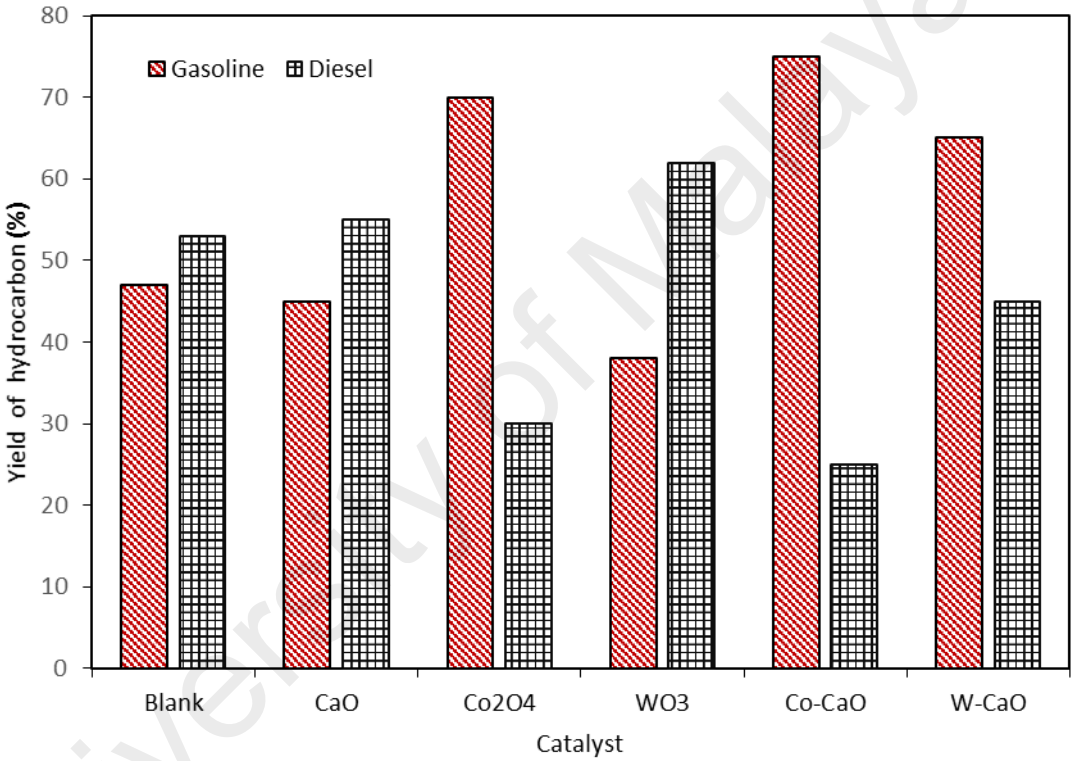

Figure 4.5: Gasoline and diesel selectivity for free catalyst, TMOs and TMO-CaO catalysed deoxygenations reaction

Amongst the catalysts, Co-CaO catalyst rendered highest yield of liquid hydrocarbon (32 %) and gasoline selectivity (75 %) with lowest total acid number (TAN) value of 67 mg KOH g^{-1} (Table 4.3). The TAN analysis is an indication study of cracking-deoxygenation reaction by detect the existence of free fatty acids formed. Based on the results obtained from Figure 4.3 and Table 4.3, all the liquid products showed high TAN value (> 100 mg $KOHg^{-1}$) as compared to triolein (0.5 mg $KOHg^{-1}$),

which implied that the cracking of triolein lead to formation of free fatty acid (FFA) intermediates. The lowest TAN value from Co-CaO catalysed product indicated that triolein successfully cracked into fatty acids and deoxygenized into hydrocarbon products. The Co-CaO catalysed product rendered lowest TAN value with remaining of 33 wt.% of acid compound, where the current percentage is within acceptable copper corrosion value (Schwab et al., 1988).

Table 4.3: Properties of the feed and liquid products obtained after the catalysed deoxygenation reaction

Oils	Density (kg L^{-1}) at 25 °C	TAN number (mg $KOHg^{-1}$)
Triolein	0.913	5.0
Blank[a]	0.916	177.3
CS-CaO	0.900	105.5
Co-CaO	0.850	67.0
W-CaO	0.801	131.4

[a]Deoxygenation of triolein without catalyst

Furthermore, it was found that the present deoxygenized rendered lower acid value/acid index (calculated by titration) as compared to several studies that discussed acidity index of deoxygenized products (Schwab et al., 1988;Mello et al., 2008;Bacha et al., 2007). According to Lima's study, green diesel derived from soybean, palm and castor oil with high acid value 116, 133 and 207.5 mg $KOHg^{-1}$ yielded Cetane number of 50.1, 52.7 and 30.9, respectively (Lima et al., 2004) which comparable/better than Standard Ultra-Low Sulphur Diesel (ULSD) Fuel specification (45) (Bacha et al., 2007). Generally, higher Cetane number indicate the fuel combust easily in the diesel engine, which avoid unburned fuel in the cylinder and reduce the intense knock. Thus, we estimate better fuel efficiency (higher Cetane number) for deoxygenized liquid product with 67 mg $KOHg^{-1}$ as compared to literature study with acid value >100 mg $KOHg^{-1}$ (Lima et al., 2004). However, post-treatment of the product such as washing or

neutralization was suggested to remove the remained organic acid in order to prevent unfavourable by-product in the biofuel product.

Based on the finding, we realized that other than basicity/acidity density of catalyst, the basicity strength and acidity strength also play and important factor to control the reactivity of deoxygenation reaction. The Co-CaO catalyst with strong acid and basic strength able to enhance the deCOx for C-C bonds scission of carboxylic acid, which leads to the formation of hydrocarbon fractions. It was in agreement with TPD-CO_2 and TPD-NH_3 result where, Co-CaO showed additional CO_2 desorption peak appears above 800 ^oC and NH_3 desorption peak at higher temperature (840 ^oC). Meanwhile W-CaO showed CO_2 and NH_3 desorbed at lower temperature < 800 ^oC than Co-CaO catalyst, with lower basic-acid strength that may slightly less effective in deoxygenation process.

Besides, BET profile (Table 4.2) shows less significant correlation of this catalysts' pore size and surface area towards deoxygenation activity. Although W-CaO showed largest pore size diameter (2.98-152.88 nm) and higher surface area (7.48 m^2g^-) than Co-CaO, however the deoxygenation performance was less efficient than Co-CaO catalyst. Hence, it can be assumed there was less reaction occurs in the pore of catalyst. It can be suggested that the small micropores of CaO-based catalyst has become a limitation for accessibility of large compound of triolein.

4.4.3 Product distribution of deoxygenated liquid

The chemical composition of deoxygenated liquid product was identified by GCMS analysis (Figure 4.6). Result shows that 70.69% of triolein composed of both unsaturated and saturated C_{18} fatty acids such as 9-octadecenoic acid, 9-octadecanoic

acid and aldehyde (13-octadecenal). For deoxygenized liquid products, it was mainly composed of unsaturated and saturated hydrocarbon chains within the range of C_8-C_{24} and accompanied by minor content of oxygenated intermediates such as coupling products (ketone), aldehydes and acids. Based on the results, Co-CaO successfully converting ~75% of 9-octadecenoic acid into hydrocarbons, followed by CaO (~68%) and W-CaO (~53%).

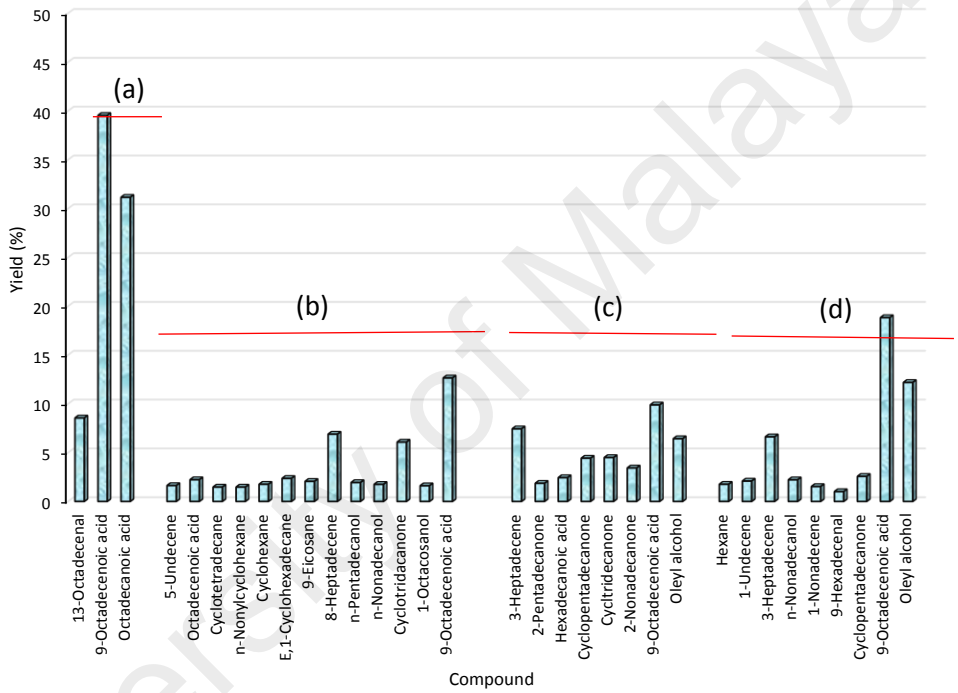

Figure 4.6: GCMS of product distribution of (a) the feedstock, liquid deoxygenated product catalysed by (b) CaO, (c) Co-CaO and (d) W-CaO catalysts

The existence of coupling products in deoxygenated liquid indicated the ketonization side reaction occurred during deoxygenation process. The Co-CaO catalysed reaction rendered the highest formation of cyclic ketone compound (14.28%), while CaO catalysed reaction showed 11.06% ketonization intermediates. However, W-CaO catalysed reaction showed the best in inhibiting the ketonization reaction with only 2.57% of ketone compounds formed during deoxygenation process. In summary, the ketonization selectivity was increased in the order of Co-CaO > CaO > W-CaO. It was

suggested that the ketonization rate was promoted by basic-ity of the catalyst and it is in agreement with the previous studies (Renz, 2005;Kamimura et al., 2003;Nagashima et al., 2005).

Furthermore, FTIR analysis was performed to determine chemical functional group of deoxygenated liquid products (Figure 4.7). The FTIR spectrum of triolein showed absorption band at 3600 cm^{-1} (-O-H), 2925 cm^{-1} and 2858 cm^{-1} (-CH) stretching, 1749 cm^{-1}(-C=O ester) stretching, 1455 cm^{-1} ($-CH_2$) bending, 1425 cm^{-1} (CH_2) bending, 1285 cm^{1}(-C-O-C) and 726 cm^{-1}–(CH)n- rocking for alkane (Santillan-Jimenez et al., 2013;Santillan-Jimenez and Crocker, 2012b;Snare et al., 2006). Besides, chemical functional group for deoxygenized liquid product composed mainly of alkane and alkene compounds with functionalities of –CH (stretching), $-CH_2$ (bending),$-CH_3$ (bending), alkene –($=CH_2$)- and alkane –(CH_2)n-) present at vibration bands of 2950 cm^{-1}, 2858 cm^{-1}, 1465 cm^{-1}, 1300 cm^{-1}, 970 cm^{-1} and 730 cm^{-1}, respectively. It was noteworthy that the liquid products showed significant shifting of FTIR stretching band from 1749 cm^{-1} for C=O group (in triolein) to 1710 cm^{-1}, which indicating the cracking of the ester structure to acid intermediates product (Romero et al., 2015a). This is in agreement with acid value test, where the acidity of the triolein increased drastically from 5 mg $KOHg^{-1}$ in liquid product (Table 4.3, Figure 4.6). Furthermore, an appearance of new peak at 1300 cm^{-1} was attributed to new bending of $-CH_2$ and $-CH_3$ alkyl chain in hydrocarbon compounds. The indication of oxygen removal was proved by the absent of C-O-C absorption band at 1150 cm^{-1}, which agreed to the occurrence of deCOx reaction.

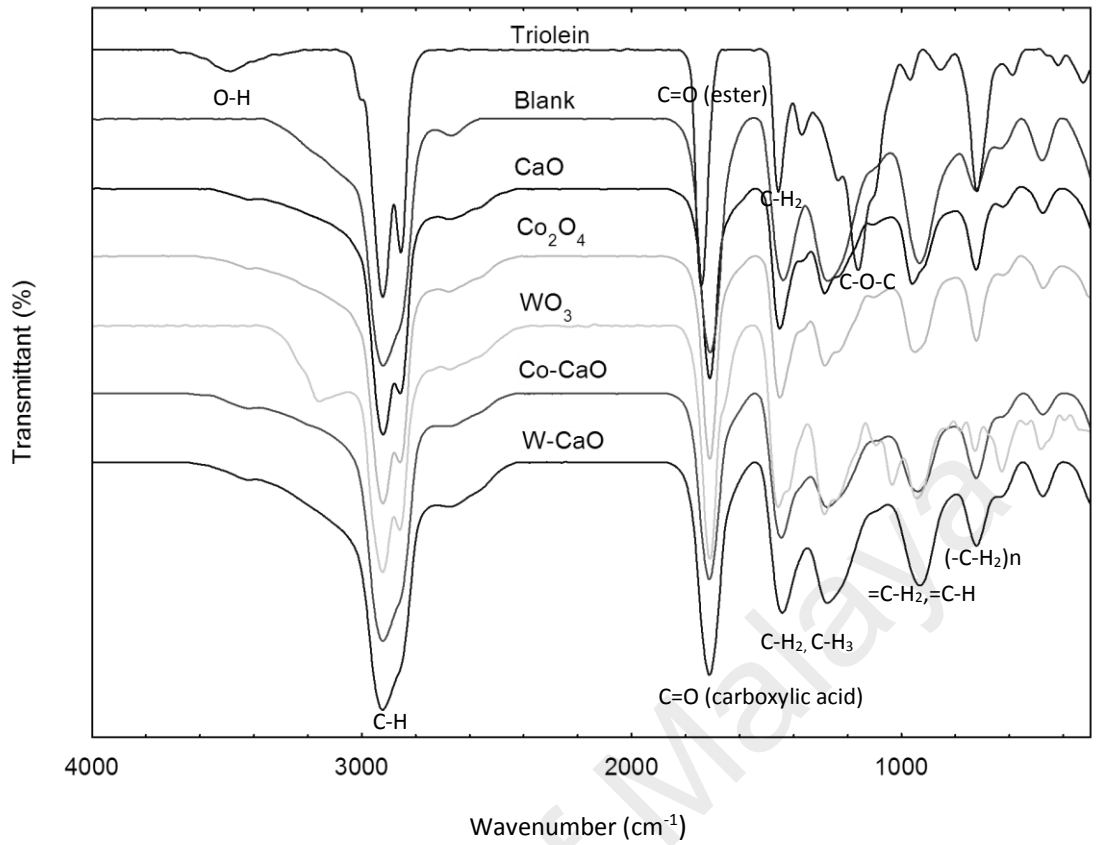

Figure 4.7: FTIR spectrum of triolein deoxygenation of triolein in catalyst free, CaO, TMOs and TMOs-CaO catalysed systems

Density analysis for the triolein and deoxygenized liquid product were evaluated using ASTM standard D975 method (Table 4.3). It was found that the density of deoxygenated liquid product was reduced when compared with the density of triolein. The density values of liquid products catalysed by CaO, Co-CaO and W-CaO were 0.9 kg L^{-1}, 0.850 kg L^{-1} and 0.801 kg L^{-1}, respectively. The densities of the deoxygenated liquid products were closely within the range of petroleum gasoline standard and diesel standard, which is 0.71–0.78 kg L^{-1}, and 0.86-0.9 kg L^{-1}) respectively (Tariq et al., 2011;Al-Hamamre and Al-Salaymeh, 2014). However, further post-treatment step is necessary to remove remained oxygenated compounds in the final products before ready as biofuel for engine usage.

4.4.4 Effect of the cobalt ratio towards deoxygenation reactivity

As indicated in Sections 4.3.2 and 4.3.3, the Co-CaO catalyst was highly effective in deoxygenation of triolein with highest selectivity towards hydrocarbon fraction, especially in the gasoline range. Thus, further stoichiometric study on active cobalt metal ratios (10–40 wt.%) was investigated to determine optimized catalyst composition for higher yield of hydrocarbon and gasoline-diesel selectivity (Figure 4.8a–d).

XRD patterns (Figure 4.8a) shows slightly decreased of intensity and broader peak of CaO phase ($2\theta = 37.21^{o}$) with reduced of crystallite sizes as the content of Co loading increased from 20 to 40 wt.% (Table 4.4). The presence of low intensity peak for Co_2O_4 at 33.76^{o} indicated high metal dispersion in the CaO support (Yu et al., 2014). Besides, the acid-basic density and active strength distribution were increased as the dosage of Co metal increased (Figure 4.8b1 and Figure 4.8b2) (Table 4.4). Based on both acidity and basicity studies, the density was increased followed order of 40 wt.% > 30 wt.% > 20 wt.% > 10 wt.%. Furthermore, new absorption peak was generated at temperature > 800 ^{o}C for cobalt concentration range 20–40 wt.%, which indicating that super strong basic and acid strength was formed. This result was in agreement with gasoline selectivity (Figure 4.8d), where increment of cobalt concentration prone to crack long fatty chain into shorter hydrocarbon chain in range of gasoline, followed by deCOx into paraffin-based products. These features capable to enhance the reactivity of deoxygenation process where highest hydrocarbon yield (65%) with highest selectivity of gasoline fractions (84%) was obtained with 40 wt.% of Co dosage on CaO support (Figure 4.8c and 4.8d). Based on our best finding, 65% of hydrocarbon yield were achieved with acid value 31 mg $KOHg^{-1}$ when 40 wt.% of cobalt were impregnated on

the CaO. It is expected to have better fuel properties (higher Cetane number) than liquid product with acid value >100 mg $KOHg^{-1}$ as reported by Lima et al. (Lima et al., 2004).

Table 4.4: Physicochemical properties of Co-CaO with different dosage of Co content

Catalyst	XRD	TPD-NH_3		TPD-CO_2	
	Crystallite size (nm)	Temperature (^oC)	Acid sites ($\mu molg^{-1}$)	Temperature (^oC)	Basic sites ($\mu molg^{-1}$)
Co10-CaO	52.98	532	180.92	678	1344.84
Co20-CaO	53.54	488, 840	257, 486.91	603, 826	260.79, 307.77
Co30-CaO	45.14	851	605.81	641,831	310.00, 284.77
Co40-CaO	35.38	909	970.32	663, 839	742.08, 333.49

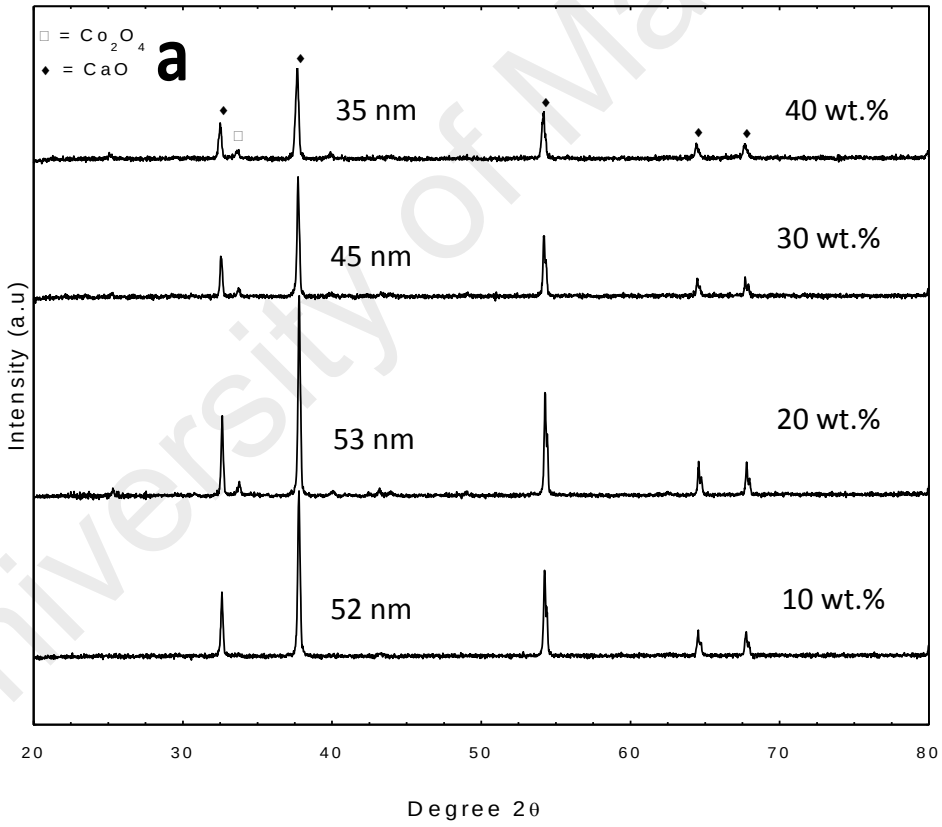

Figure 4.8: Effect of the cobalt dosage from 10 to 40 wt.% on (a) XRD diffraction peak, (b1) acidity of the catalyst, (b2) basicity of the catalyst , (c) the hydrocarbon yield and (d) selectivity toward gasoline and diesel

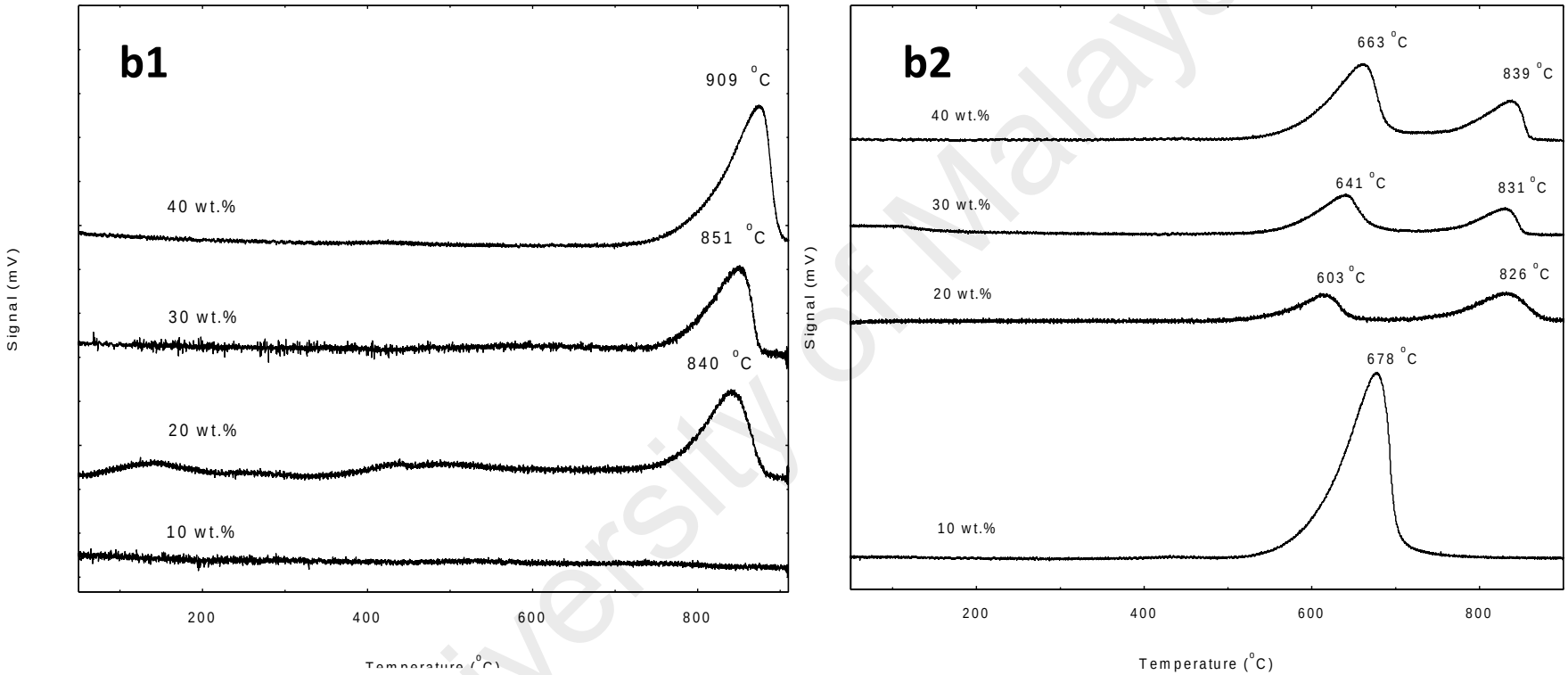

Figure 4.8, continued: Effect of the cobalt dosage from 10 to 40 wt.% on (a) XRD diffraction peak, (b1) acidity of the catalyst, (b2) basicity of the catalyst , (c) the hydrocarbon yield and (d) selectivity toward gasoline and diesel

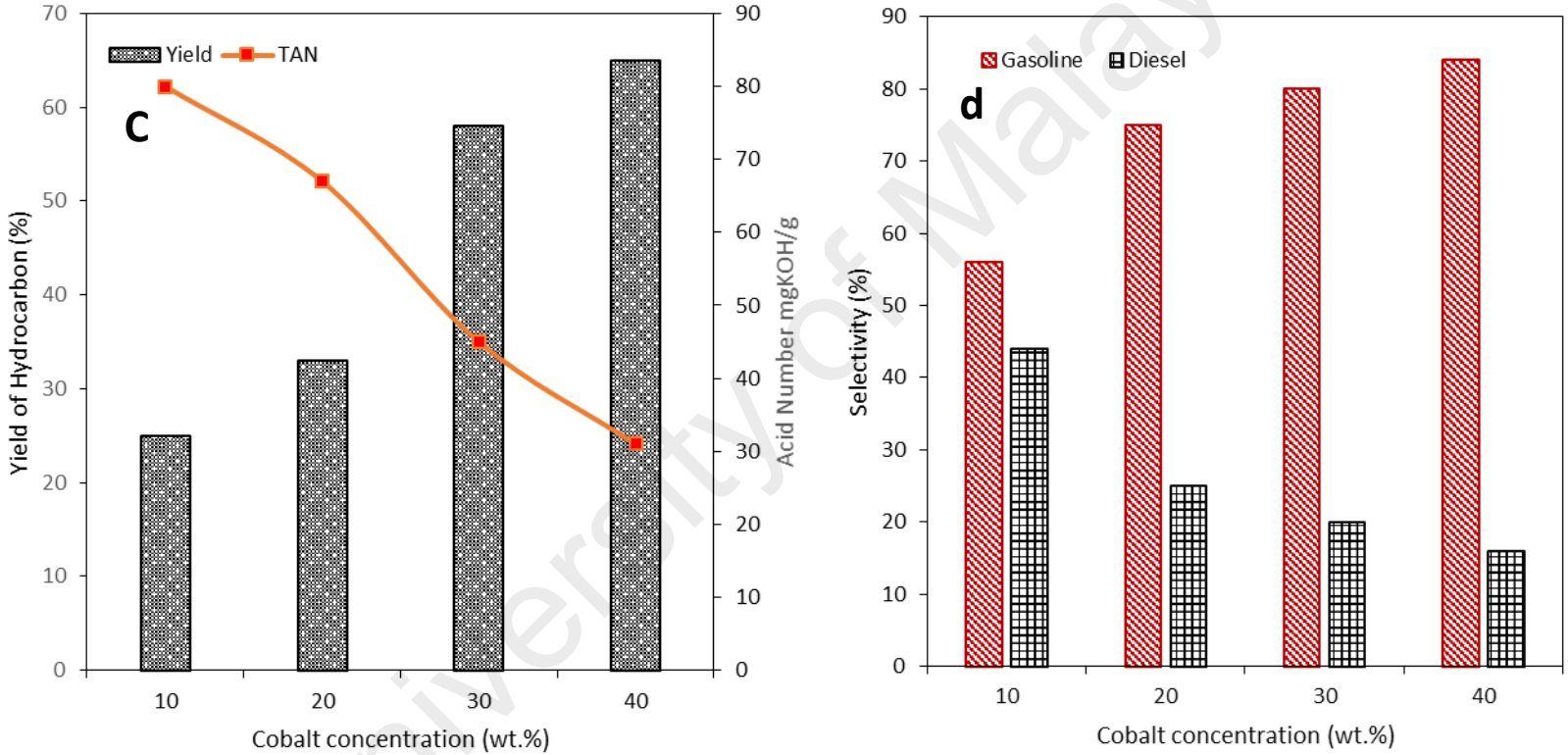

Figure 4.8, continued: Effect of the cobalt dosage from 10 to 40 wt.% on (a) XRD diffraction peak, (b1) acidity of the catalyst, (b2) basicity of the catalyst, (c) the hydrocarbon yield and (d) selectivity toward gasoline and diesel

In order to study the stability of Co-CaO catalyst for deoxygenation reaction, the chemical characteristic of spent catalysts (Co-CaO catalysts with Co dosages within range 10–40 wt.%) was further investigated. From XRD analysis, the spent Co-CaO catalysts showed the presence of carbonate phases at 2θ = 23.26º, 29.61º, 36.19º, 39.63º, 43.39º, 47.74º, 48.74º, 57.63º, 60.87º, 64.90º and 73.21º (JCPDS Card No: 00.005-0585) (Figure 4.9). It was indicated that CaO support reacted with carboxylic acid and further deactivated into carbonate phase. This suggested that CaO able to promote deCOx by absorbed the CO_2/CO gaseous from acid and converted into inactive $CaCO_3$ material (Tymchyshyn et al., 2013;Han et al., 2010). The inactive $CaCO_3$ phases from Co-CaO catalyst will re-covert into active CaO phases by thermal activation at high calcination temperature.

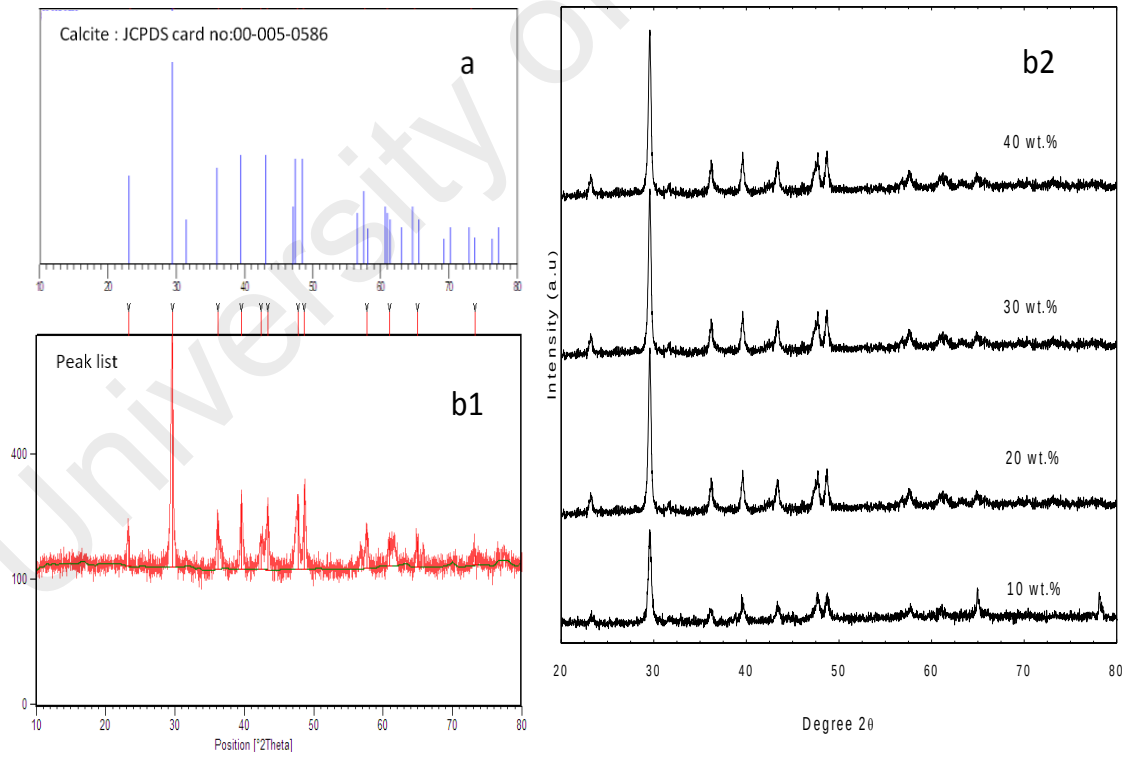

Figure 4.9: XRD diffraction peak for (a) raw clamshell, (b1) spent Co-CaO catalyst with Co concentration of 40 wt.% and (b2) spent Co-CaO catalyst with Co concentration of 10-40 wt.%

The thermal decomposition profile of spent Co-CaO catalysts was analysed using TGA analysis (Figure 4.10). The spent Co-CaO catalysts (cobalt dosage of 10–40 wt.%) showed two major degradation peaks of weight loss. The first weight loss was identified as the degradation of organic matter, which contributed to the coke burning. TGA profile indicated that the coke formation was reduced from 14% to 8.2% as the cobalt dosage was increased from 10 wt.% to 40 wt.%. The second degradation peak at temperature of 530–780 ^{o}C showed the decomposition of $CaCO_3$ to active CaO by releasing CO_2 gas (Lewandowski and Sarbak, 2000;Asikin-Mijan et al., 2015b). The total weight loss was increased from 32.1% to 37.2% as continuous increased of Co dosage from 10 to 40 wt.%. This implied that high acid and basic density originated from cobalt species leads to an active oxidation reaction, which transformed inactive $CaCO_3$ to active CaO catalyst. Therefore, we suggested that synergic effect of bi-metallic system (Co_2O_4 and CaO) capable to prolong the reusability of catalyst for deoxygenation process.

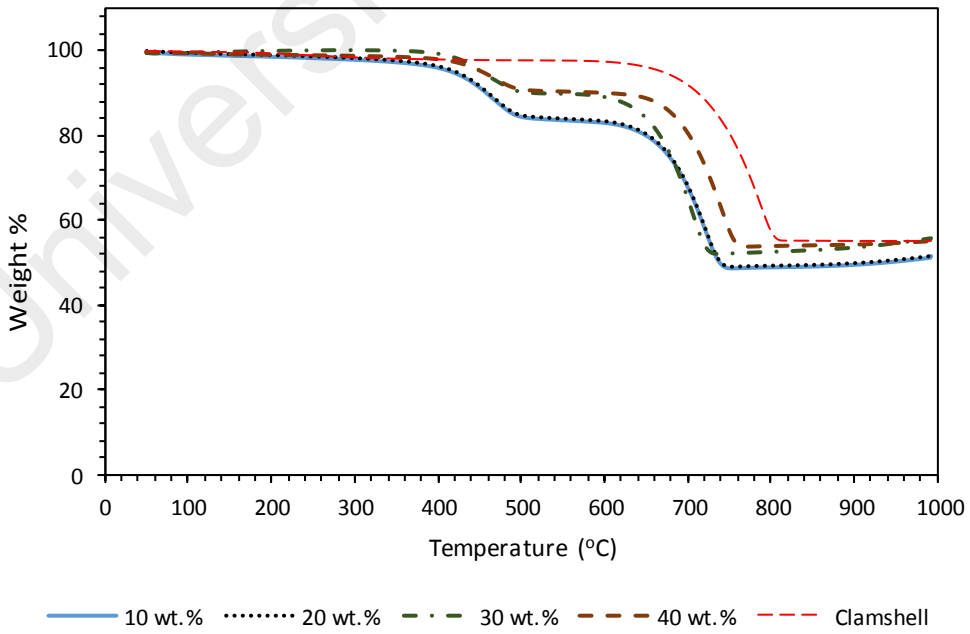

Figure 4.10: TGA analysis for raw clamshell and spent Co-CaO catalysts for 10-40 wt.% Co dosage

Catalyst reusability is an important stability features of the catalyst system for long term usage in large scale production. In the present study, catalyst re-activation for spent Co-CaO (different Co concentration: 10, 20, 30 and 40 wt.%) was investigated for deoxygenation study (Figure 4.11a-b). The spent Co-CaO catalyst were re- activated via hydrothermal treatment using hexane to removed oily coating, followed by thermal activation at 800◦C for 1 h to convert inactive $CaCO_3$ phases into active CaO phases. Results showed that the hydrocarbon yields for reactivated catalysts were comparable as fresh Co-CaO catalyst, while gasoline selectivity was slightly reduced, which indicated that the treated catalyst capable to remain the active sites for further reaction.

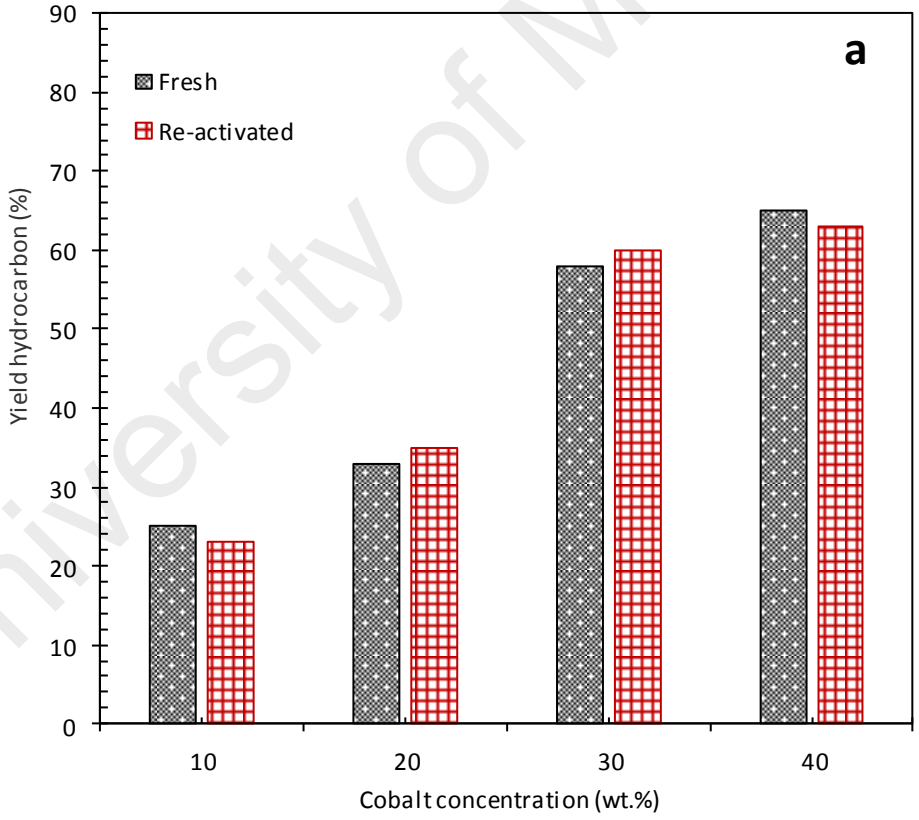

Figure 4.11: Effect of fresh and re-activated Co-CaO catalyst (different Co concentration) toward (a) hydrocarbon yield and (b) gasoline and diesel selectivity

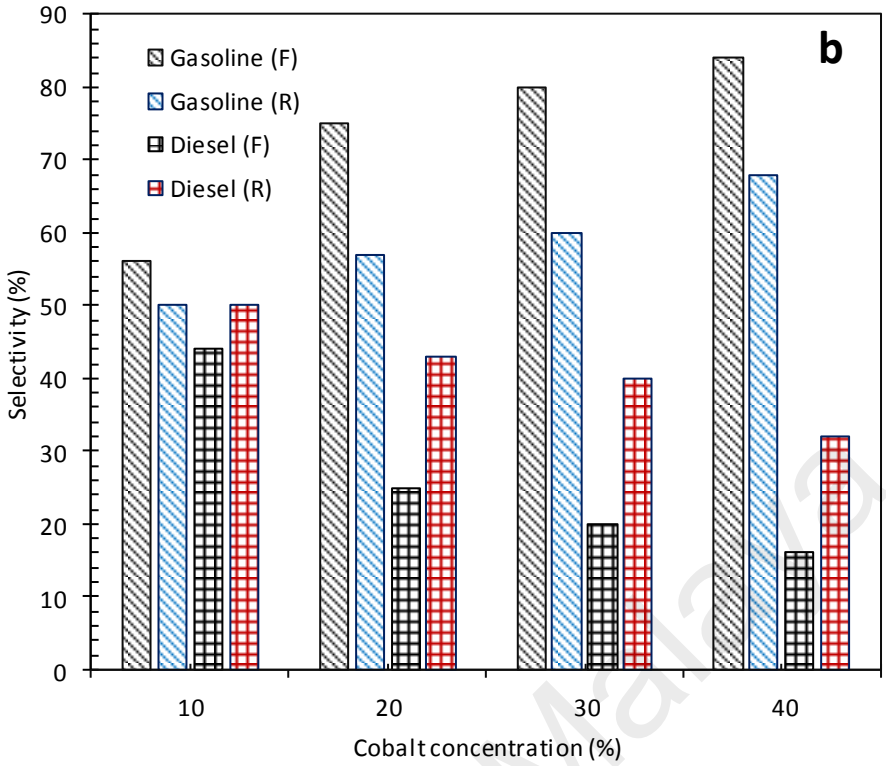

Figure 4.11, continued: Effect of fresh and re-activated Co-CaO catalyst (different Co concentration) toward (a) hydrocarbon yield and (b) gasoline and diesel selectivity

Catalytic activity of Co-CaO (as a microporous catalyst) was further compared with mesoporous-zeolite supported catalyst (H-ZMS5 zeolite) (Lima et al., 2004;Guo et al., 2009) and noble metal-based catalyst (Rh/C) (Wildschut et al., 2010) (Table 4.5). The summary shows Co-CaO catalysed reaction capable to render better hydrocarbon yield via deoxygenation reaction instead of reaction catalysed by mesoporous zeolite (H-ZMS5) and noble metal-based catalysts (Ru/C). In additional, the Co-CaO yielded deoxygenated liquid product rendered lowest acid value, which indicated that the presence of catalyst basicity-acidity successfully cracked majority of the fatty acids and deoxygenized the intermediate into hydrocarbon products. Moreover, it also found that deoxygenation reaction without presence of H_2 gas rendered comparable hydrocarbons yield as hydrodeoxygenation reaction. This prove that deoxygenation reaction is highly efficient as hydrodeoxygenation reaction in removing of oxygen content via cracking-deCOx pathways. The tendency of catalyst deactivation is one of the greatest challenge

to influence deoxygenation activity. It was observed that Co-CaO catalyst showed maximal resistance to coke-induced deactivation with < 10 wt.% of coke as compared to other catalysts. Thus, it is important to note that the Co-CaO catalyst derived from low cost waste material is economically effective as compared to expensive mesoporous zeolite and noble metal-based catalyst.

Table 4.5: Comparison studies of Ca-based, mesoporous zeolite and noble metal catalyst in catalytic deoxygenation and hydrodeoxygenation

Properties	**Present study**	**Literatures**		
Type of catalyst	Microporous Ca-based	Mesoporous zeolite		Noble metal
Catalyst	Co-CaO	H-ZMS5 zeolite (Lima et al., 2004)	H-ZMS5 zeolite (Guo et al., 2009)	Rh/C(Wildschut et al., 2010)
Type of reaction	[a]DO	[a]DO	[a]DO	[b]HDO
Type of oil	Triolein	Bio-oil	Soybean oil	Beech wood oil
Hydrocarbon yield [%]	65	60	<49	>60
Acid value [mg KOH/g]	31	116	[c]N/A	[c]N/A
Coke [wt.%]	8.2	[c]N/A	33.1	8.4

[c]N/A = Not available

4.5 Conclusion

Production of hydrocarbon-based biofuel was prepared via deoxygenation of triolein in the presence of clamshell-derived CaO supported Co- and W- catalysts. The presence of acid-base effect of Co-CaO and W-CaO were favour for the cracking and deCOx reactions, where majority paraffin-based hydrocarbons in the range of C_8-C_{17} was obtained. Besides, Ca-based catalysed reaction rendered higher selectivity towards gasoline products (C_8-C_{12}) as compared to that of diesel ranged products (C_{13}-C_{17}). Amongst the catalysts, Co-CaO with Co content of 40 wt.% showed the highest hydrocarbon yield (65%) with gasoline fraction of 84% under optimum conditions: 5 wt.% catalyst, 45 min, 350 ^oC at partial vacuum condition. In addition, the strong stability of spent Co-CaO system was potentially to be reactivated for reusability as the

high acid density of catalyst favour to oxidation reactivation process by transformed inactive $CaCO_3$ into active CaO catalyst.

CHAPTER 5: CATALYTIC DEOXYGENATION OF TRILGYCERIDES TO GREED DIESEL OVER MODIFIED CaO-BASED CATALYSTS

Chapter 5 is sets out its purpose, viz. the continuation of Chapter 4. Apparently, mild acidic catalyst (Co-CaO) catalyst showed high deoxygenation activity as compared to stronger acidic catalyst (W-CaO). Thus, the study on a series of mild acidic transition metals (ie: Ni, Zn and Fe) are required. Overall, the reaction were proceed under inert N_2 flow condition instead of vacuum condition. This is because deoxygenation via selective decarboxylation/decarbonylation (deCOx) could be controlled effectively than under partial vacuum condition. Thus, more formation of diesel-range product will be obtained instead of gasoline-range product. The present chapter had been published in *Journal of RSC Advances".* The work presented with title of ***"Catalytic deoxygenation of triglycerides to green diesel over modified CaO-based catalysts*"** and the authors including N. Asikin-Mijan, H.V. Lee, J.C. Juan, A.R. Noorsaadah and Y.H. Taufiq-Yap.

5.1 Introduction

Production of liquid biofuel is becoming more important, this is mainly due to the increase of global consumption of fossil fuel especially in the transportation sector which has contributed to the depletion of natural petroleum fossil resources. New alternative solution is very much needed to sustain the future fuel production. Diesel is an important liquid hydrocarbon-based fuel derived primarily from fractional distillation of petroleum crude oil. This type of fuel is comprised of medium to long chain hydrocarbons within the range of (C_{13}-C_{20}) with specific concentration of aromatic additive as octane enhancers (Song et al., 2015). Diesel is preferable by the industry users as it converts 20% more fuel energy to actual energy compared to gasoline (range (C_8-C_{12})) and subsequently produces less waste heat. The higher cetane

number of diesel also results in shorter ignition delaying time which will help to achieve complete combustion. Moreover, it also lasts longer and safer as diesel not release as much fume as gasoline. The global demand on diesel has increased tremendously while world crude oil reserve is continuously depleting. An alternative route for diesel production from non-fossil sources is a necessity. Deoxygenation (DO) of vegetable oil is one of the suggested alternative routes to produce green-diesel. Deoxygenation of vegetable oil is one of the suggested alternative routes to produce renewable green diesel. The deoxygenation of vegetable-based feedstock is typically related to cracking of hydrocarbon chain with the hydrocarbon chain being broken and the oxygen being removed in the form of CO_2/CO via decarboxylation/decarbonylation (deCOx) reactions. The produced green diesel presented similar properties to conventional petroleum derived fuels and deoxygenation also is an economical process as there is no H_2 is used as compared to well-established refinery process (hydrodeoxygenation(HDO)). Hydrodeoxygenation, is a process involves an exothermic reaction which removes oxygen in the form of water in the presence of H_2 (Ding et al., 2014).

The studies on the effect of alkali metal and alkaline earth metal, especially on Mg (Chiam and Tye, 2013) and Ca metals were widely investigated to improve the quality of diesel via deoxygenation reaction due to their unique basic properties. It was found CaO helped in oxygen removal by being able to absorb more CO_2 in gas phase (Lin et al., 2010). Moreover, application of basic over calcined dolomite (MgO-CaO) catalyst also showed reduction of tar formation with an increase of H/C ratio (Lin et al., 2010). In brief, these observations indicated that MgO and CaO presence will produce a better route for oxygen removal in the form of CO_2 through catalytic deoxygenation. Eventhough those basic catalyst was found to be reactive but acidic sites of catalyst is

required for enhancing the cracking reaction. Recently, we have studied the catalytic deoxygenation over CaO support Co and W catalyst and found this catalyst is highly active toward C-C cleavage for formation of gasoline-range product via secondary reaction of deoxygenation reaction (cracking reaction). In order to enhance the deoxygenation reaction via desired deCOx reaction through C-O cleavage, more studies on the usage binary metal oxide system (TMO-doped CaO) is necessary for producing green fuel rich diesel-range hydrocarbon. In this present work, integrated catalysts with binary metal oxide system (TMO-doped CaO: Ni-CaO, Zn-CaO, Fe-CaO and Co-CaO) were prepared via impregnation method. The CaO derived from waste clamshell was used as the catalyst support for the TMO promoters and all the reaction were proceed under N_2 flow condition. The physicochemical properties of prepared catalysts were further investigated by XRF, XRD, SEM, FESEM-EDX mapping, BET and TPD analysis. In addition, chemical composition and product distribution of deoxygenized liquid products were analyzed using FTIR, GC-FID, GC–MS and CHNOS analysis.

5.2 Literature Review

Transition metal oxides (TMOs) are important materials and widely applied for various processes such as oxidation, dehydrodeoxygenation, selective/reduction, ammoxidation, metathesis and etc. TMOs is a good promoter in catalyst synthesis which acted as an alternative catalyst family to noble metals such as Pt and Pd in the field of catalytic cracking activity. Promoter played an important role in tuning product selectivity towards monofunctional hydrocarbon intermediates, which then further proceeded to desired hydrocarbon-like chain (Chen et al., 2012). Application of noble metals in catalytic cracking activity is still being widely explored and studied but it is still unattractive due to the high cost constrain (Zhang et al., 2013). Thus, it is more reasonable to develop a new inexpensive catalyst. Several literatures had reported that

the rule over transition metal catalysts in enhancing the formation of unsaturated hydrocarbon from saturated fatty acid and fatty acid ester. Several studies had reported on the application of bimetallic fraction cooperation of Co/Pt, Co/Mo, Ni/pristine and Fe/MSN to enhance the effectiveness of converting model triglycerides compound into desired hydrocarbons (Dietrich et al., 2014;Tymchyshyn et al., 2013;Chen et al., 2013;Kandel et al., 2014). These reports had successfully proved that TMOs are active and selective in the mentioned reactions because of its unique properties such as existence of both basic and acid properties, cationic and anionic vacancies and high mobility of lattice oxygen (He and Wang, 2014)

5.3 Experimental

5.3.1 Material

The CaO was prepared from waste clamshell based on previous study (Asikin-Mijan et al., 2015c). The nickel (II) nitrate hexahydrate ($Ni(NO_3)_2.6H_2O$) with purity >99% was obtained from R&M Company. Iron (III) nitrate nanohydrate ($Fe(NO_3)_3.9H_2O$) with 99% purity was purchased from Analar, zinc (II) nitrate hexahydrate ($Zn(NO_3)_2.6H_2O$) with 98% purity, cobalt (II) nitrate hexahydrate ($Co(NO_3)_2.6H_2O$) with 99.9% purity, triolein (glyceryltrioleate) with 65% purity, standard solution of alkane and alkene (C_8–C_{20}) and internal standard 1-bromohexane with purity >98% (GC grade) were purchased from sigma Aldrich. The *n*-Hexane (GC grade) with purity >98% from Merck was used for dilution.

5.3.2 Catalyst development

Calcium-based catalysts were synthesized using wet impregnation method. 5 g of clamshell-derived calcium oxide (CaO) was impregnated with an aqueous solution of metal salts containing 20 wt.% concentration of nickel (II) nitrate hexahydrate and the

mixture was stirred for 6 h. The mixture was then dried in the oven at the temperature of 100 ^{o}C for 24 h. The dried samples were grounded into fine powder before thermally activated at the temperature of 900 ^{o}C for 2 h under atmosphere condition. The 900 ^{o}C calcination temperature is in agreement with Taufiq-Yap et al., (2012). The procedures above were repeated using cobalt (II) nitrate hexahydrate, iron (III) nitrate 9-hydrate and zinc (II) nitrate hexahydrate. The samples were denoted as Ni-CaO, Zn-CaO, Fe-CaO and Co-CaO.

5.3.3 Catalyst characterization

X-ray fluorescence (XRF) spectrometry was used to trace elemental composition in the catalyst. In this study, the XRF (Philips PWI404) was equipped with a scandium anode tube. The powder X-ray diffraction (XRD) analysis was carried out to identify the crystallography of the mixed metal oxide catalysts. The XRD analyses were performed using Shimadzu diffractometer model XRD-6000. The specific surface area and pore distribution of the catalysts were determined by Brunauer-Emmet-Teller (BET) method with N_2 adsorption/desorption analyzer using Thermo-Finnegan Sorpmatic 1990 series. The catalysts were degassed overnight at 150 ^{o}C to remove moisture and foreign gases on the surfaces of the catalysts. Adsorption and desorption processes of N_2 on the catalysts surfaces were analyzed in a vacuum chamber at −196 ^{o}C. The basicity and basic strength distribution of the catalysts were studied by using temperature-programmed desorption with CO_2 as probe molecule. TPD-CO_2 experiment was performed using a Thermo Finnegan TPDRO 1100 apparatus equipped with a thermal conductivity detector. Catalysts (0.05g) were pre-treated with N_2 gas flow for 30 min at 250 ^{o}C to remove the moisture in the sample. This was followed by CO_2 gas flow for 1h under ambient temperature to allow adsorption of CO_2 onto the surfaces. The excess CO_2 was subsequently flushed with N_2 gas flow at 20 mL/min for 30 min. The

desorption of CO_2 from the basic sites of the catalysts was detected by thermal conductivity detector (TCD) in helium gas flow (30 mL/min) from 50 ^oC to 900 ^oC and hold for 30 min. The acidity of the catalyst was determined by using ammonia (NH_3) as probe gas. The adsorption and desorption of NH_3 utilized the same procedures as in TPD-CO_2 method. The amount of basicity/acidity of the catalyst were determined using peak area of CO_2/NH_3 desorption peaks. The temperatures of the peak maximum (T_{max}) at which the desorption of CO_2/NH_3 had occurred were used to study the characteristics and the basic/acid site distribution of the active sites for the catalysts. The morphology of the catalysts were then investigated by using scanning electron microscope (SEM) (SEM JOEL 6400). The determination of elemental compositions such as Ca, Ni, Zn, Fe and Co on the surface of catalysts were determined by FESEM-EDX mapping analysis using LEO 1455 VP electron microscope via Rayny EDX-720 spectrometer.

5.3.4 Activity test

Catalytic deoxygenation of triolein was carried out in a 250 ml two-necked round bottom flask equipped with magnetic stirrer bar, heating mantle and connected to a distillation system. Approximately 20 g of triolein and 5 wt.% of synthesized catalyst was added into the flask. The deoxygenation reaction of triolein was performed by heating the reaction medium to 350 ^oC under inert condition (N_2 flow = 20 cc/min) for 60 min. The cracked/deoxygenated product was then collected in a receiver flask and at the end of the test, the reactor was cooled to room temperature using an external water circulation cooling system and the liquid products was further weighted and analyzed using acid number (AN) test, Fourier transform infrared spectroscope (FTIR), gas chromatography flame ionization detector (GC-FID) and gas chromatography mass spectrometry (GCMS). All the reactions were repeated 3 times and the reported data were the mean values of the 3 repetitions. The analyses of mass balance were conducted

in all reactions. The solid catalysts were separated by mixing the liquid residue inside the flask with hexane to determine the mass of the retained products (char+residue) after reaction. The hexane was removed via rotary evaporator and the dark viscous liquid was identified as (char + residue). The analyses of carbon balance were conducted by collecting the liquid product every 15 min over a period of 135 min. The changes in the hydrocarbon product and acid values were observed by GC-FID and total acid number (TAN) test.

5.3.5 Experimental design

The optimization studies were carried out via the Box–Behnken design to maximize the hydrocarbon yield from triolein by optimizing the 3 combinations of variables. Three independent variables such as A: reaction temperature (300–390^{o}C), B: reaction time (60–120 min) and C: catalyst loading (1–9wt.%) was applied. The coded and non-coded (actual) levels of the independent variables are given in Table 6.1. All the 17 experiments were augmented with 5 replications and were carried out at the center points to evaluate the pure error.

Table 5.1: Independent variables used for Box–Behnken design in deoxygenation of triolein

Factor	Coding	Units	Levels		
			-1	0	1
Reaction temperature	A	^{o}C	300	330	360
Reaction time	B	min	60	90	120
Catalyst loading	C	wt.%	3	5	7

In the present study, the Design Expert 6.0.4 software was used to obtain the regression and graphical analysis of the data. The maximum values of hydrocarbon yield were taken as the response of the design experiment for deoxygenation process. The experimental data obtained from the above procedure was analyzed by the response

surface regression using polynomial equation Eq. (5.1), where Y is the predicted response; β_o, β_j, β_{ij} and β_{jj} are constant coefficients; x_i and x_j are the coded independent variables or factors; ε is random error.The equation was also being validated by carrying out confirmatory experiments.

$$Y = \beta o + \sum_{j=1}^{k} \beta_j x_j + \sum_{i<j} \beta_{ij} x_i x_j + \sum_{j=1}^{k} \beta_{jj}{}^2 x_j + \varepsilon \quad (5.1)$$

5.3.6 Product analysis

The deoxygenated liquid products were identified using standard alkanes (C_8-C_{20}) and were quantitatively analyzed in gas chromatography (Shimadzu GC-14B) equipped with a HP-5 capillary column (length: 30 m × inner diameter: 0.32 mm × film thickness: 0.25 μm) and a flame ionization detector (FID) operating at 300 ^oC. The liquid product was diluted with GC grade *n*-hexane prior to the yield analysis. 1-bromo hexane was used as internal standard for quantitative analysis. An aliquot of 1 μL sample was injected with into the GC column. The injection temperature was at 250 ^oC. Nitrogen gas was served as the carrier gas. The initial temperature of the oven was set at 40^oC and held for 6 min, then ramped up to 270 ^oC at the heating rate of 7 ^oC/min. The hydrocarbon yield and product selectivity were determined by comparing the retention time of standard hydrocarbons (C_8-C_{20}) with experimental-based products which shown Appendix A. In the present study, the catalytic performances of the catalysts was studied by determining the yield of saturated and unsaturated straight-chain hydrocarbons (*X*) (Eq. 5.2) (Asikin-mijan et al., 2016;Asikin-Mijan et al., 2016b).

$$X = \frac{\sum n_o + \sum n_i}{\sum n_z} \times 100\% \quad (5.2)$$

Where, n_o= Total area of alkene (C_8–C_{20}), n_i = Total area of alkane (C_8–C_{20}), n_z= Total area of the product.

The hydrocarbon selectivity (S_c) or carbon balance were determined by Eq. 5.3

$$S_{carbon} = \frac{C_o + C_i}{\sum n_o + \sum n_i} \times 100\% \quad (5.3)$$

Where, S_{carbon}= Hydrocarbon selectivity or carbon balance (%), C_x= Area of desired range of carbon number, n_x = Area of hydrocarbons

The analyses were conducted for 3 times to confirm the reproducibility of the results. The product distribution in the liquid product were qualitatively characterized using GC-MS (model SHIMADZU QP5050A) equipped with a non-polar DB-5HT column (30 m × 0.32 mm × 0.25 µm) with split-less inlet. The samples were diluted with GC grade *n*-hexane (purity >98%) to 100 ppm. The generated fraction peaks from the GC-MS spectrum were identified through the National Institute of Standards and Testing library. The compound identification was based on a probability match equal to or higher than 95%. The yield of the organic compound (hydrocarbon fractions, carboxylic acid, alcohol and etc.) was determined using Eq. 5.4:

$$S_{product} = \frac{C_y}{\sum n_y} \times 100\% \quad (5.4)$$

Where, $S_{product}$ = Yield of organic compound (%), C_y = Area of the desired organic compound, n_y = Total area of organic compounds

The degree of oxygen to carbon (O/C) atomic ratio and degree of hydrogen to carbon (H/C) atomic ratio were determined by molar O/C ratio and molar of H/C ratio of the obtained deoxygenated product. The similar method has been reported by several high inter-disciplinary article focused on deoxygenation reaction (Payormhorm et al., 2013)(Asikin-Mijan et al., 2015a). The results were depicted in terms of H/C and O/C ratio in Krevelen diagram. The acid values of the feedstock and liquid products were determined using standard method of AOAS Cd 3d-63. It is important to determine the amount of carboxylic acid/fatty acid in deoxygenated product. The acid value was calculated using equation as shown in Eq. 5.5.

$$Total\ acid\ number\ (TAN) = (V_f - V_i)N\frac{56}{W_{oil}} \quad (5.5)$$

Where, V_f = The volume of titrant (ml) consumed by the oil sample, V_i = the volume of titrant (ml) consumed by 1 ml of spiking solution at the equivalent, N = Concentration of HCI W_{oil}= Mass of the sample in grams, 56 = Molecular weight of KOH.

Furthermore, Fourier Transform–Infrared Spectrometer (FT-IR) analysis was performed using PerkinElmer (PC) Spectrum 100 FTIR with a resolution of 4 cm^{-1} in the IR range of 300-4000 cm^{-1} which principally followed the concept of Attenuated Total Reflection (ATR) method. This analysis was to determine the chemical functional group contained in the liquid product.

5.4 Results and discussion

5.4.1 Catalyst characterization

The bulk elemental composition for transition metal oxide-doped with CaO was studied by using XRF analysis (Table 5.2). The results showed that the presence of

transition metal oxides (NiO, ZnO, Fe_2O_3 and Co_2O_4) at 15-19 atomic% for each catalyst. Calcium (Ca) content was found as the major element (>80 atomic%) in all catalysts. Thus, experimental ratio (TMO:CaO) of synthesized catalysts (20% of active metal oxide and 80% of CaO) were in agreement with the intended ratio, which is 2:8. The TMO-doped catalysts were characterized using FESEM-EDX mapping (Figure 5.1) to further verify the dispersion of Ca Ni, Zn, Fe and Co on the surface of support. The result found Ca-rich regions was clearly observed. The speckled pattern of TM species indicated that the uniform distribution of metallic active sites over the CaO matrix particles contributed to the efficient reactions. Furthermore, the EDX analysis reported that the TMO-doped CaO catalyst rendered the average of 77-87±3.1 wt.% of calcium, 14.2±2.1 wt.% of Ni for Ni-CaO, 10.4±3.2 wt.% of Zn-CaO, 22.9±2.4 wt% of Fe-CaO and 14.9±3.1 wt.% of Co-CaO. The high content of CaO in the TMO-doped CaO catalysts acted as effective basic sites which had enhanced the catalysts stability and simultaneously enhanced the occurrence of deCOx reactions.

XRD analysis of CaO, Ni-CaO, Zn-CaO, Fe-CaO and Co-CaO catalysts were shown in Figure 5.2. The Ca-based catalysts showed intense diffraction peaks of CaO phases and low crystallinity peaks of transition metal oxides phases. Based on the XRD results, all the TMO and CaO were segregately presented in individual metal oxide phases. The XRD characteristic of CaO peaks appeared at $2\theta = 32.21^o$, 37.21^o, 54.34^o, 64.62^o and 67.76^o that supported by JCPDS card no. 00-037-1497. Ni-CaO catalyst showed the presence of XRD peak at 43.76^o, which was attributed to NiO phase (JCPDS card no. 00-047-1049). The Zn-CaO catalyst revealed diffraction peak at 36.76^o, which confirmed the presence of ZnO phase composited in CaO (JCPDS card no. 00-036-1451). Besides, Fe_2O_3 phases from Fe- CaO catalyst exibited at peaks of 25.8^o and 32.61^o, respectively (JCPDS card no. 00-021-0917). While Co-CaO catalyst

showed the presence of Co_2O_4 peak at 33.76° (JCPDS card no. 00-042-1467). Moreover, it is observed that a shifting of the diffraction TMO doped CaO peaks to the higher 2θ values compared to pure CaO. The peak shift is well explained with the presumption that Ca^{2+} lattice parameter (1.06 Å) is partially substituted by the TM lattice (Ni^{2+}:0.55 Å, Zn^{2+}: 0.6 Å, Fe^{3}+: 0.49 Å and Co^{4+}: 0.40 Å) in TMO-CaO catalysts (Shim et al., 2014). The lattice parameter for pure CaO was a =2.407 Å whereas for CaO peak in Ni-CaO, Zn-CaO, Fe-CaO and Co-CaO catalysts were a= 2.39 Å, 2.39 Å, 2.37 Å and 2.38 Å, respectively. These results has suggested that the Ni^{2+}, Zn^{2+}, Fe^{3+} and Co^{4+}cations from TMO-doped CaO were replacing the Ca^{2+}cations in the CaO structure. Therefore, minor content of solid ($TM_{(x)}Ca_{(1-x)}O$) was formed in the solution. As shown in Table 5.2, the crystallite size decreased with the addition of TM metals in CaO catalysts. The crystallite size of cubic phase of CaO catalysts were remarkably decreased from 64 nm to the range of 48-55 nm for TM-CaO catalyst. This indicated that the insertion of the Ni^{2+}, Zn^{2+}, Fe^{3+} and Co^{4+} in CaO lattice would reduce the crystallite size.

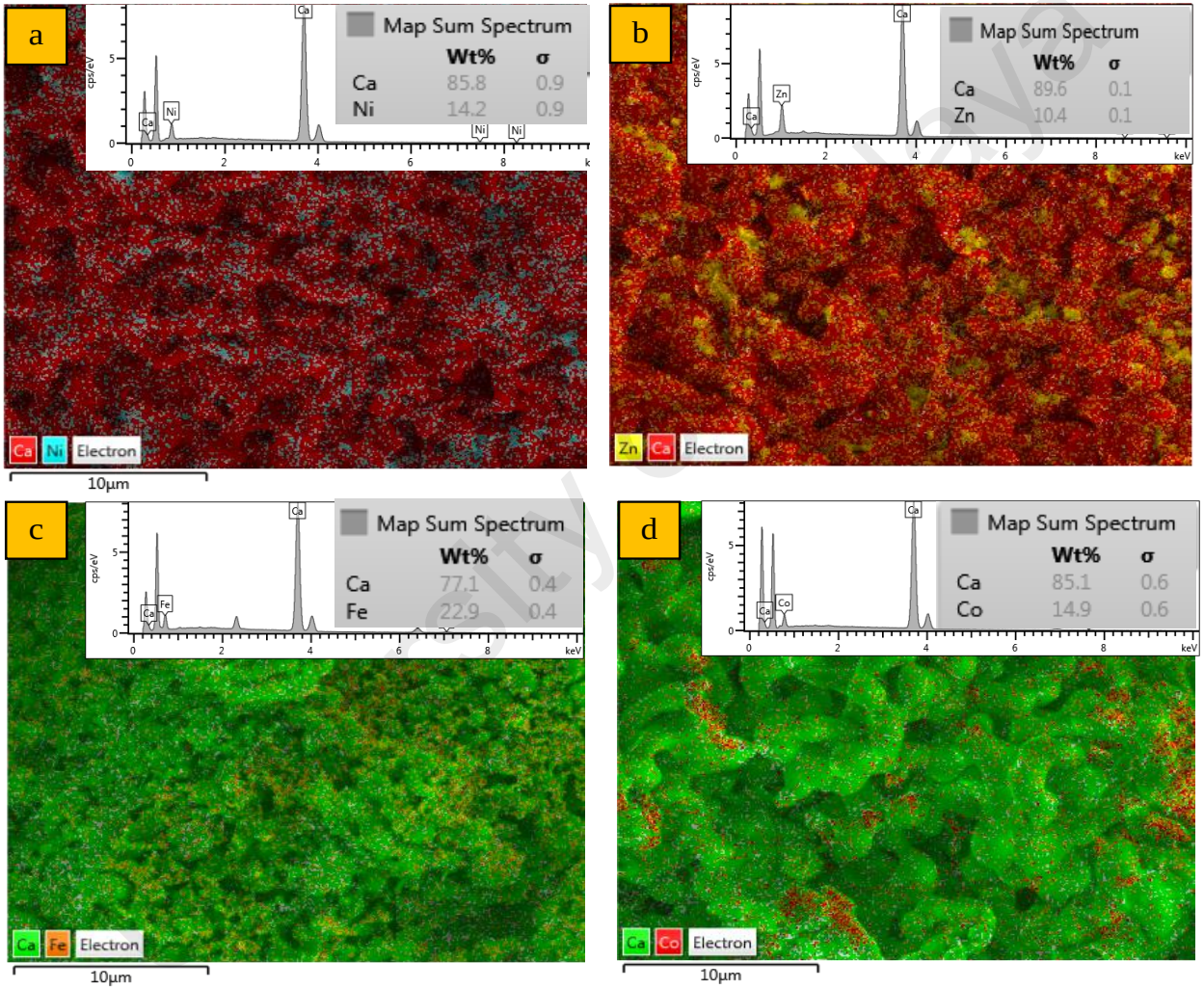

Figure 5.1: FESEM-EDX mapping for (a) Ni-CaO, (b) Zn-CaO, (c) Fe-CaO and (d) Co-CaO catalysts

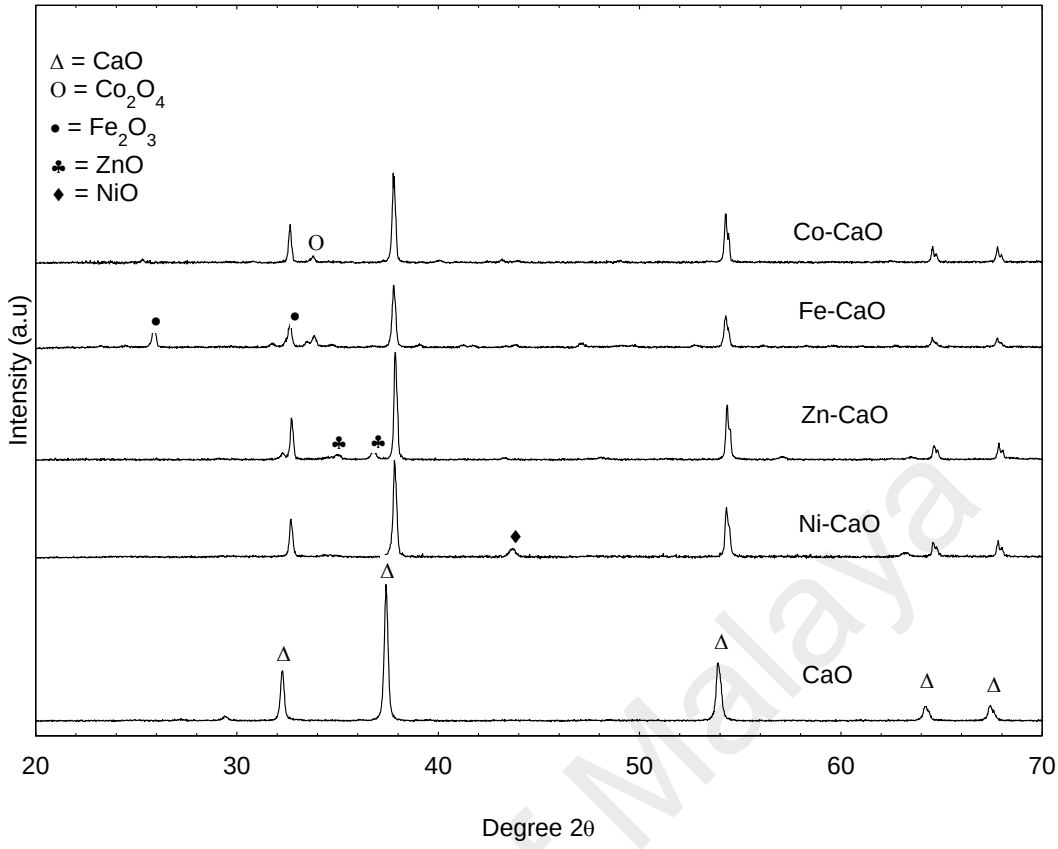

Figure 5.2: XRD diffraction patterns for CaO and TMO-doped CaO catalysts

The textural properties of clamshell-derived CaO and TMO-doped CaO catalysts were summarized in Table 5.2. The surface area of CaO was 9.8 m^2/g, while Ca-based catalysts (Ni-CaO, Zn-CaO, Fe-CaO and Co-CaO) rendered lower specific surface area, which were 7.58 m^2/g, 7.37 m^2/g, 7.88 m^2/g and 7.46 m^2/g, respectively. This finding indicated that the transition metal oxides were successfully impregnated onto the surface of CaO supports and partially covered the CaO (Siahvashi and Adesina, 2013). It is also observed that the pore diameters of all TMO-doped CaO catalysts were increased in the range of 2-188 nm and varied based on different TMO precursor. The results indicated that the catalysts were mainly consisted of mesoporous (2-50 nm) and macroporous (>50 nm) structure. The significant increase of the pore diameters for TMO-doped CaO catalysts was likely associated with the thermal activation temperature of the synthesized precursor which collapsed the pore walls (Lee et al., 2014). This had led to the pitting and erosion on the newly formed TMO-doped CaO

catalyst surfaces. This had provided a wide channel for diffusion of reactant and product into the TMO-doped CaO pores (Chandra Mouli et al., 2011) thus enhanced the catalytic activity.

The SEM micrographs for all synthesized catalysts were shown in Figure 5.3. The CaO prepared from clamshell showed irregular shape with agglomerated structure demonstrated sintering effect of CaO due to high calcination temperature at 900^{o}C (Figure 5.3a) (Sirisomboonchai et al., 2015). However, SEM morphology for all TMO-doped CaO catalysts rendered significant changes of morphology for surface structure. The images for both Ni-CaO and Zn-CaO catalysts revealed that irregular cubic-like structures which were larger in size of particles were observed in Zn-CaO catalyst (Figures 5.3b and 5.3c). Interestingly, the particles of Fe-CaO exhibited flat flakes-like structures, which had changed the dominant structure of CaO after the impregnation process (Figure 5.3d). In the case of Co-CaO, the aggregated particles consisted of interconnected sheet-like structure with rough surfaces (Figure 5.3e). The TMO-doped CaO catalysts were found to comprise of large cluster, which had resulted in lower surface area of the catalyst which is shown in Table 5.2.

Table 5.2: Elemental composition, crystallite sizes, textural properties, acidity and basicity profile of synthesized catalysts

Catalyst	XRF			XRD		BET		TPD			
	[a]Elemental composition (%)			[b]Crystallite size (nm)		[c]Surface area (m^2/g)	[c]Pore size diameter range (nm)	[d]CO_2 desorption Temperature (^oC)	[d]Basic sites (µmol/g)	[e]NH_3 desorptionTemperature (^oC)	[e]Acid sites (µmol/g)
	CaO	TMO	Others*	CaO	TMO						
CaO	98.81	-	1.19	64.29±0.21	-	9.8	2.86-78.32	636	548.52	-	-
Ni-CaO	81.96	15.70	0.48	50.50±0.18	38.97±0.16	7.58	2.88-121.94	650	549.71	467	106.66
Zn-CaO	84.11	17.81	0.19	55.40±0.11	33.32±0.14	7.37	2.96-152.35	664	624.57	151,442	73.91, 100.23
Fe-CaO	81.75	19.37	0.44	48.02±0.16	40.65±0.17	7.88	2.87-188.68	631	523.74	456	32.13
Co-CaO	80.29	17.56	0.34	53.54±0.13	36.71±0.18	7.46	2.96-116.50	603,826	260.79, 307.77	488,840	257.00, 486.91

Determined by XRF analysis, *Others minor component of metal oxides: Sc, Sr,Cu,Br,K and Fe
Determined by using Debye–Scherrer equation. All determinations were carried out twice for each sample.
Determined by BET analysis
Determined by TPD-CO_2 analysis
Determined by TPD-NH_3 analysis

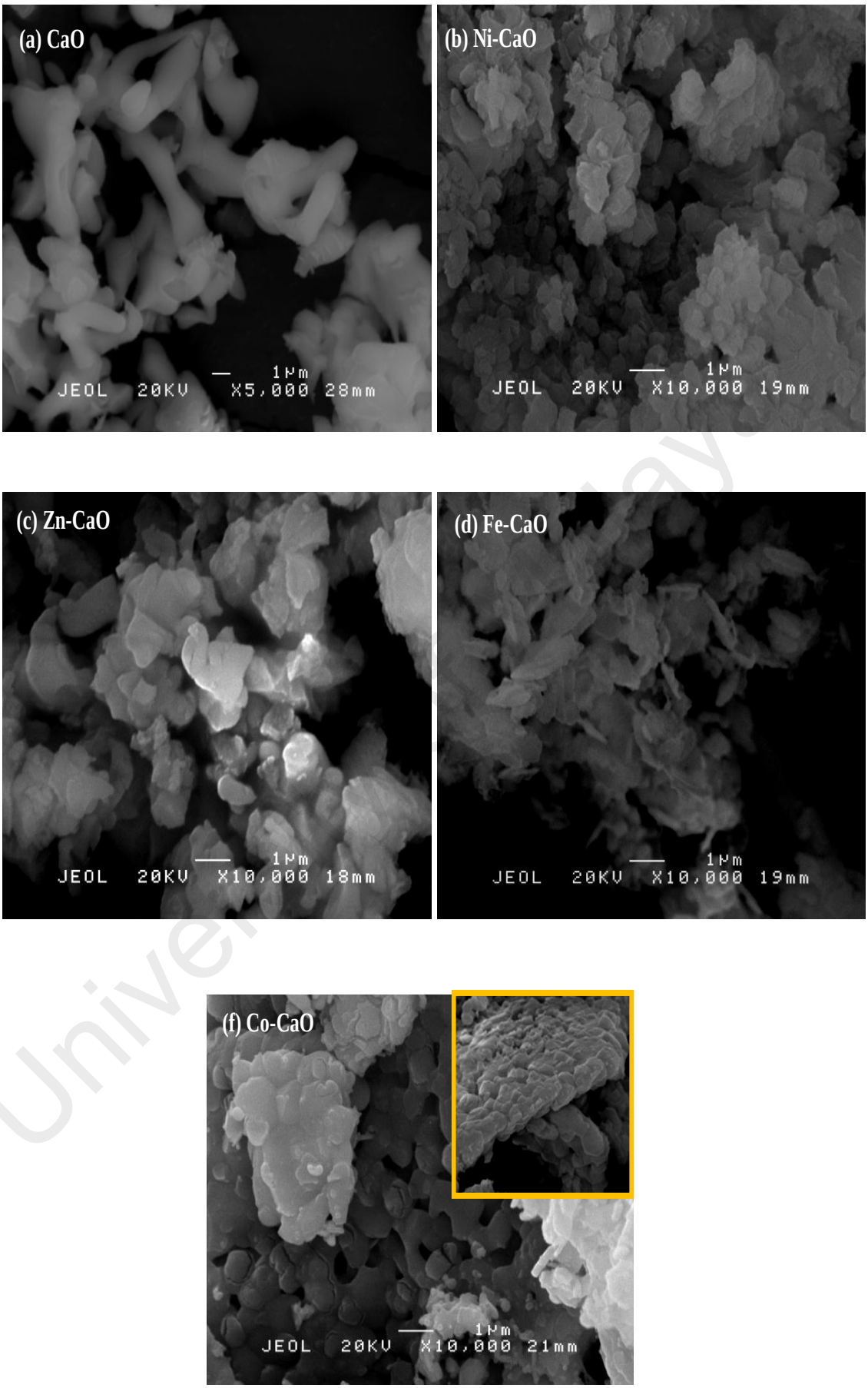

Figure 5.3: SEM images for CaO and TMO-doped CaO catalysts

The results of XRF and XRD showed that CaO is the dominant metal oxide in the prepared catalysts (Ni-CaO, Zn-CaO, Fe-CaO and Co-CaO). Thus, it was estimated that the catalysts were strong base contributed by Ca^{2+}-O^{2-} phases(Asikin-Mijan et al., 2015b). The basicity study of TMO-doped CaO catalysts was determined by TPD-CO_2 analysis (Figure 5.4a and Table 5.2). TMO-doped CaO catalysts showed broad and intense desorption peak at temperature higher than 500 ^oC. This had proven the presence of stronger bronsted basic sites(Wu et al., 2014). Furthermore, basicity trend of synthesized catalysts in the order of Zn-CaO>Co-CaO>Ni-CaO>CaO>Fe-CaO has showed that Zn, Co and Ni-doped CaO were capable of rendering higher amount of basicity than CaO catalyst. This is due the interaction between bi-metal ions, which had promoted synergy effect by enhancing the basicity between active TMO (Zn, Co and Ni) and CaO (Nair et al., 2012). The acidity profile of synthesized catalysts was studied using TPD-NH_3 analysis. TMO-doped CaO catalysts (Ni-CaO, Zn-CaO and Fe-CaO) showed low intensity on NH_3 desorption peaks in the range of 151 ^oC to 450 ^oC (refer to Figure 5.4b and Table 5.2). This has suggested that the presence of a considerable amount of weak and medium acidic sites on the surfaces of catalysts (Kandel et al., 2014). The presence of acid sites were attributed to Brønsted acid sites associated with the bridging of OH groups and/or Lewis acid sites associated with the presence of transition metal ions [$Ni^{2+,}$ Zn^{2+}, and Fe^{3+}] (Kandel et al., 2014;Taufiq-Yap et al., 2012). From the findings, the acidity of TMO-CaO catalysts were in the order of Co-CaO>Zn-CaO>Ni-CaO>Fe-CaO. Co-CaO catalyst rendered the highest acidity (743.91 μmol/g) with presence of medium and strong acid strength, which had proven the presence of synergy effect between the bonding of Co_2O_4 and CaO.

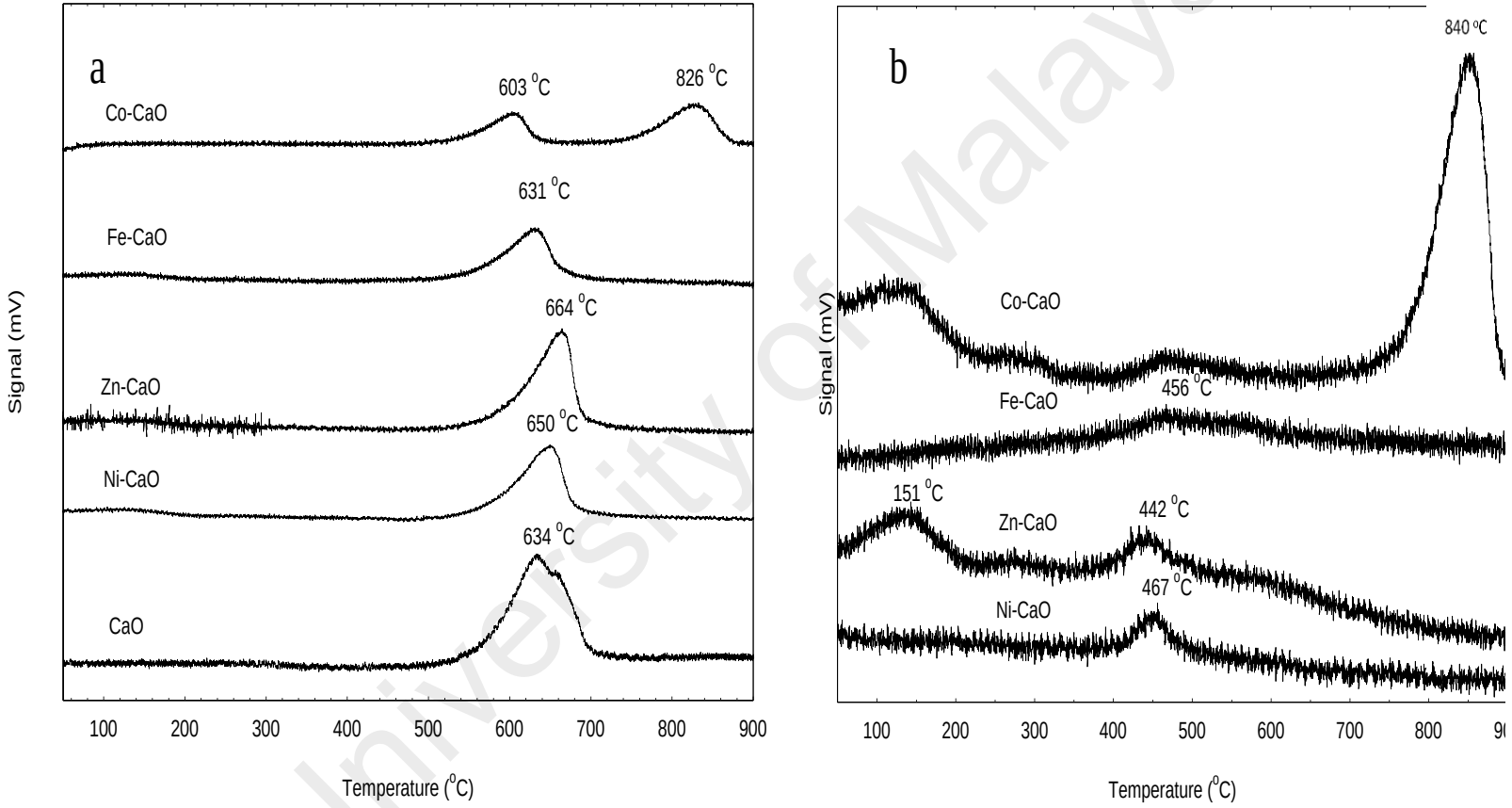

Figure 5.4: (a) TPD-CO_2 and (b) TPD-NH_3 profile for CaO and TMO-doped CaO catalysts

5.4.2 Deoxygenation activity

5.4.2.1 Chemical composition study

The catalytic activity of synthesized Ca-based catalysts (Ni-CaO, Zn-CaO, Fe-CaO, and Co-CaO) was investigated via deoxygenation of triolein at the reaction conditions of 350 ^{o}C, 60 min, 5 wt.% of catalyst loading under inert condition. Furthermore, the bulk metal oxide catalysts (CaO, NiO, ZnO, Fe_2O_4, Co_2O_4) (TM-oxides) were used as comparison study. FTIR analysis was performed to study the chemical functional group of triolein (feedstock) and deoxygenized products (Figure 5.5). The FTIR spectrum of triolein showed the absorption band at 3600 cm^{-1} (-O-H), 2925 cm^{-1} and 2858 cm^{-1} (-CH), 1749 cm^{-1} (-C=O) stretching, 1455 cm^{-1} ($-CH_2$) scissoring, 1398 cm^{-1} ($-CH_2$), 1285 cm^{-1} (-C-O-C) and 726 cm^{-1} –(CH)n- bending for alkane (Asikin-Mijan et al., 2015a). FTIR results for triolein and liquid deoxygenated product showed that all spectrum were normalized by the intensity of the absorption band centered at 2858–2950 cm^{-1}(CH stretching, aliphatic). It was noteworthy to mention that the liquid deoxygenated products showed significant shifting of absorption band from 1749 cm^{-1} that belonged to C=O (ester) in molecule triglycerides to the absorption band at 1715 cm^{-1} which was attributed to C=O of carboxylic acid). This implied the occurrence of cracking reaction of ester to intermediates products of carboxylic acid. This fact was in agreement with the acid value test, where the acidity of the triolein was increased drastically from 5 mg KOH/g to >100 mg KOH/g after deoxygenation reaction (Figure 5.6a). Besides, deoxygenation reaction also resulted in the absent of C-O-C absorption features at 1285cm^{-1} which belonged to carbonyl group in triolein, these was in agreement with the removal of oxygen species via deCOx pathways.

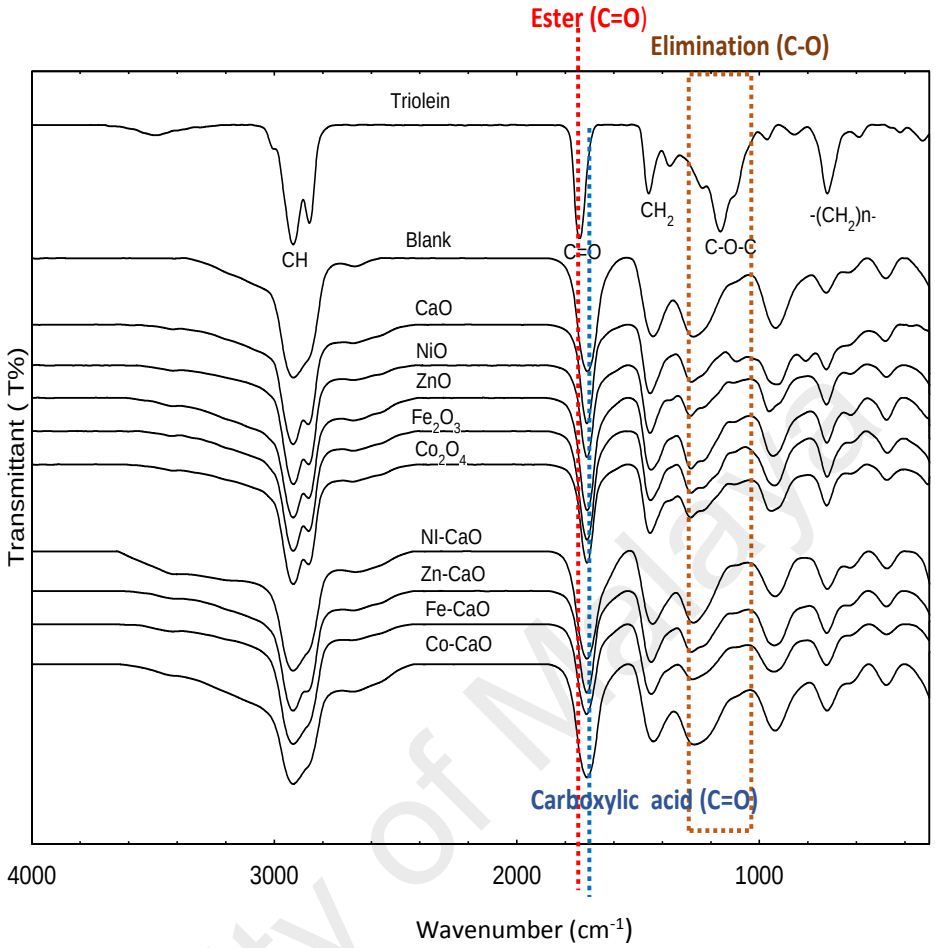

Figure 5.5: FTIR spectra of triolein and deoxygenated liquid products for both blank and different catalysed reaction

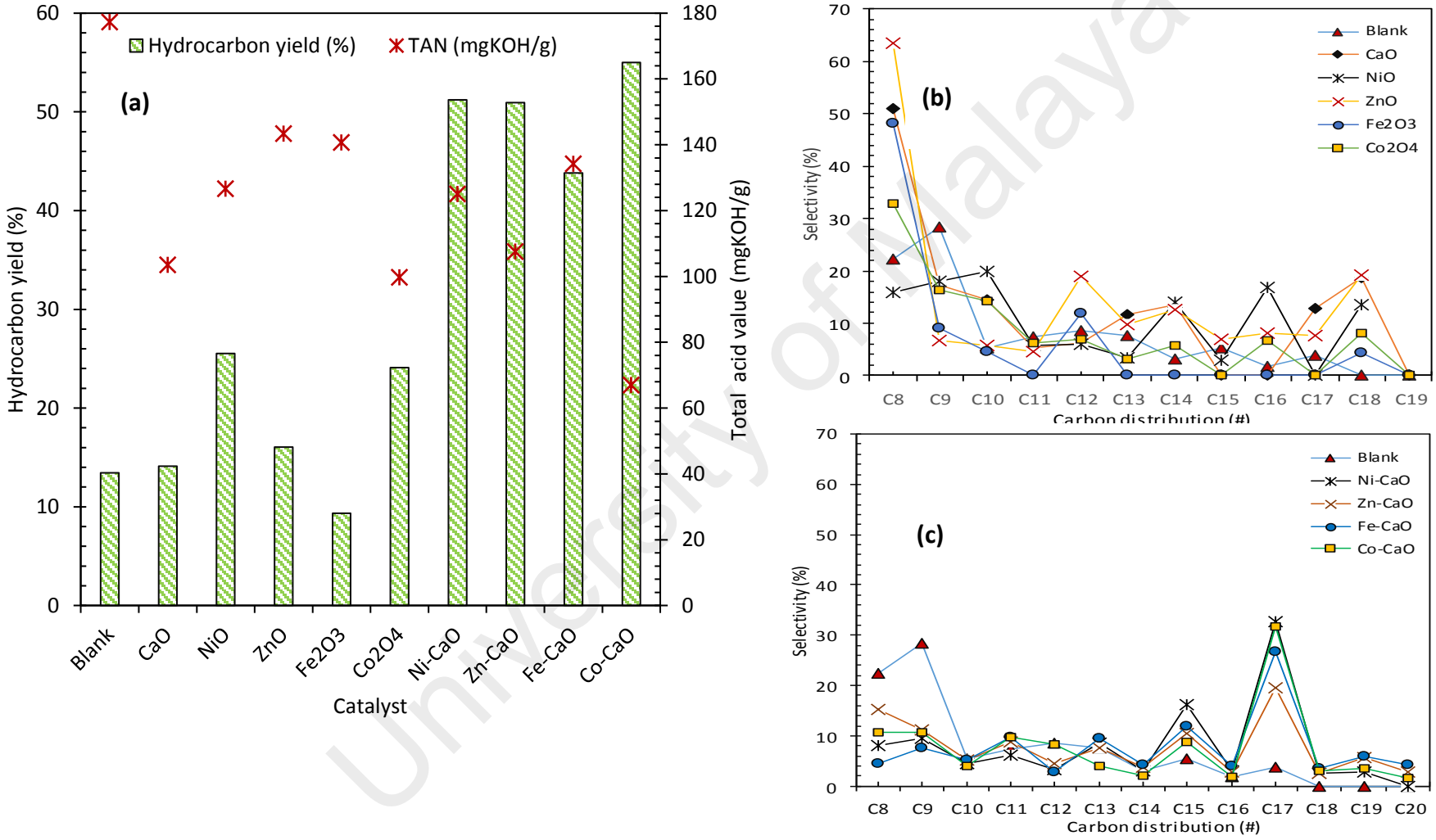

Figure 5.6: (a) Hydrocarbon yield and (b-c) product selectivity of the liquid deoxygenated product

5.4.2.2 Quantification analysis

Figure 5.6a showed that the deoxygenation profile of triolein using catalyst-free (blank) and catalyzed reaction using different TM-oxide and TMO-doped CaO catalysts. The catalyst-free (blank) deoxygenation reaction rendered low yield of liquid hydrocarbon (13.4%), with high acidity of product (117.3 mg KOH/g) which corresponded to low deoxygenation reactivity of triglycerides in the absence of catalyst. As compared to bulk TM-oxide and TMO-doped CaO catalyzed reaction, the yields of liquid hydrocarbon were increased in the order of Co-CaO>Ni-CaO>Zn-CaO>Zn-CaO>NiO>Co_2O_4>ZnO> CaO>blank>Fe_2O_3. The results showed that the addition of transition metal oxide in CaO systems were capable to render high hydrocarbon yield and low TAN value compared to TM-oxide alone. It was suggested that synergistic effect from of acid-base interaction between binary metal oxide CaO and TMO were able to perform actively in deoxygenation process as mixed metal oxides. Based on the results obtained, Co-CaO catalyst showed better catalytic activity with the highest yield of 54% hydrocarbon and lowest TAN value of 67 mg KOH/g. This indicated that Co-CaO is able to convert majority of acid compounds in the triolein to non-acidic compounds including hydrocarbons.

As shown in our recent study (Asikin-Mijan et al., 2016b), the GC-MS chromatogram of the trioleins revealed that this feedstock was dominant toward saturated and unsaturated C16 and C18 fatty acids. The product of the subsequent fatty acid deCOx process are predicted to be resulted in formation of the long-chain hydrocarbon of *n*-C_{15} and *n*-C_{17} fractions. Based on the carbon distribution profile of the product Figures 5.6b-c, all the catalyst-free and TM-oxide catalyzed reaction showed wide distribution of hydrocarbon within the range of *n*-(C_8-C_{20}). Our observations also showed that majority of the hydrocarbons fractions tended to form light hydrocarbon *n*-

C_8. Nevertheless, the product distribution from TMO-doped CaO catalyzed deoxygenation of triolein was improved compared to deoxygenation reaction without catalyst and with TM-oxide catalysts. TMO-doped CaO catalysts were more selective to form desired deCOx product (*n*-C_{15}, *n*-C_{17}) and there were only minor formation of *n*-(C_8-C_{12}). Co-CaO and Ni-CaO catalysts showed the highest (*n*-C_{15}+*n*-C_{17}) selectivity at 41% and 48%, respectively. Thus, it can be suggested that the use Co- and Ni-doped CaO catalyzed deoxygenation was in favor to the formation of C_{n-1} hydrocarbons, which has implied higher deCOx activity. Formation of *n*-(C_8-C_{12}) hydrocarbon fractions were detected in the reaction which indicated that cracking reaction via C-C scission had also occurred, this was then proved that TMO-doped CaO had catalyzed simultaneous cracking-deCOx reaction. Co-CaO is more favored toward deoxygenation reactivity with the highest hydrocarbon yield (54%) and high production of desired deCOx product (*n*-C_{15}+*n*-C_{17}). The efficiency of Co-CaO catalyst in deoxygenizing triolein was confirmed by producing the lowest acid value (67 mg KOH/g) in deoxygenated liquid product (Figure 5.6a).

Figure 5.7a showed the chemical composition of deoxygenated liquid products catalyzed by TMO-doped CaO catalysts. Results had showed that 91% of the total unsaturated and saturated $C_{18+}C_{16}$ fatty acids in triolein had gone through remarkable changes after catalyzed by TMO-doped CaO catalysts. All the catalyst produced desired hydrocarbon fraction in saturated and unsaturated alkenes and alkanes (C_8-$C_{20)}$ in the range of 60% to 76% with minor coupling products (ketone), alcohol, cyclic, heavy hydrocarbon *n*-(C_{21}-C_{24}) fractions and acid compounds. Ketones were found in large amount in the product catalyzed by Zn-CaO and Fe-CaO. Meanwhile, Ni-CaO and Co-CaO had shown promising results in inhibiting the ketonization side reactions with <8% of ketone compounds produced during deoxygenation reaction. It was suggested that

ketonization reaction were promoted by a catalyst with excellent basicity and poor acidity properties which was in agreement with our recent findings(Asikin-Mijan et al., 2016d). We also found that the Fe-CaO promoted significant formation of heavy hydrocarbon *n*-(C_{21}-C_{24}). It is possible to infer that the polymerization reaction in deoxygenation of triolein was expected to occur due to poor acidic properties of Fe_2O_3 and CaO metal oxides. Both Co-CaO and Ni-CaO rendered similar trend of product selectivity, which is in the range of 29-35% for gasoline and 38-44% for diesel based on the gasoline and diesel profile (Figure 5.7b). As a summary, Co-CaO showed the highest hydrocarbon yield compared to other catalysts, thus it is selected for further optimization study to improvise on the catalytic activity and product selectivity.

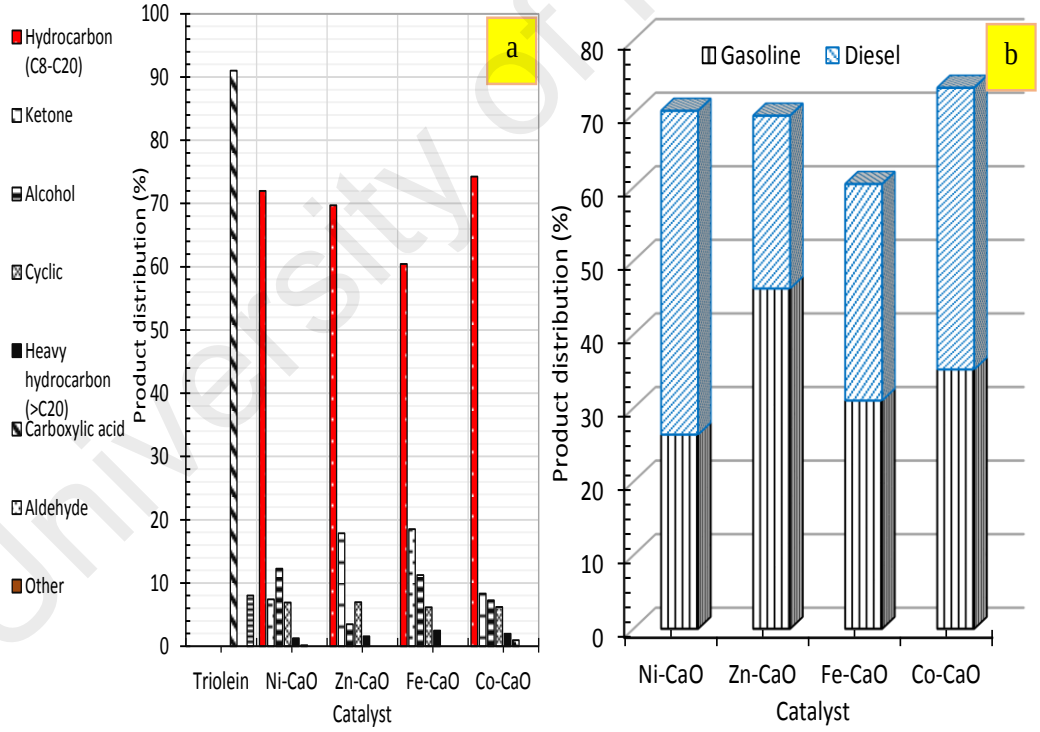

Figure 5.7: (a) Product distribution of deoxygenated liquid product and (b) gasoline and diesel distribution catalysed by TMO-doped CaO catalysts

5.4.2.3 Mass balance profile for catalytic deoxygenation of triolein

A mass balance profile for deoxygenation of triolein into liquid hydrocarbon product using TMO-doped CaO catalyst was studied under reaction conditions of 350

ºC, 5 wt.% catalyst loading, 60 min reaction time under inert condition. Based on Eq. 5.6, the deoxygenation reaction of triolein had led to the production of liquid product via deCOx reaction accompanied by the release of CO_2 gas, CO gas and water as by-products. The theoretical and experimental mass fraction of each compounds including triolein feedstock, liquid product, by products (CO_2 gas, CO gas, water and mixture of char+residues) was tabulated in Table 5.3. The overall experimental liquid mass balance is 40-68% lesser than theoretical value. The deviation of the liquid mass collected were due to high occurrence of cracking activity of deoxygenated product into volatile matter and the formation of undesired char+residue after reaction. This phenomenon was particularly obvious on the TMO-doped CaO catalysts due to significant formation of gaseous product (25-31 wt.%). This is in consistent with higher basicity of catalysts (refer to TPD-CO_2 analysis), which contributed to the formation of more gaseous product via cracking reaction. This was in agreement with Zhang studies which had stated that basic catalysts generated more low molecular weight (LMW) products which were consisted one, two, or three carbons (Zhang et al., 2016a). Char and residue shall not form during the deoxygenation reaction in ideal reaction. However, the significant amount of solid char and residue were observed in catalytic deoxygenation process. The formation of char and residue (char+residue) was caused by low degree volatilization of triolein during deoxygenation at high temperature (350 ºC) (Vitolo et al., 1999) and was partially due to $CaCO_3$ formation during the reaction (Zhang et al., 2016a), which had been proven by our previous study (Asikin-Mijan et al., 2016d). Nevertheless, the Co-CaO catalysts yielded low formation of char+residue (26 wt.%) compared to pure CaO (34 wt.%) and other TMO-doped catalysts (38-46 wt.%). The low char+residue yielded from Co-CaO catalyzed reaction might be attributed to the suppression of formation of carbon species via the existence of large amount of acid/basic active sites. The mass balance of the water was found lesser than

theoretical, as it was easily vaporized during high temperature deoxygenation reaction. The mass balance profile suggested Co-CaO catalyst did the most promising deoxygenation activity with the highest amount of liquid product yield (38 wt.%) and produced the least by-product (char+residue) (26 wt.%).

5.4.2.4 Oxygen removal rate

Elemental analysis for oxygen, carbon and hydrogen content of deoxygenized product was determined via CHNOS analysis. The H/C and O/C atomic ratios were calculated and depicted in the Van Krevelen diagram (Figure 5.8). It could be seen that the H/C and O/C atomic ratios of the triolein feedstock were 2.07 and 0.20 respectively, which consisted the highest amount of oxygen content. However, our results had shown that the liquid products rendered reduction of O/C ratio, which is the result of oxygen removal via deCOx process. The catalyst-free deoxygenation reaction showed reduction of oxygen content via cracking process, which favored the formation of short unsaturated hydrocarbon chain (low H/C ratio = 1.92). The same applied to CaO catalyzed deoxygenation reaction, where low H/C ratio (1.88) resulted in undesired short and unsaturated hydrocarbon fractions. It was discovered that CaO catalysed deoxygenation reaction showed lowest H/C ratio as compared to blank reaction. This is due to the high basicity of CaO, which highly favorble toward the occurence of C-C cleavage via cracking reaction and forming shorter hydrocarbon fractions. Co-CaO catalyst rendered significant reduction of O/C atomic ratio = 0.04 with the highest H/C ratio amongst the Ca based catalyst. The cobalt promoter showed significant dehydration and deCOx process thru elimination of hydroxyl, carboxyl, and carbonyl groups from triolein structure. In the absence of H_2, oxygen had the tendency to be removed in the form of CO_2 or CO gases without additional hydrogen atom to yield most of the alkene compounds.

Table 5.3: Mass balance profile of catalytic deoxygenation of triolein

Theoritical deCOx:	**Triolein ⟶ liquid (oil) + 3mol CO_2/CO (g) + 3mol H_2O (aq) + By product (5.6)**								
Reaction[a]	Feedstock	Liq-product[b]		Gas[c]		Water[d]		Char + residue[e]	
	(g)	(g)	(wt.%)	(g)	(wt.%)	(g)	(wt.%)	(g)	(wt.%)
Theoritical data (deCOx)	10.00	6.89	68.90	2.49	24.90	0.62	6.20	-	-
CaO	10.05	3.25	32.33	2.82	28.05	0.55	5.23	3.43	34.12
Ni-CaO	10.01	2.20	21.97	2.65	26.47	0.52	5.19	4.64	46.35
Zn-CaO	10.01	2.36	23.57	2.88	28.87	0.61	6.09	4.16	41.55
Fe-CaO	10.02	3.03	30.23	2.54	25.34	0.55	5.48	3.90	38.92
Co-CaO	10.09	3.80	37.66	3.20	31.71	0.62	6.14	2.67	26.46

[a]Deoxygenation condition : reaction temperature of 350 °C, 60 min reaction time, 5 wt.% of catalyst, under vacuum condition 10 mbar pressure and stirring 400 ppm.
[b]Mass fraction for Liq-product = [(mass of Liq-product/mass of feedstock)x 100]
[c]Material fraction for gas = [(mass of feedstock – mass of Liq-product- mass of (char+residue)- mass of water)/ mass of feedstock x100]
[d]Material fraction for water = [(mass of water/ mass of feedstock x100]

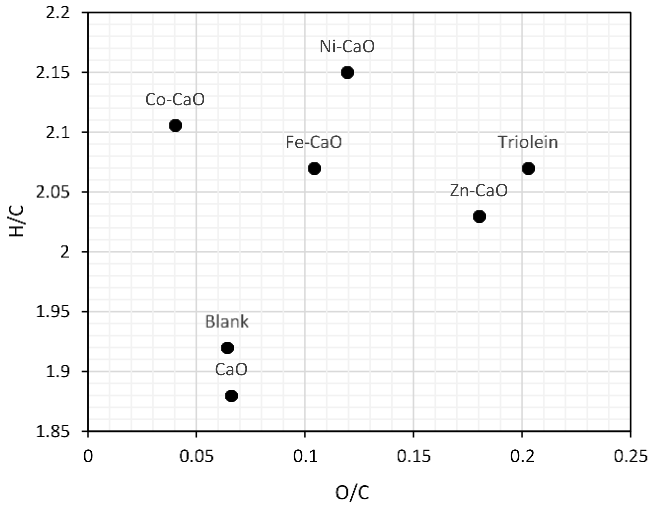

Figure 5.8: H/C and O/C ratio for deoxygenized liquid product (Van Krevelen diagram)

5.4.2.5 Basicity and acidity correlation

The synergic effect between active cobalt oxide and calcium oxide had promoted the deoxygenation mainly via C-O cleavage of the oxygenated compound than C-C cleavage (Romero et al., 2015b). The presence of excellent acidity and basicity profile (acid/basic density and strength distribution) played an important role in the occurrence of prominent C-O scission and mild C-C scission (Fig. 5.4a, Fig. 5.4b), and subsequently producing higher diesel-range (*n*-C_{15}+*n*-C_{17}) and minor gasoline-range *n*-(C_8-C_{12}) hydrocarbons deCOx product. It is estimated that the presence of acidic sites has induced the cracking of triolein into acid molecule (Zhang et al., 2017), while the basic sites reacted with fatty acid and were further deoxygenized via deCOx reaction into hydrocarbons (Xu et al., 2010). It has been agreed by Tani et al., (2011) and our recent findings Asikin-Mijan et al., (2015a) that MgO and CaO promote deCOx reaction thru reaction with carboxylic acid and further transformed to inactive carbonate phase. This study suggested that relatively strong surface acidity and strong surface basicity is crucial for deoxygenation of carboxylic acids. Based on catalytic activity study, deoxygenation activity hardly to correlated with textural properties of the catalysts (Fig. 5.1, Table 5.2) since the surface area and pore size of catalyst is close in value.

5.4.3 Optimization studies via Box-Behnken design

5.4.3.1 Statistical analysis

In the present work, the relationship between response (hydrocarbon yield) and 3 independent variables were studied. The experimental and predicted values the response at the design point and the 3 variables in non-coded form were given in Table 5.4. The regression Eq. (5.7) for the determination of predicted values of output parameter (i.e. hydrocarbon yield) were given as follows

$$\text{Hydrocarbon yield} = 54.38 + 3.62A + 1.66B - 3.63C - 5.53A^2 - 8.41B^2 - 6.90C^2 - 8.57AB - 0.050AC - 8.61BC \quad (5.7)$$

Table 5.4: Responses for deoxygenation of triolein

Run	A: Reaction temperature (°C)	B: Reaction time (min)	C: Catalyst loading (wt.%)	Hydrocarbon yield (%)	
				Experimental response	Predicted response
1	300	60	5	25.73	26.59
2	360	60	5	52.26	50.97
3	300	120	5	45.75	47.04
4	360	120	5	38.00	37.14
5	300	90	3	42.80	41.91
6	360	90	3	48.00	49.25
7	300	90	7	36.00	34.75
8	360	90	7	41.00	41.89
9	330	60	3	32.40	32.44
10	330	120	3	53.36	52.97
11	330	60	7	42.00	42.40
12	330	120	7	28.53	28.49
13	330	90	5	53.52	54.38
14	330	90	5	54.42	54.38
15	330	90	5	55.00	54.38
16	330	90	5	55.26	54.38
17	330	90	5	53.69	54.38

Positive sign in front of the terms indicates synergistic effect, while negative sign indicates antagonistic effect (Halim et al., 2009). The generated model equation implied that positive coefficient of A and B rendered linear effect toward the response.

Meanwhile, the quadratic term of C, A^2,B^2,C^2, AB, AC, and BC showed negative effect, which decreased the hydrocarbon yield. Table 5.4 showed the percentage of hydrocarbon yield was varied between 26-54%. The highest hydrocarbon yield was at 330 ^oC, 90 min, 5 wt.% catalyst loading and the lowest yield was at 300 ^oC, 60 min, 5 wt.% catalyst loading. It was proven that the modeled and experimental values were similar, hence, validating the reliability of the model developed for establishing a correlation between the process variables and the hydrocarbon yield.

5.4.3.2 Effect of reaction parameters

The response surface profile and its contour of the optimal production of hydrocarbon yield based on Eq. (5.7) was shown in Figure 5.9, for which the rate of reaction ramping was fixed at 400 rpm. There were 3 factors which had affected the deoxygenation reaction. Hence, it is impossible to present all the effects on the same 3D plot. Therefore, the interaction effect of the two parameters was plotted with the third parameter fixed to be constant in each of the figure. Figures 5.9a-ai showed the influence of temperature (A) and reaction time (B), 5.9b-bi: temperature (A) and catalyst loading (C), and 5.9c-ci: reaction time (B) and catalyst loading (C) to the hydrocarbon yield. Figures 5.9a-ai showed the interaction effect between reaction temperature (A) and reaction time (B) towards straight chain hydrocarbons yield, with catalyst loading (B) was fixed at 5 wt.%. The interaction temperature and reaction time showed significant effect on hydrocarbon yield, which is illustrated in Figure 5.9a. The yield of hydrocarbons increased significantly from 27% to 54% with increased reaction temperature. Meanwhile, the contour lines indicated that hydrocarbon fractions yield was maximum at high temperature ~330^oC and longer reaction time ~105 min with 54% yield (Figure 5.9ai). However, the hydrocarbon yield began to decrease after a prolonged retention time (>105 min), which can be explained by the cracking of

deoxygenated product or intermediate products to gases and char formation by condensation, cyclization and re-polymerization(Gan and Yuan, 2013). The results also showed that the optimum hydrocarbon products can be achieved under shorter reaction time (~75 min) but the reaction must be sustained at high temperature (360 ^{o}C). It was expected that more non-volatile light fractions (C_8-C_{12}) were obtained as the aggressive C-C scission occurred more easily at high reaction temperature than C-O scission. Generally, the C-O scission is favored at lower temperature (330-340 ^{o}C) and it was in agreement with our recent finding (Asikin-mijan et al., 2016) which had shown that jatropha oil was successfully converted to desired *n*-C_{15}+*n*-C_{17} with total selectivity >65% and to *n*-(C_8-C_{10}) with total selectivity <12% at the temperature of 330-350 ^{o}C. The trend of *n*-C_{15}+*n*-C_{17} selectivity reduced with the increase of *n*-(C_8-C_{10}) formation to 26% when the reaction temperature was increased to 400 ^{o}C.

The simultaneous interaction effects towards hydrocarbons yield by varying reaction temperature (A) and the catalyst loading (C) at constant reaction time of 90 min and 400 rpm was presented by 3D and contour lines plot in Figure 5.9b-bi. The results showed that the catalyst loading rendered low impact on the hydrocarbon yield. The hydrocarbon yield increased with the increment of catalyst loading within the range of 3-5 wt.% at reaction temperature up to 330 ^{o}C. The trend was reversed when catalyst loading was further increased to >5 wt% and reaction temperature exceeded 330^{o}C. Theoretically, higher catalyst loading would increase the availability of catalyst sites for deoxygenation reaction, thus increase the hydrocarbon yield. However, the usage of excess of catalyst would increase the possibilities of secondary reactions such as polymerization and cracking reactions. Polymerization reaction will lead to the formation of heavy product such as large aromatic-by product and asphaltenes which is unhealthy for the catalyst surface and lead to deactivation of catalyst (Kwon et al.,

2011). Moreover, further increment of the catalyst loading had resulted in high thermal cracking efficiency towards the formation of shorter hydrocarbon fraction like gaseous product (Hengst et al., 2015). The occurrence of secondary reactions due to thermal cracking at high temperature will eventually resulted in production of more volatile species and caused reduction in the yield.

The effect of reaction time (B) and catalyst loading (C) on the hydrocarbon yield under constant reaction temperature at 330 ^{o}C were shown in both surface and contour plots in Figure 5.9c-ci. Analysis of these two effects showed that the increment in both reaction time and catalyst loading increased the hydrocarbon yield up to a certain point. It has clearly shown that hydrocarbon yield was increased with the increment of reaction time from 60 to 105 min. Similar trend was also observed thru the increment of catalyst loading from 3 to 5 wt.%. The contour plot (Figure 5.9ci) indicated similar results with 3D-surface plot. It is obvious that the maximum hydrocarbon yield region can be obtained around ~55% within 105 min using 5 wt.% catalyst loading. It can be concluded that reaction temperature and reaction time shall have significant effect to deoxygenation of triglycerides into hydrocarbon fractions. The effect of increasing catalyst loading towards hydrocarbon yield is unsubstantial compared to reaction temperature and reaction time. It was suggested that increasing of all parameters above the optimum level will reduce the product yield. This was in agreement with Eq. 5.7 when all the interaction of AB, BC and AC showed negative interaction. The model predicted that the maximum yield can be obtained at 340 ^{o}C, reaction time, 5wt.% catalyst loading within 105 reaction time. The optimum response variables were then tested following suggested conditions to verify the model prediction. The experimental results indicated that the hydrocarbons yield was reasonably close to the predicted value generated from the model (Table 5.5).

Table 5.5: Verification of experimental results under optimum conditions

Optimum condition			Hydrocarbon yield (%)	
Reaction temperature (°C)	Reaction time (min)	Catalyst loading (wt.%)	Model predicted	Experimental result
340	105	5	55	56

Mean ± standard deviation (n = 2)

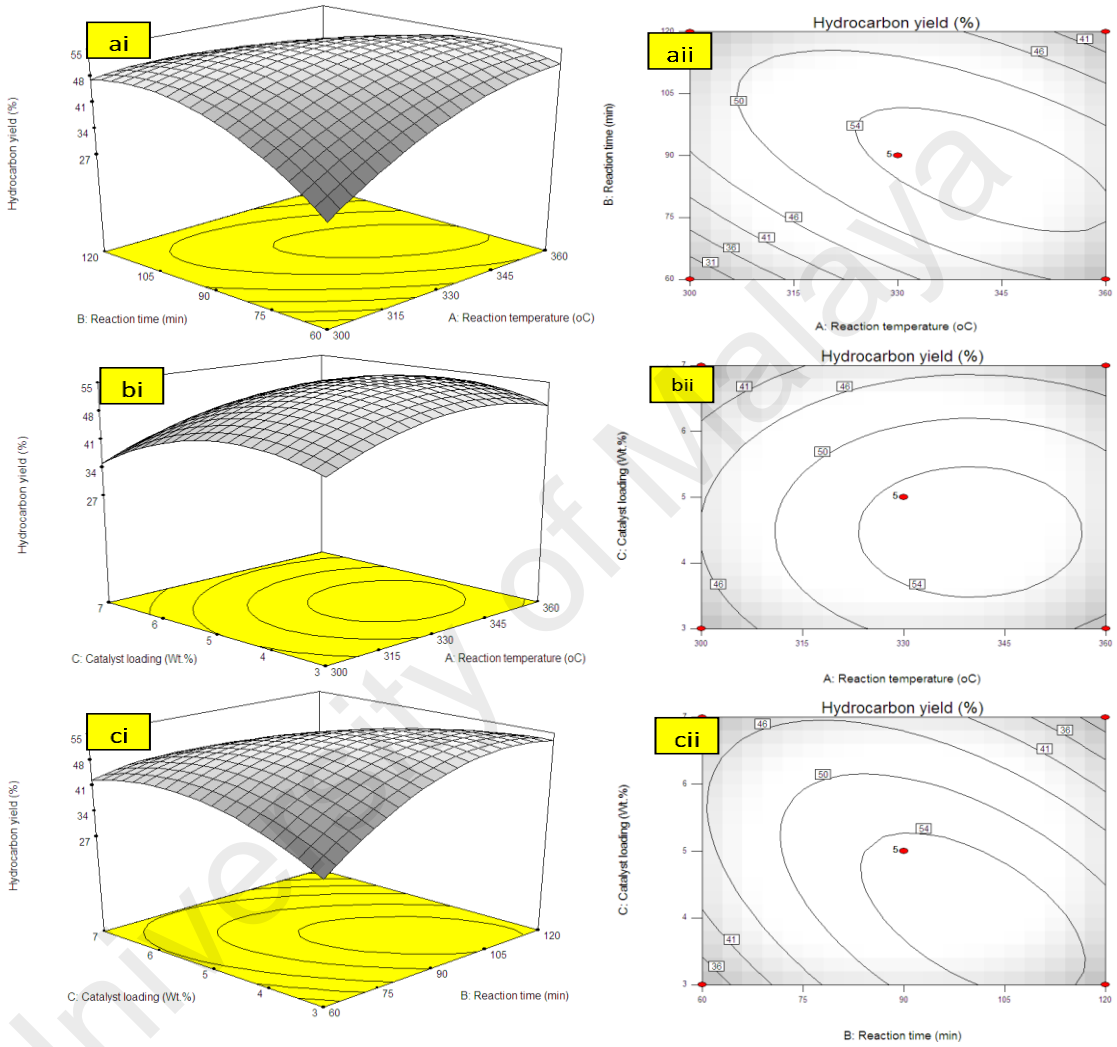

Figure 5.9: 3D-response surface plot and 2D-contour plot for (ai-aii) interaction of reaction temperature and reaction time (AB), (bi-bii) interaction of reaction temperature and catalyst loading (AC), and (ci-cii) interaction of reaction time and catalyst loading (BC)

5.5 Co-CaO derived waste clamshell versus commercial CaO

The catalytic deoxygenation of triolein at 340°C, 5wt.% catalyst loading within 15-135 min reaction time using Co-$CaO_{clamshell}$ and Co-$CaO_{commercial}$ under inert condition was shown in Figures 5.10(a-d). The total amount of hydrocarbon fractions

for Co-$CaO_{clamshell}$ and Co-$CaO_{commercial}$ achieved 77% and 72%, respectively at the reaction time of ≥105 min. This finding indicated that the deoxygenation activity of Co-$CaO_{clamshell}$ is comparable to Co-$CaO_{commercial}$ catalyst. Further study on carbon distribution profile was shown in Figures 5.10(c-d). The results showed similar trend of carbon distribution curve for both catalysts. The desired product for *n*-C_{17} fraction showed maximum content at 60 min of reaction time. The product in carbon range of *n*-(C_{13}-C_{16}) increase after 60 min, this suggested that C-C dissociation of fatty acid has occurred. The lower yield in product range of *n*-(C_8-C_{12}) after 60 min indicated that the cracking reaction has occurred mildly. The efficiency of Co-$CaO_{clamshell}$ and Co-$CaO_{commercial}$ catalysts in converting the free fatty acids into hydrocarbon were in agreement with changes in acid values, FTIR analysis and GC-MS analysis. It can be seen that both Co-$CaO_{clamshell}$ and Co-$CaO_{commercial}$ catalysts resulted in drastic changes in the acid values of liquid product from high-acid-value (145-135 mg KOH/g) in the first 15 min of reaction time to low-acid value-value (< 2 mg KOH/g) after 105 min of reaction time. This is equivalent to acid value conversion of ~98% (Figures 5.10(c-d)). The elimination of intermediates acid species were further confirmed by FTIR analysis (Figure 5.11a) with a significant reduction of C=O stretch at 1713-1705 cm^{-1} which is belonged to carboxylic acid and elimination of C-O stretch at 1285 cm^{-1} which is belonged to carbonyl. Meanwhile, GC-MS analysis showed that zero detection of carboxylic acid compound (Figures 5.11(b-c)). These observations had shown that the gradual formation of the hydrocarbon-based liquid fuel along with the elimination of intermediate acid compound during the deoxygenation reaction. Moreover, GC-MS also showed a trace amount of oxygenates and non-oxygenates compound which consisted of ketone, alcoholic, cyclic and heavy hydrocarbons *n*-(C_{21}-C_{25}). In contrast, straight chains alkanes and alkenes compounds with carbon number *n*-(C_8–C_{20}) was the most predominant in its concentration (>70%). This had shown that the product selectivity is

leaning towards diesel-range hydrocarbon product (Figure 5.11b). These findings suggested that both Co-$CaO_{clamshell}$ and Co-$CaO_{commercial}$ catalyzed the reaction toward diesel-range hydrocarbon formation via cracking-deCOx reaction and retarded the side reactions (polymerization, cyclization, ketonization and etc.) simultaneously. However, the utilization of Co-$CaO_{clamshell}$ as a catalyst has more benefits as it was derived from natural sources which are abundant in nature, economical and environment friendly.

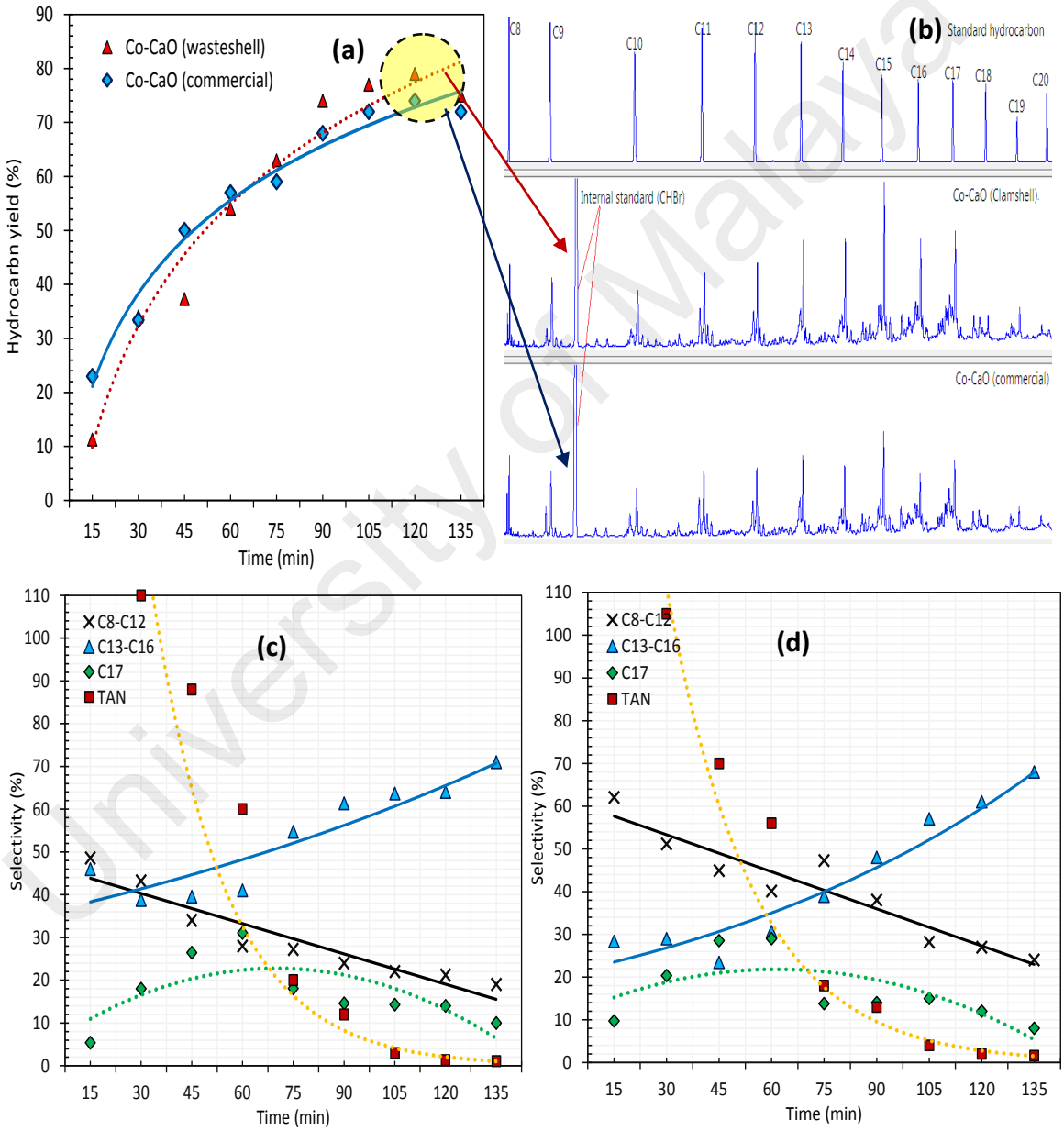

Figure 5.10: (a) Hydrocarbon yield, (b) GC chromatogram of the optimize sample and (c-d) carbon balance for deoxygenation of triolein via Co-CaO (wasteshell) and Co-CaO (commercial)

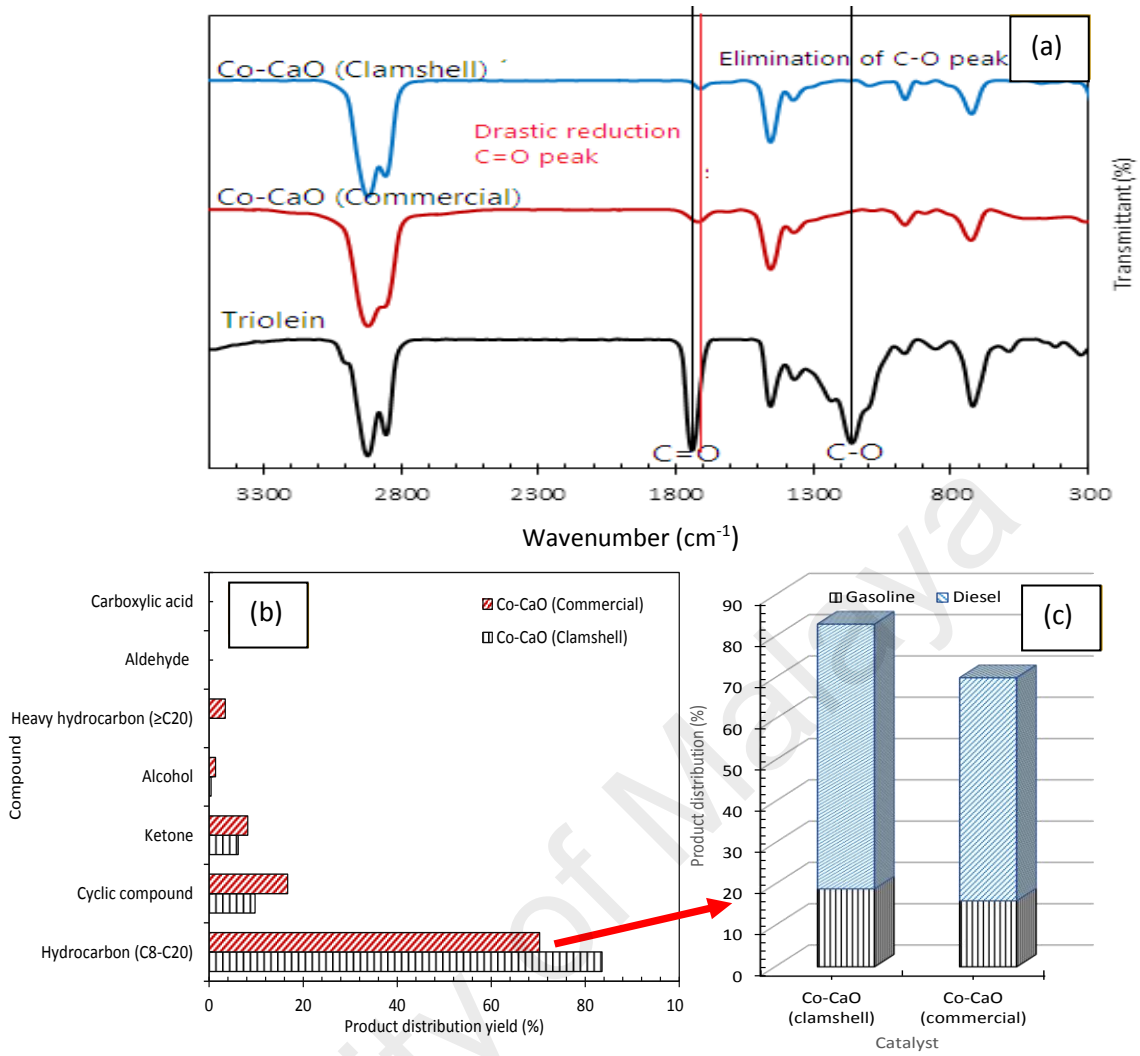

Figure 5.11: (a) FTIR spectra, (b) product distribution and (c) gasoline and diesel distribution for triolein and deoxygenated liquid products

5.6 Comparison studies and the reaction pathway of deoxygenation of triolein.

The catalytic activity of Co-CaO at optimum conditions was further compared to other Ca-based catalysts which tabulated in Table 5.6 (Asikin-Mijan et al., 2016d;Abdulkareem-Alsultan et al., 2016b;Asikin-Mijan et al., 2016b). The summary showed that Co-CaO (present study) rendered better hydrocarbon yield (56%) and selectivity toward diesel range (77%) at optimized conditions (reaction time: 105 min, temperature: 340°C and 5 wt.% catalyst loading) under inert N_2 flow condition via deoxygenation reaction compared to mesoporous CaO/AC, MgO-SiO_2, Co- and W-supported catalysts (Abdulkareem-Alsultan et al., 2016b;Asikin-Mijan et al.,

2016b;Tani et al., 2011). Our former study shown that Co-supported catalyst rendered higher yield in gasoline-range product via cracking reaction in a shorter reaction time (45 min) under partial vacuum condition. Meanwhile, in our recent study, Co-CaO rendered higher selectivity towards diesel-range within 105 min via cracking-deCOx reaction under inert condition (N_2 flow). Therefore, other than the synergy effect between TMO and CaO with improved acidity-basicity profile, the reaction parameters especially time and reaction atmospheres were also some of the crucial criteria to look into to enhance the product selectivity toward diesel-range hydrocarbon. This was in agreement with former studies, where deoxygenation under inert N_2 or He flow condition rendered hydrocarbon within diesel-range fractions(Romero et al., 2015a;Abdulkareem-Alsultan et al., 2016b;Tani et al., 2011). Continuous flow of N_2 and He during the reaction has helped in maintaining a high catalytic activity by avoiding CO_2/CO gases produced by the deCOx reaction from poisoning the active catalyst surface (Bernas et al., 2010). Furthermore, flowing N_2 and He has the ability to promote desorption of organic contaminants at the active surfaces of the catalyst, therefore conserving its activity for longer reaction time.

Table 5.6: Comparison studies of alkaline-based catalyst in catalytic deoxygenation

Catalyst	Reaction condition	Feeds	H/C yield (%)	Reaction mode	Product selectivity (%)	References
CaO/AC	Time= 60 min Temperature= 350 ^{o}C Catalyst loading =5 wt.% Under inert N_2 flow	WCO	~50	DeCOx[a]	Diesel	(Abdulkareem-Alsultan et al., 2016b)
Co_x-CaO W_x-CaO	Time= 45 min Temperature = 350 ^{o}C Catalyst loading =5 wt.% Under partial vacuum condition	Triolein	~32 ~22	Cracking	Gasoline	(Asikin-Mijan et al., 2016d)
CaO	Time = 360 min Temperature=400 ^{o}C Catalyst loading= 3 wt.% Under inert N_2 flow	WCO JCO	70 <75	Cracking-deCOx[a]	Diesel	(Romero et al., 2015a)
$MgO-SiO_2$	Oil feed rate: 15 ml/h, catalyst: 50 ml, LHSV: 0.3 h^{-1}, temperature=430 ^{o}C, Under inert He flow	Palm oil	50	Cracking-decarboxy[b]	Diesel	(Tani et al., 2011)
Co-CaO	Time = 105 min Temperature = 340 ^{o}C Catalyst loading = 5 wt.% Under inert N_2 flow	Triolein	56	Cracking-deCOx[a]	Diesel	Present study

[a]deCOx: Decarboxylation/decarbonylation
[b]decarboxy: decarboxylation

5.7 Conclusion

The present study has investigated the performance of clamshell-derived catalysts (Ni-CaO, Zn-CaO, Fe-CaO and Co-CaO) for deoxygenation reaction of triolein. The binary metal oxide system between TMO promoters (NiO, ZnO, Co_2O_4 and Fe_2O_3) and CaO support has created both acidic-basic active sites that synergically contributed to the production of diesel-range product mainly composed of desired deCOx product. It is predicted that the presence of acidic sites helps in cracking the triolein into acid molecule, while the basic site reacted with fatty acids and further deoxygenized via deCOx reaction into hydrocarbons. Based on the deoxygenation profile, the liquid hydrocarbon yield increased in the order of Co-CaO>Ni-CaO>Zn-CaO>Fe-CaO. Co-CaO catalyst rendered the highest yield (55%) with product selectivity towards diesel-range and gasoline-range due to the presence of excellent acidity/basicity profile (density, strength). The optimization study via RSM Box-Behnken suggested that the optimal value of ~55% hydrocarbon yield were achieved under reaction conditions of 5 wt.% of catalyst, 340^{o}C within 105 min of reaction time with product selectivity towards diesel-range product (77%). The optimization study also proposed that the interaction effect between reaction temperature-time would greatly influence the product yield. The application of clamshell derived CaO-based support in catalytic deoxygenation to produce green diesel is proven effective by comparison study between Co-$CaO_{clamshell}$ and Co-$CaO_{commercial}$, which found both catalysts rendered comparable deoxygenation activity with Co-$CaO_{clamshell}$ having an edge over Co-$CaO_{commercial}$ as it was derived from natural clamshells which were abundant in nature, economical and environment friendly.

CHAPTER 6: PYROLYTIC-DEOXYGENATION OF TRIGLYCERIDES MODEL COMPOUND AND NON-EDIBLE OIL TO HYDROCARBONS OVER SUPPORTED Ni AND Ca CATALYSTS

Chapter 6 described the study of deoxygenation of triglycerides over mesoporous acid-base catalyst derived NiO-CaO/SiO_2-Al_2O_3 for production of diesel range hydrocarbon. This study required in order to overcome the low deoxygenation activity and detrotriation of active Ca-based catalyst which found in Chapter 4-5. The present work focused enhancing the stability of the catalyst by the implementation of the CaO and NiO as a promoter. NiO is used as it gave the highest potential in tuning the deoxygenation via deCOx reaction. This chapter have been accepted to be published in *Journal of analytical and Applied Pyrolysis*" entitle of "***Pyrolytic-deoxygenation of triglycerides model compound and non-Edible Oil to hydrocarbons over supported Ni and Ca catalysts***" and the authors including N. Asikin-Mijan, H.V. Lee, T.S. Marliza and Y.H. Taufiq-Yap.

6.1 Introduction

Dwindling global petroleum deposits and environmental concerns have triggered the search for alternatives for fossil fuels. Over the past decades, mono alkyl esters of long-chain fatty acids (i.e., fatty acid methyl esters [FAME]) or biodiesel are widely used as alternative fuel, however biodiesel is less than ideal fuel due to its oxygen content which leads to a low heating value, as well as a high cloud and pour point (Miao et al., 2016). Hydrodeoxygenation (HDO) and deoxygenation (DO) are among the well-known technologies that have been used extensively to remove oxygen from fatty acids (Asikin-Mijan et al., 2015a) and resulted in production of hydrocarbon-based fuel that are capable of replacing petroleum derived fuel. Due to the considerable consumption of

H_2 in hydrodeoxygenation process which has become an obstacle to the widespread application of the hydrodeoxygenation process. Therefore, catalytic deoxygenation through decarboxylation (-CO) and decarbonylation (-CO_2) (deCOx) of triglycerides and fatty acids are proposed to enhance the economic feasibility of hydrodeoxygenation.

There was a numbers of solid acid catalyst involving metal sulfide-, noble metal-, metal phosphide-, and metal carbide-, metal, transition metals oxide- with supporting material reported in deoxygenation reaction. Sulfonated acidic catalyst shows high affinity toward the production of hydrocarbon fractions, but suffers from sulfur leaching and affects the quality of oil (Deepak S. Thakur,Thomas, 1985). Meanwhile, the high acidity noble metal catalyst is costly (Mäki-Arvela et al., 2008), which makes it unattractive. Medium acidity catalysts, such as metal phosphate and carbide, and mesoporous catalysts, such as SBA-15, MCM-41, and HMS catalysts, are generally selected for biofuel production as these catalysts pose low affinity toward the deactivation of the catalyst along with high deoxygenation activity (Chen et al., 2014a;Barrón C. et al., 2011). However, the complexity of catalyst synthesis makes it unappealing (Arun et al., 2015). Thus, the drawbacks of the abovementioned catalysts encouraged the exploration of non-sulfated, low-cost, and facile catalysts for producing high-quality renewable fuel. The usage of metal oxides in deoxygenation reaction has been continuously reported and proven to be selective towards the formation of hydrocarbon fractions (Asikin-Mijan et al., 2016d;Asikin-Mijan et al., 2016c). Common transition metal oxides that were used in deoxygenation process included Ni, Co, W (Rezgui and Guemini, 2005),Mo, Cu, Fe and Zn (Chen et al., 2014a). Among these metals, Ni showed the highest deoxygenation activity. Eventhough Ni-promoted catalyst is catalytically reactive, however, it is still suffered from coke formation. Coke formation can be prevented or reduced by integrating basic metal catalyst with acid

metal catalyst. Therefore, in the present study had focused on the development of the SiO_2-Al_2O_3 supported catalyst. NiO and CaO were used as a catalyst promoter. Additionally, in the present work also contributing the detail investigation of the study of the effect of reaction atmospheres (i.e., partial vacuum and inert N_2 flow) and investigation of the role of CaO on deoxygenation reaction.

6.2 Literature review

The efficiency of the NiO in the deoxygenation reaction was consistent with Croker and coworkers who reported on the deoxygenation of tristearin over 20 wt.% Ni/C showed similar performance with those obtained over 5 wt.% Pd and 1 wt.% Pt-promoted catalyst (Morgan et al., 2010). This finding is important due to the fact that the cost of Ni is ~1750 and ~3450 times lower than Pd and Pt, respectively. Several studies indicated that Ni-promoted catalysts exhibited high deoxygenation activity via deCOx pathway during deoxygenation of triglyceride oil and model compounds (palmitic acid, methyl stearate) to produce diesel-range hydrocarbons (Miao et al., 2016;Qian et al., 2014;Asikin-Mijan et al., 2016c). Eventhough Ni-promoted catalyst is catalytically reactive, however, it is still suffered from coke formation. Coke formation can be prevented or reduced by integrating basic metal catalyst with acid metal catalyst. It was proven by Gómez et al., (2013) that the implementation of alkaline earth metal (Na) on zeolite (NaX1.4) has resulted in reduction of coke formation. Meanwhile, Danuthai reported that the increase of Cs lewis base sites from 2% to 20% has resulted in the reduction of coke formation from 4.4 wt.% to 3.5 wt.% (Danuthai et al., 2011). Similar case was reported in our previous study, Asikin-Mijan et al., (2016d) which had observed significant reduction of coke deposited from 14 wt.% to 8.2 wt.% when the basicity of the Co-CaO were improve by cobalt loading from 10% to 40%.

6.3 Experimental

6.3.1 Material

Nickel (II) nitrate hexahydrate ($Ni(NO_3)_2 \cdot 6H_2O$) with purity >99% and calcium nitrate tetrahydrate ($Ca(NO_3)_2 \cdot 4H_2O$) with purity >99% were obtained from R&M Company. Silica-alumina (SiO_2-Al_2O_3) catalyst support grade 135 was purchased from Sigma-Aldrich. The standard for gas chromatography (GC) analysis of liquid product alkane and alkene standard solutions (C_8–C_{20}) and internal standard 1-bromohexane with purity >98% were purchased from Sigma-Aldrich and used without further purification. For dilution, analytical grade *n*-hexane for GC with purity >98% was obtained from Merck. Triolein (65% purity) was obtained from Sigma-Aldrich, *jatropha curcas* oil (JCO) was purchased from Bionas Sdn. Bhd., Malaysia, waste cooking oil (WCO) was collected at restaurant within the vicinity of Serdang and palm fatty acid distillate (PFAD) was supplied by Jomalina R&D, Sime Darby Sdn. Bhd., Malaysia. These feedstocks were used for deoxygenation reaction without further treatment and purification. The physicochemical properties of the feedstocks were tabulated in Table 6.1.

Table 6.1: Analysis data of properties of the triolein, Jatropha curcas L. oil, waste cooking oil and palm fatty acid distillate

Oil properties	Triolein	JCO	WCO	PFAD	Method
Density (g/cm^3)	0.91	0.92	0.87	0.87	ASTM D1298
Moisture content (wt.%)	0.08	0.01	1-5	0.10	ASTM E203 - 08
Acid Value (mg KOH g^{-1})	5.0	30.8	36.8	172.6	AOCS Ca 5a-40
FFA Value (%)	2.5	15.4	18.4	86.3	AOCS Ca 5a-40
Fatty acid composition of Oil (%)					AOCS Ce1-62 & Ce-661
Myristic acid (C14:0)	1.2	-	1.6	1.9	
Palmitic acid (C16:0)	3.8	20.2	43.8	45.7	
Palmitoleic acid (C16:1)	4.3	-	-	-	
Stearic acid (C18:0)	1.9	7.2	4.1	4.3	
Oleic acid (C18:1)	83.3	39.8	39.4	40.2	
Linoleic acid (C18:2)	0.4	31.5	11.1	7.9	
Linolenic acid (C18:3)	0.3	-	-	-	
Others[a]	4.8	1.3	-	-	

[a]Other representing minor compound of myristoleic acid(C14:1), pentadoic acid (C15:0), arachidic acid (C20:1), gadoleic acid (C20:1) and behenic acid (C22:1).

6.3.2 Catalyst synthesis

SiO_2-Al_2O_3 supported by the NiO-CaO catalyst was prepared using the wet impregnation method via weight percent determination (wt.%). Approximately 10 g of SiO_2-Al_2O_3 powder was impregnated with an aqueous solution 10 wt.% of Ca and 10 wt.% of Ni concentration. Distillate water is used as a solvent for dissolving the metal salt and act a dispersion medium during impregnation process. Moreover, in order to maximize the metal impregnation on the support surface and avoid active metal leaching, the filtration process is avoided. Thus, the final mixtures were directly dried in the oven at a temperature of 100 °C for overnight. The dried samples were ground into fine powder before being thermally activated at a temperature of 500 °C for 2 h under atmosphere condition. The catalyst was denoted as NiO-CaO/SiO_2-Al_2O_3 or NiO-10CaO/SiO_2-Al_2O_3. The catalyst was impregnated with 10 wt.% of NiO for synthesizing NiO/SiO_2-Al_2O_3. Different content of Ca solution (5 wt.%, 15 wt.% and 20 wt.%) were synthesized using a constant wt.% of Ni solution (10 wt.%) via similar method. The catalyst denoted as NiO-5CaO/SiO_2-Al_2O_3, NiO-15CaO/SiO_2-Al_2O_3 and NiO-20CaO/SiO_2-Al_2O_3.

6.3.3 Catalyst characterization

In this study, X-ray fluorescence (XRF) (Philips PWI404) equipped with scandium anode tube was used. 2 g of catalyst was added to the sample cup (31 mm Double Open-Ended X-ray Cell with Collar) and transferred into the XRF chamber. The elemental composition of the catalyst was accurately quantified. X-ray powder diffraction (XRD) analysis was conducted to identify the dispersion states and chemical composition of modified SiO_2-Al_2O_3 supported catalysts. XRD analysis was performed using Shimadzu diffractometer model XRD-6000. The specific surface area and pore distribution of the catalysts were determined by Brunauer–Emmett–Teller (BET)

method with N_2 adsorption/desorption analyzer using Thermo-FinniganSorpmatic 1990 series. The catalyst was degassed overnight at 150 °C to remove moisture and foreign gases on the catalyst surfaces. The adsorption and desorption processes of N_2 on the catalyst surfaces were analyzed in a vacuum chamber at −196 °C. The basicity and acidity of the catalysts were investigated using temperature-programmed desorption with CO_2 and NH_3 as probe molecules (TPD-CO_2 and TPD-NH_3, respectively). The analysis was performed using Thermo-Finnigan TPD/R/O 1100 instrument equipped with thermal conductivity detector (TCD). The catalyst (approximately 0.05 g) was pretreated with N_2 gas flow for 30 min at 250 °C and exposed to CO_2 gas for an hour at ambient temperature to allow the adsorption of CO_2 onto the surfaces. The excess CO_2 was subsequently flushed with N_2 gas flow at the rate of 20 mL/min for 30 min. The desorption of CO_2 from the basic sites of the catalyst was detected by TCD under helium gas flow (30 mL/min) from 50 °C to 900 °C and held for 30 min. The adsorption and desorption of NH_3 was similar to the TPD-CO_2 method. The morphological characteristics of the catalysts were investigated by field emission scanning electron microscopy (FESEM Rayny EDX-720). The FESEM images were observed through LEO 1455 VP electron microscope. The coking tendency of the catalyst was evaluated using thermogravimetric analysis (TGA) with simultaneous thermal analyzer (TGA, Mettler Toledo 990). The extent of coke/carbon deposition on the spent catalyst was determined using TGA instrument (TGA 1000i, Instrument Specialists Inc., USA). The samples were heated from 25 °C to 1,400 °C at the heating rate of 30 °C/min under 40 mL/min of air flow.

6.3.4 Catalytic deoxygenation of triolein

Deoxygenation of triolein was performed in a 250 mL mechanically stirred semi-batch reactor under partial vacuum and N_2 flow. The schematic diagrams for these

two configurations were shown in Figures 6.1A and 6.1B. In a typical experiment, approximately 10 g of triolein and a fixed amount of catalyst were added to the reactor. However, in the partial vacuum condition, the reactor was initially vacuumed using a mechanical vacuum pump with a pressure controller to remove the air/vapor in the system and then pressurized to approximately 0.1 bar (10 mbar) before initialization of the experiment. The purpose of lowering the air pressure is to accelerate the reaction temperature of the reaction medium to the desired point at a shorter time and increase the diffusion rate between feedstocks to enhance the deoxygenation process. Meanwhile, in deoxygenation process under inert N_2 flow condition, oxygen in the reactor was removed by purging with N_2 gas at the flow rate of 20 cc/min. All deoxygenation process was proceeded at elevated reaction temperature ≥ 300 ºC, as breaking of triglycerides via C-C cleavage generally occurred at early stage of reaction condition: >190 ºC and > 30 min (Crossley et al., 1962;Santillan-Jimenez et al., 2013), forming smaller molecules with lighter weight and volatile intermediates, such as fatty acid derivatives (palmitic acid: $C_{15}H_{29}COOH$ + oleic acid: $C_{17}H_{33}COOH$) (Benson et al., 2009). Further high thermal deoxygenation (≥ 300 ºC) is necessary for promoting C-O cleavage via deCOx reaction, where the oxygen species is removed in the form of CO_2/$CO+H_2O$ (Asomaning et al., 2014;Shim et al., 2014). Vapor/volatile species generated during the deoxygenation process was condensed into the liquid product using external water cooling circulator in the temperature of 16 °C and collected using a vessel collector. Meanwhile in deoxygenation under partial vacuum condition, the generated gas/vapor during the deoxygenation process was removed by the vacuum system to control the pressure in the system at 10 mbar. Pressure buildup in the vacuum system was adjusted during the reaction by releasing the generated gas from the system. The experiment was repeated three times to obtain the average range of the results to reduce the error of the experimental results.

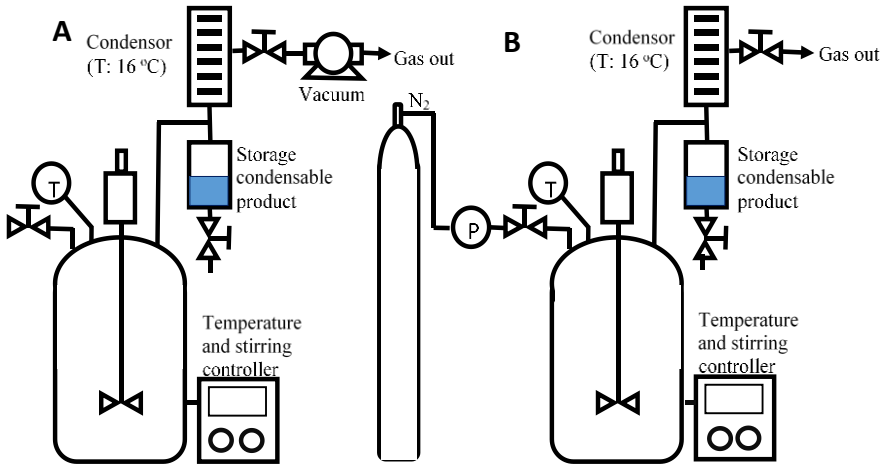

Figure 6.1: Semi-batch reactor in (A) partial vacuum atmosphere and (B) inert N_2 flow condition

6.3.5 Product analysis

The liquid products were quantitatively analyzed using GC (Shimadzu GC-14B) equipped with HP-5 capillary column (length of 30 m × inner diameter of 0.32 mm × film thickness of 0.25 µm) and a flame ionization detector operating at 300 °C. The liquid product was diluted with GC grade *n*-hexane prior to the analysis. 1-Bromohexane (CHBr) was used as internal standard for quantitative analysis. An aliquot of 1 µL sample was injected into the GC column. The injection temperature was at 250 °C and nitrogen gas was served as the carrier gas. The initial temperature of the oven was set at 40 °C and held for 6 min and then ramped to 260 °C at a heating rate of 7 °C/min. Thus, the precision and accuracy of the findings (total weight fraction of hydrocarbon and product selectivity) were determine by comparing the retention time of standard hydrocarbons (C_8-C_{20}) with experimental-based products (Appendix B). The catalytic performances of the catalyst were investigated by determining the saturated and unsaturated straight-chain hydrocarbons (*n*-alkane+*n*-alkene) weight fraction (X) using Eq. 6.1 (Asikin-Mijan et al., 2015a):

$$X = \frac{\sum n_o + \sum n_i}{\sum n_z} \times 100\% \quad (6.1)$$

where X denotes the saturated and unsaturated straight-chain hydrocarbons weight fraction (wt.%), n_o denotes the area of alkene (C_8–C_{20}), n_i denotes the area of alkane (C_8–C_{20}), and n_z denotes the area of the total product.

In addition, the chemical compositions of the feedstocks and deoxygenation liquid products were qualitatively characterized using GC-MS (model SHIMADZU QP5050A) equipped with non-polar DB-5HT column (30 m × 0.32 mm × 0.25 µm) with splitless inlet. The samples were diluted with GC grade *n*-hexane (purity > 98%) to 100 mg/L. The compounds were identified by comparing the mass spectral data through the National Institute of Standards and Testing library. Compound identification was based on a probability match equal to or higher than 95%. The selectivity of the deoxygenated products was determined using Eq. 6.2:

$$S = \frac{C_x}{\sum n_x} \times 100\% \quad (6.2)$$

where S denotes the selectivity (%), C_x denotes the area of the desired organic compound, and n_x denotes the area of the total organic compounds.

6.4 Results and discussion

6.4.1 Catalyst characterization

The elemental compositions of the SiO_2-Al_2O_3 and NiO-CaOx/SiO_2-Al_2O_3 (x=5, 10, 15, 20 wt.%) catalysts were investigated using XRF analysis (Table 6.2). The data showed that the content (SiO_2, NiO) was decreased rapidly to lower levels together with zero detection of Al_2O_3 metal when CaO content was increased from 5 wt.% to 20 wt.%. This is due to the coverage of CaO metal that has eventually covered SiO_2, NiO and Al_2O_3 active metals. The absence of Al_2O_3 composition for all NiO-CaO catalysts does not indicate zero Al_2O_3 content, but it indicates that the quantity of Al_2O_3 incorporated

onto SiO_2 is below the XRF analyzer detection limit as it is fully covered by excess CaO.

The XRD patterns of the catalysts were shown in Figure 6.2(i). Based on the XRD patterns, SiO_2-Al_2O_3 supported catalyst showed a broad peak that is attributed to low crystallinity and amorphous characteristic of SiO_2-Al_2O_3 mesoporous structure(Yoshida et al., 2002). For NiO/SiO_2-Al_2O_3 and NiO-CaOx/SiO_2-Al_2O_3 (x=5, 10, 15, 20 wt.%) catalysts, the presence of intense NiO peak at ($2\theta = 37.5°$ and 43.7°) (JCPDS card 00-047-1049) and CaO peak at ($2\theta = 37.6°$) (JCPDS card no. 00-037-1497) indicated that the active metal NiO and CaO have successfully impregnated on SiO_2-Al_2O_3 support. Further increment of CaO content which exceeded 15 wt.% has resulted in an appearance of carbonate phase at $2\theta = 29.8°$ (JCPDS Card No: 00.005-0585). This indicated that absorption of CO_2/CO gases from the surrounding was enhanced as CaO content was increased, which in turn converted some of active CaO phase to $CaCO_3$ phase. The average crystallite sizes of NiO/SiO_2-Al_2O_3 decreased with increased CaO content (Table 6.2). The reduction in crystallite size has suggested that CaO content has effect on the crystallinity of the catalysts.

The textural properties of SiO_2-Al_2O_3 and SiO_2-Al_2O_3 supported catalysts were summarized in Table 6.2. The results showed that the surface area and pore volume of SiO_2-Al_2O_3 supported catalysts were gradually decreased within the range of 199.65 m^2/g to 57.56 m^2/g and 0.46 cc/g to 0.26 cc/g, respectively, as compared to fresh SiO_2-Al_2O_3 (surface area = 382.60 m^2/g and pore volume = 0.75 cc/g). The reduction of the surface area and pore volume of SiO_2-Al_2O_3 supported catalysts is due to the pores blockage by NiO and CaO particles filled inside the SiO_2-Al_2O_3 pores. Moreover, the pore diameter of the SiO_2-Al_2O_3 supported catalysts was significantly enlarged during the course of varying the CaO content from 15 wt.% to 20 wt.%. The enlargement of the

pore size for NiO-CaO15/SiO_2-Al_2O_3 and NiO-CaO20/SiO_2-Al_2O_3 in BET analysis was consistent with the formation of visible torn-like surface in FESEM analysis (Figure 6.2(ii)). This implies that high content of CaO will induce more porous structure from the collapse of pore walls via releasing of CO_2 molecules from the carbonate-rich phase of the synthesized catalysts during calcination. Based on the finding from XRF analysis supported by XRD, BET and FESEM data confirmed CaO rich catalyst gave great effect on the textural properties of catalyst.

It is established that basicity characteristic played an important role in suppressing the coke formation along with promotion towards C-O cleavage via decarboxylation reaction (Asikin-Mijan et al., 2016d), meanwhile acidity is necessary to stimulate the C-C cleavage during deoxygenation reaction (Asikin-Mijan et al., 2016c). Among weak, medium and strong acidic sites, weak and medium acidic sites at desorption peak area T_{max}=<500 ^oC (milder acidic sites) are desired acidic sites as it favored mild cracking activity via deCOx reaction (Asikin-Mijan et al., 2016a). Table 6.2 and Figures 6.2(iii)-(iv) summarized the results obtained from TPD-CO_2 and TPD-NH_3. All the SiO_2-Al_2O_3 supported catalysts showed CO_2 desorption peaks at the temperatures within the range of 500-900 ^oC indicating all SiO_2-Al_2O_3 supported NiO and CaO exhibited strong basic sites. It was found that the total strong basic density has increased along with the increasing of CaO content, thus confirming overall basicity of SiO_2-Al_2O_3 supported catalyst associated with CaO phase (Taufiq-Yap et al., 2014). The TPD-NH_3 profile of all the SiO_2-Al_2O_3 supported catalysts showed existence of milder acidic sites. The largest existence of milder acidic sites were dominated by both of NiO/SiO_2-Al_2O_3 and NiO-5CaO/SiO_2-Al_2O_3 at total acidity of 3217.9 μmol/g and 3005.7 μmol/g, respectively. Thus, these two catalysts are capable of promoting deoxygenation via selective deCOx pathways.

Table 6.2: Physicochemical properties for SiO_2-Al_2O_3 and supported metal catalysts

Catalyst	XRF				XRD	BET			TPD			
	[a]Surface analysis (%)				[b]Crystallite size(nm)	[c]Surface area (m^2/g)	[c]Pore volume (cm^3/g)	[c]Pore size diameter (nm)	TPD-CO_2			TPD-NH_3
	SiO_2	Al_2O_3	NiO	CaO					[d]T (^oC)	[d]Basic sites (µmol/g)	[e]T (^oC)	[e]Acid sites (µmol/g)
SiO_2-Al_2O_3	86.4	10.8	-	-	-	382.60	0.75	7.65	100,904	12.4,13.7	241	1526.5
NiO/SiO_2-Al_2O_3	41.5	7.6	49.8	-	17.8	199.65	0.46	9.13	535,623, 730	116.9, 176.5, 164.2	395,567	3217.9, 6161.8
NiO-5CaO/SiO_2-Al_2O_3	33.7	-	50.0	15.9	15.2	163.51	0.42	7.97	143,301, 488, 712	31.0, 260.0, 292.4, 533.4	266,717	3005.7, 1005.2
NiO-10CaO/SiO_2-Al_2O_3	32.3	-	39.4	27.3	14.3	127.64	0.38	10.54	721	924.4	350,724	1105.0, 2994.8
NiO-15CaO/SiO_2-Al_2O_3	23.0	-	38.6	36.5	13.3	97.11	0.30	15.79	465,688	1340.7, 1335.3	239,518, 734	510.5, 1079.1, 1629.0
NiO-20CaO/SiO_2-Al_2O_3	19.4	-	32.5	47.3	11.7	57.56	0.26	17.40	450,527, 677	682.5, 941.2, 1395.9	199,514, 667	605.6, 1768.8, 1308.1

[a] Elemental composition were determined by XRF analysis
[b] Measured by using Scherer equation from XRD data (repeat twice)
[c] Determined by BET analysis
[d] Determined by TPD-CO_2 analysis
[e] Determined by TPD-NH_3 analysis

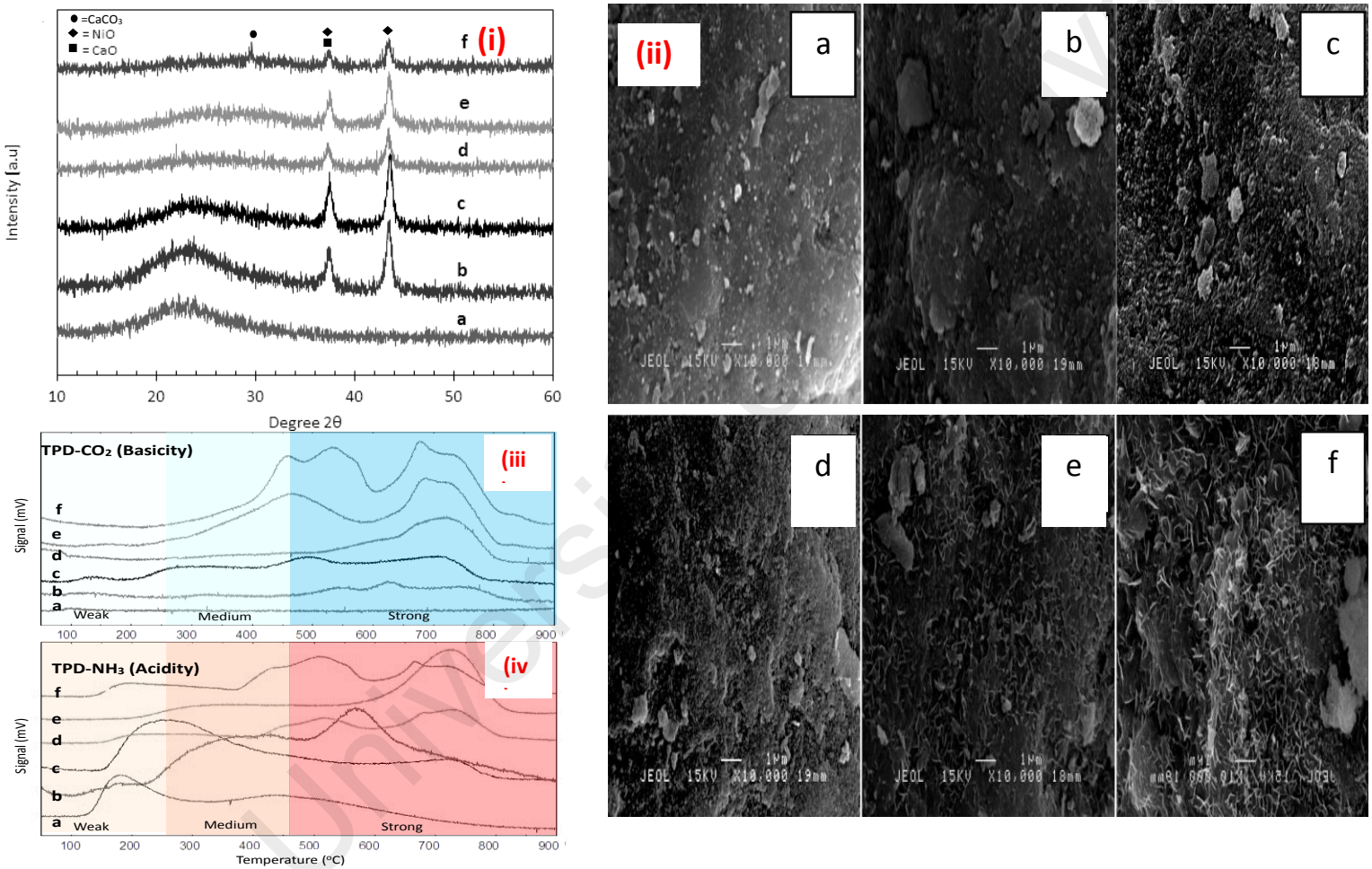

Figure 6.2: (i) The XRD patterns, (ii) FESEM images, (iii) TPD-CO_2 and (iv) TPD-NH_3 for (a) SiO_2-Al_2O_3, (b) NiO/SiO_2-Al_2O_3, (c)NiO-5CaO/SiO_2-Al_2O_3,(d) NiO-10CaO/SiO_2-Al_2O_3 or NiO-CaO/SiO_2-Al_2O_3, (e) NiO-15CaO/SiO_2-Al_2O_3 and (f) NiO-20CaO/SiO_2-Al_2O_3

6.4.2 Catalytic deoxygenation profile

In order to study the effect of bi-functional system of NiO-CaO and mono-functional system of NiO on mesoporous SiO_2-Al_3O_4 support, the deoxygenation activity under partial vacuum and inert N_2 flow were investigated over supported metal catalyst using constant 10 wt.% of NiO and 10 wt.% of CaO. The weight fractions of the saturated and unsaturated straight-chain hydrocarbons were summarized in Figure 6.3A. A blank experiment was carried out under the same conditions to determine the product distribution during the thermal composition of triolein in the absence of catalyst and results in marginal weight fraction (<20%). However, the catalytic deoxygenation over SiO_2-Al_3O_4, NiO/SiO_2-Al_2O_3 and NiO-CaO/SiO_2-Al_2O_3 were found to be reactive in deoxygenation reaction by obtaining higher hydrocarbon weight fraction. The deoxygenation reactivity of different catalysts are in the order of blank<SiO_2-Al_2O_3<NiO/SiO_2-Al_2O_3< NiO-CaO/SiO_2-Al_2O_3.

The composition of triolein was mainly C16 and C18 fatty acid derivatives based on fatty acid composition profile of triolein (Table 6.1). Theoretically, deCOx reaction of C16+C18 fatty acid derivatives will result in formation of *n*-C_{15}+*n*-C_{17} deCOx product. The results showed catalyzed deoxygenation via deCOx reaction was prominent as compared to blank reaction (Figures 6.3B-C). The blank reaction favored gasoline range (C_8–C_{12}) fractions. Meanwhile, catalyzed reaction were predominantly selective toward *n*-C_{15}+*n*-C_{17} formation hence indicated the occurrence of catalytic deoxygenation via deCOx reaction. The deCOx selectivity increased in the order of blank<SiO_2-Al_2O_3<NiO-CaO/SiO_2-Al_2O_3<NiO/SiO_2-Al_2O_3. The enhancement of deCOx selectivity in NiO/SiO_2-Al_2O_3 catalyst was consistent with highest distribution of total milder acidic sites (3217.9 µmol/g) in Table 6.2 and Figure 6.2(iv). Although NiO/SiO_2-Al_2O_3 catalyst was more efficient in deCOx pathways than NiO-CaO/SiO_2-

Al_2O_3 catalyst but it still suffered additional side reactions such as polymerization and cyclization reactions, which was consistent with the large formation of heavy fraction ($>C_{20}$; approximately 10%) and cyclic compound (approximately 14%) in the liquid product (Figure 6.4A-B). The NiO-CaO/SiO_2-Al_2O_3 catalyzed reaction showed the best performance in inhibiting the cyclization+polymerization reaction with total cyclic+heavy product <8% during deoxygenation process. It was suggested cyclization and polymerization rate was promoted by large density of strong acidity in NiO/SiO_2-Al_2O_3 catalyst (6161.8 μmol/g)(Table 6.2) and it was in agreement with the previous studies(Krivan et al., 2016;Lou et al., 2016). Thus, the incorporation of basic metal (CaO) into NiO/SiO_2-Al_2O_3 has led to interesting acid-base characteristic in suppressing the occurrence of side reaction by neutralization the strong acid constituents. Based on catalytic activity performance, deoxygenation activity showed no significant correlation with the textural properties of the catalyst (pore size; Table 6.2). It was apparent that poor deoxygenation activity over NiO-CaO/SiO_2-Al_2O_3 catalyst although its pore diameter was the largest has indicated that the pore size of SiO_2-Al_2O_3-based catalysts remained a limitation to access to large compounds of triolein.

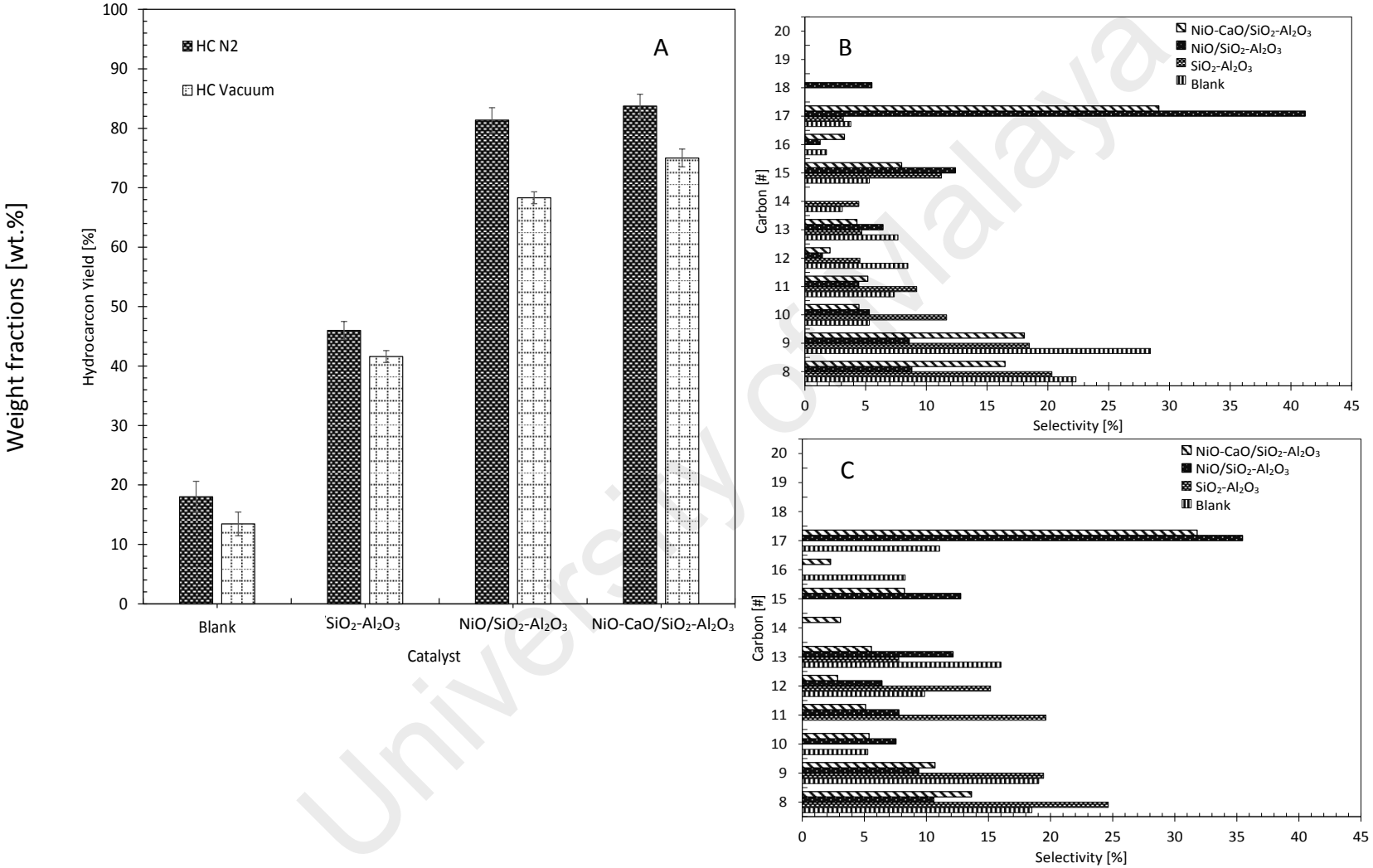

Figure 6.3: (A) Hydrocarbon weight fraction of deoxygenated liquid, (B) selectivity toward C_8-C_{20} under partial vacuum atmosphere and (C) selectivity towardC_8-C_{20} under inert N_2 flow condition

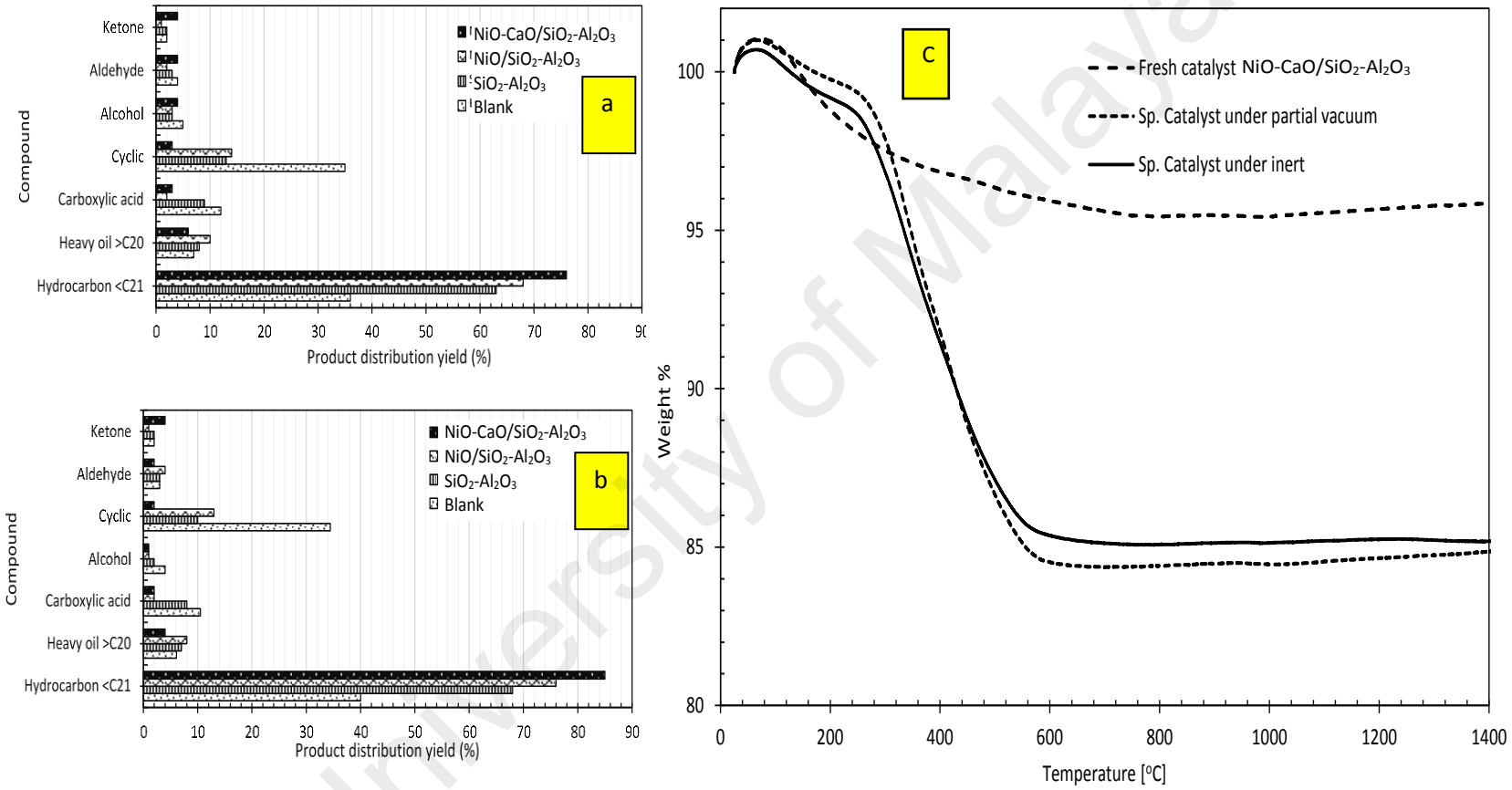

Figure 6.4: Fractional distribution of deoxygenated liquid produced under (A) partial vacuum and (B) inert N_2 flow and (C) TGA result for NiO-CaO/SiO_2-Al_2O_3 spent catalyst deoxygenized under partial vacuum and inert N_2 flow condition

Overall deoxygenation activity was found to be more prominent under inert N_2 flow than in partial vacuum condition (Figures 6.3A-C, Figures 6.4A-B). It was found that continuous N_2 flow was capable of maintaining high deoxygenation activity by preventing CO_2/CO gases produced by the deCOx reaction from poisoning the active catalyst surface (Bernas et al., 2010). Furthermore, flowing N_2 was capable of promoting desorption of organic contaminants on the active surface of the catalyst. Thus, conserving its activity for longer period. The suggestion is consistent with GCMS finding (Figures 6.4A-B), where catalytic deoxygenation under inert N_2 flow has resulted in lower formation deoxygenation intermediate products (i.e., carboxylic acid) and side products (i.e., alcoholic, heavy fraction hydrocarbon, and cyclic compound) than in partial vacuum condition. The formation of those oxygenates and cyclic compound have made the catalysts more prone to coke build up. The extent of coke deposited on the spent catalyst were measured by the deduction of total weight loss of fresh catayst and spent catalyst obtained in TGA analysis. The extra weight loss for spent catalyst will be generated as coke will be decomposed at temperature > 400 ^oC which due to the oxidation of carbon based material. TGA analysis had shown that the catalyst reacted in deoxygenation under partial vacuum produced highest coke formation (Figure 6.4C). This indicated that the amount of carbonaceous deposits on the spent catalyst surface showed a closely dependence on the atmospheric condition applied during the deoxygenation reaction. In all cases, catalytic deoxygenation under inert N_2 flow was determined to be beneficial for catalyst stability by having highest hydrocarbon weight fractions and lowest coke formation.

6.4.3 Role of Ca metal in deoxygenation of triolein

The catalytic deoxygenation activity and product selectivity profile from deoxygenation under inert N_2 flow over NiO-xCaO/SiO_2-Al_2O_3 (x=5, 10, 15, 20 wt.%)

catalysts were displayed in Figure 6.5. It was observed that the hydrocarbon weight fractions and *n*-C_{15}+*n*-C_{17} selectivity were entirely dependent on the CaO content. The results showed that low CaO metal content (5 wt.%) has promoted highest deoxygenation activity by producing 85% hydrocarbon weight fractions and product selectively toward *n*-C_{15}+*n*-C_{17} (48%). As the CaO content of the catalyst was increased, the *n*-C_{15}+*n*-C_{17} selectivity was reduced and light fraction selectivity increased. This implies that the richness of the high-strength basic and acidity sites existed in high CaO content catalyst has promoted cracking via C-C cleavage rather than deCOx reaction via C-O cleavage(Asikin-Mijan et al., 2016d) (see TPD-CO_2 and TPD-NH_3 (Figure 6.2(iii-iv), Table 6.2). The great deCOx promotion over NiO-5CaO/SiO_2-Al_2O_3 was in line with largest existence of milder acidic sites (3005.7 µmol/g). Again, this implies that milder acid sites is highly involved in deCOx mechanism. However, no correlation was observed between catalytic activity and pore properties. It was proven that NiO-20CaO/SiO_2-Al_2O_3 consisted of the largest pore size diameter (17.4 nm) among catalysts (Table 6.2). However, the result showed that the catalyst reacted with an outcome of low hydrocarbon weight fractions (63%) and poor deCOx activity (29%). This showed that the effect of pore size diameter can be neglected in the reactivity.

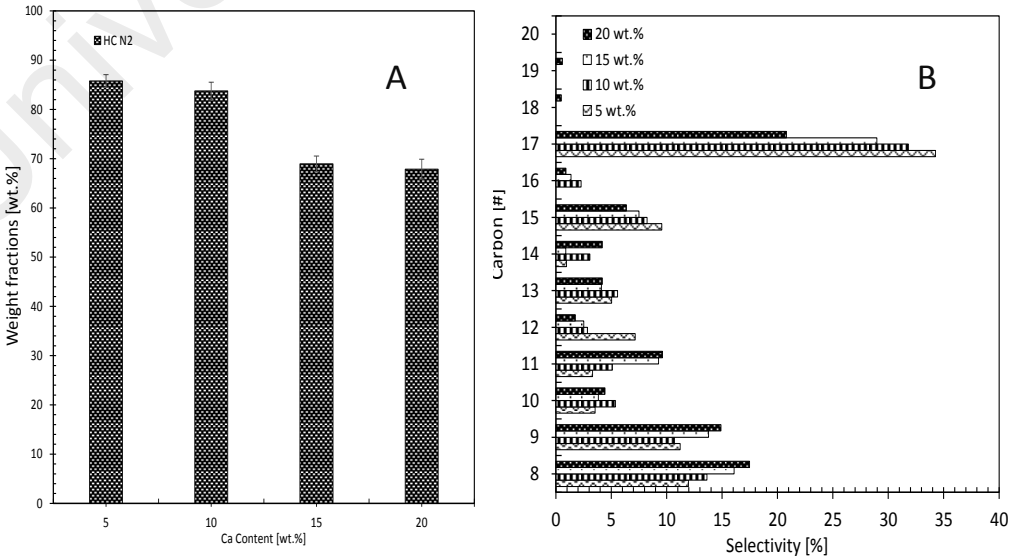

Figure 6.5: Effect of Ca content from 5-20 wt. % on (A) Hydrocarbon weight fraction and (B) Selectivity toward C_8-C_{20}

6.4.4 Optimization studies

The influence of catalyst loading (1-9 wt.%), reaction temperature (300-380 ^{o}C) and reaction time (30-240 min) were investigated via one-variable-at-a-time technique (Figure 6.6). The effect of catalyst loading on the hydrocarbon weight fractions and *n*-C_{15}+*n*-C_{17} selectivity (deoxygenation activity) were studied and summarized in Figure 6.6A-A1. It was found when the catalyst loading was increased from 1 wt.% to 7 wt.% within 60 min reaction time and 350 ^{o}C reaction temperature, the hydrocarbon weight fractions and *n*-C_{15}+*n*-C_{17} selectivity increased from 80% to 92% and 44% to 61%, respectively. This implies that 7 wt.% catalyst loading provided more active sites than 1 wt.% catalyst loading which induced deoxygenation activity (Kwon et al., 2011). However, excess of active sites may render the occurrence of secondary reactions such as polymerization and promote coke formation and subsequently reduced the deoxygenation activity. Evidently, drastic reduction of deoxygenation activity was observed when 9 wt.% catalyst loading was used. To maximize deoxygenation activity at a given time, high NiO-5CaO/SiO_2-Al_2O_3 loading (7 wt.%) was chosen for further study. The effect of reaction temperature on deoxygenation activity was studied. It was found that deoxygenation activity was retarded with the increased of reaction temperature >350 ^{o}C (Figure 6.6B-B1), indicating thermal cracking via C-C cleavage is favored at high temperature and resulting in formation of volatile species and light fractions (Bezergianni et al., 2009). This finding is in consistent with the increment of *n*-(C_8-C_{12}) from 35% to 44% and reduction of *n*-C_{15}+*n*-C_{17} selectivity from 61% to 52% when the reaction temperature was increased from 350 ^{o}C to 380 °C. Further study on the effect of reaction time towards deoxygenation activity was studied. Results showed that deoxygenation activity was mainly affected by reaction duration (Fig. 6.6C-C1). Low deoxygenation activity degree was observed when the deoxygenation reaction proceeded within 30 min, which implied the amount of energy available at early

reaction time was insufficient for the catalyst to initiate the deoxygenation reaction. Besides, reduction of deoxygenation activity was observed as well when prolong the reaction to 240 min. This is due to excessive cracking of the deoxygenated liquid product into unfavourable lighter fractions. Evidently, the *n*-C_{15}+*n*-C_{17} selectivity decreased with the increase of light fractions as the reaction time prolonged from 120 min to 240 min. Based on the results, 60 min was found to be the most efficient duration for deoxygenation reaction, with hydrocarbon weight fraction= 92% and *n*-C_{15}+*n*-C_{17} = 61%. In comparison with previous RSM optimization study of the SiO_2-Al_2O_3 supported catalyst under partial vacuum deoxygenation condition (Asikin-Mijan et al., 2016a), the inert N_2 flow system rendered better efficiency for the conversion of triolein.

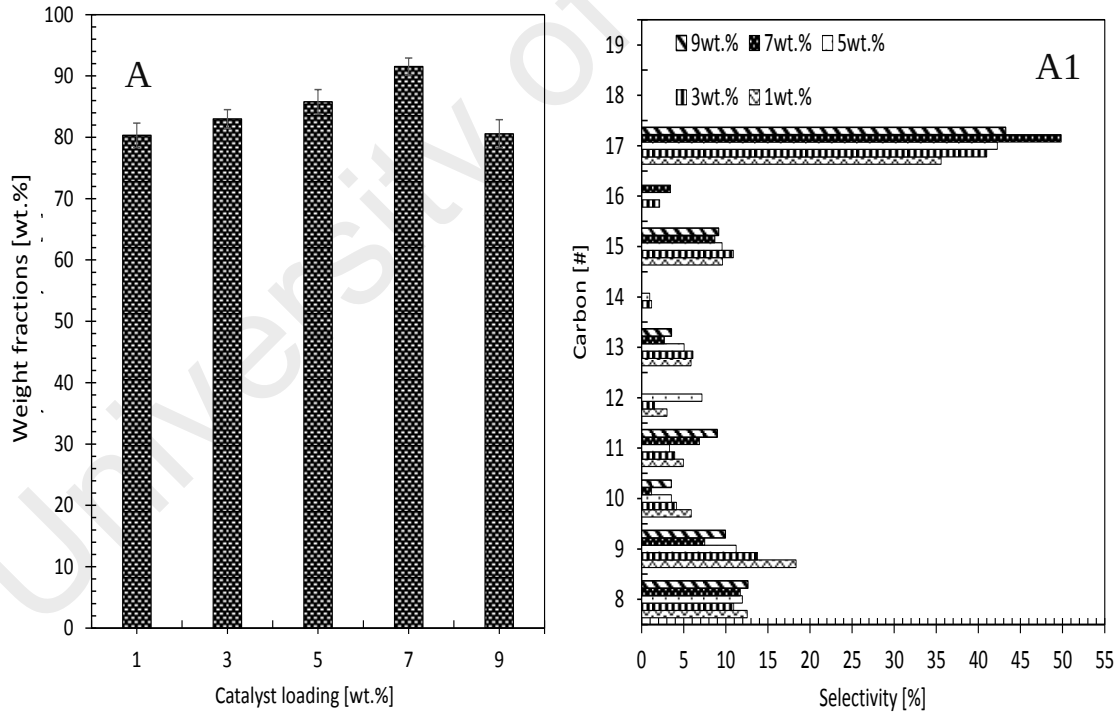

Figure 6.6: Optimization studies of triolein (A-A1) deoxygenation reactions of NiO-5CaO/SiO_2-Al_2O_3 catalyst affected by catalyst amount; reaction conditions: 350 ^oC, 1 h, (B-B1) deoxygenation reactions of NiO-5CaO/SiO_2-Al_2O_3 catalyst affected by reaction temperature; reaction conditions: 7 wt.% catalyst loading , 1 h, (C-C1) deoxygenation reactions of NiO-5CaO/SiO_2-Al_2O_3 catalyst affected by reaction time; reaction conditions: 7 wt.% catalyst loading, 350 ^oC for 400 rpm under N_2 flow

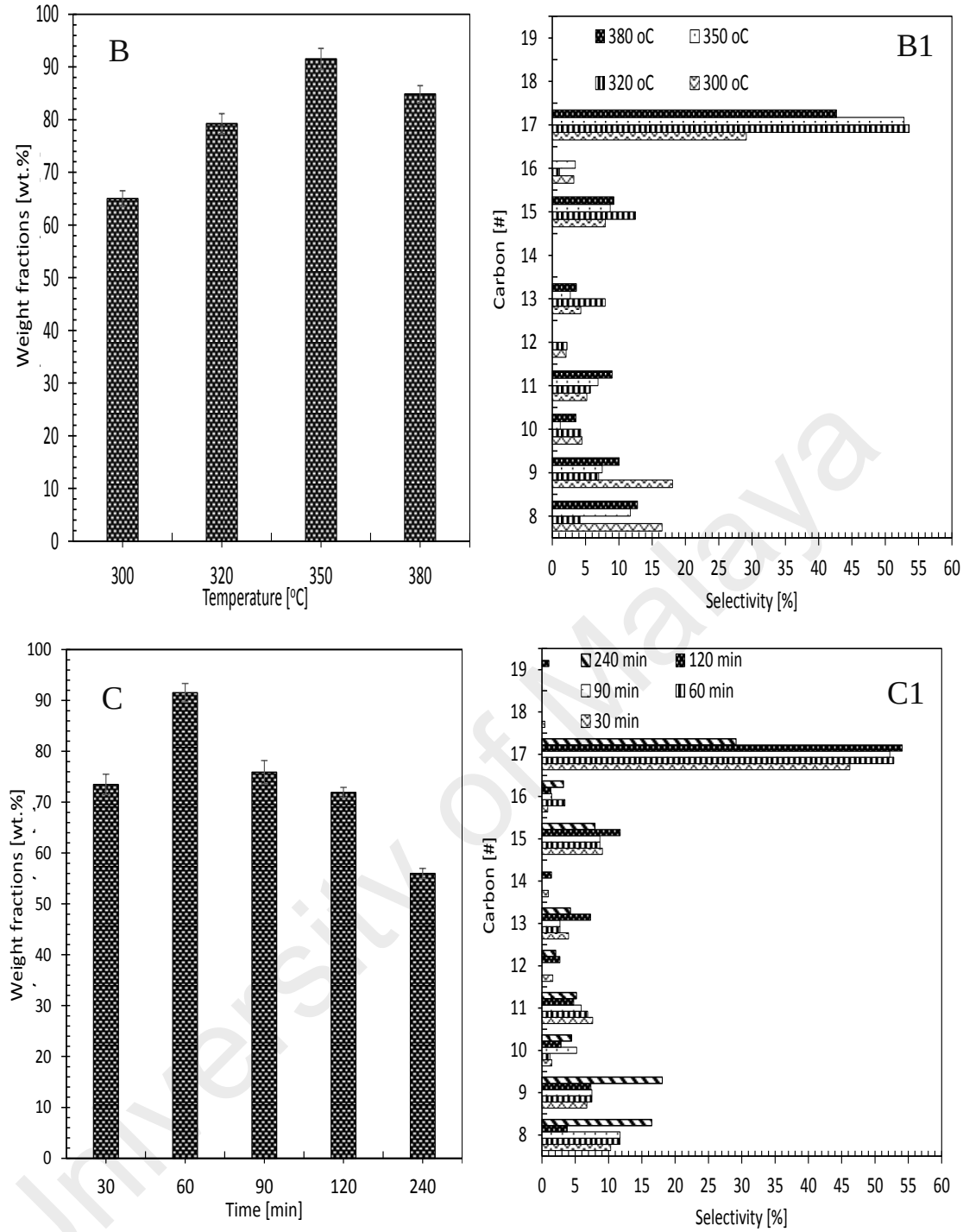

Figure 6.6, continued: Optimization studies of triolein (A-A1) deoxygenation reactions of NiO-5CaO/SiO_2-Al_2O_3 catalyst affected by catalyst amount; reaction conditions: 350 ^oC, 1 h, (B-B1) deoxygenation reactions of NiO-5CaO/SiO_2-Al_2O_3 catalyst affected by reaction temperature; reaction conditions: 7 wt.% catalyst loading , 1 h, (C-C1) deoxygenation reactions of NiO-5CaO/SiO_2-Al_2O_3 catalyst affected by reaction time; reaction conditions: 7 wt.% catalyst loading, 350 ^oC for 400 rpm under N_2 flow

6.4.5 Effect of free fatty acid on catalytic deoxygenation activity

The effect of the NiO-5CaO/SiO_2-Al_2O_3 catalyst in converting triglycerides-based feeds (WCO, JCO and PFAD) at optimum reaction condition were evaluated to

gain insight into the deoxygenation of realistic non-edible feedstocks. Based on fatty acid composition in Table 6.1, the products of the subsequent fatty acid deCOx process were predicted to form long-chain hydrocarbon of *n*-C_{15} and *n*-C_{17} fractions. The deoxygenation of these feedstocks are expected to be differed from triolein model compound as it contained high free fatty acid (FFA). The FFA values for JCO, WCO, and PFAD were determined at 15%, 18%, and 86%. High FFA value of all feedstocks were due to high degree of unsaturation (Silva et al., 2016) and it might induce coke formation which simultaneously reduced the deoxygenation activity. Based on the TGA analysis in Figure 6.7, spent NiO-5CaO/SiO_2-Al_2O_3 catalyst from deoxygenation of PFAD (FFA: 86%) showed the highest coke formation with weight loss of 14.48 ± 0.12% at the temperature range of 300 °C to 600 °C. Meanwhile, spent NiO-5CaO/SiO_2-Al_2O_3 catalyst from deoxygenation of WCO (FFA: 18%) and JCO (FFA: 15%) showed a weight loss of 13.68 ± 0.31% and 12.95 ± 0.46%, respectively. The higher content of unsaturated FFA in PFAD suggested to easily undergoes very fast aromatization (via sequential cyclization, de-hydrogenation and condensation reactions) to form (poly) aromatic compound (coke precursor). This finding was in agreement with formation of significant cyclic compound in the residue of deoxygenized PFAD (Figure 7.8). This finding is particularly relevant with Absi-Halabi study (Absi-Halabi et al., 1991) and it is in consistent with the previous finding of Morgan and coworkers (Morgan et al., 2012). Theoretically, the coke formation will block the active centers and prevent further reaction on the surface of the catalyst, which will simultaneously result in the lower weight fraction of hydrocarbons.

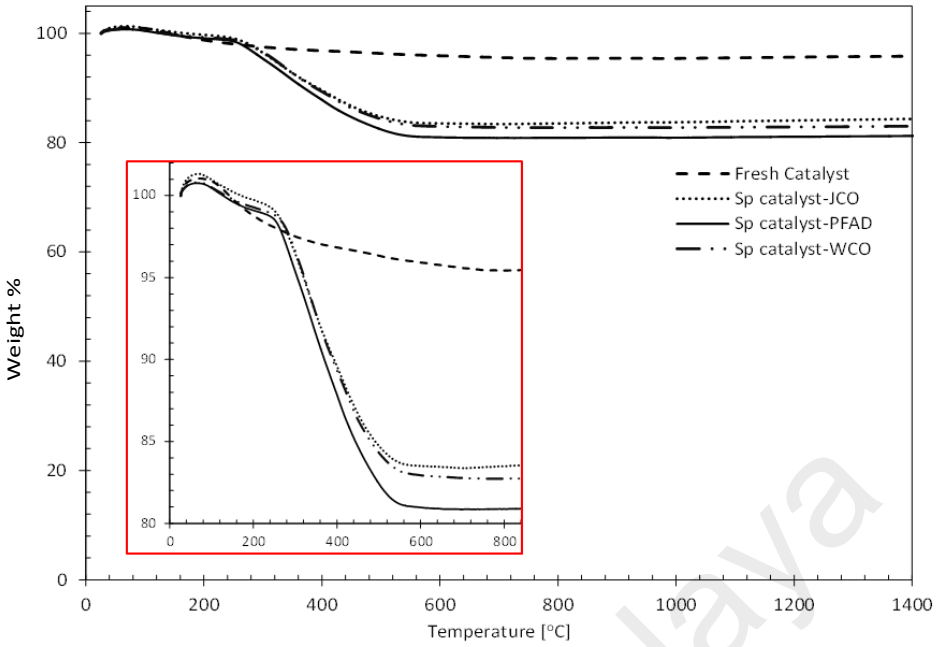

Figure 6.7: TGA profiles for NiO-5CaO/SiO_2-Al_2O_3 spent catalyst from catalytic deoxygenation of JCO, PFAD and WCO

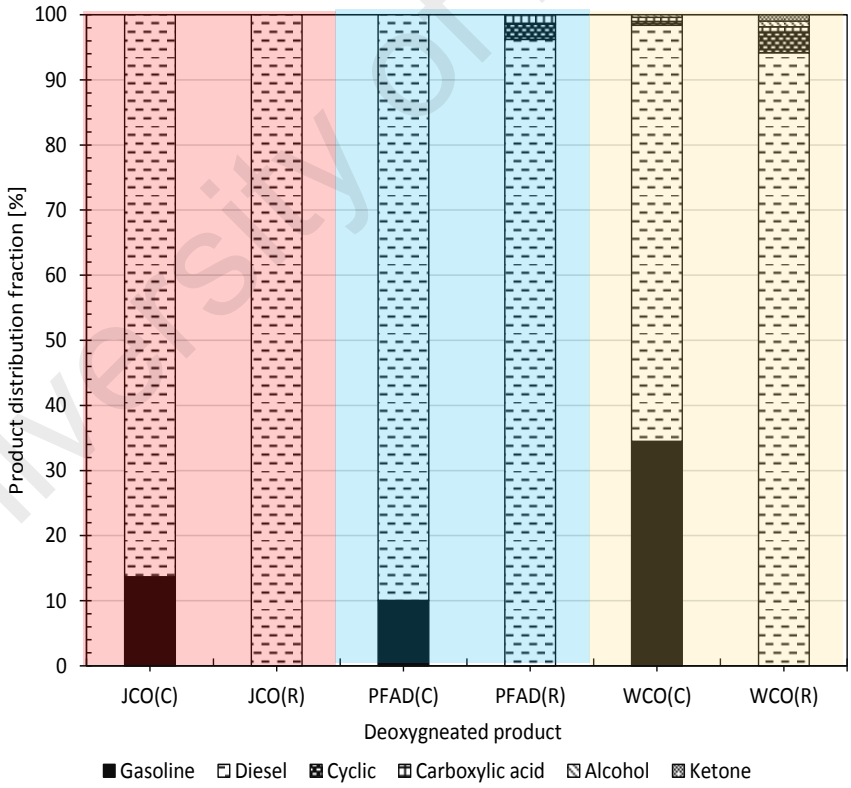

C: condensed liquid product, R: liquid product in the reactor.

Figure 6.8: Effect of NiO-5CaO/SiO_2-Al_2O_3 in product distribution fractions from deoxygenation of JCO, PFAD and WCO

Although coke was found significantly in deoxygenation of PFAD, WCO and JCO feedstocks, all the feedstocks were effectively deoxygenized via selective deCOx reaction with higher hydrocarbon weight fractions >74% and the product was predominantly selective toward *n*-C_{15}+*n*-C_{17} fractions (Figures 6.9A-C). The hydrocarbon weight fractions were in the order of PFAD>WCO>JCO and *n*-C_{15}+*n*-C_{17} selectivity were in the order JCO=PFAD>WCO. The deCOx products was the lowest in deoxygenation of WCO with 54% of *n*-C_{15}+*n*-C_{17} selectivity, while the gasoline-range *n*-(C_8-C_{12}) was the highest (46%). This implies that the deoxygenation of WCO majorly induced both C–C cleavage via cracking and C-O cleavage via deCOx reaction. This phenomenon is due to the high content of polar molecules in WCO which formed during the continuous oxidation and thermal reaction when the oil was reused multiple times during the cooking process. The high content polar molecules has enabled ion exchange on the catalyst surface (Bezergianni et al., 2009), which simultaneously enhanced the occurrence of the cracking reaction and resulted in the significant formation of the light fraction of gasoline(C_8-C_{12}). This finding is in consistent with the GC-MS results, which has revealed the detection of significant gasoline fractions in the WCO deoxygenized product and significant polar molecules from intermediate products, such as ketone (cyclic ketone), alcohol (cyclododecanemethanol), and carboxylic acid (pentadecanoic acid) (Figure 6.8).

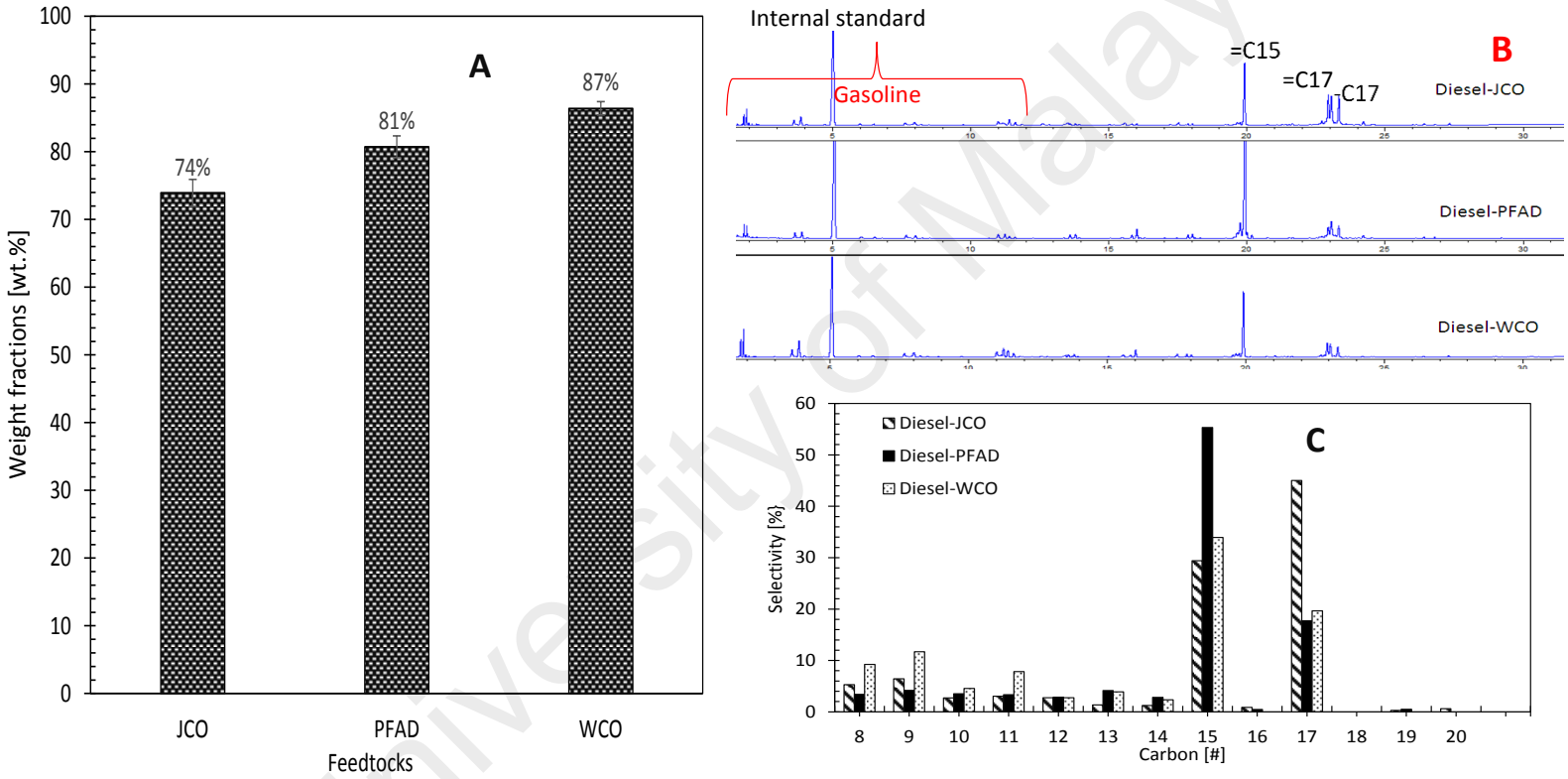

Figure 6.9: Effect of NiO-5CaO/SiO_2-Al_2O_3 in A) hydrocarbon weight fraction, (B) GC-FID chromatogram and (C) product selectivity for deoxygenation of JCO, PFAD and WCO

6.4.6 Comparison study on catalytic cracking catalysts

Catalytic activity of NiO-5CaO/SiO_2-Al_2O_3 catalyst (as mesoporous catalyst) was further compared with mesoporous zeolite-supported catalyst (Ni-ZSM 5, H-ZSM, Pd/HY) (Botas et al., 2012;Guo et al., 2009;Echeandia et al., 2014), noble metal-based catalyst (Rh/C) (Wildschut et al., 2010) and microporous alkaline-earth metal-based catalyst (CaO, $Ca(OH)_2$, Co-CaO) (Asikin-Mijan et al., 2016d;Asikin-Mijan et al., 2015a) (Table 6.3). The summary showed NiO-5CaO/SiO_2-Al_2O_3 catalyzed reaction rendered better hydrocarbon production via deoxygenation reaction instead of reaction catalyzed by mesoporous zeolite-supported catalyst (Ni-ZSM 5, H-ZSM, Pd/HY), noble metal-based catalyst (Rh/C) and alkaline-earth metal catalysts (CaO, $Ca(OH)_2$, Co-CaO). Moreover, the NiO-5CaO/SiO_2-Al_2O_3 catalyst also yielded lower coke formation compared to strong acidic-based catalyst listed in Table 6.3, which attested that strong acidic catalyst promotes the formation of coke precursor more than acid-base catalyzed deoxygenation reaction (Bui et al., 2011). Thus, the reduction of coke deposited on the NiO-5CaO/SiO_2-Al_2O_3 catalyst demonstrated the importance of the acid-base sites in changing the relative rates of coking mechanism. Evidently, acid-base catalyst (Co-CaO) in our recent study also showed maximal resistance to coke-induced deactivation with < 10 wt.% of coke (Asikin-Mijan et al., 2016d). Again it implies that basic sites lead to an important improvement in the catalyst stability. Additionally, it is also discovered that deoxygenation reaction over NiO-5CaO/SiO_2-Al_2O_3 catalyst under H_2-free atmospheres is highly promising since it could rendered higher hydrocarbon production than in hydrodeoxygenation catalyzed reaction (Yang et al., 2013b;Castaño et al., 2007). Thus, it is strongly proved that utilization of H_2 can be excluded as NiO-5CaO/SiO_2-Al_2O_3 catalyst effectively deoxygenized the feeds to optimum level along with excellent production of hydrocarbon fractions. This is a very important result to be

highlighted, since non-economical hydrodeoxygenation process is still being widely applied in the industries rather than the economical deoxygenation process.

Table 6.3: Comparison study on catalytic cracking catalysts

Type	Catalyst	Type reaction	Feed	H/C yield [%]	Coke [wt.%]	Reference
Acid catalyst	Rh/C	[a]HDO	Beech wood oil	>60	8.4	(Wildschut et al., 2010)
	Ni/ZSM-5	[b]DO	Rapeseed oil	<45	~45	(Botas et al., 2012)
	H-ZSM	[b]DO	Bio-oil	<24	33-43	(Guo et al., 2009)
	Pd/HY	[a]HDO	Phenol	28 21 63 11	16.3	(Echeandia et al., 2014)
Acid-base catalyst	NiO-5CaO/SiO_2-Al_2O_3	[b]DO	Triolein JCO PFAD WCO	91 74 81 86	12-15	Present study
	Co-CaO	[b]DO	Triolein	65	<10	(Asikin-Mijan et al., 2016d)
Base catalyst	$Ca(OH)_2$	[b]DO	Triolein	47	-	(Asikin-Mijan et al., 2015a)
	CaO	[b]DO	Triolein	35	-	(Asikin-Mijan et al., 2015a)

[a]HDO = Hydrodeoxygenation
[b]DO = Deoxygenation
[c]H/C= Hydrocarbon

6.5 Conclusion

In the present work, an effective approach was disclosed for converting triolein to the desired hydrocarbon fraction over bi-functional NiO-CaO/SiO_2-Al_2O_3 catalyst. The improvement of deoxygenation activity over bi-functional acid-base catalyst was due to the neutralization of the strong acidity catalyst. Deoxygenation under inert N_2 flow are predominantly more reactive than partial vacuum condition due to the advantages of N_2 flow which is beneficial in maintaining a high catalytic activity by preventing CO_2/CO gases produced by the deCOx reaction from poisoning the active catalyst surface. Cracking was found to be enhanced with increase of CaO content due to the richness of the high-strength basic and acid sites of the catalyts. The optimum

content for optimizing the deCOx reaction CaO was 5 wt.%. The effects of reaction time, catalyst loading and temperature were investigated and the optimum catalytic deoxygenation (hydrocarbon weight fraction = 92%, *n*-C_{15}+*n*-C_{17}= 61%) was achieved within 60 min and 7 wt.% catalyst loading at 350 °C under inert N_2 flow condition. The efficiency of bi-functional NiO-CaO/SiO_2-Al_2O_3 catalyst has been proven to be capable of deoxygenizing triglycerides-based feeds (JCO, WCO, PFAD) through selective deCOx pathways by rendering 54%, 74%, and 73% of *n*-C_{15}+*n*-C_{17} fractions and total hydrocarbon weight fraction of >74%. In addition, the reason for the high degree of coke formation was determined, which is to be related to the high existence of unsaturated FFA chains.

CHAPTER 7: OPTIMIZATION STUDY OF SiO_2-Al_2O_3 SUPPORTED BIFUNCTIONAL ACID-BASE NiO-CaO FOR RENEWABLE FUEL USING RESPONSE SURFACE METHODOLOGY

The present (chapter 7) describes the optimization study on NiO-5CaO/SiO_2-Al_2O_3 catalysed deoxygenation of triolein towards hydrocarbon yield via response surface methodology in order to evaluating the interactions between a set of independent experimental and were compared with finding in chapter 6, which optimized via one-variable-at-a-time technique. the present work is available as a published *Energy Conversion Management* article. The authors including Asikin-Mijan, N. Lee, H.V. Taufiq-Yap, Y.H. Abdulkrem-Alsultan, G. Mastuli, M.S. and Ong, H.C., under 2016 publication with title: ***Optimization study of SiO_2-Al_2O_3 supported bifunctional acid-base NiO-CaO for renewable fuel using response surface methodology.***

7.1 Introduction

Due to the concern on environmental, economical and social demand integrated with global warming effect, rising of crude oil price and diminishing of the fossil energy resources crisis have triggered further research's on use of alternative renewable resources. Therefore, several processes have been developed over the years to produce renewable fuel that is compliant with the modern infrastructure. Notably, there are several established process including cracking, transesterification/esterification and deoxygenation (Gosselink et al., 2013;Kordulis et al., 2015;Cheryl-Low et al., 2015;Yigezu and Muthukumar, 2014). Apparently, cracking and transesterification/esterification have found relatively widespread in commercial application but these process have their own drawbacks: cracking involve thermal or

catalytic decomposition of triglycerides but the product favour large range of hydrocarbons (unselective). Meanwhile, biodiesel which produce via transesterification/esterification reactions not compatible with the conventional diesel engine as it contained high oxygen content of fatty ester. Thus, greener alternative route producing less oxygenated compound and selective diesel range process are necessary in order to produce large amount of selective diesel with higher oxidative stability. This, could be achieved by deoxygenation (DO) of vegetable oil-based via selective decarboxylation/decarbonylation (deCOx) reactions, where CO_2/CO + H_2O were removed from molecule. Albeit hydrodeoxygenation (HDO) via hydrotreating reaction is more preferred pathways under certain condition, but deoxygenation reaction permit the use of more simpler catalyst and require less hydrogen which make these reactions more appealing from an economic standpoint (Santillan-Jimenez and Crocker, 2012c).

Nowadays, a significant number of acidic metal catalyst such as Ni, Ni/Mo, Ru, Pd, Pd/Pt, Pt, Ir, Os and Rh have been tested on different supports (metal oxides and charcoal) for their deoxygenation performance (Lestari et al., 2009;Arend et al., 2011). It was found the used of noble catalyst (Pt and Pd) was the most active for fatty acid deoxygenation reaction and their derivatives to fuel-like hydrocarbon via COx reaction. However, despite the high performance of Pd-based and Pt-based, their high cost is the most critical restriction to their viability as industrial scale catalysts. In this connection, it is necessary to develop alternative catalyst such as less expensive metallic catalysts, high deoxygenation ability with selective deCOx reaction. Ni-based catalysts are promising candidates, which had confirmed by several reports on the performance in deCOx reaction (Roh et al., 2011;Santillan-Jimenez et al., 2013). Croker and co-workers reported the deoxygenation of triglycerides by using 20 wt.% Ni/C, 5 wt.% Pd/C and 1 wt.% Pt/C catalysts under N_2. Results showed that 20 wt.% Ni/C able to convert >81%

of tristearin, triolein and soybean oil to hydrocarbons fractions (<C_8,C_8–C_{17} and C_{18}) which rendered highest activity than 5 wt.% Pd/C and 1 wt.% Pt/C (Morgan et al., 2010). Although Ni-based catalyst showed potential for deoxygenation process, however, the presence of acidity properties limited to the reaction, which the acidic catalyst suffered extensive deactivation that attributed by catalyst coking and tar formation (Arun et al., 2015). Recently found, coke and tar formation could be inhibited via introduction of basic catalyst derived CaO and MgO in deoxygenation reaction (Tani et al., 2011;Lin et al., 2010;Romero et al., 2015b). The use of mesoporous acidic support such as SiO_2-Al_2O_3 was found to be effectively work in deoxygenation process (Yang et al., 2013b;Calemma et al., 2000). Catalyst mesoporous support not only improve the catalyst stability but able to improve the product selectivity during the reaction. It was in agreement with previous finding, who observed high cracking reaction (selectively toward paraffin-range hydrocarbon formation) via deCOx when mesoporous support like SiO_2-Al_2O_3 is used as catalyst support. Therefore, combination of acid-base catalyst derived SiO_2-Al_2O_3 promoted by acid-base active promoter might be the key of high occurrence of deoxygenation via selective deCOx.

Other than the present of effective deoxygenation catalyst, optimization study for catalysed deoxygenation reaction in renewable fuel production is the crucial part to obtain better yield of product with high selectivity and further scale up manufacturing process. Therefore, in this work, instead of using the traditional optimization via the variation of one component at a time, which the response was a function to a single parameter (one-variable-at-a-time technique) (Bezerra et al., 2008). According to Bas and Boyaci, one-variable-at-a-time technique excludes the interactive effects among the parameter and eventually, it does not depict the complete effects of the parameters on the process (Baş and Boyacı, 2007). Therefore, in order to overcome this weakness, the

optimization studies can be carried out by using response surface methodology (RSM), which is among the most relevant multivariate techniques. Thus, it the present study, we focused on the optimization study for renewable fuel process via response surface methodology (RSM) over mesoporous SiO_2-Al_2O_3 support Ni-Ca catalyst. In the optimization study, the major variables chosen for optimization studies are catalyst amount, reaction time and reaction temperature.

7.2 Literature Review

Yang et al., (2009), Tani et al., (2011), Lin et al., (2010), and Romero et al., (2015b) have recently reported on the deoxygenation of vegetable oil-based via deCOx and cracking over solid base catalyst (MgO-based and CaO-based catalyst) for the deoxygenation process. Despite showing excellent oxygen removal and highly active in deoxygenation activity, it apparently exhibited superior in suppressing the coke formation. Admittedly, the high activity of deoxygenation reactivity accompanies with better catalyst coke resistance might be achieved by the co-existence of acid and basic sites promoters. Acidic supports such as amorphous silica–aluminas can be used in combination with metals promoter for achieving ‘‘ideality” from metal–acid site balance and affect the reaction patterns and selectivity. It has been established that optimization study for catalyzed deoxygenation reaction in renewable fuel production is an important stage in the production process. Process optimization is often time-consuming and requires repeated, expensive experiments. Furthermore, due to the simultaneous effects of some operating variables on the system, the design and application of modeling tools such as the response surface methodology (RSM) are essential for maximizing the productivity and reducing the production process costs. RSM is a set of mathematical and statistical methods for modeling and problem

analysis. This methodology is suitable for optimizing complicated systems where response is influenced by several parameters (Hamze et al., 2015).

7.3 Experimental and methods

7.3.1 Material

The nickel (II) nitrate hexahydrate ($Ni(NO_3)_2.6H_2O$) with purity > 99% and calcium nitrate tetrahydrate ($Ca(NO_3)_2.4H_2O$) with purity > 99% were obtained from R&M Company. Silica-Alumina (SiO_2-Al_2O_3) catalyst support grade 135 were purchased from Sigma Aldrich. Triolein feedstock was obtained from sigma Aldrich, which GCMS analysis showed the triolein (65%) composed of saturated fatty acids and unsaturated fatty acid (Table 7.1) (Morgan et al., 2010). Standard solution of alkane and alkene (C_8-C_{20}) and internal standard 1-bromohexane with purity > 98% (GC grade) were purchased from Sigma Aldrich. For dilution purpose, n-Hexane solvent (GC grade) with purity > 98% from Merck was used.

Table 7.1: Physicochemical properties of triolein

Oil properties	Triolein	Methods
Density (g/cm^3)	0.91	ASTM D1298
Viscosity at 40^o C (cSt)	38.62	ASTM D445 - 15a
Moisture content (wt.%)	0.08	ASTM E203 - 08
Acid Value (mg KOH/g)	5.0	AOCS Ca 5a-40
FFA Value (%)	2.5	AOCS Ca 5a-40
Fatty acid composition of Oil (%)		AOCS Ce1-62 & Ce-661
Myristic (C14:0)	1.2	
Myristoleic (C14:1)	0.3	
Pentadoic (15:0)	0.4	
Palmitic (16:0)	3.8	
Palmitoleic (C16:1)	4.3	
Stearic acid (C18:0)	1.9	
Oleic acid (C18:1)	83.3	
Linoleic (18:2)	0.4	
Linolenic acid (C18:3)	0.2	
Arachidic (C20:0)	0.1	
Gadoleic (C20:1)	0.8	
Behenic (22:0)	<0.1	
Others	3.2	

7.3.2 Catalyst synthesis

Silica-Alumina (SiO_2-Al_2O_3) supported NiO-CaO catalyst was prepared by using wet impregnation method. Approximately 10 g of SiO_2-Al_2O_3 powder was impregnated with an aqueous solution 5 wt.% of Ca and 10 wt.% of Ni concentration. The mixtures were stirred for 6 h, then left to continue drying in the oven at the temperature 100 ^oC for overnight. The dried samples were grounded into fine powder before thermally activated at temperature of 500 ^oC for 2 h under atmosphere condition and known as NiO-CaO_5/SiO_2-Al_2O_3.

7.3.3 Catalyst characterization

The catalysts were characterized by XRD, TPD-CO_2, TPD-NH_3, FESEM-EDX analysis. The powder X-ray diffraction (XRD) analysis was employed to identify the crystallography of the mixed metal oxide catalysts. The powder X-ray diffraction (XRD) analysis was carried out to identify the crystallography of the mixed metal oxide catalysts. The XRD analysis was performed using Shimadzu diffractometer model XRD-6000. Furthermore, the basicity and acidity of the catalysts were studied using temperature programmed desorption (TPD-CO_2) and (TPD-NH_3) with CO_2 and NH_3 as probe molecules, respectively. The analysis was carried out by using Thermo Finnigan TPD/R/O 1100 instrument equipped with thermal conductivity detector (TCD). The catalyst (~0.05 g) was pre-treated with N_2 gas flow for 30 min at 250 ^oC, followed by CO_2 gas flow for an hour at ambient temperature to allow adsorption of CO_2 on the surfaces of catalyst. The excess CO_2 was subsequently flushed with N_2 gas flow at rate 20 ml/min for 30 min. The desorption of CO_2 from the basic sites of the catalyst was detected by TCD under helium gas flow (30 ml/min) from 50 ^oC to 900 ^oC and held for 30 min. The adsorption and desorption of NH_3 was similar to TPD-CO_2 method. Morphological and elemental compositions of the catalysts were investigated by the

FESEM images were recorded on LEO 1455 VP electron microscope. The FESEM device was fitted with EDX analysis was performed by Rayny EDX-720 spectrometer for the determination of elemental composition of Ca, Ni, Si and Al on the synthesized catalysts. The coking tendency of catalyst was evaluated using thermogravimetric analysis (TGA) with simultaneous thermal analyzer (TGA, Mettler Toledo 990). The extent of coke/carbon deposition on the spent catalyst was determined by thermogravimetric analysis (TGA) instrument (TGA 1000i, Instrument Specialists Inc, USA). The samples were heated from 25 to 900 ^{o}C at a heating rate of 30 ^{o}C/min under 40 mL/min air flow.

7.3.4 Catalytic deoxygenation of triolein

The deoxygenation of triolein was performed in a mechanically stirred 250 mL of semi-batch reactor (Figure 7.1). In a typical experiment, approximately 10 g of triolein and a fixed amount of catalyst were added to the reactor. Initially, the reactor was vacuumed by using a mechanical vacuum pump attached with pressure controller to remove the air/vapour in the system and later pressurized to approximately at 0.1 bar (10 mbar) before start the experiment. The purpose to lowering the air pressure will accelerate the reaction temperature of reaction medium to the desired point at shorter time and increase the diffusion rate between feedstock to enhance the deoxygenation process. During the deoxygenation process, generated vapour/volatile species was condensed into liquid product by using external water cooling circulator under temperature of 16 ^{o}C and then collected by using a vessel collector. The generated gas/vapour during deoxygenation process was removed by the vacuum system in order to control the pressure in the system at 10 mbar. Pressure builded up in vacuum system was adjusted during the reaction by released the generated gas from system. The reaction condition of deoxygenation experiments was determined by RSM-CCD

method. Final deoxygenized liquid products were further analyzed by using FITR, GC-FID and GCMS analysis. The spent solid catalyst was further washed with hexane to remove the organic compounds and dried in an oven at 110 ^{o}C for 12 h for further analysis**.**

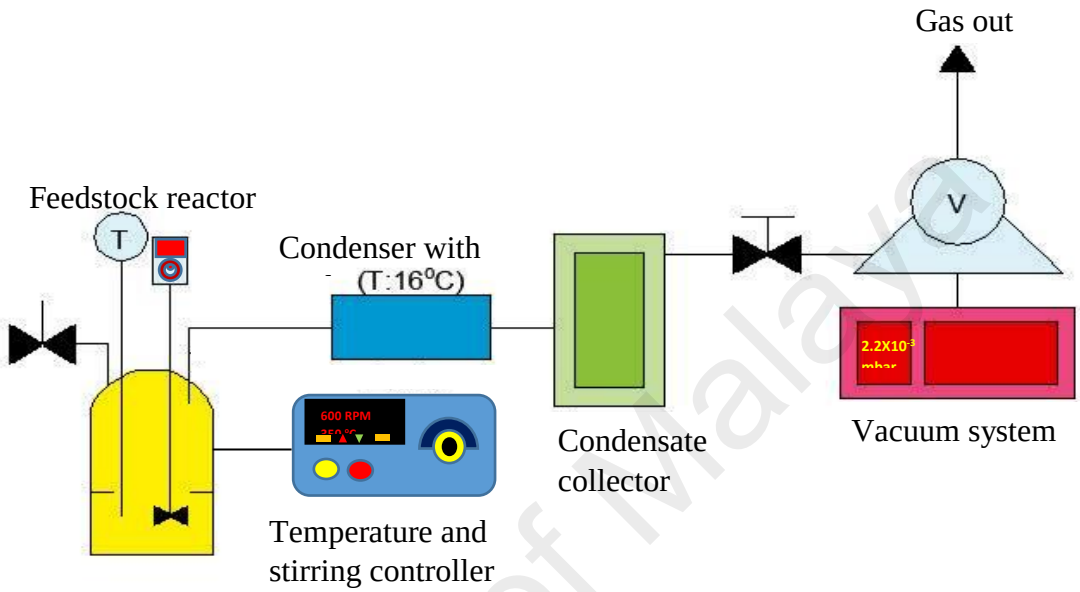

Figure 7.1: Schematic diagram for semi-batch reactor

7.3.5 Experimental design

In the present study, statistical analysis of straight chain hydrocarbons yield (C_8–C_{20}) production via deoxygenation process was performed using Statsoft Statistica 8.0 software. The central com- posite design (CCD) was applied to study the NiO-5CaO/SiO_2-Al_2O_3 catalysed deoxygenation reaction variables. Three identified independent variables are A: reaction temperature (270–390 ^{o}C), B: reaction time (30–150 min) and C: catalyst loading (1–9 wt.%). The response chosen was straight chain hydrocarbons yield, which were obtained from the deoxygenation reaction of triolein. The actual and coded levels of the independent variables are given in Table 7.2. The independent variables are coded to two levels namely: low (−1) and high (+1), whereas the axial points are coded as −2 (−α) and +2 (+α). In this study, the α value was fixed at 2, which is the distance of the axial point from center and makes the design rotatable.

The 20 designs of the experiment were produced to fit the CCD model including 8 experiments at the factorial point, 6 at the axial point and another 6 replicates at the center point (Table 7.3). Each experiment was run in replicate to reduce the experimental error.

Table 7.2: Five-level-four-factor central composite design of deoxygenation variables

Factor	Coding	Units	Levels				
			-2	-1	0	1	2
Reaction temperature	A	^{o}C	270	300	330	360	390
Reaction time	B	min	30	60	90	120	150
Catalyst loading	C	wt.%	1	3	5	7	9

Table 7.3: Experimental design generated by RSM and responses from each reaction

Type	A: Reaction temperature (^{o}C)	B: Reaction time (min)	C: Catalyst loading (wt.%)	Straight chain hydrocarbon yield (%)
Fact	300	60	3	28.10
Fact	360	60	3	51.60
Fact	300	120	3	66.40
Fact	360	120	3	70.32
Fact	300	60	7	50.01
Fact	360	60	7	74.61
Fact	300	120	7	53.11
Fact	360	120	7	65.01
Axial	270	90	5	9.60
Axial	390	90	5	40.10
Axial	330	30	5	55.01
Axial	330	150	5	80.10
Axial	330	90	1	60.14
Axial	330	90	9	73.23
Center	330	90	5	70.50
Center	330	90	5	72.20
Center	330	90	5	70.46
Center	330	90	5	70.61
Center	330	90	5	71.80
Center	330	90	5	71.52

7.3.5 Statistical Analysis

The data obtained from the experiments were analyzed by response surface methodology to develop a mathematical model. A second-order polynomial equation was used to relate the response to the selected factors (Halim et al., 2009). The general form of the second-order polynomial equation shown at Eq. 7.1, where Y is the predicted response; β_o, β_j, β_{ij} and β_{jj} are constant coefficients; x_i and x_j are the coded independent variables or factors; ε is random error.

$$Y = \beta o + \sum_{j=1}^{k} \beta_j x_j + \sum_{i<j} \beta_{ij} x_i x_j + \sum_{j=1}^{k} \beta_{jj}{}^2 x_j + \varepsilon \quad (7.1)$$

The quality of fit for the model was evaluated by the coefficients of determination (R_2) and its regression coefficient significant (analysis of variances (ANOVA) were checked with Fisher's test (F-test) (Montgomery, 2001). Response surfaces and contour plots were developed using the quadratic polynomial equation obtained from regression analysis of experimental data by keeping two of the independent variables at a constant value while changing the other two variables.

7.3.6 Product analysis

FTIR analysis was performed using Perkin-Elmer Spectrum (PS) 100 FT–IR spectrometer with resolution of 4 cm^{-1} operating in the range of 300–4000 cm^{-1}. This analysis helps to determine the chemical functional group of the liquid product. The deoxygenated liquid products were identified using alkane and alkene standards (C_8–C_{20}), which were purchased from Sigma Aldrich. The liquid products were quantitatively analyzed by using on a gas chromatography (Shimadzu GC-14B) equipped with a HP-5 capillary column (length: 30 m × inner diameter: 0.32 mm × film

thickness: 0.25 µm) with a flame ionization detector (FID) operating at 300 ^{o}C. The liquid product was diluted with GC grade *n*-hexane prior to the analysis. 1-Bromo hexane was used as internal standard for quantitative analysis. An aliquot of 1 µL of sample was injected with into GC column. The injection temperature was 250 ^{o}C and nitrogen gas has been served as the carrier gas. The initial temperature of the oven was set at 40 ^{o}C and held for 6 min, then ramped to 260 ^{o}C at heating rate of 7 ^{o}C/min. The catalytic performances of the catalyst was investigated by determine the saturated and unsaturated hydrocarbons straight chain hydrocarbons yield (X) (Eq. (7.2)) (Asikin-Mijan et al., 2015a). Based on fatty acid composition of triolein (Table 7.1), the unsaturated fatty acid in form of oleic acid was found notably (83.3%). Upon performing the catalytic deoxygenation of triolein to straight chain hydrocarbons under hydrogen deficiency condition, the decarboxylation of unsaturated oleic acid (from triolein) tends to form *n*-heptadecenes (mono-unsaturated; $C_{17}H_{34}$) via scission of C-C bond of fatty acid (oleic acid), which leads to the oxygen removal in the form of CO_2 gas as by products. For decarbonylation reaction, di-unsaturated *n*-heptadecene ($C_{17}H_{32}$) was produced by removing oxygen in the form of CO gas and water as a by-product (Snare et al., 2006)(Asikin-Mijan et al., 2015a). Theoretically, under H_2 deficiency condition, all of the hydrocarbon chain tends to form unsaturated hydrocarbons instead of saturated hydrocarbon chain as absence of hydrogenation pathway for saturation of alkene products. Therefore, calculation for both unsaturated and saturated straight chain hydrocarbons must be included.

$$X = \frac{\sum n_o + \sum n_i}{\sum n_z} \times 100\% \qquad (7.2)$$

Where:

X = saturated and unsaturated straight chain hydrocarbons yield (%)

n_o = Area of alkene (C_8-C_{20})

n_i = Area of alkane (C_8-C_{20})

n_z = Area of the total product

In additional, the chemical composition of feedstock and deoxygenated liquid product was qualitatively characterized using gas chromatography mass spectrometer (GC-MS) (model SHIMADZU QP5050A) equipped with a non-polar DB-5HT column (30 m x 0.25 mm x I.D µm) with split less inlet. The samples were diluted with GC grade n-hexane (purity > 98%) to 100 ppm. Generated fraction peaks from GC-MS spectrum were identified via National Institute of Standards and Testing (NIST) library. Compound identification was based on a probability match equal or higher than 95%. The selectivity of the deoxygenated products was determined followed Eq. 7.3.

$$S = \frac{C_x}{\sum n_x} \times 100\% \quad (7.3)$$

Where:

S = Selectivity (%)

C_x = Area desired organic compound

n_x = Area of total organic compounds

7.4 Results and discussion

7.4.1 Physicochemical properties of NiO-5CaO/SiO_2-Al_2O_3 catalyst

The XRD patterns of SiO_2-Al_2O_3 support doped with 10 wt.% of Ni and 5 wt.% of Ca metal are shown in Figure 7.2a. Based on the XRD patterns, SiO_2-Al_2O_3 catalyst support showed an broad peak that attributed to low crystallinity and amorphous characteristic of silica-alumina mesoporous structure (Yoshida et al., 2002). For NiO-5CaO/SiO_2-Al_2O_3 catalyst., the presence of intense NiO peak at $2\theta = 43.74^o$ (JCPDS

card no. 00-047-1049) and CaO peak at 2θ value 37.76º (JCPDS card no. 00-037-1497) indicated the active mixed metal oxide (NiO-CaO) successfully impregnated on the SiO_2-Al_2O_3 support.

Basicity and acidity profile of synthesized catalyst were evaluated by using temperature programmed desorption of CO_2 and NH_3, respectively. The TPD-CO_2 and TPD-NH_3 pattern of NiO-5CaO/SiO_2-Al_2O_3 catalyst was displayed in Figures 7.2b and 7.2c. The mixture of both NiO-CaO able to enhance the basicity and acidity of the catalyst. NiO-5CaO/SiO_2-Al_2O_3 catalyst showed the presence of weak, moderate and strong basic strength at T_{max} range 100-200 ºC (31.07µmol/g), 200-400 ºC (552.4 µmol/g) and > 500 ºC (523.65 µmol/g), respectively. Meanwhile, SiO_2-Al_2O_3 catalyst support rendered negligible amount of weak basic sites at T_{max} = 100 ºC with total basic density of 12.39 µmol/g. A similar pattern has been observed from the acidity study, where NiO-5CaO/SiO_2-Al_2O_3 catalyst showed the highest weak acid density at T_{max} at 100–200 ºC (3157.52 µmol/g) as compared to SiO_2-Al_2O_3 catalyst support (1430.68 µmol/g). Besides, the synthesized catalyst also showed the formation of strong acid strength at T_{max} = 717 ºC, with total acid density of 845.23 µmol/g. It can be suggested that the enhanced basicity and acidity of catalyst was due to the incooperation of mixed metal oxide NiO-CaO system with SiO_2-Al_2O_3 catalyst support. The surface morphology and elemental composition study of the NiO-5CaO/SiO_2-Al_2O_3 catalyst was shown in Figure 7.2(d1) and (d2), respectively. The FESEM image showed the changes of smooth surface from SiO_2-Al_2O_3 support to rougher surface with sheet torn-like morphologic surface, which consisted of triangle-like aggregates (NiO-5CaO/SiO_2-Al_2O_3). Elemental analysis (Figure 7.2e) indicated that Ni and Ca phases was presence on the surface of SiO_2-Al_2O_3 support, which composed of 8 at.% of Ni and 4.3 at.% Ca, which is comparable to intended ratio of NiO (10 wt.%):CaO (5 wt.%).

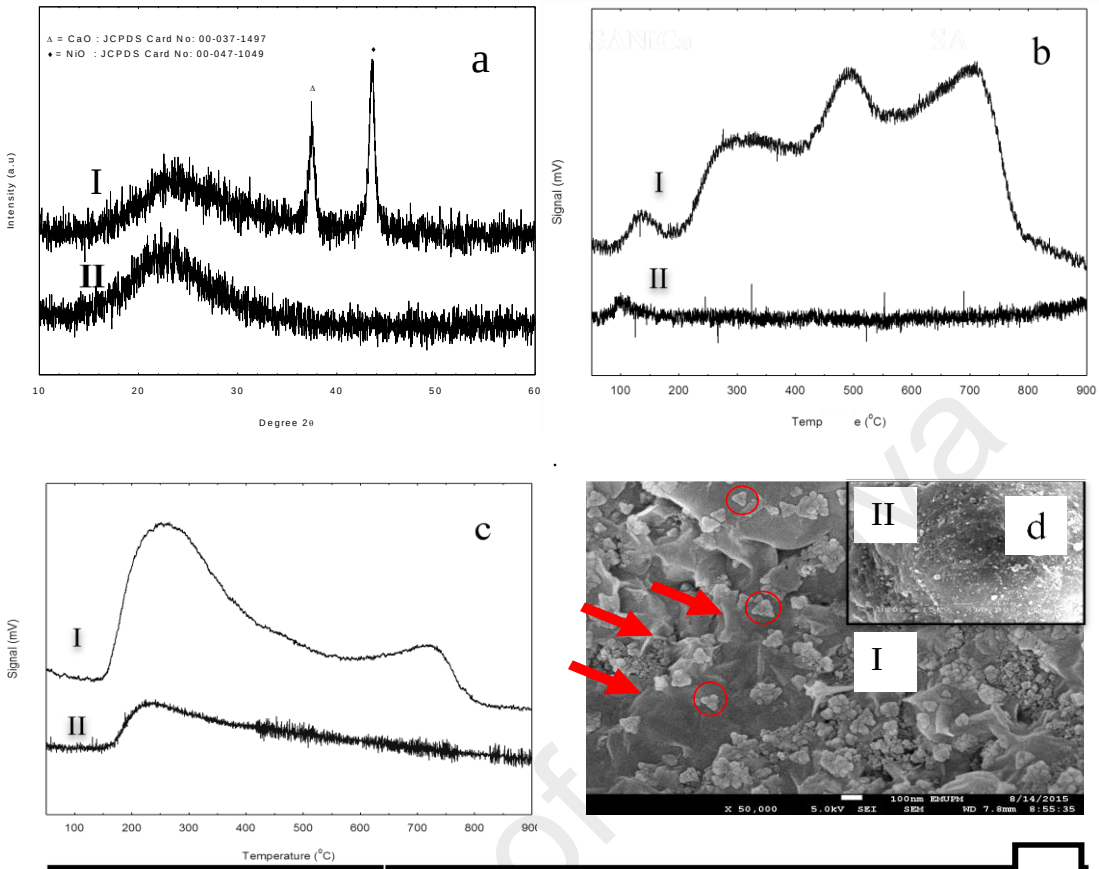

Catalyst	Elemental composition (wt.%)				e
	Si	Al	O	Ni	Ca
SiO_2-Al_2O_3	35.1	10.1	54.8	-	-
NiO-CaO_5/SiO_2-Al_2O_3	19.4	6.1	62.0	8.0	4.3

Figure 7.2: Characterization of catalysts: (I) NiO-5CaO/SiO_2-Al_2O_3 and (II) SiO_2-Al_2O_3 for (a) XRD diffractogram and (b) TPD-CO_2 (c) TPD-NH_3; (d) FESEM; and (e) FESEM-EDX

7.4.2 Development of regression model

Regression analysis was used to study the relationship of empirical or predicted model that is generated from experiment data. Among the models (linear, two factor interaction (2FI), quadratic and cubic polynomial) that can fit the response, the quadratic model was suggested as the best model for the response generated from experimental design. Table 7.4 depicts the sequential model sum of the square for the generated data. The fitting summary for the model was selected based on the sequential model sum of the square, the lack of fit test, and the model summary statistics. Besides,

the quadratic model was selected as the best model due to its highest order polynomial with significant reaction terms. The reaction model revealed insignificant lack of fits, which ensured that the model was good with low error (Rashid et al., 2011). Furthermore, the model equation based on the coded values (A, B, and C as reaction temperature, reaction time, and catalyst amount, respectively) for straight chain hydrocarbons-based fuel production is expressed in Eq. (7.4). The generated model equation indicated that positive coefficients of A, B, C, and AC rendered linear effect towards the response. However, the quadratic terms of A^2,B^2,C^2, AB, and BC showed negative effects, which decreased the product yield.

Table 7.4: Sequential model sum of squares

Source	Sum of Squares	DF	Mean Square	F Value	Prob > F	
Mean	72512.11	1	72512.11	-	-	-
Linear	1778.93	3	592.98	2.30	0.1166	-
2FI	645.17	3	215.06	0.80	0.5146	-
Quadratic	3475.85	3	1158.62	1231.06	< 0.0001	Suggested
Cubic	6.45	4	1.61	3.27	0.0949	Aliased
User Added Terms	0.11	1	0.11	0.20	0.6731	Aliased
Residual	2.84	5	0.57	-	-	-
Total	78421.47	20	3921.07	-	-	-

$$\text{Hydrocarbons yield} = 71.15 + 7.81A + 6.28B + 3.28C - 11.60A^2 - 0.93B^2 - 1.14C^2 - 4.04AB + 1.14AC - 7.94BC \quad (7.4)$$

Experimental data obtained were analyzed via ANOVA analysis in order to assess the goodness of fit. The significant quadratic models and the corresponding significant model terms for all responses are tabulated in Table 7.5. Based on 95% confidence level, the reaction model was found significant as the computed F value of 696.54 reflected very low probability value ($p < 0.001$). With that, the high significance

of the fitted model exhibited the reliability of the regression model for predicting the straight chain hydrocarbons yield. Other than that, the p-value (probability of error value) was used as a tool to determine the significance of each regression coefficient, which also indicated the interaction effect of each cross product. The smaller the p-value, the bigger the significance of the corresponding coefficient (Lee et al., 2011). Therefore, this regression model had been found reliable in predicting the straight chain hydrocarbons yield. In the case of model terms, p-values less than 0.05 showed that the particular model terms were statistically significant (Rashid et al., 2011;Lokman et al., 2015b). Referring to the ANOVA results, the reaction variables that significantly influenced the straight chain hydrocarbons yield were reaction temperature (A), reaction time (B), and catalyst loading (C). In addition, the interactions between AB, AC, and BC also significantly affected the response of straight chain hydrocarbons yield. The ANOVA analysis summarized thatreaction temperature (A) was the most influence parameter (F value = 1036.46), while interaction between reaction time catalyst loading (BC) also playing main role to positively enhance the straight chain hydrocarbons yield significantly (F value = 536.05).

Table 7.5: ANOVA analysis of response surface quadratic model

Source	Sum of Squares	DF	Mean Square	F Value	Prob > F	
Model	5899.95	9	655.55	696.54	< 0.0001	significant
A	975.47	1	975.47	1036.46	< 0.0001	
B	631.39	1	631.39	670.87	< 0.0001	
C	172.07	1	172.07	182.83	< 0.0001	
A^2	3381.10	1	3381.10	3592.50	< 0.0001	
B^2	21.93	1	21.93	23.30	0.0007	
C^2	32.54	1	32.54	34.57	0.0002	
AB	130.33	1	130.33	138.48	< 0.0001	
AC	10.33	1	10.33	10.97	0.0078	
BC	504.51	1	504.51	536.05	< 0.0001	
Residual	9.41	10	0.94	-	-	
Lack of Fit	6.57	5	1.31	2.31	0.1899	not significant
Pure Error	2.84	5	0.57	-	-	
Cor Total	5909.36	19	-	-	-	
Std. Dev.[a]		0.97		R-Squared		0.9984
Mean		60.21		Adj R-Squared[b]		0.9970
C.V.[c]		1.61		Pred R-Squared[d]		0.9915
PRESS		50.27		Adeq Precision[e]		103.253

[a] Standard of deviation.
[b] Adjusted R^2.
[c] Coefficient of variation.
[d] Predicted R^2.
[e] Adequate precision

The lack of fit with F-value of 2.31 implies that there were 2.31% chances that 'Lack of fit for F-value' might have occurred due to noise (Lokman et al., 2015b). However, insignificant lack of fit model shown by the ANOVA analysis proved that the model satisfactorily fitted to the experimental data (Noordin et al., 2004). In addition, the predicted value versus the actual value for hydrocarbon yield with adjusted R2 value of 0.9984 indicated that the model projected 99.84 of variability (Figure. 7.3). For this particular reason, the accuracy and the general availability of the polynomial model was adequate for usage. Furthermore, the Pred. R-squared (predicted values) of 0.9915 and the Adj R-Squared (experimental values) of 0.9970 further prove that the data fit well with the model and gave a convincingly good estimate of response. The coefficiency of the variation (C.V. = 1.61) was significantly smaller, which mean that high degree of precision and the experimental value were within a good range.

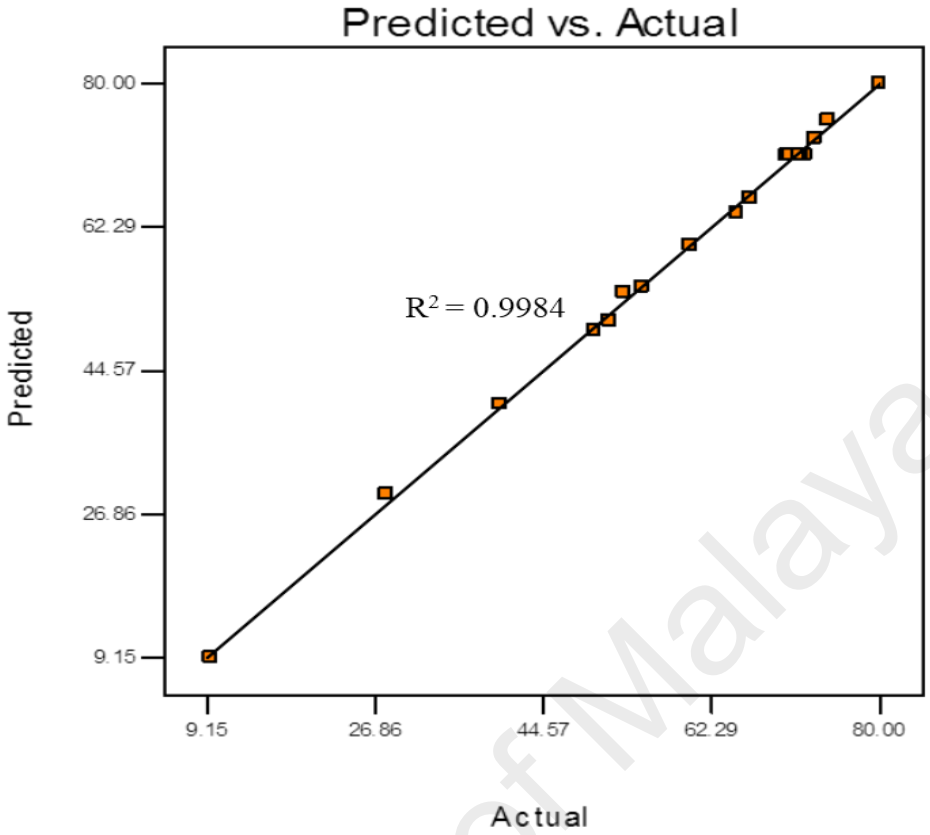

Figure 7.3: Predicted value vs. actual straight chain hydrocarbon

In addition, investigation on residuals to determine the adequacy of the reaction model was performed. Residual is the difference between the observed response and the predicted response. This analysis was carried out by using the normal probability plot of the residuals (Figure 7.4a) and the plot of the residuals versus predicted response (Figure 7.4b). The normal probability plot of the residuals specified that the errors were normally distributed in a straight line and insignificant. Meanwhile, the plot of residuals versus predicted response had been found scattered randomly within the limit. Therefore, it was expected to produce a virtuous estimation and possessed the ability to appraise the correlation of the variables (Lokman et al., 2015b).

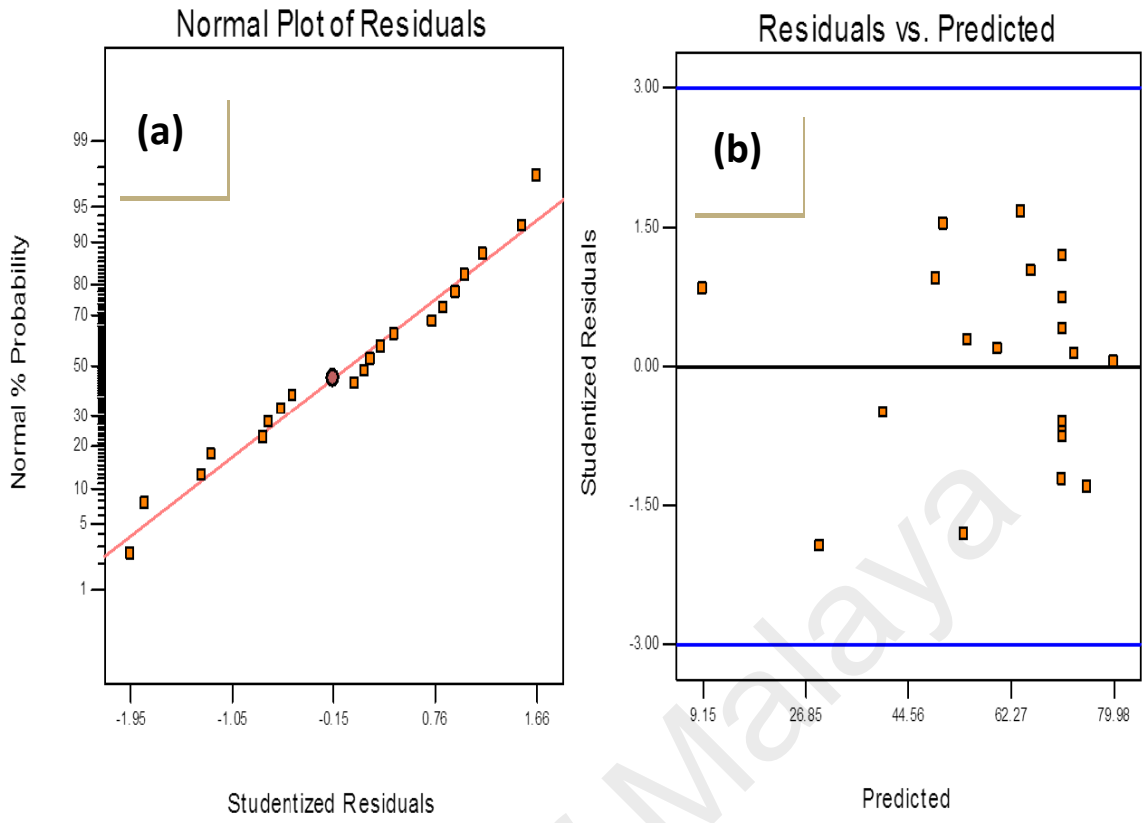

Figure 7.4: (a) Normal probability plot of the residuals and (b) plot of the residuals vs. predicted response

7.4.3 Parameter study

The general graphical represented the regression equation are given in both three-dimensional (3D) response surface plots and two-dimensional (2D) contour plots. Both 3D response surface plots and 2D contours plots (Figure 7.5) showed the effect of two variables towards straight chain hydrocarbons yield. It was observed that when the catalyst was catalyzed at high temperature, the reaction time and the increasing catalyst loading had a positive effect towards straight chain hydrocarbons yield until a maximum value was achieved.

Figure 7.5a shows the 3D plot and 2D plot for the interaction effect between reaction temperature (A) and reaction time (B) towards straight chain hydrocarbons yield, where the catalyst loading (B) was fixed at 5 wt.%. It was revealed that an

increment of reaction temperature from low level (300 ^{o}C) to high level (340 ^{o}C) led to the increase of straight chain hydrocarbons yield at continuous prolong of reaction time. However, further increment of temperature for >360 ^{o}C led to decrement of deoxygenation activity with lower straight chain hydrocarbons yield. High reaction temperature enhanced the occurrence of further cracking reaction pathway, which led to formation of lighter fractions (gaseous product) and reduced the liquid straight chain hydrocarbons yield (Arend et al., 2011;Kiatkittipong et al., 2013). Results showed that >70% of straight chain hydrocarbons yield was achieved under optimum reaction temperature of 340 ^{o}C and reaction time within 120 min.

On the other hand, Figure 7.5b shows the response surface plot and contour plot of interaction effect between reaction temperature (A) and catalyst loading (C) on straight chain hydrocarbons yield, where reaction time was fixed at 90 min. Results showed that the catalyst loading rendered mild impact on the straight chain hydrocarbons yield under constant reaction temperature (300 ^{o}C). However, varying the reaction temperature (from 300 to 340 ^{o}C) apparently enhanced the deoxygenation activity (>70% of straight chain hydrocarbons yield) under constant catalyst loading. Thus, reaction temperature plays an important role to initiate the deoxygenation process and high amount of catalyst loading was positively assisted in the reaction (Arend et al., 2011;Kiatkittipong et al., 2013). The result also showed that NiO-5CaO/SiO_2-Al_2O_3 effectively catalysed the yield of straight chain hydrocarbons by >70% using catalyst loading >4 wt.% at reaction temperature (330–350 ^{o}C).

In the present study, the simultaneous interaction effect towards straight chain hydrocarbons yield by varying reaction time (B) and the catalyst loading (C) is illustrated in Figure 7.5c. Results showed that interaction of both reaction parameters

rendered positive response towards the deoxygenation activity as the catalyst loading were within the range of 1–7 wt.% and reaction time within the range of 30–90 min. Further increased of the catalyst loading >7 wt.% along with reaction time >90 min will resulted in reduction of straight chain hydrocarbon yield. Although increment of catalyst loading resulted in more active sites for deoxygenation reaction, reaction, however, excessive of active sites caused the possibilities of parallel or secondary reactions such as polymerization, which accelerate the deactivation of catalyst life as polymerization process generated coke on the catalyst (Kwon et al., 2011;Mortensen et al., 2011). Moreover, prolonging the reaction time favour for the occurrence of undesirable side reactions (polymerization and cracking) of the deoxygenated liquid product into lighter fractions (gaseous product), which resulted in lower hydrocarbon yield. This was in agreement with Eq. (7.4) which showed negative interaction of BC, which simultaneously increase both parameters above the optimum level will reduce the product yield. Thus, this is suggested that maximum of hydrocarbon yield can be achieved at shorter time (30–90 min) and catalyst loading (1–7 wt.%.), beyond the optimum parameter will reduce the yield. The result further showed that optimum straight chain hydrocarbons yield (>70%) was achieved with 7 wt.% catalyst loading within 60 min.

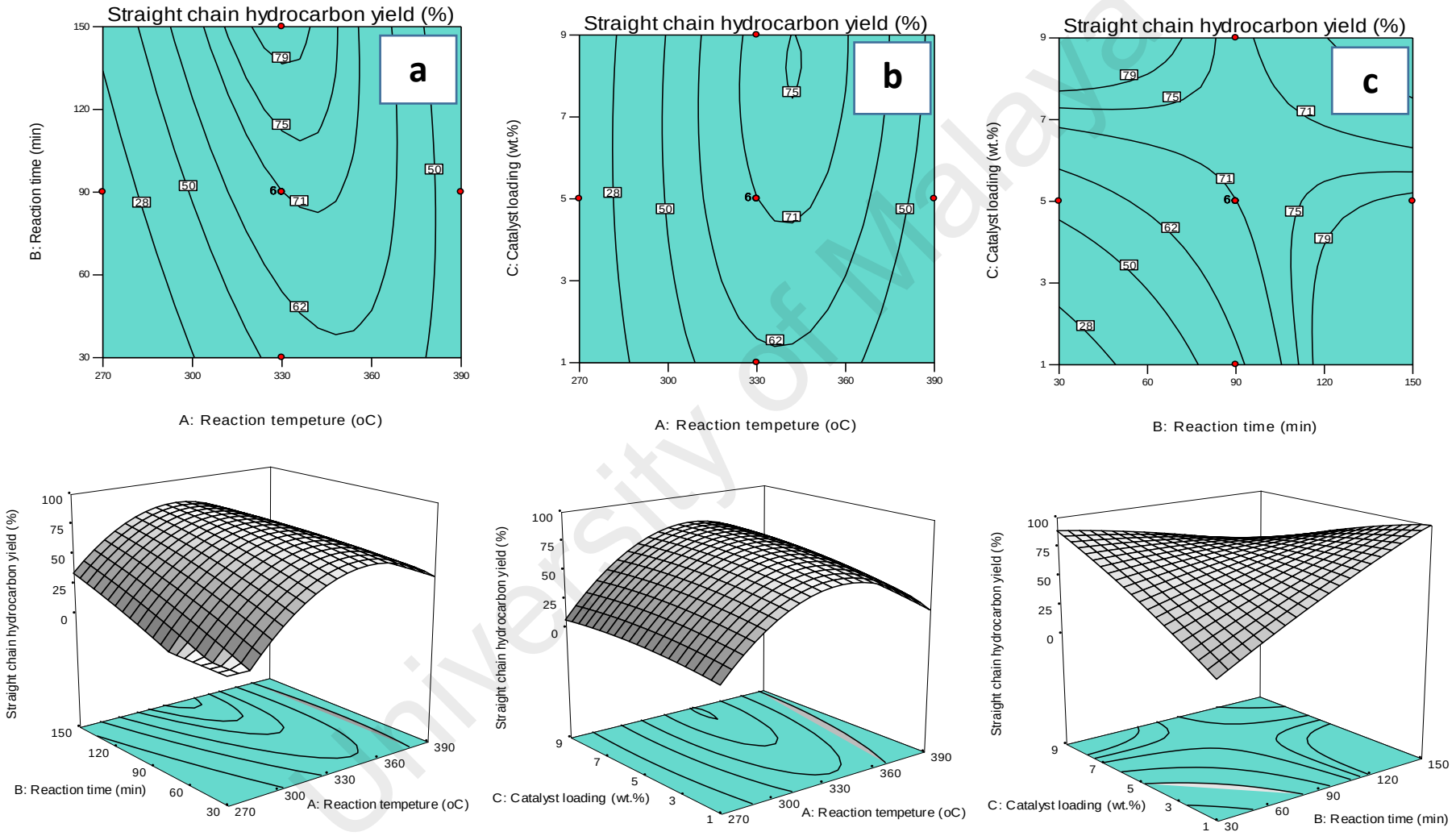

Figure 8.5: 3D-response surface plot and 2D-contour plot for (a) interaction of reaction temperature and reaction time (AB), (b) interaction of reaction temperature and catalyst loading (AC), and (c) interaction of reaction time and catalyst loading (BC)

7.4.4 Model validation study

In order to verify the prediction validity of the model, the optimal reaction conditions were applied to three independent replicates of NiO-5CaO/SiO_2-Al_2O_3 catalysed deoxygenation reaction, which the experiment condition were suggested from the reaction model (Table 7.6). The experimental results indicated that straight chain hydrocarbons yield was reasonably closer to the predicted value that generated from the model (2.6% of average error). It also revealed that the actual straight chain hydrocarbons yield had been slightly less than the RSM-predicted data. However, it clearly suggested that the generated model showed reasonable predictability and sufficient accuracy for NiO-5CaO/SiO_2-Al_2O_3 catalysed deoxygenation process.

Table 7.6: Results of model validation at optimum condition

No	Reaction temperature (ºC)	Reaction time (min)	Catalyst loading (wt.%)	Predicted straight chain hydrocarbon yield (%)	Experimental straight chain hydrocarbon yield (%)	% error
1	330	90	5	70.7	68.1	2.6
2	340	60	7	74.6	73.3	1.3
3	340	120	3	76.8	72.8	4.0

7.4.5 Chemical composition profile of deoxygenized product.

The chemical composition of the triolein and optimized deoxygenized products obtained by model validation (Table 7.6) was investigated by studied the chemical functional groups (Figure 7.6). Each spectrum was normalized by the intensity of the absorption band centered 2850–2921 cm^{-1} (CH stretching, aliphatic) (Satyarthi and Srinivas, 2011). Several different features were observed in the samples after deoxygenation reaction. The deoxygenation process of triolein led to the formation intermediated oxygenated products, which shifting absorption band from 1740 cm^{-1} that belonged to C=O (ester) in molecule triglycerides to the absorption band at 1709 cm^{-1}

(attributed to C=O of carboxylic acid) (Asikin-Mijan et al., 2016d). Besides, deoxygenation process also resulted in disappearance of C-O-C absorption features at 1159 cm^{-1} that belonged to carbonyl group in triolein, which was in agreement with the occurrence of deCOx reaction.

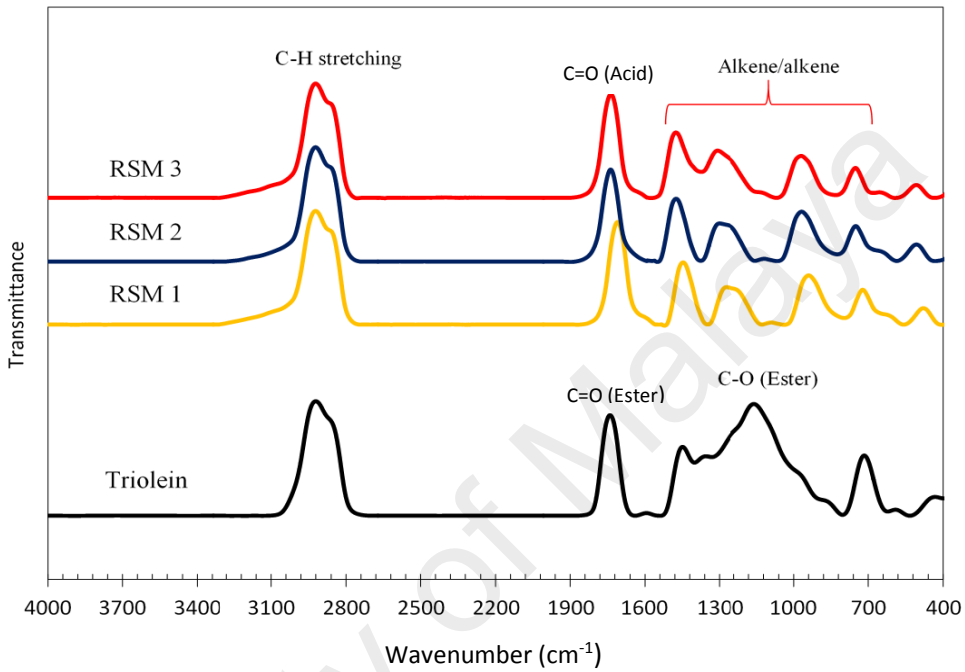

Figure 7.6: FTIR profile for deoxygenated liquid product under RSM modelling generated optimum condition.

GCMS analysis was further performed to study product distribution of deoxygenized liquids. As refer to Figure 7.7, majority constituents of deoxygenated liquid included straight chain of alkanes and alkenes and aromatic compounds (selectivity >70%), followed by minority of carboxylic acid, aldehydes (heptanal, octanal, decenal, hexadecenal, octadecanal (selectivity <1.3%)), ketone (2-undecanone and 9-octadecanone (selectivity <1.4%)) and alcoholic intermediates (*n*-nonadecanol-1 and 9-octadecenol-1-ol (selectivity <3.9%)). The straight chain hydrocarbons yield at different carbon distribution (C_8–C_{20}) was shown in Figure 7.8. The carbon distribution (C_8–C_{20}) showed that highest selectivity of C_{17} (>35%) was formed, and followed by C_{15} (<8%) and short chain (C_8 and C_9) fractions (<8%). Comparing the product

selectivities of various reports, it can be suggested the use of mixed metal oxide NiO-CaO incooperated with SiO_2-Al_2O_3 support resulted in mostly C_{n-1} hydrocarbons, suggesting high deCOx selectivity Principally, the deCOx reaction involved an elimination step, which both saturated and unsaturated hydrocarbons with one carbon atom less than the fatty acid of origin will generated(Lestari et al., 2009). The deCOx of unsaturated oleic acid (from triolein) showed the tendency to form *n*-heptadecenes (mono-unsaturated; $C_{17}H_{34}$) via scission of C-C bond of oleic acid, which led to oxygen removal in the form of CO_2 gas as a by-product. As for decarbonylation reaction, di-unsaturated n-heptadecene ($C_{17}H_{32}$) was produced by removing oxygen in the form of CO gas and water as a by-product (Asikin-Mijan et al., 2015a).

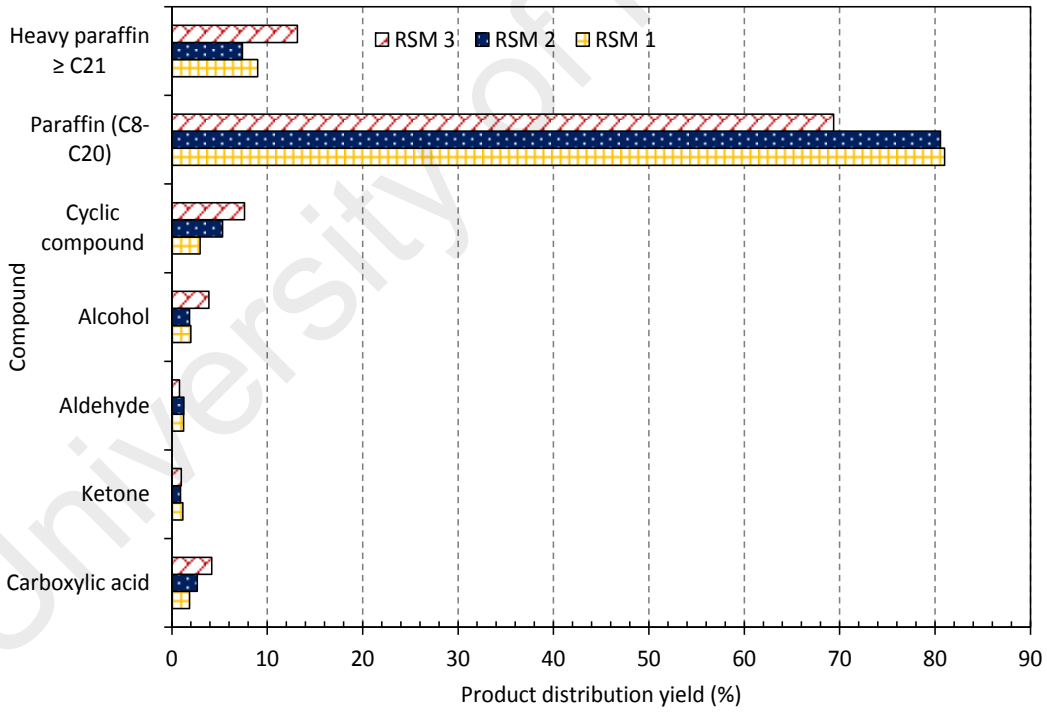

Figure 7.7: Product distribution of deoxygenated liquid product catalysed by NiO-5CaO/SiO_2-Al_2O_3 catalyst under RSM modelling generated optimum condition

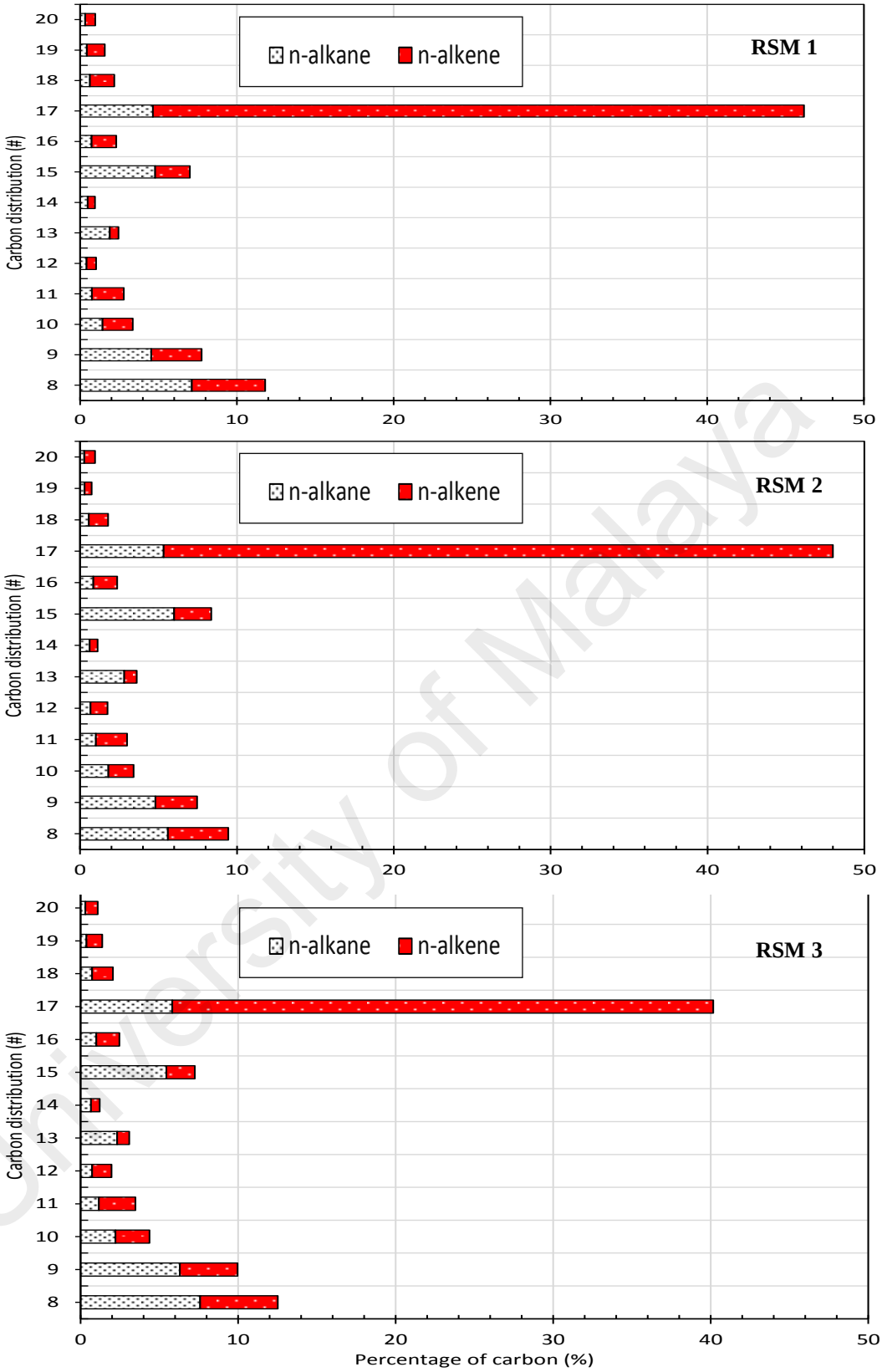

Figure 7.8: Carbon distribution of *n*-alkane and *n*-alkene of deoxygenated liquid products under RSM modelling generated optimum condition

7.4.6 Study of stability and reusability spent catalyst in triolein deoxygenation

The NiO-5CaO/SiO_2-Al_2O_3 catalyst was tested for its recoverability and stability in the deoxygenation system. It was carried out four times under a constant operating condition (reaction temperature: 360 ^oC, reaction time: 60 min, catalyst amount: 7 wt.%). Upon the completion of each cycle, the catalyst was reactivated by simply washing with hexane and reused for the next cycle. Results indicated that the catalytic activity of NiO-5CaO/SiO_2-Al_2O_3 catalyst was slightly reduced throughout the 4 cycles, which the straight chain hydrocarbons yield was slightly reduced from 73% to 65% with gentle decreased of the carbon chain of C_{17} (Figures 7.9 and 7.10).

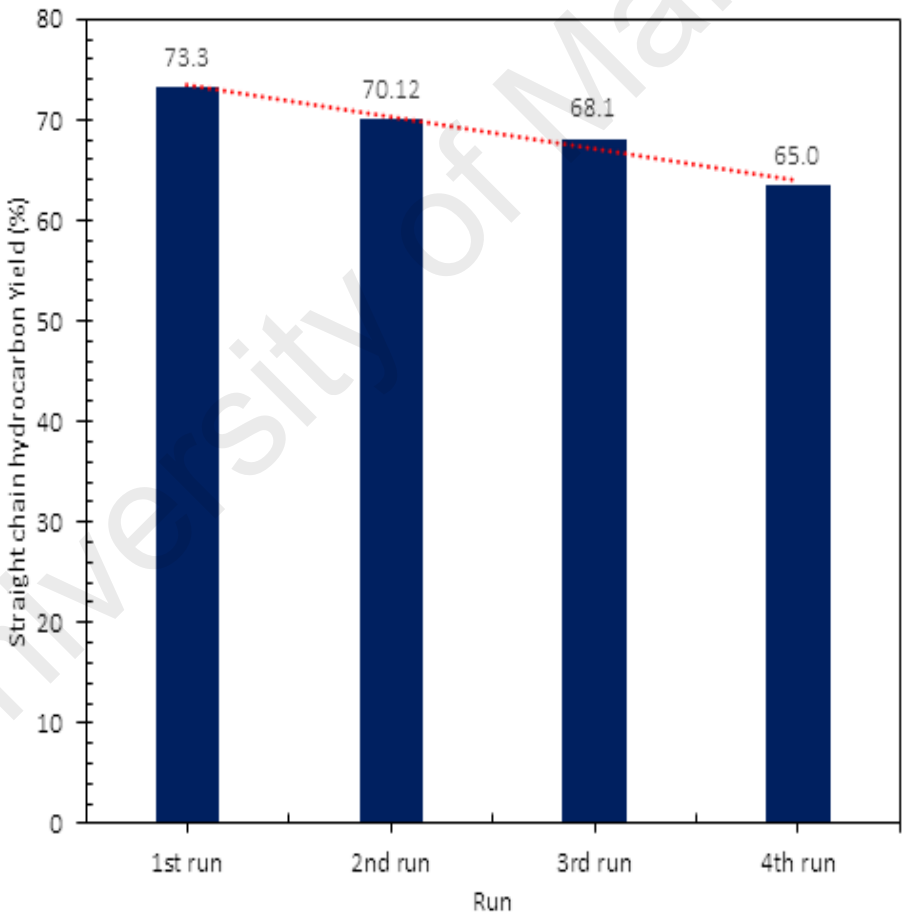

Figure 7.9: Reusability of the NiO-5CaO/SiO_2-Al_2O_3 catalyst towards straight chain hydrocarbon

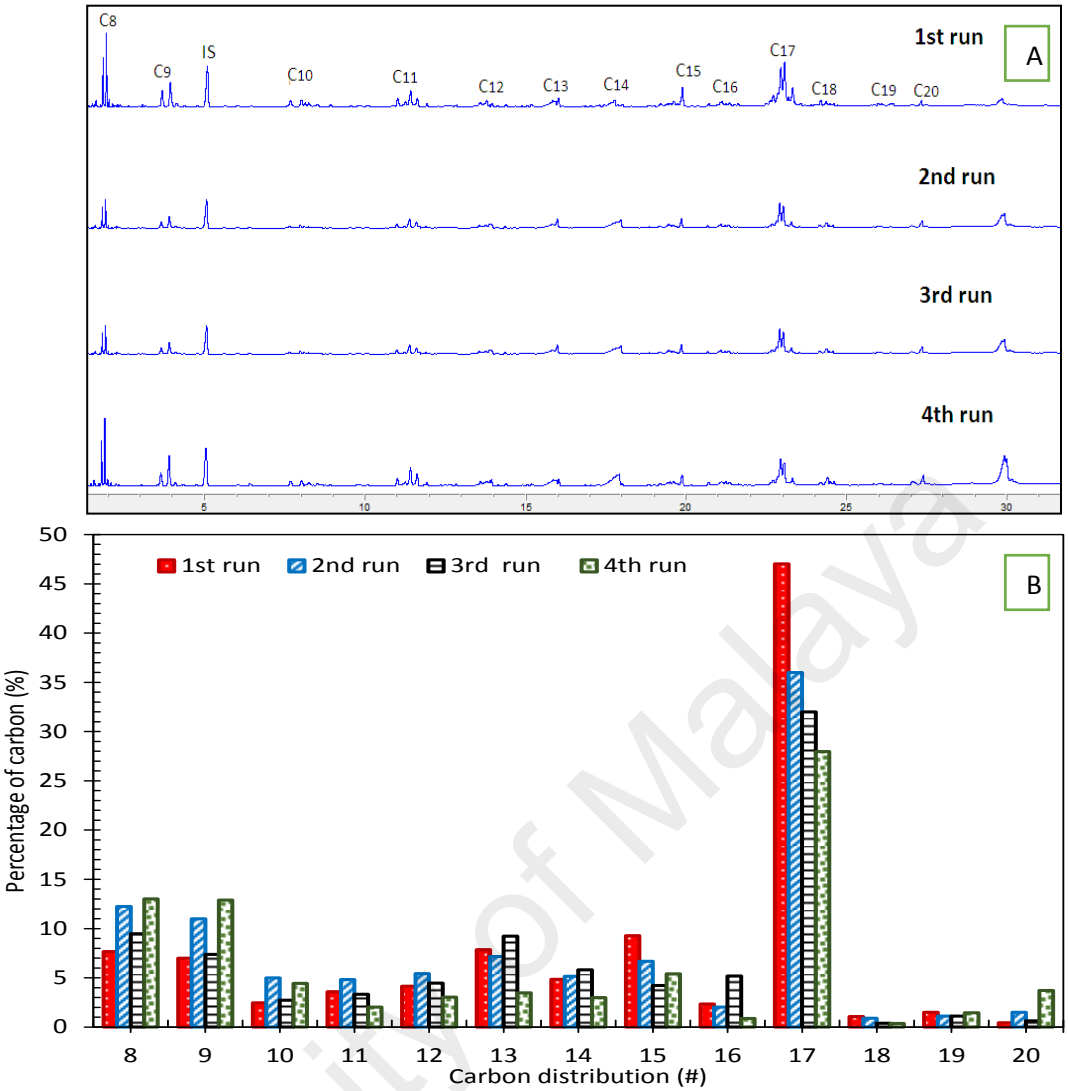

Figure 7.10: (a) GC-FID chromatogram and (b) carbon distribution for 1st–4th run deoxygenation reaction

Furthermore, the product composition study showed that the increased formation of intermediates products, such as carboxylic acid, aldehyde, and alcohol, after the fourth cycle (Figure 7.11). This might due to the leaching of the active metals during the deoxygenation reaction. Elemental analysis of fresh and used catalysts was performed to investigate the catalyst leaching for four reaction cycles (Table 7.7). Results show that the concentration of Ni^{2+}, Ca^{2+}, Si^{2+}, and Al^{3+} from NiO-5CaO/SiO_2-Al_2O_3 catalyst was gradually reduced from 30.8 to 18.1ppm, 20.1 to 12.4ppm, 60.1 to 55.8ppm, and 26.0 to 20.1ppm for fresh and fourth-use catalysts, respectively. This indicated that the leached of active metals, especially Ca and Ni, have lead to the reduction of deoxygenation activity and reduced the deCOx process toward C_{17} selectivity. Furthermore, the metal

content in deoxygenated products for the 4 cycles of reaction was further investigated, results showed that Ni^{2+}, Ca^{2+}, Si^{2+}, and Al^{3+} concentrations had total metals leaching of (< 0.15ppm) for 1st to 4th run, which suggested the concentration are within the maximum range of EN 12662 Standard Specification for Diesel Fuel Oils contamination content (max 24 ppm) (John Bacha et al., 2007). Further simple washing of deoxygenated product will remove the metals prior for the engine usage. It also observed that the elemental content for catalyst samples were not similar as amount of leached metal in the deoxygenated liquid product. This is because the spent catalyst and final liquid product was collected from different container as shown in schematic diagram in Figure 7.1. The deoxygenated liquid was generated from the condensable organic compounds from feedstock reactor and further transfer to condensate collector, while spent catalyst remained in feedstock reactor. Thus, leached metal from the catalyst do not affect much on the purity of the final product as the product was totally separated from the reaction system. Moreover, the occurrence of slight metals leaching during the reaction, indicated that the deoxygenation process do not performed truly in heterogeneous pathway. Thus, further improved of NiO-5CaO/SiO_2-Al_2O_3 catalyst by using different synthesis method (sol-gel or coprecipitation method) is necessary to enhance the stability of catalyst system under high temperature.

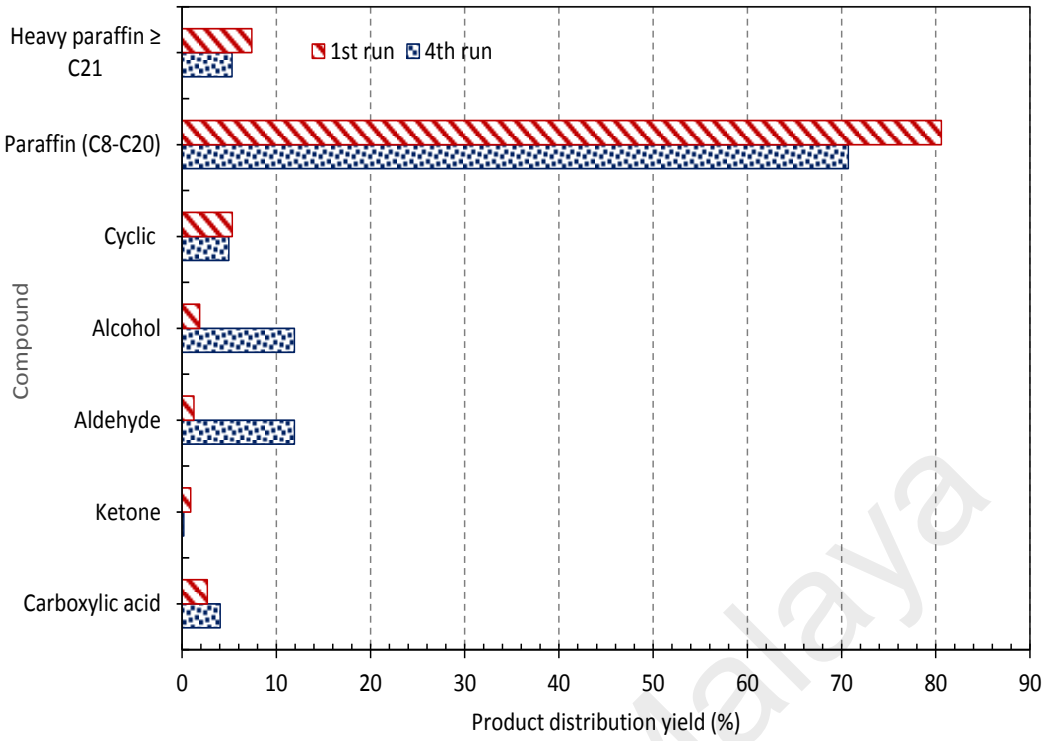

Figure 7.11: GCMS product distribution for 1st run and 4th run deoxygenation reaction

Table 7.7: Reusability and leachate study of NiO-5CaO/SiO_2-Al_2O_3 catalyst

Number on run[a]	**Deoxygenated product**			
Catalyst	**Ni[b] (ppm)**	**Ca[b] (ppm)**	**Si[b] (ppm)**	**Al[b] (ppm)**
Fresh catalyst	30.8±0.51	20.1±0.12	60.1±0.14	26.0±0.15
Used catalyst (2nd run)	28.7±0.45	18.7±0.34	58.2±0.23	24.0±0.45
Used catalyst (3rd run)	24.4±0.34	15.2±0.47	57.0±0.45	23.8±0.57
Used catalyst (4th run)	18.1±0.41	12.4±0.42	55.8±0.35	20.1±0.98
Liquid product				
1st run	0.020±0.0002	0.010±0.0003	0.010±0.0002	0.013±0.0003
2nd run	0.028±0.0004	0.013±0.0002	0.023±0.0004	0.019±0.0002
3rd run	0.031±0.0007	0.020±0.0004	0.024±0.0006	0.026±0.0004
4th run	0.040±0.0003	0.024±0.0009	0.029±0.0005	0.030±0.0008

[a]Deoxygenation reaction condition; reaction temperature 340 °C, 60 min of reaction time, 7 wt.% NiO-5CaO/SiO_2-Al_2O_3 catalyst loading under vaccum condition.
[b] Ni, Ca, Si and Al concentration was determined by ICP analysis.

In order to examine the extent of coke formation on NiO-5CaO/SiO_2-Al_2O_3 catalyst during the deoxygenation of triolein, thermogravimetric analysis of fresh and spent catalysts was carried to determine the accumulation of carbonaceous deposits on the catalyst surface (Figure 7.12). It was observed that both of the catalysts resulted in

weight gain (1.01 ± 0.006%) at initial temperatures between 50 and 90 °C. The scenario of weight gain was attributed to the adsorption of gas on the catalyst surface, which revealed the catalyst render an ability as gas absorber (Abdulkareem-Alsultan et al., 2016a). The significant variation of fresh and 4th used catalyst is based on their weight loss stage. The fresh catalyst resulted in a minor weight-loss stage about 2.22 ± 0.24% at the temperature of 100–250 °C, which corresponded to decomposition of water. However, the 4th used catalyst appears two weight-loss stages. The first stage is within the range of 100–250 °C with a weight loss of water (2.04 ± 0.32%). The second stage is within the range of 300–580 °C with a weight loss of 13.7 ± 0.21%, which attributed to desorption of coke as CO or CO_2. The coke desorbed at this temperature range are physisorbed carbonaceous residues or side products (altogether can be termed as 'soft coke') (Sahoo et al., 2004). Therefore, it was highly confirmed that reduction of reaction reactivity (straight chain hydrocarbons yield: 73– 65%) (Figure 7.9), C_{17} selectivity (47–28%) (Figure 7.10) with an increase of the side product selectivity towards alcohol, aldehyde and carboxylic acid (Figure 7.11) were due to deactivation of catalyst as coke formation deposited on the catalyst surface.

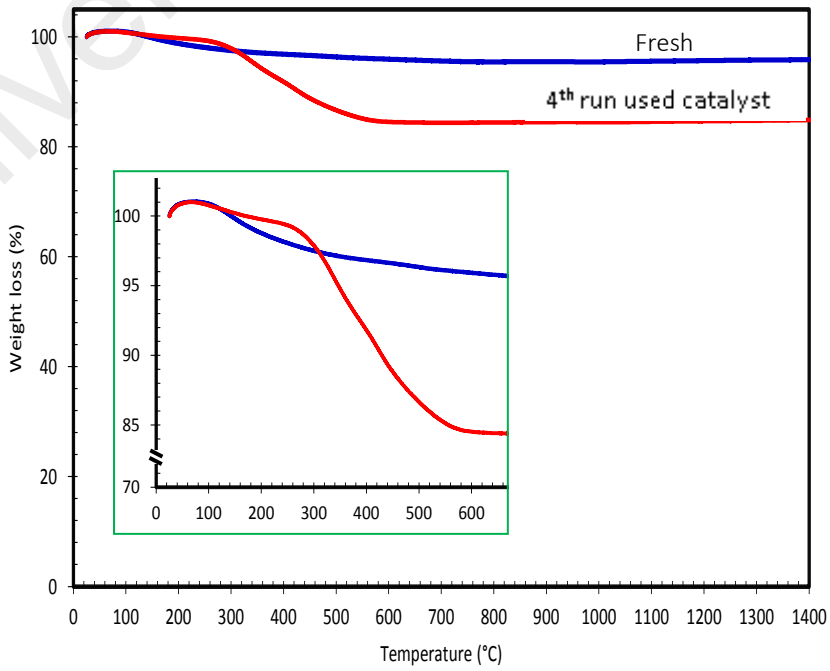

Figure 7.12: TGA profiles for fresh catalyst and 4th run used catalyst

7.5 Conclusion

A central composite design and response surface methodology (CCD-RSM) was conducted to study the interaction effects of reaction temperature, reaction time and catalyst loading towards NiO-5CaO/SiO_2-Al_2O_3 catalysed deoxygenation of triolein. The physico-chemical properties of NiO-5CaO/SiO_2-Al_2O_3 indicate that active metals (NiO and CaO phases) were dispersed well in SiO_2-Al_2O_3 catalyst support with presence of both acidity-basicity active sites. In addition, the catalytic performance of NiO-5CaO/SiO_2-Al_2O_3 catalyst resulted in optimal value of 73.3% straight chain hydrocarbons yield with diesel selectivity (C_{13}–C_{20}) > 67% under reaction condition of 7 wt.% of catalyst, 340 ^oC within 60 min of reaction. The reaction model suggested that the interaction effect between reaction temperature-catalyst amount greatly influence the product yield. Furthermore, the NiO-5CaO/SiO_2-Al_2O_3 catalysed deoxygenation reaction able to produce majority of straight chain hydrocarbons in carbon ranged of C_{17} (>28%) with total straight chain hydrocarbons yield (>65%) for 4 consecutive reaction cycles.

CHAPTER 8: PROMOTING DEOXYGENATION OF TRIGLYCERIDES BY Co AND Ca LOADED SiO_2-Al_2O_3 CATALYST

Chapter 8 describes the study of promoting deoxygenation of triglycerides by Co and Ca loaded SiO_2-Al_2O_3 catalyst. This study is important for evaluating the performance of bifunctional Co_3O_4-CaO supported SiO_2-Al_2O_3 catalyst as comparison to our former chapter 6 and chapter 7. The present study entitle "***Promoting deoxygenation of triglycerides by Co and Ca loaded SiO_2-Al_2O_3 catalyst***" currently has been accepted to be published in *Journal of Applied Catalysis A: General* journal. The authors including Asikin-Mijan, N, Lee H.V., Juan J.C., Noorsaadah A.R., Ong H.C., Razali S.M. and Taufiq-Yap Y.H.

8.1 Introduction

Due to rising of fuel demand, depletion of the fossil resources along with deteriorating climate conditions have raised concerns for energy crisis. These kinds of environmental problems have triggered further researches on searching for new alternative future green fuel from renewable resources. Biodiesel or fatty acid methyl esters (FAMEs) is one of the diesel substitutes which is already a well-established commercial biofuels (Abdulkareem-Alsultan et al., 2016a). However, the use of pure biodiesel (B100) is not applicable due to the existence of oxygenates compound which might result in lower energy densities and poor low-temperature properties (Shi et al., 2012;Kaewmeesri et al., 2015). In view of this, attention has been shifted to catalytic processes known as deoxygenation (DO). The oxygenates species is eliminated under milder condition either as H_2O or COx, which will then lead to the formation of hydrocarbon-based green fuels that are entirely fungible with fossil fuels (Ayodele et al., 2014b). Deoxygenation process has paramount advantages than existing refinery

process which implement hydrodeoxygneation (HDO) process in daily practices. hydrodeoxygenation was commonly practiced under H_2 environment and high pressure, which is less environmental and non-economical friendly as compared to deoxygenation process as it consumes substantial amount of conventional hydrogen gas to allow hydrogenation reaction of triglycerides (Huber et al., 2007). There are many deoxygenation study involve the usage of triglycerides and fatty acid model compound (i.e: triolein, oleic acid, palmitic acid, stearic acid, methyl oleate and etc.) and less deoxygenation study report the utilization of non-edible feedstock such as *jatropha curcas* oil and waste cooking oil. Meanwhile, the usage of non-edible oil derived ceiba oil and sterculia oil still relatively unknown in deoxygenation reaction. Thus, this study reported the catalytic deoxygenation of triglycerides model compound (triolein) and realistic feedstock (ceiba oil and sterculia oil) over mesoporous SiO_2-Al_2O_3 supported Co_3O_4-CaO under inert N_2 flow condition. The influence of ceiba and sterculia oils on the efficiency of catalytic deoxygenation of their fatty acid derivatives was investigated for direct comparison with the deoxygenation of triolein.

8.2 Literature Review

It was reported the feedstock covers more than 75% of the overall green fuel production cost (Lee et al., 2014). Thus, in order to improve the efficiency of green fuel cost production, the usage of various types non-edible oils in deoxygenation reaction have focused (Romero et al., 2015a;Asikin-Mijan et al., 2016c), but none for ceiba oil and sterculia oil. Ceiba oil is generally derived from *Ceiba petandara L.*, a seed from the plant that belongs to the Malvaceae family and locally known as *kekabu* or kapok. This plant either grows naturally or being cultivated in Southeast Asia, Malaysia, Sri Lanka, other parts of East Asia and Africa. The seeds are brownish black in color and contain about 25-28% of oil in each fruit. Meanwhile, sterculia oil is extracted from

sterculia foetida L., a seed from the plant that belongs to sterculiaceae family. Generally, this plant is abundantly found in the western and southern parts of India, Burma, Ceylon and occasionally in east tropical Africa. The average kernel *sterculia foetida L.* seeds consist 50–60% of light yellow fatty oil (Varma et al., 1957;Ong et al., 2013). Both the ceiba oil and sterculia oil were reported to be rich in both saturated and unsaturated fatty acids – containing a variable proportion of cyclopropenoid fatty acids (sterculoyl acid and malvaloyl acid) (Silitonga et al., 2013). The high degree of saturated and unsaturated (straight chain and cyclic) fatty acid derivatives content (>98%) in ceiba and sterculia oils are estimated as an "optimistic case" to undergo commercial upgrading process as deoxygenation process will converted all subsequent fatty acid derivatives to high quality of green fuel, which is usable for existing engines. Mesoporous support (SiO_2-Al_2O_3) was selected as the support due to its excellent textural properties and mild acidity properties(Regali et al., 2014). Both criteria are essential for giving a good balance between cracking and limiting the occurrence of secondary cracking (Regali et al., 2013). Utilization of acidic metal (Co) was proved to be able to accelerate fatty acid deCOx reactions (Zhang et al., 2014). Meanwhile, basic Ca metal was proved to able to accelerate fatty acid decarboxylation reaction (Asikin-Mijan et al., 2016d) and minimize the coke formation by acidic metal (Lin et al., 2010). Thus, this ideal combination of mesoporous acid-base catalyst is estimated to show excellent deoxygenation activity in converting the fatty acid to hydrocarbon with low affinity toward coke formation.

8.2 Experimental

8.2.1 Material

The cobalt(II) nitrate hexahydrate ($Co(NO_3)_2.6H_2O$) with purity > 99% and calcium nitrate tetrahydrate ($Ca(NO_3)_2.4H_2O$) with purity > 99% were obtained from

R&M Company. SiO_2-Al_2O_3 catalyst support grade 135 were purchased from Sigma Aldrich. The standard for gas chromatograph (GC) analysis of liquid product alkane and alkene standard solution (C_8-C_{20}) with internal standard of 1-bromohexane with purity > 98% were purchased from Sigma Aldrich and used without further purification. For dilution, GC analysis grade *n*-Hexane for gas chromatography with purity > 98% from Merck was used. The feedstock of this work triolein (65% purity) was obtained from Sigma Aldrich, *S. foetida L.* while *C. pentandra L* seeds were purchased from West Java, Indonesia. The ceiba and sterculia oils were extracted from its seeds by using similar method reported by Ong et al., (2013). These feedstocks were used for the deoxygenation reaction without further treatment and purification. The physicochemical properties of the feedstock were tabulated in Table 8.1.

Table 8.1: Analysis data of properties of the triolein, ceiba oil. and sterculia oil

Oil properties	**Triolein**	**Sterculia oil**	**Ceiba oil**	**Method**
Acid Value (mg KOH g^{-1})	5.0	5.1	11.9	AOCS Ca 5a-40
FFA Value (%)	2.5	2.5	5.9	AOCS Ca 5a-40
Fatty acid composition of Oil (%)				AOCS Ce1-62 & Ce-661
Lauric (C12:0)	-	0.1	0.1	
Myristic (C14:0)	1.2	0.2	0.1	
Palmitic (C16:0)	3.8	18.4	19.2	
Palmitoleic (C16:1)	4.3	0.3	0.3	
Stearic (C18:0)	1.9	7.6	2.6	
Oleic (C18:1)	83.3	4.0	17.4	
Linoleic (C18:2)	0.4	11.1	39.6	
Linolenic (C18:3)	0.3	0.7	1.5	
Arachinic (C20:0)	0.1	2.3	0.56	
Behenic (C22:0)	<0.1	-	-	
Malvaloyl (18:CE)	-	11.1	18.5	
Sterculoyl (19:CE)	-	44.1	-	
Others	4.8	0.1	0.34	

*Other representing minor compound of pentadoic acid (C15:0), gadoleic acid (C20:1), lignoceric (24:0)
[a]Data from previous study (Ong et al., (2013)

8.2.2 Catalyst synthesis

SiO_2-Al_2O_3 supported mixed Co and Ca oxides catalyst were prepared by using wet impregnation method. Approximately 10 g of SiO_2-Al_2O_3 powder was impregnated with an aqueous solution of 10 wt.% Ca and 10 wt.% of Co. The mixtures were stirred for 360 min at ambient temperature and dried overnight in an oven at a temperature of 100 °C. The dried samples were grounded into fine powder before thermally activated at temperature of 500 ^oC for 120 min under atmosphere condition. The catalysts were denoted as Co_3O_4-CaO/SiO_2-Al_2O_3. Furthermore, Co_3O_4/SiO_2-Al_2O_3 and CaO/SiO_2-Al_2O_3 with 10 wt.% of Co metal and 10 wt.% of Ca metal, was prepared via similar preparation step. In addition, optimization Co content study was further performed by varying the Co content at 5 wt.%, 10 wt.%, 15wt.% and 20 wt.%. All Co content optimization study catalysts were synthesized using constant 10 wt.% of Ca solution.

8.2.3 Catalyst Characterization

The powder X-ray diffraction (XRD) analysis was carried out to identify the dispersion states and chemical composition of modified SiO_2-Al_2O_3 catalysts. The XRD analysis was performed using Shimadzu diffractometer model XRD-6000. The specific surface area and pore distribution of the catalysts were determined by Brunauer-Emmet-Teller (BET) method with N_2 adsorption/desorption analyser using Thermo-FinniganSorpmatic 1990 series. The catalyst was degassed overnight at 150 ^oC to remove moisture and foreign gases on the surfaces of the catalyst. Adsorption and desorption processes of N_2 on the catalyst surfaces were analyzed in a vacuum chamber at -196 ^oC. The basicity and acidity of the catalysts were studied using temperature programmed desorption (TPD-CO_2) and (TPD-NH_3) with CO_2 and NH_3 as probe molecules, respectively. The analysis was carried out by using Thermo Finnigan TPD/R/O 1100 instrument equipped with thermal conductivity detector (TCD). The

catalyst (~0.05 g) was pre-treated with N_2 gas flow for 30 min at 250 ^oC, followed by exposed with CO_2 gas for an hour ambient temperature to allow adsorption of CO_2 onto the surfaces. The excess CO_2 was subsequently flushed with N_2 gas flow at rate 20 ml/min for 30 min. The desorption of CO_2 from the basic sites of the catalyst was detected by TCD under helium gas flow (30 ml/min) from 50 ^oC to 900 ^oC and held for 30 min. The acidity of the catalyst was determined by using ammonia (NH_3) as a probe gas. The adsorption and desorption of NH_3 adapted the same steps as TPD-CO_2 method. The amount of basicity/acidity of the catalyst were determined by the shape of the CO_2/NH_3 desorption peak from the data of area under the graph provided. The temperature of the peak maximum (T_{max}) at which the desorption of CO_2/NH_3 occurred used to study the characteristic and basic/acid site distribution of the active sites for the catalysts. The FESEM images were recorded on LEO 1455 VP electron microscope. The FESEM device coupled with EDX analysis was performed by Rayny EDX-720 spectrometer for determination of elemental composition of Si, Al, Co and Ca on the synthesized catalysts and spent catalyst.

8.2.4 Catalytic Deoxygenation of triolein

The deoxygenation of triolein was performed in a mechanically stirred 250 mL of semi-batch reactor under inert N_2 flow condition. In a typical experiment, approximately 10 g of triolein and 5 wt.% of catalyst were added to the reactor. Initially, oxygen in the reactor was removed by purging with N_2 gas under flow rate 20 cc/min. The temperature was increased to reach the desired temperature 350 ^oC and maintained for 60 min. During the deoxygenation process, generated vapour/volatile species was condensed into liquid product by using external water cooling circulator under temperature of 16 °C and then collected using a vessel collector. In order to reduce the error of experimental results, the experiment was repeated for three times to obtain the

average range of results. Final deoxygenized liquid products were further analyzed by using FTIR, GC-FID and GCMS analysis.

8.2.5 Product analysis

The occurrence of deoxygenation using various types of feedstock was observed by performing Fourier transform mid-infrared spectroscopy (FTIR) using Perkin-Elmer Spectrum (PS) 100 FT–IR spectrometer with resolution of 4 cm^{-1} operating in the range of 300–4000 cm^{-1}. The reduction of the C=O absorption bands corresponded to stretching of carboxylic acid carbonyls (1710–1715 cm^{-1}) and esters (1740–1745 cm^{-1}) present in the feedstock were monitored. Further reduction of C-O absorption bands at 1285 cm^{-1} was also focused. The liquid products were quantitatively analyzed using a gas chromatography (Agilent Technologies 7890A) equipped with a HP-5 capillary column (length: 30 m × inner diameter: 0.32 mm × film thickness: 0.25μm) and a flame ionization detector (FID) operating at 300 ^{o}C. The deoxygenated liquid products were identified using alkane and alkene standards (C_8-C_{20}). The liquid product was diluted with GC grade *n*-hexane prior to the analysis. 1-bromo hexane was used as internal standard for quantitative analysis. An aliquot of 1 μL of sample was injected with into GC column. The injection temperature was 250 ^{o}C and nitrogen gas has been served as the carrier gas. The initial temperature of the oven was set at 40 ^{o}C and held for 6 min, then ramped to 260 ^{o}C at heating rate of 7 ^{o}C/min. The catalytic performances of the catalyst was investigated by determining the saturated and unsaturated hydrocarbons straight chain hydrocarbons yield (*X*) (Eq. 8.1)(Asikin-Mijan et al., 2015a).

$$X = \frac{\sum n_o + \sum n_i}{\sum n_z} \times 100\% \quad (8.1)$$

Where:

X = Saturated and unsaturated straight chain hydrocarbons yield (%)

n_o = Area of alkene (C_8-C_{20})

n_i = Area of alkane (C_8-C_{20})

n_z = Area of the total product

The hydrocarbon selectivity (S_c) or carbon balance were determined by Eq. 8.2

$$S_{carbon} = \frac{C_o + C_i}{\sum n_o + \sum n_i} \times 100\% \quad (8.2)$$

Where,

S_{carbon}= Hydrocarbon selectivity or carbon balance (%)

C_o= Area of desired alkene

C_i= Area of desired alkane

In addition, the feedstock was qualitatively characterized using GC-MS (model SHIMADZU QP5050A) equipped with a nonpolar DB-5HT column (30 m × 0.32 mm × 0.25 µm) and splitless inlet. The samples were diluted with GC grade *n*-hexane (purity > 98%) to 100 ppm. The generated fraction peaks from the GC-MS spectrum were identified through the National Institute of Standards and Testing library. Compound identification was based on a probability match equal to or higher than 95%. The acid number value of the feedstock was determined using standard method of AOAS Cd 3d-63. The acid value was calculated as shown in Eq. 8.3.

$$Acid\ Number\ (AN): (V_f - V_i) N \frac{56}{W_{oil}} \quad (8.3)$$

The concentration of the elements in the deoxygenation liquid was determined using inductively-coupled plasma-atomic emission spectrometer (ICP-AES) analysis. The analysis was done using Perkin–Elmer Emission Spectrometer Model Plasma 1000.

8.3 Results and discussion

8.3.1 Characterization of SiO_2-Al_2O_3 -based catalysts

The XRD pattern shown in Figure 8.1 confirms the amorphous nature of SiO_2-Al_2O_3 support (Yoshida et al., 2002). The characteristic diffraction peaks of Co_3O_4/SiO_2-Al_2O_3 and Co_3O_4-CaO/SiO_2-Al_2O_3 exhibited at 2θ=31.29°, 36.97°, 44.92°, 59.43° and 65.33° corresponded to 220, 311, 400, 511 and 440 crystal planes of Co_3O_4 (JCPDS File No:01-073-1701)(Figure 8.1a-b). The presence of diffraction peaks confirm that Co_3O_4 are embedded in the SiO_2-Al_2O_3 matrix. In comparison with CaO/SiO_2-Al_2O_3, the XRD patterns exhibit only broad amorphous characteristic of SiO_2-Al_2O_3 without appearance of any crystalline Ca-containing phases. This suggests Ca species to be well dispersed in porous SiO_2-Al_2O_3 materials (Liu et al., 2016). The amorphous phase characteristic disappeared with further addition of Co metal solution, indicating that the dispersion of Co metal was saturated and it covered the amorphous phase of SiO_2-Al_2O_3 (Rabiah Nizah et al., 2014). The crystallite size of Co_3O_4 was calculated by the Debyee Scherrer equation based on the highest intense peak centered at 36.97° and results were tabulated in Table 8.2. The crystallite size of the Co_3O_4 in Co_3O_4-CaO/SiO_2-Al_2O_3 prepared by wet-impregnation was smaller than that of the Co_3O_4/SiO_2-Al_2O_3 catalyst. It can be summarized that Ca addition into the Co_3O_4/SiO_2-Al_2O_3 catalyst led to a smaller decrease in Co_3O_4 crystallite size, suggesting presence of interaction between the Ca and Co species that helped in Co_3O_4 dispersion. These results are consistent with the ones previously reported in Lee's finding(Lee et al., 2015b).

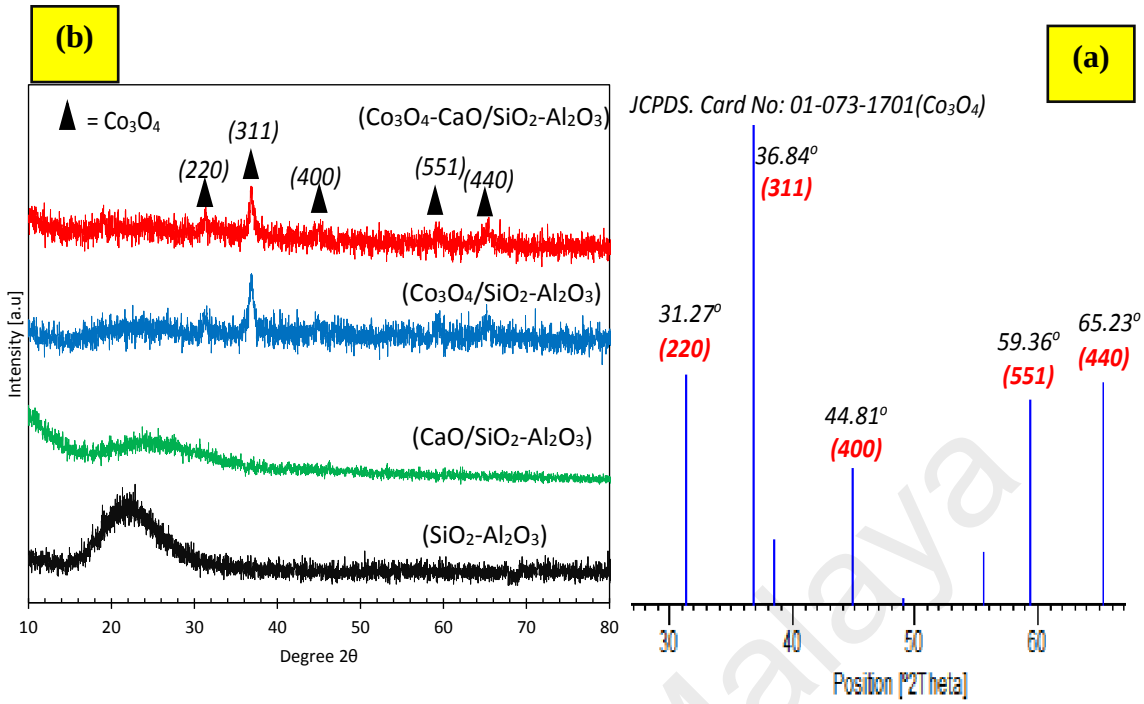

Figure 8.1: (a) XRD diffraction patterns for SiO_2-Al_2O_3, CaO/SiO_2-Al_2O_3, Co_3O_4/ SiO_2-Al_2O_3, Co_3O_4-CaO/SiO_2-Al_2O_3 catalysts and (b)Reference pattern for Co_3O_4

The BET surface area of all the catalysts are shown in Table 8.2. The surface area for SiO_2-Al_2O_3 support catalyst was found 382.60 m^2/g and pore volume 0.60 cc/g. The SiO_2-Al_2O_3 supports were mainly consisted of mesoporous structure with pore diameter within the range of 2-50 nm (Lokman et al., 2015a). As expected, the surface area and pore volume of supported Co_3O_4-CaO catalysts were somewhat lesser than pure support and single metal oxide supported catalyst. The decrease in the specific surface area was higher after the impregnation of Co_3O_4-CaO species on the SiO_2-Al_2O_3 support in comparison with the impregnation of individual Co and Ca species on SiO_2-Al_2O_3 support. The addition of Co_3O_4-CaO species on the SiO_2-Al_2O_3 support decreased the specific surface area (from 382 m^2 g^{-1} to 132 m^2 g^{-1}) and total pore volume (from 0.60 $cc^{-1}g^{-1}$ to 0.31 $cc^{-1}g^{-1}$) suggesting that the impregnated Co_3O_4 and CaO species blocked some pores in SiO_2-Al_2O_3 support (Abdulkareem-Alsultan et al., 2016a). It was found that among the supported catalysts, CaO/SiO_2-Al_2O_3 resulted in the largest pore volume (0.54 cc/g) and pore diameter (9.18 nm), which can be ascribed due to the

collapsing of the pore walls from Ca rich metal from releasing of CO_2 molecule during calcination. This would provide a wide channel for diffusion of reactant and product into the CaO/SiO_2-Al_2O_3 pores (Chandra Mouli et al., 2011;Zhao et al., 2016) thus enhancing the catalytic deoxygenation activity.

As seen in Figures 8.2a-d, it revealed the addition of Co rendered significant effect on the morphology of catalyst. It was proven by morphology changes from small aggregates of pure SiO_2-Al_2O_3 and CaO/SiO_2-Al_2O_3 to a more exfoliated morphology in all Co-promoted catalysts. The elemental compositions of all catalysts are shown in Table 8.3. The EDX result showed the Co_3O_4-CaO supported catalyst exhibits the presence of metal species (Ca and Co) at range of 9–14 wt.%. The value was close with theoretical ration Co+Ca: SiO_2-Al_2O_3 (10+10:80), where 20 wt.% of catalyst corresponded to active metal species and 80 wt.% was SiO_2-Al_2O_3 support. The SiO_2-Al_2O_3 content reduced significantly as both the Co and Ca oxides incorporated on the SiO_2-Al_2O_3 support due to the metal coverage by the active metals, this was in agreement with the disappearance of amorphous characteristic of SiO_2-Al_2O_3 in XRD analysis. Moreover, based on FESEM-EDX spot analysis (Figures 8.2ai-di), it showed that the Ca and Co were found to be homogeneously distributed on the SiO_2-Al_2O_3 surface with standard deviation of Ca(< 0.8 wt.%) and Co (<2.8 wt.%), respectively (Yu et al., 2014).

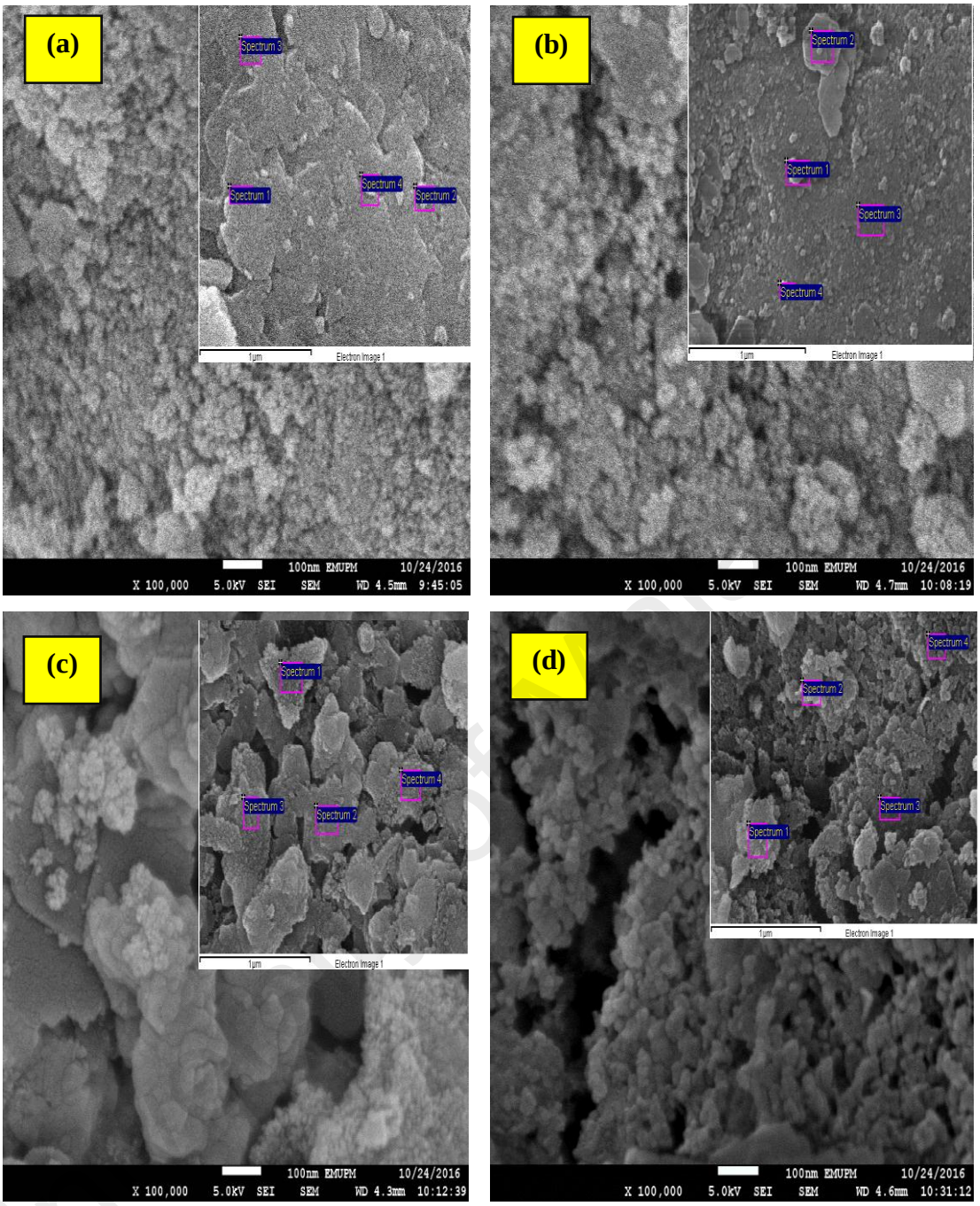

Figure 8.2: FESEM-EDX profile for (a) SiO_2-Al_2O_3, (b) CaO/SiO_2-Al_2O_3, (c) Co_3O_4/ SiO_2-Al_2O_3 and (d) Co_3O_4-CaO/SiO_2-Al_2O_3 catalysts

Table 8.2: Physicochemical properties for SiO_2-Al_2O_3 and metals promoted SiO_2-Al_2O_3 support

Catalyst	XRD	BET			TPD			
					TPD-CO_2			TPD-NH_3
	[a]Crystallite size(nm)	[b]Surface area (m^2/g)	[b]Pore volume (cc/g)	[b]Pore size diameter (nm)	[c]Temperature (^oC)	[c]Basic sites (µmol/g)	[d]Temperature (^oC)	[d]Acid sites (µmol/g)
SiO_2-Al_2O_3	-	382.60	0.60	15.00	100,904	12.4,13.7	241	1526.5
CaO/SiO_2-Al_2O_3	-	206.69	0.54	10.44	487,651,701	98.99,309.31, 274.50	514,703	1007.91,6367.29
Co_3O_4/SiO_2-Al_2O_3	27.87	230.29	0.43	7.47	888	127.32	186,459	1646.88,606.99
Co_3O_4-CaO/SiO_2-Al_2O_3	25.67	132.95	0.31	9.18	500,664,908	448.66,212.08, 366.45	124,402,638, 780	3141.52,3548.99, 1997.23,1819.39

[a] Measured by using Scherer equation from XRD data (repeat twice)
[b] Determined by BET analysis
[c] Determined by TPD-CO_2 analysis
[d] Determined by TPD-NH_3 analysis

Table 8.3: Elemental composition of SiO_2-Al_2O_3 and metals promoted SiO_2-Al_2O_3 support

Catalyst	Elemental surface analysis[a] (%)				
	O	Al	Si	Ca	Co
SiO_2-Al_2O_3	70.25±0.4	16.67±0.2	13.80±0.3	-	-
CaO/SiO_2-Al_2O_3	57.78±1.5	5.98±0.1	26.48±0.5	9.75±0.5	-
Co_3O_4/SiO_2-Al_2O_3	60.13±1.9	5.09±0.4	19.92±2.8	-	14.55±2.8
Co_3O_4-CaO/SiO_2-Al_2O_3	60.13±2.1	3.93±0.3	14.91±1.0	9.65±0.8	14.35±2.1

[a] Elemental composition were determined by FESEM-EDX analysis

As agreed by former studies, basicity characteristic is important for inhibiting the coke formation along with promotion toward decarboxylation reaction formation(Asikin-Mijan et al., 2016d) and acidity is required for enhance the cracking reaction(Asikin-Mijan et al., 2016a;Asikin-Mijan et al., 2016c). Among the acidic sites characteristics (weak, medium, strong), mildly acidic (weak and medium) acidic sites is necessary rather than strong acidic sites characteritic as the weak and medium are favored to mild cracking activity via deCOx reaction(Asikin-Mijan et al., 2016a). Therefore, the basicity and acidity profile of synthesized catalysts were further evaluated by TPD-CO_2 and TPD-NH_3. The basic/acidic sites of the catalyst were determined by desorption peak area of CO_2/NH_3 and the basic/acid strength with the maximum peak temperature (T_{max}) of the desorption peak. The results were displayed in Figure 8.3a-b and the total amount of CO_2/NH_3 desorbed is listed in Table 8.2. It was observed that pure SiO_2-Al_2O_3 support showed a negligible amount of weak basic sites and strong basic sites at lower T_{max}=100 ^oC and T_{max}=904 ^oC with total basic density of 26.10 µmol/g (Figure 8.3a). Meanwhile, the CaO/SiO_2-Al_2O_3 showed an intense desorption of mixed medium and strong basicity with total basic density (682.80 µmol/g) appeared at T_{max} =487 ^oC, 651 ^oC and T_{max}=701 ^oC which corresponded to the synergism interaction of SiO_2-Al_2O_3 support and association of Ca^{2+}–O^{2-} pairs(Lee et al., 2013). Moroever, the Co_3O_4/SiO_2-Al_2O_3 was also found to have a number of strong basic sites (127.32 µmol/g) at T_{max}=888 ^oC which indicated the association of Co^{3+}–O^{4-}

pairs. The strong basic sites in Co_3O_4-CaO/SiO_2-Al_2O_3 varied significantly as it resulted in a new appearance of three distinct mixed medium-strong basicity peaks at T_{max}= 487 ^oC, 651 ^oC and 701 ^oC with total basic density 1027.19 µmol/g, which attributed due to the synergistic interaction between Co and Ca metals on the acidic mesoporous SiO_2-Al_2O_3 support. According to TPD-NH_3 profile, all catalysts show clear differences in the strength and density of strong acid sites. As illustrated in Figure 9.3b and Table 9.2, the TPD curve of the parent SiO_2-Al_2O_3 presents a major mildly acidic peak at T_{max}= 241 ^oC with total acid density 1526.5 µmol/g. A mildly acidic SiO_2-Al_2O_3 support was in agreement with former findings and this characteristic will give a good balance between cracking, isomerization and limit secondary cracking (Castaño et al., 2007;Regali et al., 2013;Roussel et al., 2005). Among the modified SiO_2-Al_2O_3 catalyst, the Co_3O_4-CaO/ SiO_2-Al_2O_3 catalyst showed the largest amount of mildly acidic sites (6690.51 µmol/g) at T_{max}= 124 ^oC and 402 ^oC, whereas Co_3O_4/SiO_2-Al_2O_3 just exhibited the low amount of mildly acidic sites with total acid density 2253.87 µmol/g at T_{max}=186 ^oC and 459 ^oC, respectively. Meanwhile, the CaO/SiO_2-Al_2O_3 catalyst only showed a formation of strong acid strength at T_{max}= 514 ^oC and 703 ^oC with total acid density 7375.20 µmol/g. The presence of large density of strong acid catalyst generally favored formation of light hydrocarbons via C-C cleavage though cracking reaction (Asikin-Mijan et al., 2016e). Again, the difference of Co_3O_4-CaO/SiO_2-Al_2O_3 catalyst indicated that catalyst with multi-metal ion interaction showed synergy effect by enhancing the total midly acidity density. From the results, Co_3O_4-CaO/SiO_2-Al_2O_3 showed highest amount of basicity and midly acidity albeit lower amount of surface area. It has been suggested by our former study (Asikin-mijan et al., 2016) that chemical properties (basicity, acidity) are the main reason in improving the deoxygenation reaction compared to textural properties. In this case, the Co_3O_4-CaO/SiO_2-Al_2O_3 catalyst was expected to give high deoxygenation activity via desired deCOx reaction

due to the largest amount of basicity and mildly acidic characteristics generated on it albeit lowest surface area.

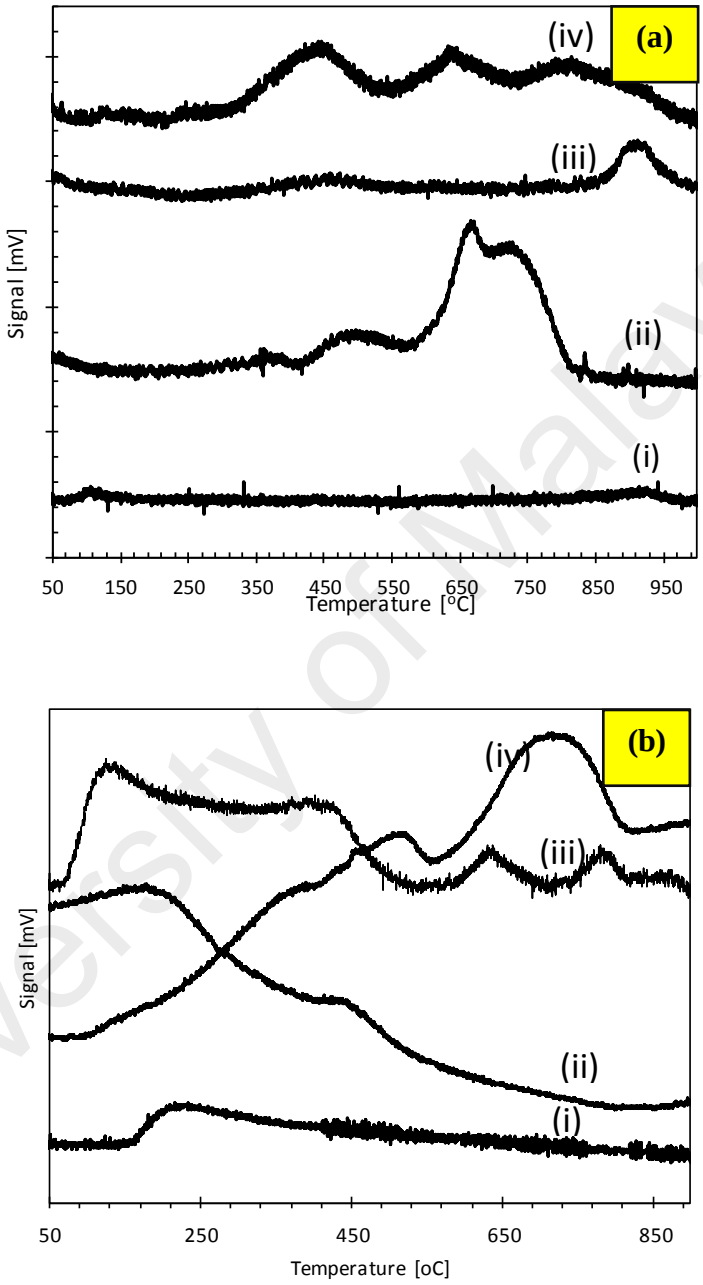

Figure 8.3: (a) TPD-CO_2 and (b) TPD-NH_3 profile for (i) SiO_2-Al_2O_3, (ii)CaO/SiO_2-Al_2O_3, (iii) Co_3O_4/SiO_2-Al_2O_3 and (iv) Co_3O_4-CaO/SiO_2-Al_2O_3 catalysts

8.3.2 Deoxygenation activity profile

8.3.2.1 Quantification analysis

The catalytic activity and product selectivity profile was summarized in Figures 8.4a-b. The result showed the deoxygenated liquid product was mainly composed of saturated and unsaturated hydrocarbon fractions within the range of *n*-(C_8-C_{20}). A blank experiment was carried under the same condition and parameters in order to determine the product distribution during the thermal composition of triolein in the absence of catalyst. Results showed that low hydrocarbon yield (18.1%) was achieved. However, the catalytic deoxygenation over SiO_2-Al_2O_3, CaO/SiO_2-Al_2O_3 and Co_3O_4-CaO/SiO_2-Al_2O_3 were found to be reactive in deoxygenation reaction by obtaining higher hydrocarbon yield. The hydrocarbon yield is decreasing as follow Co_3O_4-CaO/SiO_2-Al_2O_3 > Co_3O_4/SiO_2-Al_2O_3 > CaO/SiO_2-Al_2O_3 > SiO_2-Al_2O_3 >blank.

Based on fatty acid composition profile for triolein, it was mainly composed of C18 and C16 fatty acid derivatives (Table 8.1). Theoretically, deCOx reaction of C18 and C16 fatty acid derivatives will result in formation of *n*-heptadecenes (*n*-C_{17}) and *n*-pentadecenes (*n*-C_{15}) (Asikin-mijan et al., 2016). The result showed catalyzed deoxygenation via deCOx reaction was prominent as compared to blank reaction. The blank reaction yielded product selectively toward shorter chain of *n*-C_8, *n*-C_9 and *n*-C_{13}. However, significant *n*-C_{15}+*n*-C_{17} selectivity (38-43%) was achieved using both Co/SiO_2-Al_2O_3 and Co_3O_4-CaO/SiO_2-Al_2O_3 catalysts followed by CaO/SiO_2-Al_2O_3 (21%) and SiO_2-Al_2O_3 (7%). In summary, Co_3O_4/SiO_2-Al_2O_3 catalyst showed a comparable promotion effect toward deCOx pathways as Co_3O_4-CaO/SiO_2-Al_2O_3 catalyst. But, Co_3O_4/SiO_2-Al_2O_3 also favored the occurrence of cracking reaction and resulting in formation of light fraction (i.e: non-condensable gasses). Thus, reduced the yield of hydrocarbon. It can be concluded that high strong basic and strong acid of

Co_3O_4/SiO_2-Al_2O_3 catalyst exhibits higher cracking-deCOx reaction, while significant midly acidic of Co_3O_4-CaO/SiO_2-Al_2O_3 favored deCOx reaction. This finding concurs with previous study where high density of milder acidic catalyst play main factor in enhancing the deCOx reaction (Asikin-Mijan et al., 2016a), while cracking reaction is favored over strong basicity and strong acidity catalysts (Asikin-Mijan et al., 2016e).

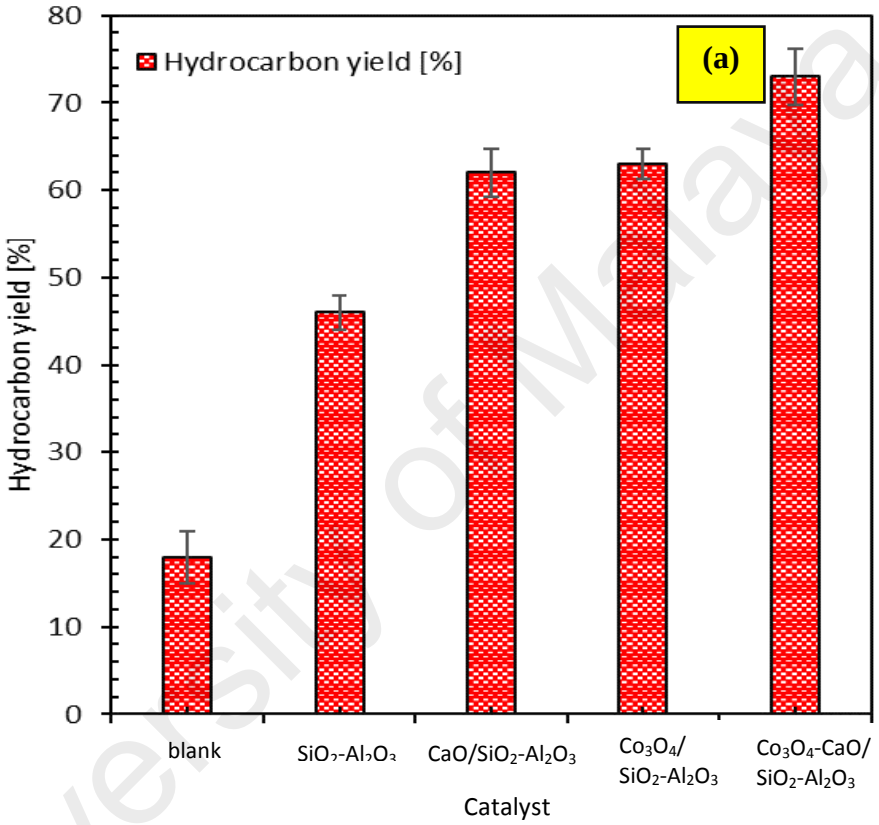

Figure 8.4: (a) Hydrocarbon yield and (b) product selectivity of the liquid deoxygenated product

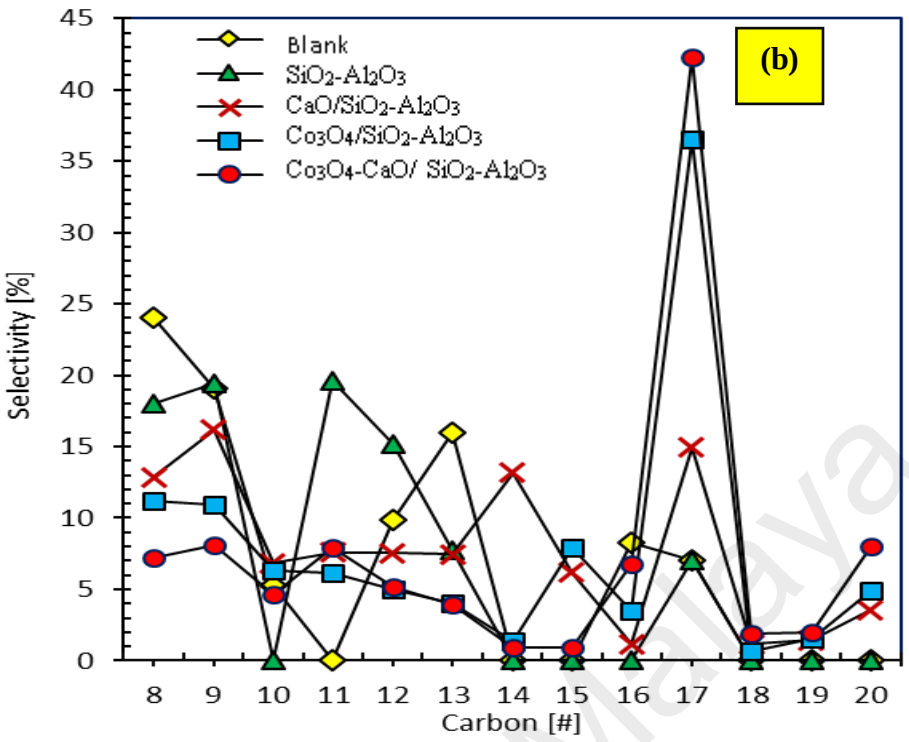

Figure 8.4, continued: (a) Hydrocarbon yield and (b) product selectivity of the liquid deoxygenated product

.

8.3.2.2 Mass balance profile for catalytic deoxygenation of triolein

A mass balance profile for deoxygenation of triolein into liquid hydrocarbon product by using SiO_2-Al_2O_3-supported catalyst was included in Table 8.4. Based on Eq. (8.4), the deoxygenation reaction of triolein will lead to the production of liquid product via deCOx with the release of CO_2 gas, CO gas and water as the by-product. The theoretical and experimental mass fraction of each compound include triolein feedstock, liquid product and by products (CO_2 gas, CO gas, water and mixture of char+residues). Ideally, the complete reaction is free from the formation of char and residue. However, the experiment yielded substantial solid char and residue as the by-product of deoxygenation process. Tellingly, a considerably less mass fraction of liquid product (< 38 wt.%) was obtained in experimental than theoretical value (68 wt.%) was observed in deoxygenation reaction with deviation of >30.7 wt.%. These contradictory results were most readily explained by the formation of undesirable by-products (char +

residue) which contained total of 30-49 wt.% remaining in the semi-batch reactor after reaction. The formation of (char + residue) was caused by low degree volatilization of triolein during deoxygenation at high temperature (350 ^{o}C), which had also been reported elsewhere (Vitolo et al., 1999). Furthermore, in all cases, the gaseous balance from the catalytic deoxygenation of triolein released approximately 26% to 31% of volatile matter which was comparable with theoretical value. Based on the mass balance of water, the experimental resulted in significantly lesser with range of 4% to 6% than theoretical, as it easily vaporised into gas during high temperature in deoxygenation reaction. Overall, the Co_3O_4-CaO/SiO_2-Al_2O_3 catalyst effectively deoxygenized the triolein via selective deCOx reaction with highest mass liquid fraction (38.2 wt.%) as compare to the others. This finding is predictable as Co_3O_4-CaO/SiO_2-Al_2O_3 owns the largest distribution mildly acidic characteristic which contributes to a good balance on the occurrence of C-O cleavage and limits secondary cracking leading to formation of volatile species.

Table 8.4. Mass balance profile of catalytic deoxygenation of triolein

Theoritical deCOx:	**Triolein⟶**	**liquid (oil) + 3mol CO_2/CO (g) + 3mol H_2O (aq) + By product (8.4)**							
Reaction[a]	Feedstock	Liq-product[b]		Gas[c]		Water[d]		Char + residue[e]	
	(g)	(g)	(wt.%)	(g)	(wt.%)	(g)	(wt.%)	(g)	(wt.%)
Theoritical data (deCOx)	10.00	6.89	68.90	2.49	24.90	0.62	6.20	-	-
SiO_2-Al_2O_3	10.08	1.98	19.64	2.69	26.68	0.50	4.96	4.91	48.71
CaO/SiO_2-Al_2O_3	10.10	2.20	21.78	3.07	30.39	0.63	6.23	4.20	41.58
Co_3O_4/SiO_2-Al_2O_3	10.03	2.51	25.02	3.11	31.00	0.42	4.18	3.99	39.78
Co_3O_4-CaO/SiO_2-Al_2O_3	10.01	3.82	38.16	2.61	26.07	0.51	5.00	3.07	30.66

[a]Deoxygenation condition : reaction temperature of 350 °C, 60 min reaction time, 5 wt.% of catalyst, under inert condition with 400 rpm stirring rate.
[b]Mass fraction for Liq-product = [(mass of Liq-product/mass of feedstock)x 100]
[c]Material fraction for gas = [(mass of feedstock – mass of Liq-product- mass of (char+residue)- mass of water)/mass of feedstock x100]
[d]Material fraction for water = [(mass of water/ mass of feedstock x100]

8.3.3 Optimization studies

The effect of the Co_3O_4-CaO/SiO_2-Al_2O_3 catalyst loading (1-9 wt.%) on the hydrocarbon yield and product selectivity at 350 ^oC, 60 min reaction time under inert condition with stirring rate 400 rpm were shown in Figures 8.5a-b. Based on the result obtained, the hydrocarbon yield increased from 65% to 73% with catalyst loading within the range 1 wt.% to 5 wt.%, which due to existence of more active sites provided by 5 wt.% Co_3O_4-CaO/SiO_2-Al_2O_3 catalyst loading. Further increase in catalyst loading to 9 wt.% resulted in reduction of yield (53%). In case of deCOx selectivity (total *n*-C_{15}+*n*-C_{17}), the deCOx product was enhanced when catalyst loading was increased from 1 wt.% to 7 wt.% and reduced with further increase in catalyst loading to 9 wt.%. It can be summarized that an increase in the number of active sites (increased catalyst loading) might induce the increase of deCOx reaction but excess of active sites will promote the occurrence of secondary reaction such as cracking of deCOx product to volatile species and polymerization reaction. The brisk increment in polymerization at the catalyst surface is unhealthy for the catalyst life span as polymerization reaction has been known to be prominent for coking hydrotreating catalysts (Mortensen et al., 2011;Kwon et al., 2011). In the present study, optimum hydrocarbon yield (73%) with 43% deCOx product selectivity were obtained with 5 wt.% loaded Co_3O_4-CaO/SiO_2-Al_2O_3 catalyst.

The results in Figure 8.5c-d showed the effect of reaction time (30 min to 240 min) on the catalytic deoxygenation reaction at 350 ^oC, 5 wt.% of Co_3O_4-CaO/SiO_2-Al_2O_3 catalyst loading under inert condition with 400 rpm stirring rate. As the deoxygenation reaction time proceeded to 60 min, the yield of hydrocarbon progressively increased to optimum value (73%). Reduction of hydrocarbon yield was observed after the optimum yield. Again, the reduction of hydrocarbon yield might have occurred due to cracking of the already deoxygenated liquid product into lighter

fractions. It has been proven, when judged on the reduction of the yield and increased of the formation of *n*-C_{12}, *n*-C_{13}, *n*-C_{14} and *n*-C_{16} hydrocarbons at reaction time > 60 min, it is clear that longer reaction time results in further cracking of deoxygenated product. It can be summarized that deCOx reaction was more quickly performed under shorter time than longer reaction time. Therefore, after considering the hydrocarbon yield and *n*-C_{15}+*n*-C_{17} selectivity, 60 min reaction time was found to be the most efficient for deCOx interval.

Besides, heating needs to set at optimum to enhance the deoxygenation activity and in the present work, the deoxygenation reaction was carried out at temperatures that vary from 300 ^{o}C to 400 ^{o}C using 5 wt.% catalyst loading within 60 min. It was evident that the deoxygenation activity increased as temperature increased from 300^{o}C to 350 ^{o}C and reduced as the reaction temperature increased to 400 ^{o}C Figures 8.5e-f. At 350 ^{o}C the hydrocarbon yield approached 73% and reduced to 60% at 400 ^{o}C. While observing the deCOx selectivity, it was found that the temperature has a negative effect where, gradual increase of temperature from 350 ^{o}C to 400 ^{o}C resulted in reduction of the *n*-C_{15}+*n*-C_{17} formation with simultaneous rise of lighter hydrocarbon. From this result, it can be concluded that tendency of thermal cracking of oxygenated intermediates or hydrocarbons enhanced with rise of temperature. It was supported by the increment of the cracking product of *n*-C_{8} to *n*-C_{13} as the deoxygenation reaction temperature reached 400 ^{o}C. Reddy et al. also reported increasing trends of light hydrocarbon fractions and reduction of yield product with increasing reaction temperature(Reddy Yenumala et al., 2016). Based on the result obtained, it showed that the maximum hydrocarbon yield (73%) and 43% *n*-C_{15}+*n*-C_{17} selectivity were achieved at 350 ^{o}C reaction temperature, 5 wt.% catalyst loading within 60 min.

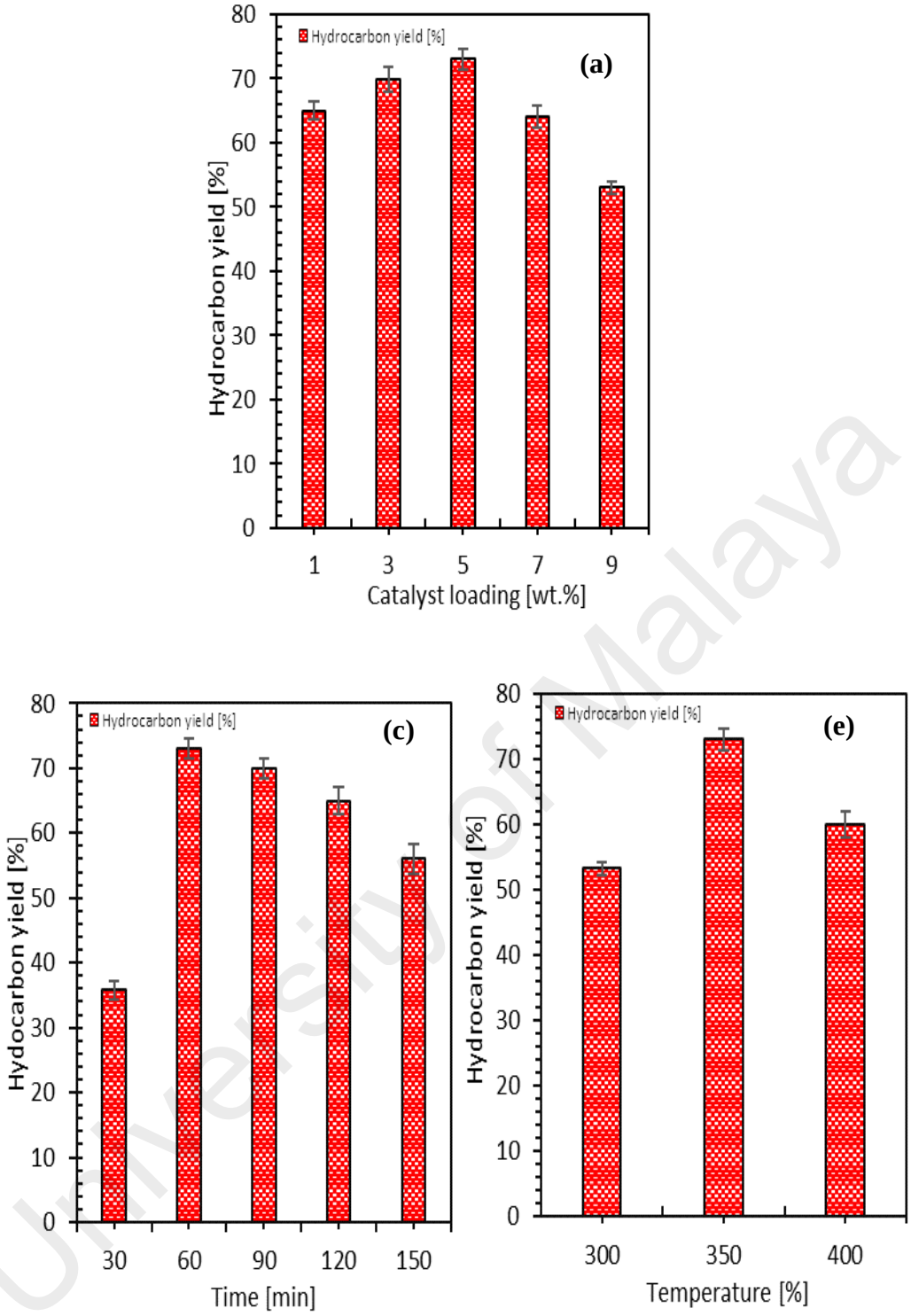

Figure 8.5: Optimization studies of triolein (a-b) Effect of catalyst amount, reaction conditions: 350 ºC, 60 min (c-d) Effect of reaction time, reaction conditions: 350 ºC, 5 wt.% catalyst amount (e-f) Effect of reaction temperature, reaction conditions: 60 min, 5 wt.% catalyst loading under inert N_2 flow condition with stirring rate 400 rpm

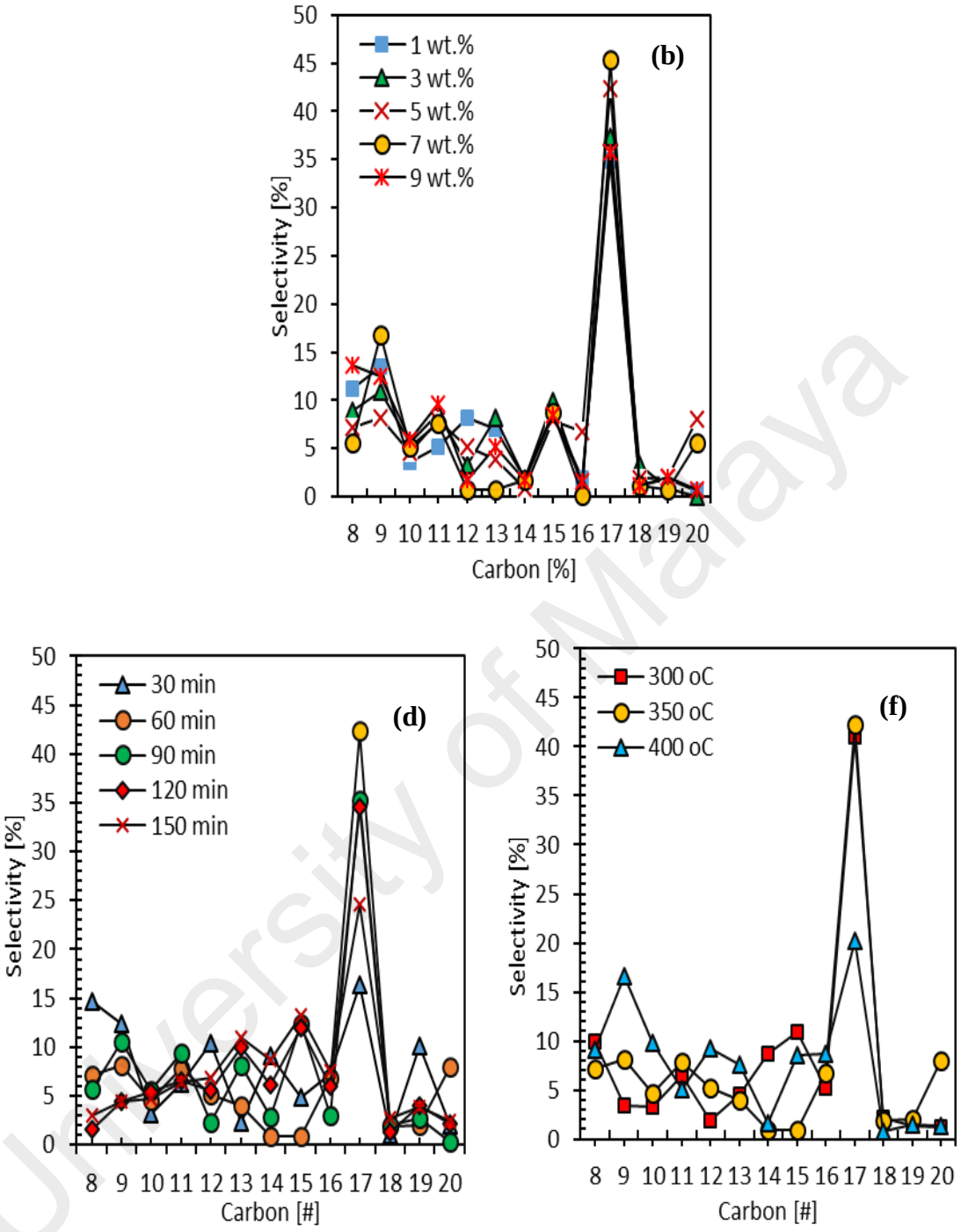

Figure 8.5, continued: Optimization studies of triolein (a-b) Effect of catalyst amount, reaction conditions: 350 ^{o}C, 60 min (c-d) Effect of reaction time, reaction conditions: 350 ^{o}C, 5 wt.% catalyst amount (e-f) Effect of reaction temperature, reaction conditions: 60 min, 5 wt.% catalyst loading under inert N_2 flow condition with stirring rate 400 rpm

8.3.4 Effect of Co content on Co_3O_4-CaO /SiO_2-Al_2O_3 catalysts

Based on the finding on optimization study using Co_3O_4-CaO/SiO_2-Al_2O_3, the maximum hydrocarbon yield and product selectivity were achieved at reaction parameter: 5 wt.% catalyst loading, 60 min reaction time, 350 ^oC reaction temperature under inert N_2 flow condition with stirring rate 400 rpm. In order to further optimize the hydrocarbon yield and desired deCOx product, further stoichiometric study on active Co metal ratios (5–20 wt.%) was investigated (Figures 8.6a-f). As can be further seen from XRD analysis in Figure 8.6a, with the increase of Co content from 5 wt.% to 20 wt.%, the intensity of Co_3O_4 diffraction peaks increased – which indicated that the increasing addition of Co metal favored the formation of Co_3O_4 (Su et al., 2013). Besides, the acid-basic density and active strength distribution were increased as the concentration of Co metal increased (Figure 8.6b-c) (Table 8.5). Based on both acidity and basicity studies, the density increased following the order of 20 wt.%> 15 wt.%>10 wt.%>5 wt.%. Furthermore, a new absorption CO_2 and NH_3 peak was generated at temperature > 800 ^oC for Co concentration range 15–20 wt.%, which indicated that super strong basic and acid strength was formed. Overall, 10 wt.% Co content showed the highest density of mildly acidic characteristic which expected to give better deCOx performance than other catalysts.

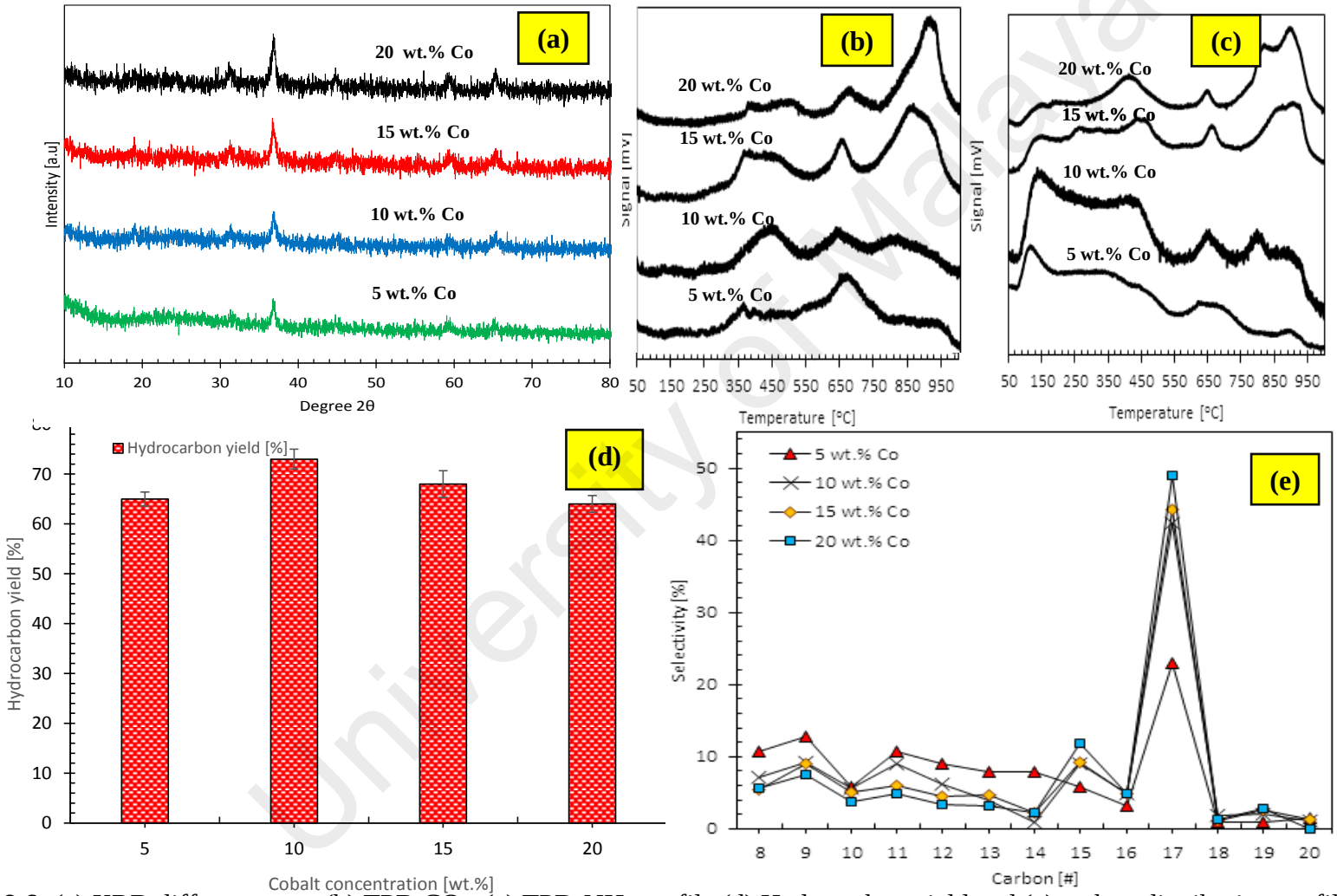

Figure 8.6: (a) XRD diffragtogram, (b) TPD CO_2, (c) TPD-NH_3 profile (d) Hydrocarbon yield and (e) carbon distribution profile for catalytic deoxygenation of triolein over Co_3O_4-CaO/SiO_2-Al_2O_3 with cobalt concentration (5-20 wt.%)

Table 8.5: Physicochemical properties of Co_3O_4-CaO/SiO_2-Al_2O_3 catalyst with Co concentration from 5 to 20 wt.%

Co concentration (wt.%)	XRD	TPD-CO_2		TPD-NH_3	
	[a]Crystallite size (nm)	[b]Temperature (^oC)	[b]bacic sites (µmol/g)	[c]Temperature (^oC)	[c]Acid sites (µmol/g)
5	20.89	336,650,911	88.66,508.60,201.62	111,333,657,887	933.60,2364.41,765.18,90.22
10	25.07	500,664,908	448.66,212.08,366.45	124,402,638,780	3141.52,3548.99,1997.23,1819.39
15	17.91	391,634,829	302.52,225.03,682.31	145,257,433,658,896	842.03,1410.68,1992.07, 1123.38,2950.17
20	20.90	365,483,66,886	19.39,57.38,124.95,593.43	404,637,807,884	1886.73, 585.49,585.49, 1594.94,2109.06

[a]Measured by using Scherer equation from XRD data
[b]Determined by TPD-CO_2 analysis
[c]Determined by TPD-NH_3 analysis

From the results, all series Co_3O_4-CaO/SiO_2-Al_2O_3 with different Co content showed higher hydrocarbon yield (>64%) with product selectively toward *n*-C_{15} and *n*-C_{17}(Figures 8.6e-f). An increment of yield and deCOx product was observed as the Co content was increased from 5 wt.% to 10 wt.%, with hydrocarbon yield increased from 65% to 73% and total *n*-C_{15}+*n*-C_{17} from 28% to 43%. Nevertheless, further increment of Co content to 20 wt.% has led to a decrement of hydrocarbon yield while the reaction was still favorable toward deCOx pathways. Nevertheless, high Co content >10 wt.% promoted cracking of high molecular weight compound to volatiles species which consequently reduced the hydrocarbon yield. This was due to the large existence of strong acid and strong basic density in 15 wt.% and 20 wt.% Co content which further resulted in high occurrence of C-C cleavage. Thus, based on the product yield and desired deCOx selectivity, all subsequent studies were therefore performed over 10 wt.% of Co content or denoted as 10 wt.% Co_3O_4-CaO/SiO_2-Al_2O_3

8.3.5 Deoxygenation of triolein and non-edible oil

The performance of the 10 wt.% Co_3O_4-CaO/SiO_2-Al_2O_3 catalyst from the deoxygenation of triolein was finally evaluated under realistic feedstock. The ceiba oil and sterculia oil were obtained from the extracted *ceiba pentandra L.* and *sterculia foetida L.* seeds from the same method in Ong et al., (2013). The fatty acid composition of the feedstock is shown in Table 8.1. The fatty acid profile showed the primary composition were palmitic acid (19.2%), oleic acid (17.2%), linoleic acid (39.6%) and malvaloyl* 18 CE (18.5%) for the sterculia oil. Moreover, fatty acid profile of ceiba oil showed that it was consisted of 18.4% palmitic acid, 11.1% linoleic acid, 11.1% malvaloyl*18 CE and 44% sterculoyl*19 CE. These pair of unique cyclopropene fatty acid such as sterculoyl and malvaloyl acids being present in the feedstock might result in more reactive radical formation by atmospheric oxygen than the double bond carbon

(polyunsaturated)(Yu et al., 2011). The product yield and carbon distribution from catalytic deoxygenation of ceiba oil and sterculia oil are displayed in Figure 8.7a-b. Consistent with the strong deoxygenation reactivity proven in the study of catalytic deoxygenation triolein, a dramatic increase in the yield of *n*-(C_8-C_{20}) fractions within the range of 77-80% was observed over deoxygenation of ceiba oil and sterculia oil (Figure 8.7a). The reaction order of each feedstock with respect to the deoxygenation reactivity is following this order: triolein<ceiba oil<sterculia oil. Chromatograms of all products are shown in Figure 8.7b which identified majority of the *n*-C_{15}+*n*-C_{17} observed on the deoxygenation of triolein and significant formation of light fractions within range *n*-C_8-C_{12} were observed for both deoxygenation of ceiba oil and sterculia oil with 46% and 80% selectivity's. Meanwhile, the *n*-C_{15}+*n*-C_{17} selectivity in deoxygenation of ceiba and sterculia oil occurred in small extent with only total 25% and 10%, respectively. The trend of deCOx activity of over 10 wt.% Co_3O_4-CaO/SiO_2-Al_2O_3 catalysts was observed in the order of triolein>ceiba oil>sterculia oil. Meanwhile, the trend of gasoline-range formation were in this order: sterculia oil>ceiba oil>triolein. It can be concluded that the catalytic of deoxygenation of triolein rendered deCOx reaction, while deoxygenation of ceiba oil and sterculia oils rendered both cracking and deCOx reactions. This is due to the presence of the double bond in unique pair of cyclopropene fatty acid, thus majority of the C-C cleavage occurred at the allylic C-C bond compared to the C-C bond next to the carboxyl group (Asomaning et al., 2014). The occurrence of deCOx reaction was consistent with the disappearance of C-O at absorption 1285 cm^{-1}, shifting of C=O (ester) at 1740 cm^{-1} to C=O(carboxylic acid) along with significant reduction of C=O at absorption 1710 cm^{-1} (Figure 8.7c-f).

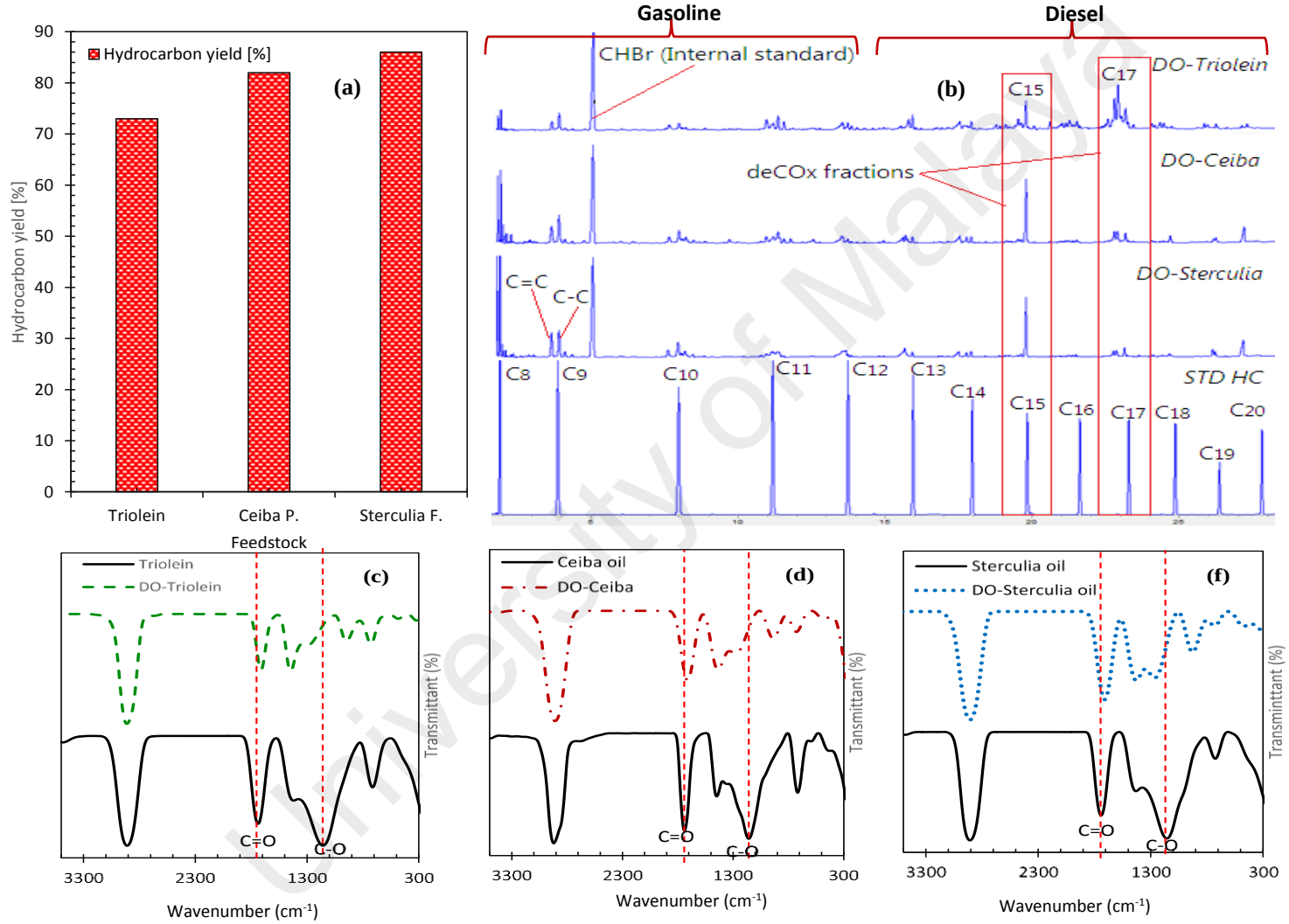

Figure 8.7: (a)Hydrocarbon yield, (b) GC-FID chromatogram and (c-f) FTIR spectra for catalytic deoxygenation of triolein, ceiba oil and sterculia oil

8.3.6 Reusability profile for 10 wt.% Co_3O_4-CaO/SiO_2-Al_2O_3 catalyst

As shown in Figure 8.8 and Figure 8.9, the catalyst stability during the catalytic deoxygenation of triolein, ceiba oil and sterculia oil over 10 wt.% Co_3O_4-CaO/SiO_2-Al_2O_3 catalyst was tested at the conditions of 10 g feedstock at 350 ^oC, 5 wt.% catalyst loading within 60 min reaction under inert N_2 flow condition. The spent catalyst underwent reactivation process by being washed repeatedly with hexane (to remove adsorbed organics). The result showed that the deoxygenation activity over the reactivated catalyst was essentially comparable with the fresh catalyst; thereby demonstrating stability of the catalyst. It could be seen that the reactivated catalyst performed progressively for 4 consecutive runs by maintaining hydrocarbon yield at range of 60-73% for deoxygenation of triolein, 75-86% for both deoxygenation of ceiba and sterculia oil (Figure 8.8a). Based on the carbon distribution profile for 4 consecutive runs, deCOx and cracking-deCOx reaction were favored by formation of > 25% *n*-C_{15}+*n*-C_{17} products for deoxygenation of triolein and > 50% of *n*-(C_8-C_{12}) for deoxygenation deoxygenation of ceiba and sterculia oil(Figure 8.8b-d). The slight reduction of deoxygenation activity over reactivated catalyst may be due to presence of adsorbed organic species and oxygenates (Reddy Yenumala et al., 2016) and formation of coke as observed from FESEM-EDX analysis(Figure 8.9a-f, Table 8.6). The result showed the presence of significant carbon amount (33-63 wt.%) were detected on the reactivated catalyst surfaces implying the decaying process of deoxygenation activity of all feedstock were attributed due to the coke formation. The reduction amount of Co, Ca, Al and Si detected via FESEM-EDX analysis in the reactivated catalyst was due to carbon coverage on the active metal species on the surface of the catalyst. The trend of coke deposited over surface of 10 wt.% Co_3O_4-CaO/SiO_2-Al_2O_3 catalysts was observed in the order of triolein<sterculia oil<ceiba oil. The variety of coke deposited among the feedstock may be derived from the higher content of unsaturated alkyl fatty acid chains

and free fatty acid, which simultaneously promoted fast aromatization reaction. Hence, it resulted in formation of polyaromatic compound (coke precursor), which in turn resulted in catalyst deactivation. Among the feedstock, ceiba oil contained the highest amount of unsaturated alkyl fatty acid (58%) and free fatty acid (11.9 mg KOH g^{-1}) which simultaneously increased the coke formation toward maximum. This assumption is particularly relevant to coking in the study of Absi-Halabi et al., (1991). Theoretically, the coke formation will block the active centers and prevent further reaction on the surface of the catalyst, which will simultaneously result in the lower deoxygenation reactivity. Besides coke deposition, sintering of the 10 wt.% Co_3O_4-CaO/SiO_2-Al_2O_3 particles may also lead to deactivation (Figure 8.9a-f). In the case of reactivated 10 wt.% Co_3O_4-CaO/SiO_2-Al_2O_3 from deoxygenation of triolein and sterculia oil, sintering was pronounced than in deoxygenation of ceiba oil by formation of smooth surface morphology of catalyst. Even though reactivated 10 wt.% Co_3O_4-CaO/SiO_2-Al_2O_3 catalyst in deoxygenation of sterculia oil showed significant sintering effect, the deoxygenation reaction was able to maintain at high reactivity within 4 runs among the others. This was likely associated with newly formation of large pores diameter which formed during deoxygenation of sterculia oil. The enhancement by deoxygenation of sterculia oil might be due to the simultaneous thermal and catalytic cracking which had resulted in the collapse of the pore walls of the catalyst(Lee et al., 2014). It has then led to the pitting and erosion on the newly formed reactivated 10 wt.% Co_3O_4-CaO/SiO_2-Al_2O_3 catalyst surfaces. As a result, it would provide a wide channel for diffusion of reactant and product into the reactivated 10 wt.% Co_3O_4-CaO/SiO_2-Al_2O_3 catalyst pores (Chandra Mouli et al., 2011;Zhao et al., 2016) thus enhancing the deoxygenation activity. Even though metal leaching is one of the factors for deterioration of catalytic activity, it was found that the total metal leaching for 4^{th} runs in the deoxygenated liquid product occurred in small extent (Table 8.7). However,

based on metal content investigation for deoxygenated liquid product from 1st and 4th runs, the results showed Co^{3+}, Ca^{2+}, Si^{2+}, and Al^{3+} concentrations had total metals leaching of negligible value within the range of < 0.2 ppm, which suggested the key factor for deterioration deoxygenation activity was due to the coke coverage. Overall, all the deoxygenated liquid products in the present study did not suffer from metal leaching which in turn lowering the risk of environmental concerns. Moreover, the metal leach in deoxygenated liquid product also meets the EN 12662 standard Specification for Diesel Fuel Oils contamination content (max 24 ppm) (John Bacha et al., 2007) and can be used in commercial applications.

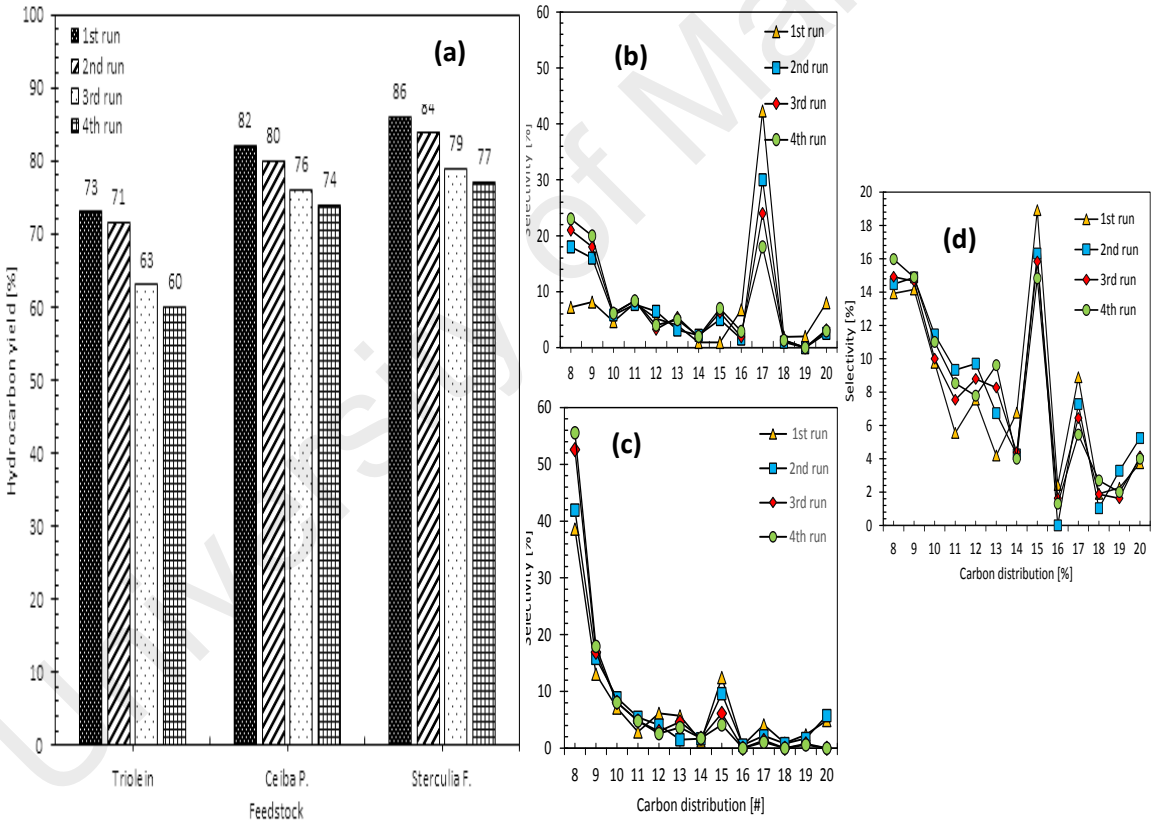

Figure 8.8: Reusability of the 10 wt.% Co_3O_4-CaO SiO_2-Al_2O_3 catalyst towards (a) straight chain hydrocarbon and carbon distribution for (b) deoxygenation of triolein, (c) deoxygenation of ceiba oil and (d) deoxygenation of sterculia oil from 1st–4th run reactions

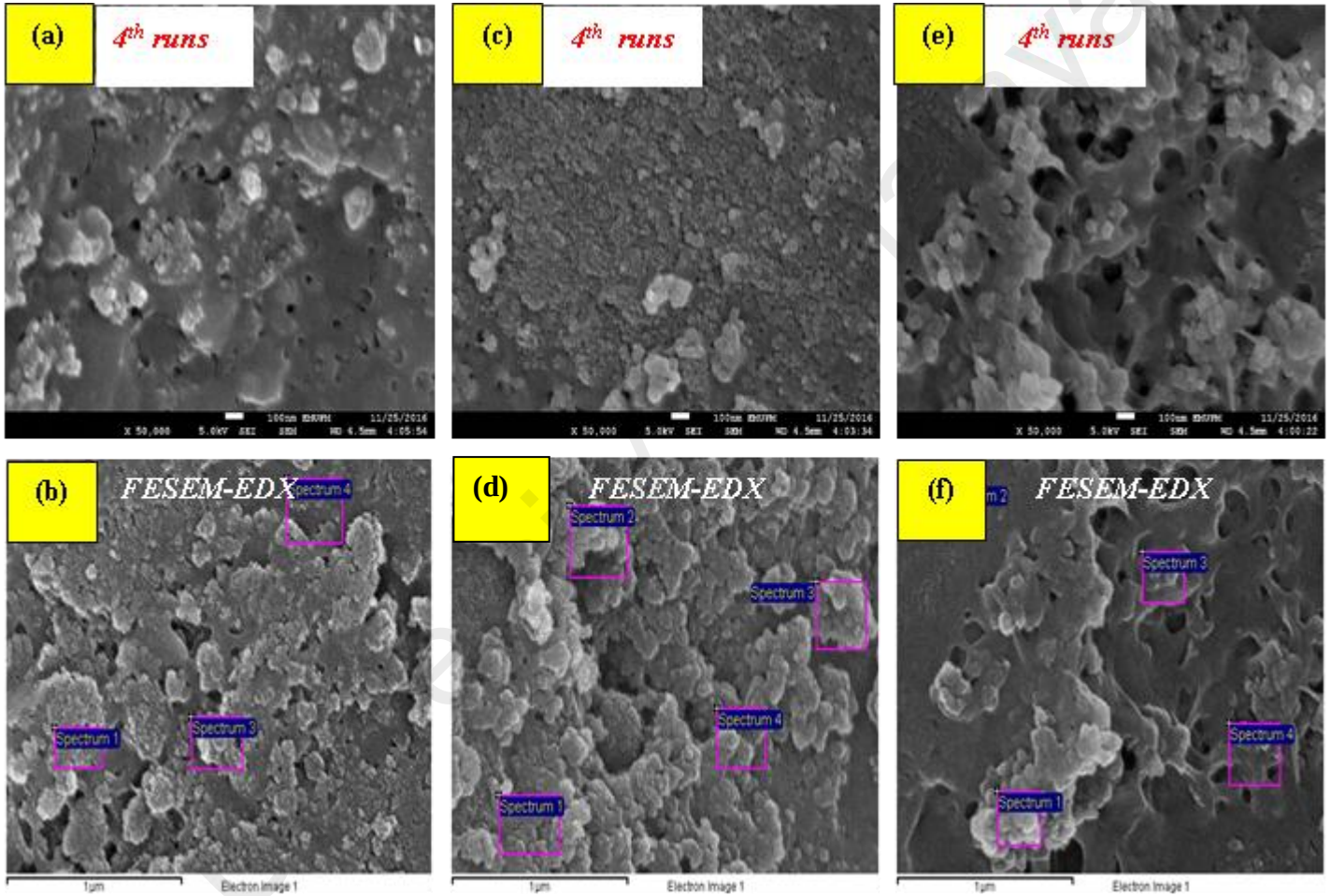

Figure 8.9: FESEM image for reactivated 10 wt.% Co_3O_4-CaO/SiO_2-Al_2O_3 catalyst from 4th runs of (a-b) deoxygenation of triolein (c-d) deoxygenation of ceiba oil and (e-f) deoxygenation of sterculia oil

Table 8.6: Physicochemical properties for fresh and reactivated 10 wt.% Co_3O_4-CaO/SiO_2-Al_2O_3 catalyst

[a]Catalyst	Feedstock	[b]Elemental composition (wt.%)					
		C	O	Al	Si	Ca	Co
Fresh catalyst	-	-	60.13±2.1	3.93±0.3	14.91±1.0	9.65±0.8	14.35±2.1
Reactivated 4th cycles spent catalyst	Triolein	33.96±0.65	45.34±0.39	3.01±0.08	14.90±0.50	1.90±0.07	0.80±0.03
	Ceiba oil	63.86±2.08	23.63±1.05	1.81±0.28	8.97±1.37	0.85±0.16	0.89±0.21
	Sterculia oil	50.19±6.04	33.88±3.57	2.38±0.40	11.41±2.27	1.34±0.25	0.80±0.31

[a]10 wt.% Co_3O_4-CaO/SiO_2-Al_2O_3 catalyst
[b]Determined by FESEM-EDX

Table 8.7: Metal leaching study in deoxygenation of liquid product for 1st and 4th runs over 10 wt.% Co_3O_4-CaO/SiO_2-Al_2O_3 catalyst

Feedstock	Number on run[a]	Elemental composition			
		Co[b] (ppm)	Ca[b] (ppm)	Si[b] (ppm)	Al[b] (ppm)
Triolein	1st run	0.010±0.0003	0.014±0.0005	0.012±0.0002	0.013±0.0001
	4th run	0.038±0.0005	0.024±0.0003	0.023±0.0005	0.036±0.0003
Ceiba oil	1st run	0.013±0.0004	0.010±0.0001	0.011±0.0004	0.016±0.0004
	4th run	0.042±0.0008	0.032±0.0004	0.021±0.0009	0.038±0.0001
Sterculia oil	1st run	0.012±0.0004	0.011±0.0003	0.016±0.0001	0.011±0.0006
	4th run	0.036±0.0001	0.028±0.0004	0.032±0.0005	0.0040±0.0005

[a]Deoxygenation reaction condition; reaction temperature 350 °C, 60 min of reaction time, 5 wt.% catalyst loading under inert condition.
[b] Co, Ca, Si and Al concentration was determined by ICP-AES analysis.

8.4 Conclusion

The deoxygenation of vegetable oil feeds is a promising route for the production of green fuel – especially the use of the non-edible sources that are of interest as this will not interfere with the food production. In the present study, the triglycerides and fatty acid derivatives can be converted to fuel-like hydrocarbon over SiO_2-Al_2O_3 supported Co_3O_4-CaO catalyst. The present Co_3O_4-CaO/SiO_2-Al_2O_3 catalyst deoxygenation reaction of triolein is capable of rendering high deCOx selectivity via formation of *n*-C_{15} and *n*-C_{17} fractions, which implies due to the presence of synergic effect between acid-basic sites associated with the present of Co_3O_4 and CaO on mesoporous SiO_2-Al_2O_3 catalyst. The optimum Co content for maximizing the yield of *n*-(C_8-C_{20}) was 10 wt.% with yield 73% and deCOx selectivity (*n*-C_{15}+*n*-C_{17}) to 43%. Furthermore, Co_3O_4-CaO /SiO_2-Al_2O_3 catalyst is capable of maintaining 4 consecutive runs with consistent hydrocarbon yield 60-73% for deoxygenation of triolein and 75-86% for deoxygenation of realistic non-edible oil derived ceiba oil and sterculia oil**.** The gradual reduction of deoxygenation activity (yield, product selectivity) in each run was mainly due to the formation of coke deposit on the Co_3O_4-CaO /SiO_2-Al_2O_3 catalyst surface. The coke was also found to be prominent with the use of higher content of unsaturated alkyl fatty acid chains and FFA acid feedstock.

CHAPTER 9: PRODUCTION OF GREEN DIESEL VIA CATALYTIC DEOXYGENATION OF JATROPHA CURCAS OIL

This chapter describes the synthesis and characterization of a novel acidic Ni and Co support MWCNT catalyst. The catalyst activity was further tested in deoxygenation of high FFA feedstock (jatropha curcas oil). This study was important in order to study performance of catalyst without the present of Ca species but with the present of the most effective transition metal oxide in deoxygenation activity which found in chapter 4-5. We also introducing the usage of neutral support: multi-wall carbon nanotube (MWCNT) in order to lowering the coke instead of the usage of basic metal (Ca) and mildly acidic mesoporous support (silica-alumina) like in chapters 4-8. This study entitle " ***Production of green diesel via catalytic deoxygenation of jatropha curcas oil*** " have been recently accepted and published in high international transdisciplinary *Journal of Cleaner Production* on 2016. The authors including N. Asikin-Mijan, H.V. Lee , G. Abdulkrem-Alsultan, A. Afandi and Y.H. Taufiq Yap.

9.1 Introduction

Increasing anthropogenic CO_2 in the atmosphere, rising of global temperature and diminishing fossil energy resources have generated a great interest in renewable biofuels (Klemeš et al., 2010; Dovì et al., 2009; Sanjid et al., 2014). Fatty acid methyl ester (FAME) or biodiesel is a potential fuel substitute with mature and proven technology (Rahman et al., 2014; Hussan et al., 2013). Biodiesel produced from the transesterification of oil or fat with a monohydric alcohol (in most cases-methanol), yielded the corresponding mono-alkyl esters (Knothe, 2005). However, FAME is composed mainly of high oxygenated compounds- which leads to many inevitable disadvantages such as high viscosity, high pour point, high acid number, low heat value

and low stability (Yang et al., 2013; Ahmed et al., 2014). These quoted detriments could cause serious problems in the conventional diesel engines.

In order to prevent the unwanted drawbacks, greener alternative routes such as deoxygenation (DO) (Romero et al., 2015; Asikin-Mijan et al., 2015) and hydrodeoxygnation (HDO) (Ayodele et al., 2014a; Boullosa-Eiras et al., 2014) were developed in order to produce bio-diesel with higher oxidative stability from various bio-feedstock biomasses such as cellulosic material, woody-biomass, crop residues , vegetable oil model compound, edible oil and non-edible oil (Ko et al., 2012; Santillan-Jimenez et al., 2013; Elkasabi et al., 2014; Lovás et al., 2015; Asikin-Mijan et al., 2016). Green diesel production was commonly prepared under hydrogen environment and high pressure, which known as hydrodeoxygenation (HDO) reaction. Thus, hydrodeoxygenation is less environmental and economical friendly as it consumes substantial amount of conventional hydrogen gas to allow hydrogenation reaction of triglycerides (Huber et al., 2007). In the presence study, a focus on development of green route for renewable diesel production under free hydrogen atmosphere, which known as deoxygenation (DO) process is discussed. The deoxygenation process is capable of producing significant amount of hydrocarbon-based fractions under milder reaction conditions compared to hydrodeoxygenation process (Lestari et al., 2010).

Recent efforts in developing suitable metal catalysed deoxygenation of fatty acid were studied by Snåre et al., (2007) and Simakova et al., (2009). Remarkably, these groups found out that the Pd supported on activated carbon display has showed promising performance in deoxygenation reaction. Lestari et al., (2010) also reported that the application Pd supported on SBA-15 was highly effective in deoxygenation of fatty acid. Eventhough palladium have reported in high catalytic activity for reaction.

However, this application is not sustainable for industrial practices as the cost of implementation is very high. Hence, an inexpensive catalyst which have similar catalytic effect as palladium is needed to be developed as a noble catalyst for bio-diesel production. Recent studies reported that Ni-based and Co-based catalysts showed similar promotional effect as noble catalysts which showed high catalytic activity for the upgrading of soybean oil and model triglycerides in batch reactor (Santillan-Jimenez et al., 2013; Zhang et al., 2014; Kordulis et al., 2015). Both of these metals gave the predominating decarboxylation/decarbonylation (deCOx) products and also yield cracked products which consisted of mainly diesel-range alkanes (Snåre et al., 2006). However, the application of bulk metal oxides will lead to the internal diffusion limitation and reduce the production of branched hydrocarbon. Instead on implementing mesoporous acidic support like previous chapter, herein, investigation on catalytic performance of neutral support (MWCNTs) for deoxygenation of non-edible and low cost jatropha oil into diesel-like hydrocarbons in the absence of hydrogen environment. The Ni and Co metals were used as metal promoters.

9.2 Literature Review

Catalyst support has significant effect in deoxygenation reaction. Carbon nanotubes (CNTs), has been investigated intensively since their discovery in 1991 by Iijima, 1991. CNTs are allotropes of carbon with a distinct structure which give outstanding mechanical properties (Park et al., 2004). There are relatively few amount of organic group in the CNTs which simultaneously reduce the possibility of the occurrence of side reaction hence making it a promising catalyst support for deoxygenation (Yang et al., 2013). In addition, the uniform and larger pore diameter of these supports facilitate relatively easier diffusion of substrates compared with conventional catalysts (Ding et al., 2014). In addition, Yang et al., 2013 has also

discussed the potential of multi-wall carbon nanorode (MWCNTs) catalyst incooperated with expensive noble metal (platinum) in hydrothermal decarboxylation of a series of fatty acids (stearic acid, palmitic acid, lauric acid, myristic acid, arachidic acid and behenic acid) model compound.

9.3 Experimental

9.3.1 Materials

Multi-walled carbon nanotube (MWCNTs) with purity > 95% were generously provided by US research Nanomaterials, Inc. Nickel(II) nitrate hexahydrate ($Ni(NO_3)_2.6H_2O$) with purity > 99%, cobalt(II) nitrate hexahydrate ($Co(NO_3)_2.6H_2O$) with purity > 99.9% and ethyl alcohol with purity 99.7% were obtained from R&M Company. Phosphoric acid (99% purity) were purchased from J.T. Baker. The liquid products are both alkane and alkene standard (C_8-C_{20}) and internal standard 1-bromohexane for gas chromatograph (GC) analysis were purchased from Sigma Aldrich and used without further purification. N-Hexane (GC grade) with purity > 98% from Merck was used for dilution. The feedstock of this work, *Jatropha curcas L*. oil (JCO), were purchased from Bionas Sdn Bhd, Malaysia. This oil was used for the reaction without further treatment and purification. The properties of the crude JCO which included FFA content and water content are given in Table 9.1 (Lee et al., 2015a). Based on the analysis, the total acid number (TAN) is 30.8 mg KOH/g, which indicated the presence of of high free fatty acids (15.4 wt.%). The chemical composition of fatty acid of JCO is composed of saturated fatty acids (i.e. palmitic acid (20.1%) and stearic acid (7.22%)), unsaturated fatty acid (i.e. oleic acid (39.77%) and linolenic acid (31.52%)).

Table 9.1: Physicochemical properties of the *Jatropha curcas L.* oil

Oil properties	**[a]JCO**
Density (g/cm^3)	0.92
Viscosity at 40^o C (cSt)	50.0
Moisture content (wt.%)	0.01
Acid Value (mg KOH g^{-1})	30.8
FFA Value (%)	15.4
Fatty acid composition of Oil (%)	
Palmitic acid (C16:0)	20.16
Stearic acid (C18:0)	7.22
Oleic acid (C18:1)	39.77
Linolenic acid (C18:2)	31.52

[a]Data from previous study (Lee et al., 2015a)

9.3.2 Synthesis of deoxygenation catalysts

Ni-Co/MWCNT catalysts was synthesized via wet-impregnation method. Initially, 5 g of MWCNT support was activated by 75 mL of concentrated H_3PO_4 (95%) at the temperature of 150 °C for 24 h. H_3PO_4 was then removed and washed by using distilled water to achieve pH 7. The activated MWCNTs particles were dried in oven at 120 °C. In order to prepare Ni-Co/MWCNT with NiO/Co_2O_4 weight percentage ratio of 10:10 (wt.%), 0.008 M of $Co(NO_3)_2.6H_2O$ and $Ni(NO_3)_2.6H_2O$ solution was added into activated MWCNT support with continuous stirring for 6 h at ambient temperature. The filtered catalyst was further thermal activated at 400 ºC for 4 h under nitrogen flow. Furthermore, Co/MWCNT and Ni/MWCNT with 10 wt. % of Co_2O_4 and 10 wt.% of NiO, respectively was prepared via similar preparation step. The synthesized catalysts are denoted as Co/MWCNT, Ni/MWCNT and Ni-Co/MWCNT, respectively. In additional, optimization study was further performed by varying the Ni content of Ni-Co/MWCNT catalyst with NiO content of 5 to 40 wt.% and remained constant for 10 wt.% of Co_2O_4 via wet-impregnation method. The series of prepare catalysts was denoted as Ni_nCo_{10}/MWCNT, where n= 5-40 wt.%.

9.3.3 Catalysts characterization

The powder X-ray diffraction (XRD) analysis was carried out to identify the dispersion states and chemical composition of modified MWCNT catalysts before and after reaction. The XRD analysis was performed using Shimadzu diffractometer model XRD-6000. The specific surface area and pore distribution of the catalysts were determined by Brunauer-Emmet-Teller (BET) method with N_2 adsorption/desorption analyser using Thermo-FinniganSorpmatic 1990 series. The catalyst was degassed overnight at 150 ^oC to remove moisture and foreign gases on the surfaces of the catalyst. Adsorption and desorption processes of N_2 on the catalyst surfaces were analyzed in a vacuum chamber at -196 ^oC. Furthermore, Fourier Transform – Infrared Spectrometer (FT-IR) analysis was performed using PerkinElmer (PC) Spectrum 100 FTIR with a resolution of 4 cm^{-1} and operating in the IR range of 300-4000 cm^{-1}. This analysis help to determine the chemical functional group comprised of the catalyst. The acidity of the catalysts were studied using temperature programmed desorption (TPD-NH_3) with NH_3 as probe molecule. The analysis was carried out by using Thermo Finnigan TPD/R/O 1100 instrument equipped with thermal conductivity detector (TCD). The catalyst (~0.05 g) was pretreated by N_2 gas flow for 30 min at 250 ^oC, followed with NH_3 gas for an hour at ambient temperature to allow adsorption of NH_3 onto the surfaces. The excess NH_3 was subsequently flushed with N_2 gas flow at rate 20 ccm/min. The desorption of NH_3 from the acid sites of the catalyst was detected by TCD under helium gas flow (30 ml/min) from 50 ^oC to 900 ^oC and held for 30 min. Morphological and elemental composition of the catalysts were investigated by FESEM-EDX analysis. The FESEM images were recorded on LEO 1455 VP electron microscope. The FESEM device coupled with EDX analysis was performed by Rayny EDX- 720 spectrometer for determination of elemental composition of carbon Ni and Co on the synthesized catalysts. The extent of coke/carbon deposition on the spent catalyst was determined by

thermogravimetric analysis (TGA) instrument (TGA 1000i, Instrument Specialists Inc, USA). The samples were heated from 25 to 900 ^{o}C at a heating rate of 30 ^{o}C/min under 40 mL/min air flow.

9.3.4 Catalytic deoxygenation of JCO

The deoxygenation of JCO was performed in a mechanically stirred 250 mL of semi-batch reactor. In a typical experiment, approximately 10 g of JCO and 5% (wt.) of catalyst were added to the reactor. Before each experiment, under constant stirring of the mixture, the reactor was vacuumed to remove the air inside and was initially pressurized to approximately 5 mbar before the heating. The temperature was increased to reach the desired temperature 350 ^{o}C and maintained for 1 h. The final pressure of around 10 mbar was achieved. The condensable products were condensed using cooler and the stored in a vessel located downstream batch reactor. The liquid product was collected every 1 h interval time for analysis. At the end of the test, the reactor was cooled down until room temperature by a cooling system based on external water circulation and the liquid products was further weighted and analysed using AN test, GC-FID. In order to determine the mass of the of retained products (char+residue) after reaction, the solid catalyst were separated by mixing the liquid residue inside the semi-batch reactor with the hexane. All solid catalyst were filtered and dried in an oven at 110 ^{o}C for 12 h. All the hexane were removed via rotary evaporator and leaving dark viscous liquid which were considered as (char+residue).

9.3.5 Product analysis

The deoxygenated liquid products were identified using alkane and alkene standards (C_8-C_{20}), which procured from Sigma Aldrich. The liquid products were quantitatively analyzed on a gas chromatography (Shimadzu GC-14B) equipped with a

HP-5 capillary column (length: 30 m × inner diameter: 0.32 mm × film thickness: 0.25 μm) with a flame ionisation detector (FID) operating at 300 °C. The liquid product was diluted with GC grade n-hexane prior to the yield analysis. The 1-bromohexane was used as internal standard for quantitative analysis. An aliquot of 1 μL of sample was injected with into GC column. The injection temperature was 250 °C and nitrogen gas was served as the carrier gas. The initial temperature of the oven was set at 40 °C and held for 6 min, then ramped to 270 °C at heating rate of 7 °C/min. The JCO was qualitatively characterized using gas chromatography mass spectrometer (GC-MS) (model SHIMADZU QP5050A) equipped with a non-polar DB-5HT column (30 m x 0.25 mm x I.D μm) with splitless inlet. The JCO was diluted with GC grade n-hexane (purity >98%) to 100 ppm. The fraction peaks from GC-MS spectrum were identified via National Institute of Standards and Testing (NIST) library. The identification of the major products was based on a probability match equal or higher than 95%. The acid value of the JCO and liquid products were determined by using the classical titration method referred to as the standard method of AOAS Cd 3d-63 (Eq. 9.1).

$$Acid\ Number\ (AN): (V_f - V_i) N \frac{56}{W_{oil}} \tag{9.1}$$

The performances of the catalysts were evaluated by GC-FID in terms of hydrocarbon yield (X) (Eq. 9.2)(Asikin-Mijan et al., 2015a).

$$X = \frac{\sum n_o + \sum n_i}{\sum n_z} \times 100\% \tag{9.2}$$

Where:

n_o =Area of alkene (C_8-C_{20})

n_i =Area of alkane (C_8-C_{20})

n_z =Area of the product

The hydrocarbon selectivity (S) of the hydrocarbon were calculated by Eq. 9.3.

$$S = \frac{C_x}{\sum n_x} \times 100\% \quad (9.3)$$

Where:

C_x =Area desired hydrocarbon fraction

n_x =Area of hydrocarbons

9.4 Results and Discussion

9.4.1 Characterization of MWCNT-based catalysts

The XRD patterns of the catalysts were shown in Figure 9.1. The XRD characteristic phase for fresh MWCNT showed diffraction peaks at 2θ = 25.82°, 44.01°, 53.18°, 64.24° and 77.46°, which corresponded to 002, 100, 110, 004 and 006 crystal planes of MWCNT. The crystallite size of 52.93 nm and d_{002} spacing of 0.34 nm. Once the MWCNT intercalated with NiO and Co_2O_4 species, the MWCNT peaks were slightly shifted and the peak intensity was also weakened. This shift over from 25.82° to a higher value 26.80° along with reduction of intensity attributed to the intercalation of NiO and Co_2O_4 which were embedded in the MWCNTs matrix and promote higher dispersion MWCNTs catalyst and cause reduction of crystallite size. This is in agreement with the significant reduction in crystallite size of Ni/MWCNT, Co/MWCNT and Ni-Co/MWCNT catalysts of about about 10.23, 12.99 and 11.53 nm and d-spacing about d_{002} = 0.33, 0.33 and 0.34 nm, respectively. Wu et al., (2014) and Qian et al., (2014) has previously proved that the support diffraction peak intensity has reduced after being impregnated with metal. No other crystalline phases are observed besides MWCNTs; which have been detected by XRD. The low amount of metal was also one of the factors in suppressing the deconvolution of new characteristic phase that belongs

to NiO and Co_2O_4, where we found only <6% of NiO and Co_2O_4 were found on the MWCNT (Table 9.2).

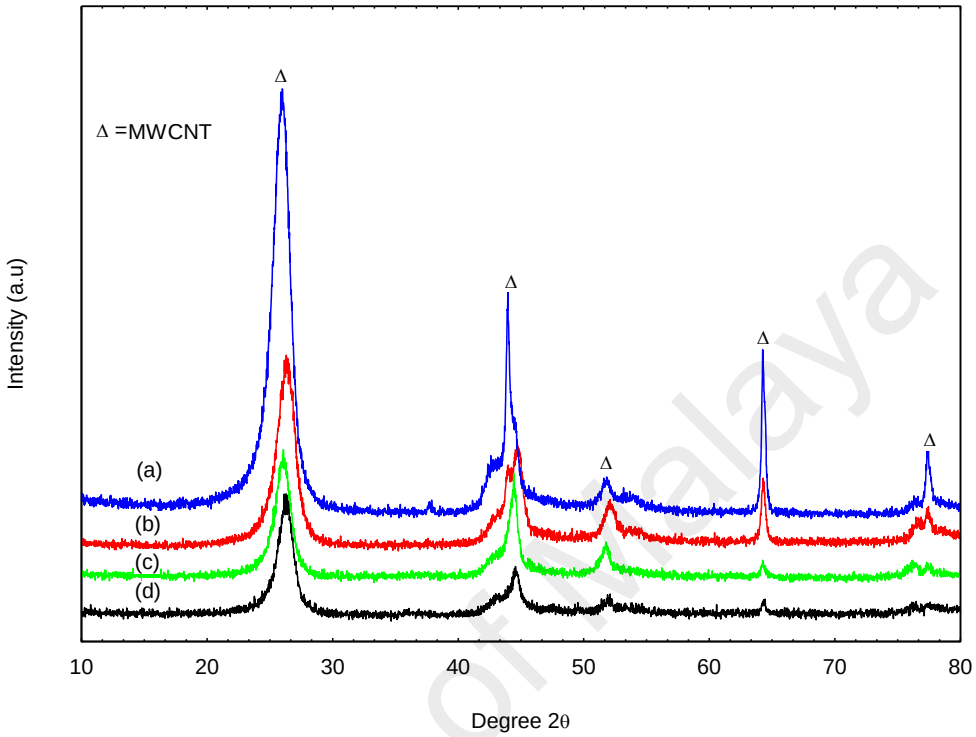

Figure 9.1: X-ray diffraction patterns of the catalysts: (a) MWCNT, (b) Ni/MWCNT, (c) Co/MWCNT and (d) Ni-Co/MWCNT

The morphology and elemental study of MWCNT-supported catalysts were determined via FESEM-EDX mapping analysis (Figure 9.2a-d). The FESEM images showed that fresh MWCNT and metal supported MWCNT catalyst present in nanotube structure with diameter <100 nm. Based on the results, majority of Ni and Co was distributed well on the MWCNT support. Furthermore, EDX analysis indicated that the MWCNT support rendered 88.53 ± 2.70 atomic % of carbon, 3.68 ± 0.42 atomic % of Ni for Ni/MWCNT, 5.43 ± 0.68 atomic % of cobalt for Co/MWCNT and Ni-Co/MWCNT (3.49 ± 0.17: 5.8 ± 0.42 atomic %) (Table 9.2). Thus, it can be suggested that the active metals were highly disperse on the MWCNT surface. The high content of carbon material in MWCNT is expected to act as effective sintering barriers and

simultaneously restraining the sintering of NiO and Co_2O_4 particles (Tan and Tsai, 2015; Ding et al., 2014).

The specific surface area of MWCNT and MWCNTs-supported catalysts was determined by using BET method (Table 9.2). The results indicated that the MWCNTs-supported catalysts has gradually reduced surface area and pore volume in the range of 41-111 m^2/g and 0.42-1.27 cc/g respectively as compared to fresh MWCNT (surface area = 220 m^2/g and pore volume = 1.34 cc/g).This is due to the excess of active metals (Ni and Co) embedded into the channel of parent materials and incorporated into the pore of support, which slightly blocked the porous structures (Abdulkareem-Alsultan et al., 2016a). Amongst the MWCNTs- supported catalysts, Ni-MWCNT catalyst showed the lowest surface area and the smallest pore volume. In the sequence of Co/MWCNT and Ni-Co/MWCNT catalysts, the surface area significantly closer except for the pore size of Ni-Co/MWCNT - it became significantly larger when NiO metal was incorporated together. The enlargement of pore size occurred due to the collapse of pore walls during impregnation/surface modification. Mixed metal NiO and Co_2O_4 metals were highly efficient in destroying the pore structure of MWCNTs support and capable to reduce the blockage of pores - which have been confirmed by having the largest pore diameter about 17.18 nm and pore volume 1.27 cc/g among other MWCNTs- supported catalysts. The large pore is beneficial for the diffusion of the reactants to catalyst and products from catalyst. Therefore, it is expected that Ni-Co/MWCNT catalyst to have high catalytic activity in the deoxygenation.

Table 9.2: Physicochemical properties of MWCNT-supported catalysts

Catalyst	Elemental composition (%)[a]				XRD[b]			BET[c]			TPD-NH_3[d]	
	C	O	Co	Ni	2θ	Cystallite size (nm)	d_{200} (nm)	Surface area (m^2/g)	Pore size diameter (nm)	Pore volume (cc/g)	Temperature (°C)	Acid sites (μmol/g)
MWCNT	88.53	11.45	-	-	25.8	52.93	3.40	220.00	15.51	1.34	-	-
Ni/MWCNT	93.49	3.33	-	3.68	26.6	10.38	3.39	41.58	15.35	0.42	709,796, 898	3225.52,4339.07, 2168.95
Co/MWCNT	88.99	5.58	5.43	-	26.9	12.99	3.31	110.98	15.34	1.05	910	7369.47
Ni-Co/MWCNT	88.90	1.80	5.80	3.49	26.8	11.53	3.40	109.05	17.18	1.27	563,777	764.21, 9711.32

[a]Determined by FESEM-EDX analysis.
[b]Measured by using Scherer equation from XRD data.
[c]Determined by BET analysis.
[d]Determined by TPD-NH_3 analysis.

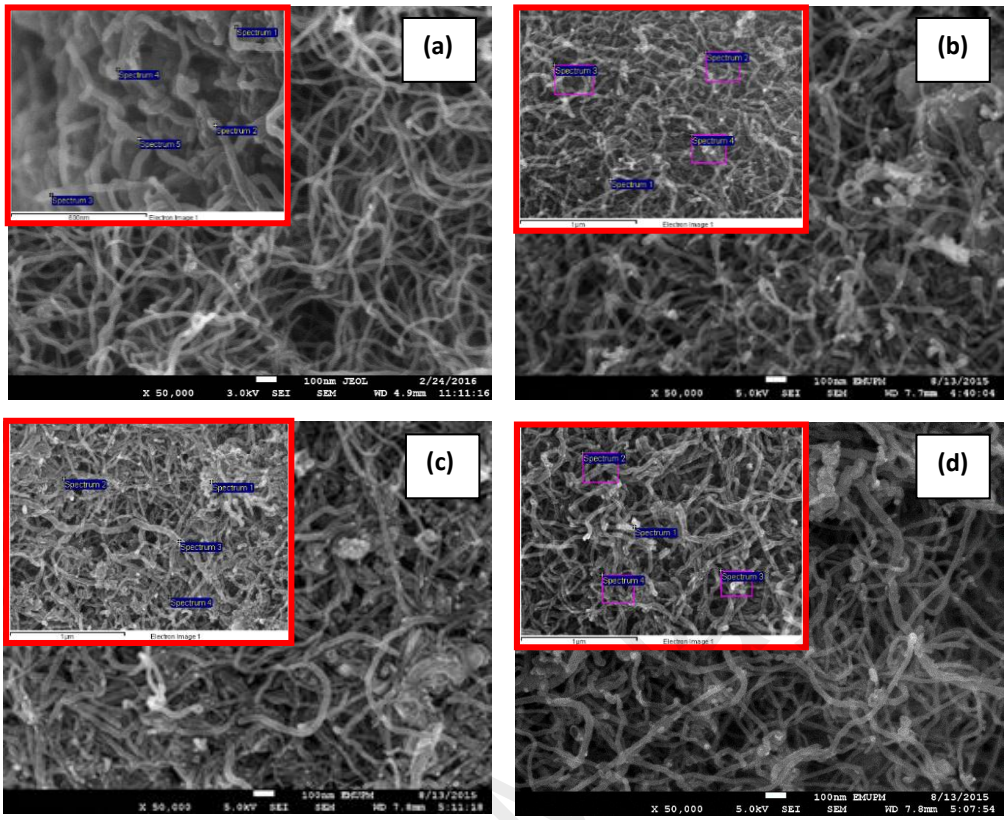

Figure 9.2: FESEM analysis for catalysts: (a) MWCNT, (b) Ni/MWCNT, (c) Co/MWCNT and (d) Ni-Co/MWCNT

The acidity profile of synthesized catalysts were evaluated by using temperature programmed desorption of NH_3. The TPD-NH_3 profiles and acidity strength distribution of the catalysts were displayed in Figure 9.3 and Table 9.2, respectively. TPD patterns of the modified MWCNT catalysts showed NH_3 desorption peaks as majority at the temperatures within the range of 500-910 ^oC, indicating all the NiO and Co_2O_4 supported MWCNT catalysts exhibited strong acid sites. MWCNT support is amphoteric material with absence of any TPD-NH_3 peak. Based on the result obtained, incooperation of Co_2O_4 and NiO on the MWCNTs support has increased the distribution of strong acid catalyst (low strength) with the highest acid density 10,475.53 mmol/g. Meanwhile, Ni/ MWCNT and Co/MWCNT rendered stronger acidity at higher strength with total acid density 9733.54 mmol/g and 7369.47 mmol/ g, respectively.

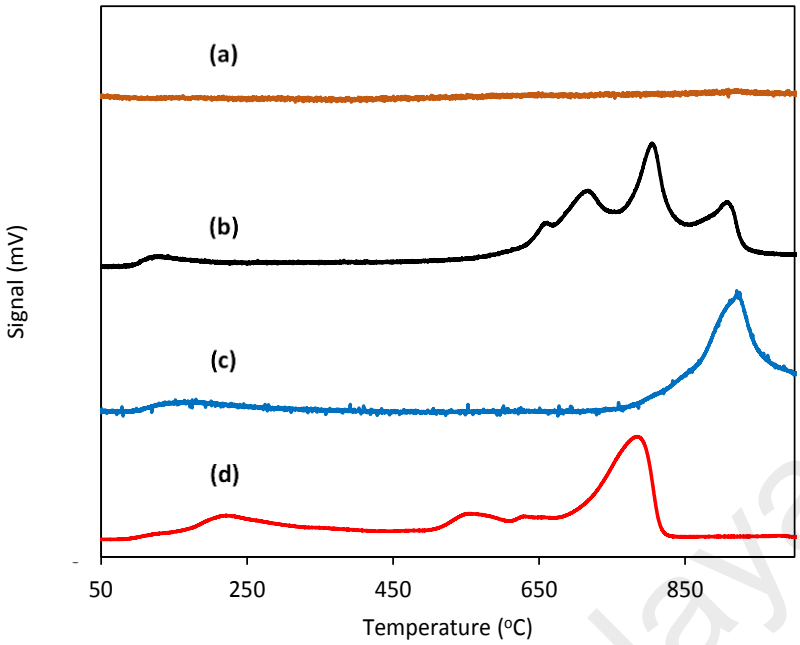

Figure 9.3: TPD-NH_3 analysis for catalysts: (a) MWCNT, (b) Ni/MWCNT, (c) Co/MWCNT and (d) Ni-Co/MWCNT

The FTIR spectra of doped MWCNTs were shown in Figure 9.4. The FTIR band at 3630 cm^{-1} corresponds to the stretching mode of O-H groups. While FTIR bands at 2814 cm^{-1} and 2682 cm^{-1} corresponded to the asymmetric and symmetric stretching modes of CH present at the sidewall surfaces of MWCNTs. Besides, the bands at 1798 cm^{-1} and 1400–1600 cm^{-1} corresponded to the stretching mode of C=O group and backbone C=C of MWCNTs, respectively. The presence of stretching of C–O group from MWCNT was also shown in FITR bands at 1615 cm^{-1} and 1320-1110 cm^{-1}. MWCNT-supported catalysts showed similar FTIR patterns with different peak intensities (2682, 1798, 1614, 1319 and 1110 cm^{-1}) for CH symmetric stretching, C=O stretching and C-O stretching, respectively. The increased peak intensity for Ni-Co/MWCNT compared to Ni/MWCNT and Co/MWCNT was due to the generation of carboxylic acids group (more defects) as an effect of the strong interaction of Ni-Co on the MWCNT support (Gao et al., 2010; Akalework et al., 2012).

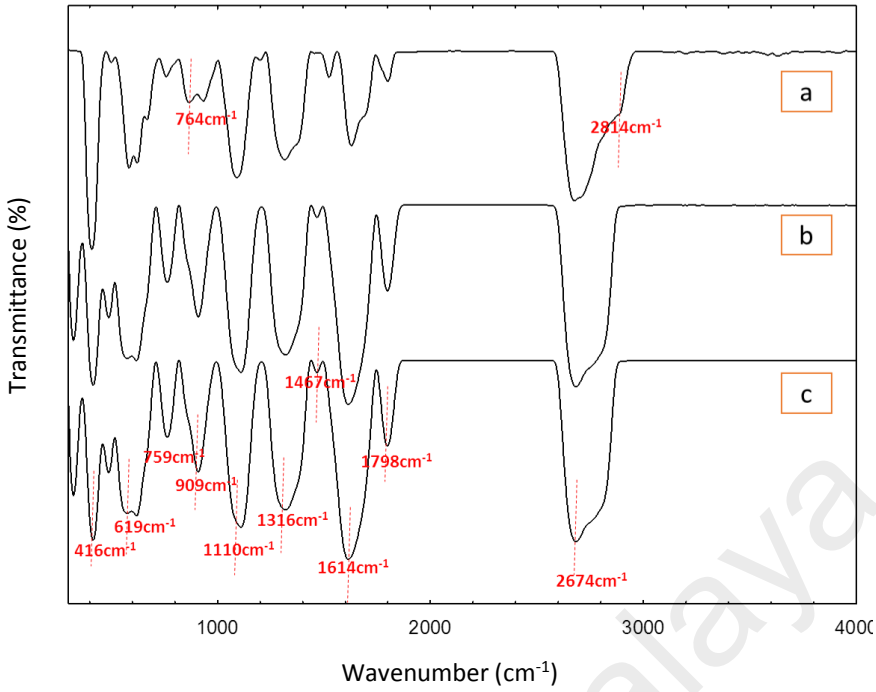

Figure 9.4: FTIR spectrum for catalysts: (a) Ni/MWCNT, (b) Co/MWCNT and (c) Ni-Co/MWCNT

9.4.2 Catalytic deoxygenation profile

Catalytic activity of MWCNT-supported catalysts was determined by deoxygenation reaction at reaction condition of 5 wt % catalyst loading, 350 ^{o}C reaction temperature for 1 h reaction time under 10 mbar pressure with stirring rate of 400 rpm. The catalytic activity and product selectivity profile was summarized in Figure 9.5. Based on the result obtained from the GC-FID analysis, the deoxygenized liquid products were composed of saturated and unsaturated hydrocarbon fractions in range of C_8-C_{20}. A blank experiment was carried under the same condition and parameters in order to determine the product distribution during the thermal composition of JCO in the absence of catalyst. Results showed that low hydrocarbon yield (18.1%) was achieved with high TAN value of 26.3 mgKOH/g. This indicated that the deoxygenized liquid product composed of large amount of non-deoxygenize carboxylic acid. Meanwhile, MWCNT-supported catalysts (Ni/MWCNT, Co/MWCNT and Ni-Co/MWCNT) were reactive in deoxygenation reaction, which obtained higher

hydrocarbon yield and low TAN value as compared to free catalysed system. Based on the results obtained (Figure 9.5a), it has demonstrated that Ni/MWCNT catalyst showed better catalytic activity with the yield of 82% hydrocarbons, followed by Ni-Co/MWCNT catalyst (70%) and the lowest was Co/ MWCNT catalyst (60%). Interestingly, Ni-Co/MWCNT catalyst showed the lowest TAN value of 8.4 mg KOH/g as compared to Ni/ MWCNT and Co/MWCNT catalysts (TAN value 13.9 mg KOH/g and 17.5 mg KOH/g, respectively). This indicated that Ni-Co/MWCNT is able to convert majority of acid compounds in the JCO to non-acidic compounds including hydrocarbons.

Although JCO composed mainly of 70% mixture oleic acid (C18:1) and linolenic acid (C18:2); and 20% of palmitic acid (C16:0), however, the product selectivity towards carbon distribution was different when various types of active metals were used in deoxygenation process (Figure 9.5b). Experimentally, the majority of product yielded under blank reaction (without catalyst) is C_{15}> C_8-C_9 > C_{17}. In fact, C_{15} and C_{17} is the liquid products yielded from C_{16} and C_{18}, respectively via deCOx reaction, while further secondary thermal cracking of C_{17} lead to the shorter chain of C_8-C_9 at high temperature. For Ni/MWCNT catalyst, the highest product selectivity is C_{15} (37%) and C_{11} (23%) compared to C_{17} (11%) fractions, which was due to further mild cracking at high temperature condition (Morgan et al., 2012). Ni/MWCNT was capable to produce both C_{15} and C_{17} hydrocarbon via deCOx pathway, however, further C-C cracking of C_{17} lead to the formation of C_{11}, which has reduced the yield of C_{17} and resulted in carbon chain distribution of C_{15}>C_{11}>C_{17}. In the case of Co-based catalyst, it was capable to reduce the cracking effect with the distribution of C_{15}>C_{17}>C_8-C_9, which is more selective than the blank test. By incorporation of Ni-Co into MWCNT system, the catalyst preferred deCOx pathway instead of cracking, which has succeeded to

selectively increase the content of C_{17}>C_{15}, while reduced the content of C_8-C_9 to minimum level under high temperature.

The catalytic activity and product distribution are mainly controlled by the pathway selection tendency of cracking or deCOx. Meanwhile, the synthesized catalysts (Ni/MWCNT, Co/MWCNT and NieCo/MWCNT) with different textural properties (e.g. surface area, pore volume and pore size) and acidity profile (acid density and acid strength distribution) played an important role to manipulate the deCOx and cracking pathway. As shown in the results (Table 9.2), Ni-Co/MWCNT catalysts rendered a high surface area with large pore diameter and pore volume which were suitable for large molecular feedstock reaction. Furthermore, the presence of sufficient acid density with strong acid strength of active sites preferred the deCOx pathway in deoxygenation process, which rendered high product selectivity of C_{17} and C_{15} products.

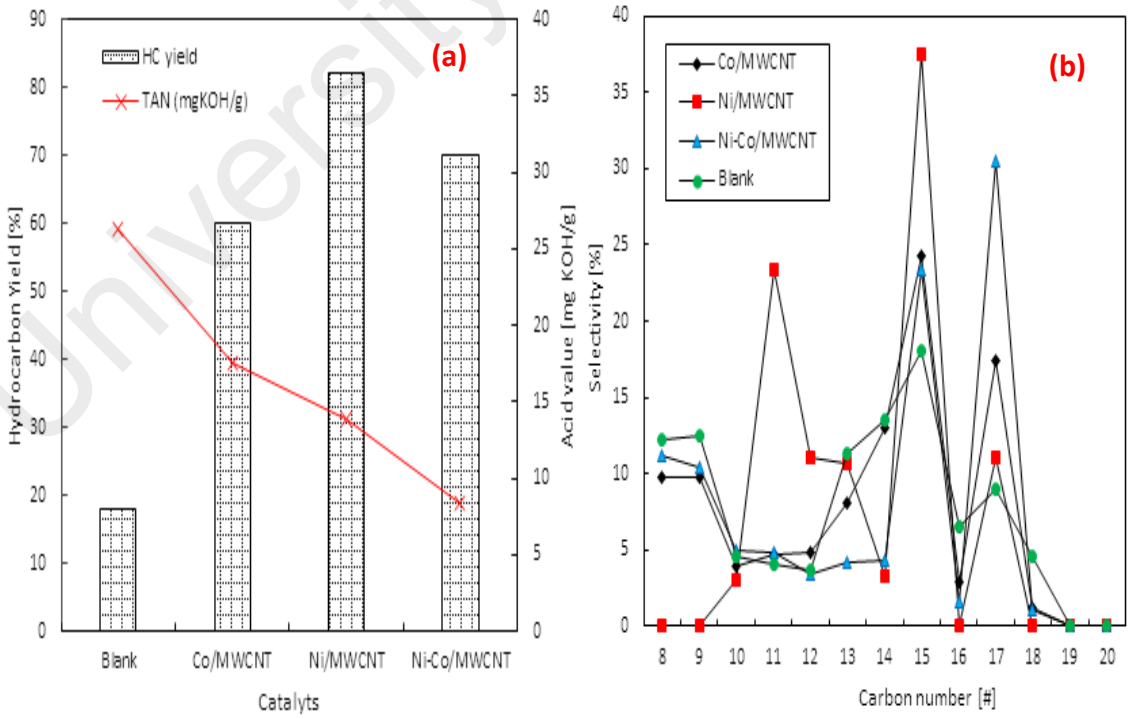

Figure 9.5: Comparison study of (a) catalytic deoxygenation and (b) hydrocarbon distribution from catalytic deoxygenation reaction of JCO by using synthesized catalysts

9.4.3 Effect of Ni content on Ni-Co/MWCNT catalysts

Based on the finding on catalytic screening of Ni/MWCNT, Co/MWCNT and Ni-Co/MWCNT, the interaction between both NiO and Co_2O_4 on the MWCNT support showed significant yield of hydrocarbon and product selectivity. Thus, different Ni content of Ni-Co/ WCNNT catalyst (5-40 wt%) was further investigated to optimize the yield and hydrocarbon products (Figure 9.6). From the results, higher hydrocarbon yield (>60%) and majority of products (C_{15},C_{17}) selectivity was produced by using series of Ni-Co/MWCNT catalysts. An increment of yield and product selectivity was observed as the Ni content was increased from 5 to 20 wt%, which maximum hydrocarbon yield at 80% with highest C_{15} and C_{17} selectivity (23%, 40%). Further increment of Ni content above 20 wt% has led to decrement in product yield and (C_{15},C_{17}) selectivity. Besides, small content of short chain (C_8-C_9) and long chain (C_{19}-C_{20}) products was found in the deoxygenation profile. Short chain of C_8-C_9 product was formed via auto-thermal cracking of C_{17} at C_8-C_9 at high temperature. While, C_{19}-C_{20} (<5%) was due to the secondary side reaction (oligomerization process), which the short chain alkene olefin (butene (C_4H_8), pentene (C_5H_{10}), and hexene (C_6H_{12}) and others) or long chain alkene (*n*-heptene (C_7H_{14}) and *n*-octene (C_8H_{16}) and others) are converted into longer carbon complex via polymerization process.

The correlation between acidity profile of Ni-Co/MWCNT with various Ni concentrations towards % of hydrocarbon yield was presented clearly in Table 9.3 and Figure 9.6. Results indicated that deCOx is the major reaction pathway instead of cracking when the Ni content increased from 5 to 20 wt.%. Low Ni content rendered highest acid density with strong acid strength (25581.84 µmol/g), which is favoured cracking pathway instead of deCox pathway, thus lead to high amount of short chain (C_8-C_9) products (Liu et al., 2012). However, further increase of Ni content to 20 wt.%

($Ni_{20}Co_{10}$/MWCNT) has reduced the acid density (9684.9 µmol/g), which turned the reaction to deCOx pathway with highest selectivity of C_{17} product. However, further increase of Ni content from 30-40 wt.% has led to decrement of acid density and generation of medium acid strength, which reduced the deoxygenation reactivity, however, the C_{17} selectivity maintained highest as compared to short chain of C_8-C_9.

Table 9.3: Correlation of deoxygenation activity towards physicochemical properties of Ni-Co/MWCNT catalyst with Ni concentration from 5 to 40 wt%

Ni conc. (%)	Hydrocarbon yield (%)	GC-FID selectivity (C_{15} + C_{17})[a]	XRD	TPD-NH_3 Acid sites ((µmol/g)[c]	
				Medium acid T = 400-499	Strong acid T = 500-799
5	66	41	12.88	-	25581.84
10	70	54	4.74	-	10475.53
20	80	60	26.22	-	9684.9
30	75	58	20.13	250.64	8469.23
40	72	54	19.43	219.88	9658.98

[a]Determined by GC-FID
[b]Measured by using Scherer equation from XRD data.
[c]Determined by TPD-NH_3 analysis.
T=Temperature(°C)

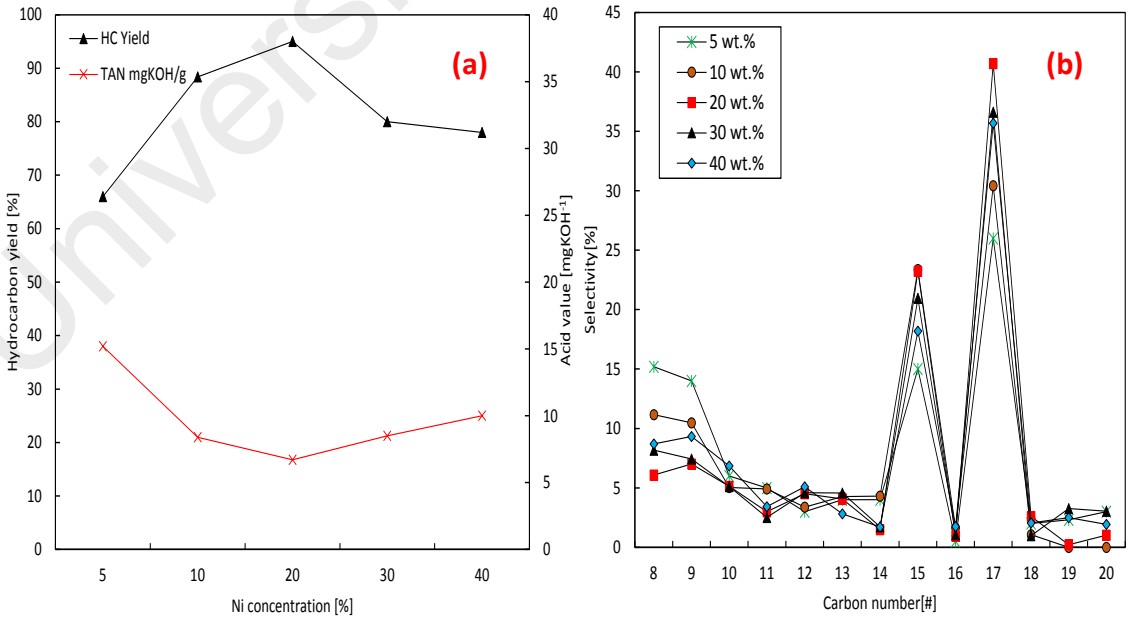

Figure 9.6: (a) Hydrocarbon yield and (b) product selectivity of deoxygenation reaction for Ni-Co/MWCNT with different Ni concentration (5-40 wt%); reaction conditions: 350 °C, 5% catalyst loading, 1 h, 10 mbar, 400 rpm.

9.4.4 Optimization studies

9.4.4.1 Effect of the catalyst loading

The effect of the $Ni_{20}Co_{10}$/MWCNT catalyst loading (1-9%) on the hydrocarbon yield and product selectivity at 350 ^{o}C, 1 h reaction time, 10 mbar reaction pressure, 400 rpm strirring rate were shown in Figure 9.7a-b. Based on the result obtained, the deoxygenation activity increased with catalyst loading within the range 1-5% (Figure 9.7a). Increasing catalyst loading has led to the increment of catalyst active sites made available for the reaction (Kwon et al., 2011) Further increasing catalyst loading to exceed 5% has resulted in reduction of hydrocarbon yield, which is due to the possibilities of parallel or secondary reactions such as polymerization. Therefore, brisk increment in polymerization at the catalyst surface means it is unhealthy for the catalyst life span as polymerization reaction has been known to be prominent for coking hydrotreating catalysts (Mortensen et al., 2011;Kwon et al., 2011). Therefore, it can be concluded that overloading of catalyst will increase the propensity of secondary reaction and parallel reaction because there are excess active site for various reaction. In the present study, optimum hydrocarbon yield (80%) was obtained with 5% loaded $Ni_{20}Co_{10}$/MWCNT catalyst. The result of deoxygenation activity is consistent with the total acid number of the liquid product. Analysis of product distribution discovered that when the catalyst loading was increased from 1 to 7%, the C_{15} and C_{17} also increased (Figure 9.7b). Based on the result obtained, 5% of catalyst loading was found to be suitable and more economical.

9.3.4.2 Effect of the reaction time

The results in Figure 9.7c-d showed the effect of reaction time on the catalytic deoxygenation reaction at 350 ^{o}C, 5% of $Ni_{20}Co_{10}$/MWCNT catalyst loading, 10 mbar reaction pressure, 400 rpm stirring rate. As the deoxygenation reaction proceed, the

amount of hydrocarbon yield were observed progressively to achieve a maximum yield of 80% within 1 h (Figure 9.7c). Yield reduction was observed after the maximum yield. The reduction might due to cracking of the already deoxygenated liquid product into lighter fractions. Similarly, the C_{15} and C_{17} selectivity increased as the reaction time prolonged to 2 h, which implied that longer reaction time is required to increasethe reaction efficiency between the reactant molecules and the catalyst surface which promote more deCOx reaction (Figure 9.7d). Therefore, after considering the hydrocarbon yield and C_{15} and C_{17} selectivity, 1 h reaction time was found to be the most efficient deCOx interval.

9.3.4.3 Effect of the temperature

To examine the effect of reaction temperature on the deoxygenation reaction, JCO deoxygenation was performed with 5% $Ni_{20}Co_{10}$/MWCNT catalyst loading, 1 h reaction time and 10 mbar reaction pressure, 400 rpm stirring rate. The effect of the reaction temperature from 330 to 400 ^{o}C on hydrocarbon yield and selectivity of ($C_{15,}C_{17}$) were shown in Figure 9.7e-f. It can be seen that as reaction temperature increases from 330-350 ^{o}C, it showed progressive increase in the proportion of hydrocarbons yield (Figure 9.7e). The high hydrocarbon yield of JCO was achieved at 350 ^{o}C reaction temperature with total hydrocarbon yield of 80% and reduced when deoxygenation temperature increased to 400 ^{o}C. The acid number was inversely proportional with the reaction temperature, which implied that more acid group detaching from JCO molecules as the deoxygenation reaction temperature increased. The hydrocarbon yield contradicted with the C_{15} and C_{17} product distribution in Figure 9.7f. It revealed that when the reaction temperature increased from 330-440 ^{o}C, the C_{15} and C_{17} selectivity was reduced. It can be inferred that deCOx reaction favours at low temperature than at high temperature. High deoxygenation temperature will enhance the

occurrence of secondary reaction which leads to formation of light product (Arend et al., 2011). It was supported by the product distribution of C_8 to C_{11} which has been increasing in its selectivity as the deoxygenation reaction temperature reached 400 ^oC. From the results obtained, 350 ^oC was selected as the optimum deoxygenation temperature after considering the yield and selectivity factors.

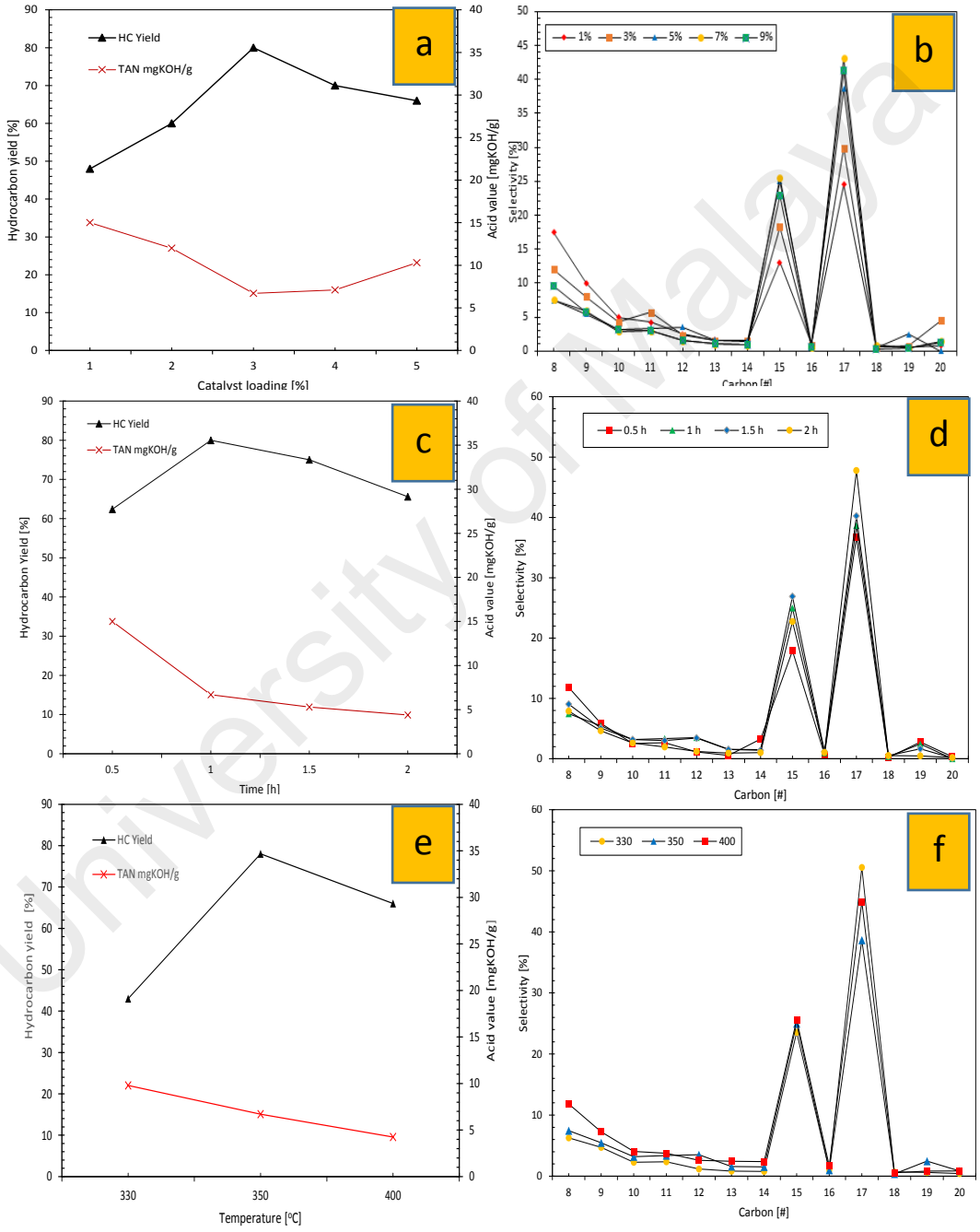

Figure 9.7: Optimization studies of JCO Optimization studies of JCO (a-b) effect of catalyst loading, reaction conditions: 350 ^oC, 1 h, (c-d) Effect of reaction time, reaction conditions: 350 ^oC, 5% catalyst amount, (e-f) Effect of reaction temperature, reaction conditions: 1 h, 5% catalyst loading, 10 mbar, 400 rpm

9.4.5 Mass balance profile for catalytic deoxygenation of JCO

A mass balance profile for deoxygenation of jatropha oil into liquid hydrocarbon product by using $Ni_{20}Co_{10}$/MWCNTcatalystwas studied under reaction condition of 350 ^{o}C, 5 wt% catalyst loading, 1 h reaction time at partial vacuum condition. Based on equation (9.4), the deoxygenation reaction of JCO will lead to the production of liquid product via deCOx with the release of CO_2 gas, CO gas and water as the by-product. The theoretical and experimental mass fraction of each compounds including JCO feedstock, liquid product, by products (CO_2 gas, CO gas,water and mixture of char & residues)was tabulated in Table 9.4. Char and residue must not form during the deoxygenation reaction which act as an indicator of an ideal reaction. However, the experiment yielded substancial solid char and residue as the by-product of deoxygenation process. Based on the results, the experimental mass faction of liquid product is 51.20 wt%, which is slightly less than theoretical value (68.90 wt% of liquid) with deviation of 17.7 wt%. The different of mass liquid balance between experimental and theoretical value might due to the formation of undesirable by-products (char + residue) which contain total of 18.47 wt% remained in the semi-batch reactor after reaction. The formation of (char þ residue) was caused by low degree volatilization of JCO during deoxygenation at high temperature (350 ^{o}C) (Vitolo et al., 1999). For the gaseous mass balance, catalytic deoxygenation of JCO released approximately 24.83 wt% of volatile matter, which is comparable with theoretical value. The mass balance of the water was significantly lesser (5.47 wt%) than theoretical, as it is easily to vaporised into gas during high temperature deoxygenation reaction. The mass balance profile suggested $Ni_{20}Co_{10}$/MWCNT catalyst is capable of performing actively and selectively for deoxygenation of JCO with sufficient product yield (5.16 g) as predicted in theoretical calculation.

Table 9.4: Mass balance profile of catalytic deoxygenation of JCO

Equation 9.4 :	**JCO ⟶ Liquid (aq) + 3mol CO_2/CO (g) + 3mol H_2O (aq) + By product**								
Reaction	Feedstock	Liq-product[b]		Gas[c]		Water[d]		Char + residue[e]	
	(g)	(g)	(wt.%)	(g)	(wt.%)	(g)	(wt.%)	(g)	(wt.%)
Theoritical data	10.00	6.89	68.90	2.49	24.90	0.62	6.20	-	-
Experimental 1	10.01	5.20	51.94	2.57	25.67	0.41	4.09	1.83	18.28
Experimental 2	10.15	5.18	51.03	2.26	22.26	0.74	7.29	1.97	19.40
Experimental 3	10.09	5.11	50.64	2.68	26.56	0.51	5.05	1.79	17.74
Average experimental :		5.16	51.20	2.50	24.83	0.55	5.47	1.86	18.47

[a]Deoxygenation condition : reaction temperature of 350 °C, 1 h reaction time, 5% of catalyst, 10 mbar pressure and stirring 400 ppm.
[b]Mass fraction for Liq-product = [(mass of Liq-product/mass of feedstock)x 100]
[c]Material fraction for gas (G) = [(mass of feedstock – mass of Liq-product- mass of (char+residue)- mass of water)/ mass of feedstock x100]
[d]Material fraction for water (G) = [(mass of water/ mass of feedstock x100]
[e]Material fraction for (char+residue) (Y) = [mass of (char+residue)/mass of feedstock)x 100)]

9.4.6 Reaction pathways for deoxygenation of high FFA jatropha oil

The reaction mechanism of converting high FFA triacylglycerides of into hydrocarbons under free hydrogen condition over metal-based catalyst has been discussed by several studies (Kaewmeesri et al., 2015; Hermida et al., 2015). Based on Table 9.1, JCO composed mainly ~ 20 % of C_{16} (palmitic acid), ~ 70 % of C_{18} (stearic acid, oleic acid, linoenic acid) and 15.4% of FFA with carbon number of C_{16} or C_{18}. The triacylglycerides and the FFAs can be converted to distillate-range hydrocarbons via catalyzed deoxygenation reaction. With reference to the reaction scheme in Figure 9.8, the triacylglycerides in JCO will initially decompose into its fatty acids by cleavage of C-O bonding via self-hydrolysis of the ester (reaction 9.8a). Subsequently, all fatty acid intermediates including FFAs present in the JCO (C_{16} and C_{18}) tends to form n-pentadecanes (saturated; $C_{15}H_{32}$), *n*-heptadecanes (saturated; $C_{17}H_{36}$) and n-heptadecenes (mono-unsaturated; $C_{17}H_{34}$, di-unsaturated; $C_{17}H_{32}$) via decarboxylation reaction, which leads to the oxygen removal in the form of CO_2 gas as by products (reaction 9.8b). Meanwhile, decarbonylation reaction is resulted in formation of n-pentadecenes and n-heptadecenes with extra double bond as different from decarboxylated products, which formed mono-unsaturated ($C_{15}H_{30}$, $C_{17}H_{34}$), di-unsaturated ($C_{17}H_{32}$) and poly-unsaturated ($C_{17}H_{28}$) (reaction 9.8c). The deoxygenated liquid product also significantly formed light fraction hydrocarbons (C_8-C_9) via C-C scission of product (Bezergianni et al., 2009) (reaction 9.8d). Moreover, the cracking reaction of fatty acid intermediates (reaction 9.8e) may also occur leading to the production of shorter chain of fatty acids and shorter hydrocarbon fractions. The short fatty acid was further deoxygenated via decarboxylation (reaction 9.8f) and decarbonylation reaction (reaction 9.8g) into hydrocarbon products.

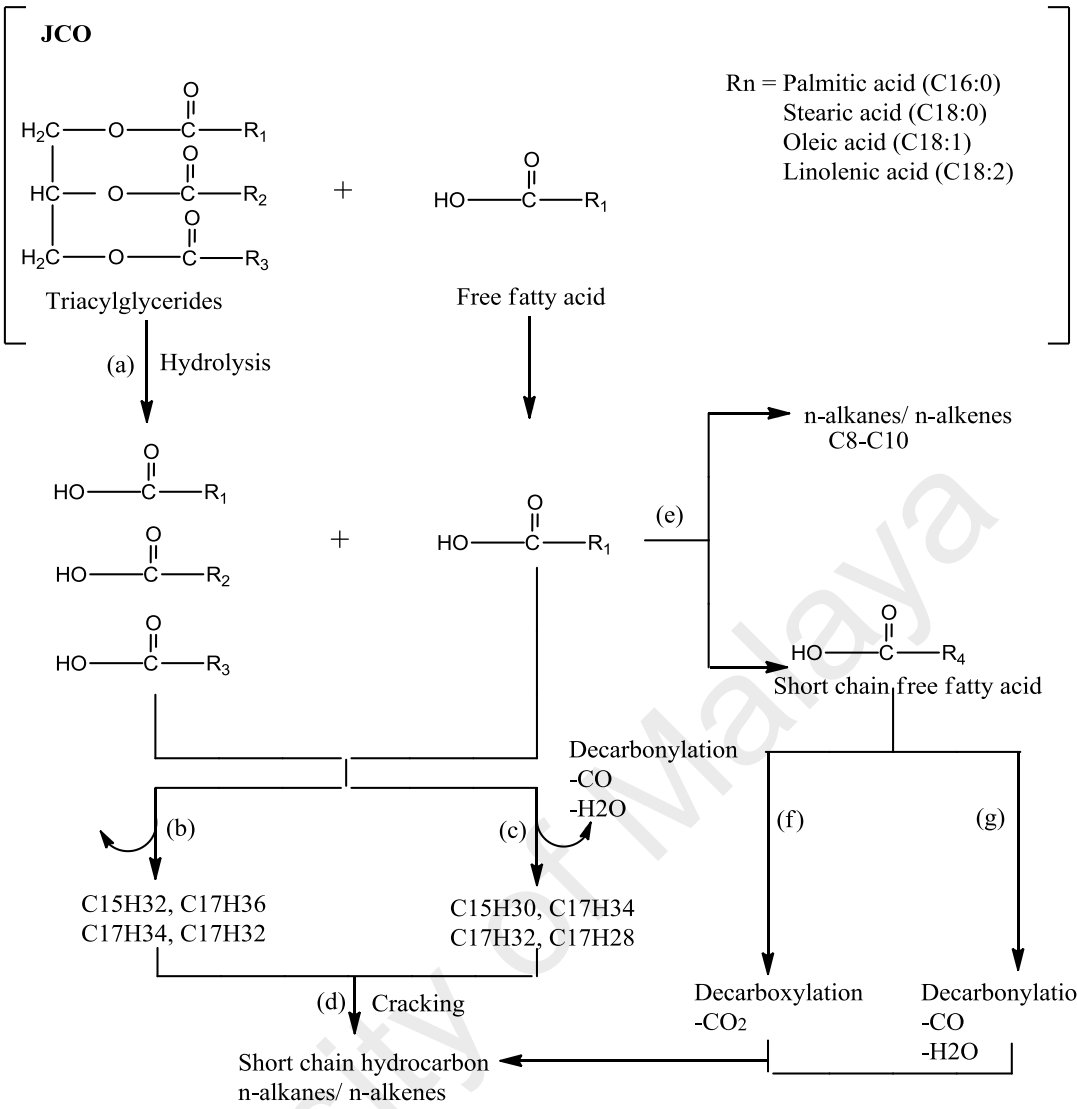

Figure 9.8: Proposed deoxygenation reaction pathway for the conversion of JCO to hydrocarbon over $Ni_{20}Co_{10}$/MWCNT catalysts

9.4.7 Reusability profile for $Ni_{20}Co_{10}$/MWCNT catalyst

The reusability profile of $Ni_{20}Co_{10}$/MWCNT catalyst was investigated via deoxygenation reaction at the conditions of 10 g JCO, 350 ^{o}C, 10 mbar, 5% catalyst loading within 1 h reaction. Results showed that $Ni_{20}Co_{10}$/MWCNT catalyst performed steadily for four consecutive runs by maintaining hydrocarbon yield at >70% with > 60% selectivity of C_{15} and C_{17} products (Table 9.5). This indicated that the $Ni_{20}Co_{10}$/MWCNT catalyst is capable of performing outstanding mechanical properties and chemical stability, which was highly resistance to heat, carbon monoxide and water. Furthermore, elemental study indicated that negligible amount of leached Ni^{2+} and Co^{4+}

species from $Ni_{20}Co_{10}$/MWCNT catalyst during each reaction (Table 9.5). The comparison of the amount of the Ni^{2+} and Co^{4+} in the liquid product using fresh and fifth-round catalyst gradually increased from 0.038 to 0.061 mg L^{-1} and 0.001 to 0.012 mg L^{-1}, respectively. Hence, the loss of the deoxygenation activity is primarily due to the dissolution of the active metal and deposition of the organic compounds on the active sites of catalyst. Furthermore, the leaching level is within the maximum range of EN 12662 Standard Specification for Diesel Fuel Oils contamination content (24 mg L^{-1}) (John Bacha et al., 2007), which confirmed that $Ni_{20}Co_{10}$/MWCNT catalyst showed high leaching resistance and revealing good stability.

Table 9.5: Reusability and metal leaching study for $Ni_{20}Co_{10}$/MWCNT catalyst

Number of run[a]	Hydrocarbon yield (%)	Selectivity C_{15+} C_{17} (%)	Ni (mg L^{-1})[b]	Co (mg L^{-1})[b]
1st run (Fresh catalyst)	80	64	0.038±0.0005	0.001±0.0009
2nd run	78	63	0.039±0.0002	0.005±0.0013
3rd run	77	61	0.041±0.0006	0.007±0.0009
4th run	76	60	0.051±0.0004	0.009±0.0007
5th run	60	50	0.064±0.0003	0.012±0.0006

[a]Deoxygenation condition : reaction temperature of 350 °C, 1 h reaction time, 5% of catalyst, 10 mbar pressure and stirring 400ppm.
[b]Ni and Co concentration in the liquid product were determined by ICP analysis.

Metal dispersion states and chemical composition study for $Ni_{20}Co_{10}$/MWCNT catalyst (fresh, reactivated catalysts) were determined by XRD and TGA analysis (Figure 9.9). Experimentally, spent catalyst was reactivated by two methods: (i) hexane washing (ii) hexane washing followed by thermal activation under inert condition at 400 °C for 2 h. XRD analysis showed that the reactivated catalysts from both methods rendered similar pattens with higher crystallinity at $2\theta = 26.12^{o}$, 44.40^{o}, 51.73^{o} and 76.13^{o}, which attributed to crystallographic planes of MWCNT. In additional, the increase of crystallite sizes for reactivated catalyst was due to exposure to high temperature, which led to the growth of particles into cluster form.

TGA analysis was performed to examine the extent of coke formation during the deoxygenation of JCO with $Ni_{20}Co_{10}$/MWCNT catalyst. Results showed that decomposition peak at temperature range from 400 to 650 ^{o}C is attributed to the the oxidation of the MWCNT nanorode (Mahajan et al., 2013). The initial decomposition temperature for fresh and reactivated catalysts was similar, however, the final decomposition temperature for reactivated catalyst was significantly higher >760 ^{o}C. Furthermore, weight loss for reactivated catalyst is 4 to 5% than that of fresh catalyst, which was due to oxidation of coke in the air.

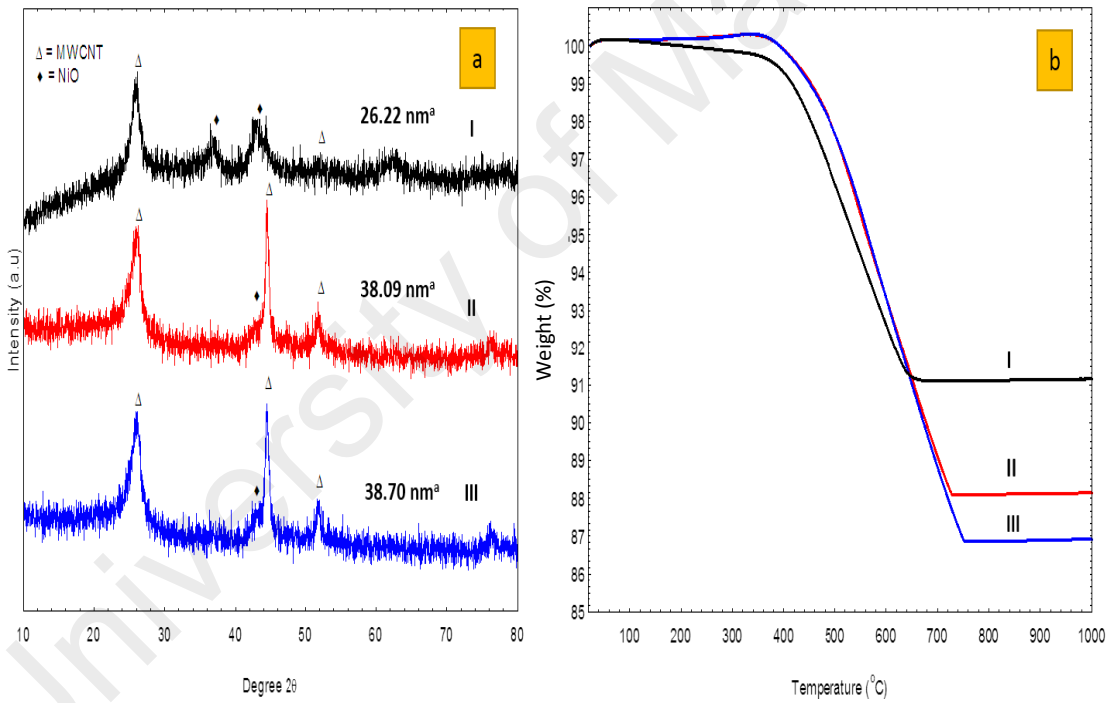

Figure 9.9: (a) XRD diffraction profile (b) TGA profiles for fresh, hexane reactivated and thermal reactivated spent $Ni_{20}Co_{10}$/MWCNT catalyst ([a]Measured by using Scherer equation from XRD data)

The hexane reactivated catalyst showed 1% extra weight loss than thermal reactivated catalyst, which can be suggested thermal treatment was able to remove certain carbonaceous compound on the spent catalyst. The coke is categorized as hard coke which decomposed completely at the temperature of 760 ^{o}C (Sahoo et al., 2004).

The coke deposition will accumulate on the catalyst surface, which covers the active site on the catalyst and reduce the catalytic deoxygenation activity. However, by evaluating the weight loss difference between fresh and reactivated catalyst, it can be considered small, insignificant difference; thus giving insignificant effect on the deoxygenation reaction activity. This result strongly suggested that NiO and Co_2O_4 supported MWCNT catalyst has showed excellent resistance to coking. From the XRD and TGA analysis results, both demonstrated similar physicochemical properties which strongly indicated that the thermal reactivation is not necessary in order to reactivate the spent $Ni_{20}Co_{10}$/MWCNT catalyst from coke contamination. Subsequently, $Ni_{20}Co_{10}$/MWCNT is expecteced to have a promising potential to be reused as its original spent catalyst. Therefore, it would save more energy and time during catalyst reactivation.

9.5 Conclusion

In the present work, an effective approach was disclosed for converting the non-edible JCO to desired hydrocarbon fractions by selectively cleaving C-O bond over MWCNT-supported Ni-Co catalyst. The present Ni-Co/MWCNT catalysed deoxygenation pathway is capable of rendering high selectivity of the hydrocarbon product of C_{15} and C_{17} fractions. It is due to the presence of synergic effect between active acidic promoter (Ni-Co), high surface area and pore diameter that contributed by MWCNT support, which has rendered active sites for bulky triglyceride for reaction. The optimum content for mixed metal oxide (Ni-Co) system was 20:10 (wt.%) for Ni:Co, which enhanced the product formation (C_{15} + C_{17}) to 64%. Furthermore, $Ni_{20}Co_{10}$/MWCNT catalyst is capable of maintaining four consecutive runs with consistent hydrocarbon yield (>76%) and C_{15} + C_{17} selectivity (>60%)

CHAPTER 10: CONCLUSION

Finally, this chapter summarizes the overall research findings from all the studies with their respective implications. The chapter also offers recommendations for future research. Nano-sized Ca-based catalyst with excellent physicochemical properties was successfully synthesized via sono-assisted wet surfactant method. This implies the collapse of the cavitational bubbles generated during sonication has caused great impact on the change of textural and chemical properties of the catalyst. Nano-sized Ca-based catalysts have been proven for being able to improve deoxygenation activity significantly than micron sized Ca-based catalyst. This has suggested that textural properties of catalyst played an important role in the enhancement of deoxygenation activity. In addition, Ca-based catalyst was also found to catalytically active in deoxygenization of the triglycerides via cracking-deCOx reaction for gasoline-range *n*-(C_8-C_{12}) green fuel production. Ca-based catalyst is an alternative catalyst for the production of gasoline-range production via C-C cleavage under partial vacuum condition. However, the inhibition of C-C cleavage has occurred when the reaction system were proceeded under continuous inert N_2 flow. Deoxygenation of triglycerides via C-O cleavage through deCOx reaction under inert N_2 flow are found to be more reactive than in partial vacuum condition as the continuous N_2 flow has prevented CO_2/CO gases produced by the deCOx reaction from poisoning the catalyst active sites. Moreover, the utilization of binary oxide consisted acid-base properties derived TMOs (NiO, ZnO, Fe_2O_3, Co_2O4 and WO_3) doped CaO has the potential of reducing the challenges associated with pure basic catalyst. NiO and Co_2O_4 were found to be the most effective metals promoter for CaO support in optimizing the deoxygenation activity. Although Ca-based catalyst is found to be effective in deoxygenizing the triglycerides, but Ca-based catalyst tends to get deactivated due to the absorption of the

CO_2/CO gas from acid compound during deCOx reaction and results in formation of inactive carbonate phase. The use of mesoporous support for TMOs (NiO, Co_3O_4) and CaO promoter offers alternative solution from catalyst alteration phase as the synergistic effect from bifunctional support catalyst has enhanced the stability of the catalyst and improved the deoxygenation activity. The deCOx reaction solely depends on the richness of mildly acidity sites of the catalyst, while C-C cleavage via cracking activity was found to have enhanced with catalyst carrying high strength basic and acid sites. Among the synthesized catalyst (Table 10.1), NiO-5CaO/SiO_2-Al_2O_3 is the most effective catalyst in deoxygenation of triglycerides over deCOx reaction which has yielded 92% hydrocarbon fractions within the range of *n*-(C_8-C_{20}) and product selectively toward *n*-C_{15}+*n*-C_{17} is 61%. Although 10 wt.%Co_3O_4-CaO/SiO_2-Al_2O_3 has shown the highest formation of mild acidic sites (6690.51 µmol/g) on the catalyst but the deoxygenation activity was found lesser than reaction catalyzed by NiO-5CaO/SiO_2-Al_2O_3 (3005.7 µmol/g). This implies that the richness of the high-strength acidity sites on 10 wt.% Co_3O_4-CaO/SiO_2-Al_2O_3 catalyst has promoted C-C cleavage rather than C-O cleavage. The reusability studies has shown that the gradual reduction of hydrocarbon yield and deCOx product selectivity in each run is mainly due to the formation of coke deposit on the catalyst surface after reaction. Moreover, coke formation was found to be prominent with the use of higher content unsaturated alkyl fatty acid chains and FFA acid feedstock. Coke formation was successfully inhibited by the utilization of basic metal with acidic metal sites in the process and it is also worth to mention that the utilization of carbon-based catalyst is also an effective approach to reduce coke formation. Overall, deoxygenation by the present catalysts are highly effective in producing a clean and high quality of green diesel with less oxygenated species.

Table 10.1: Summary of the different catalysts and their respective performances

Type	Catalyst	Feed	Reaction condition	Hydrocarbon yield [%]	DeCOx selectivity [%]
Acid catalyst	Ni-Co/MWCNT	JCO	5 wt.% catalyst loading, 60 min, 350 ^{o}C under partial vacuum condition	80	64
Acid-base catalyst	10 wt.% Co_3O_4-CaO /SiO_2-Al_2O_3	Triolein Ceiba oil Sterculia oil	5 wt.% catalyst loading, 60 min, 350 ^{o}C under inert N_2 flow condition	73 77 80	43 25 10
	NiO-5CaO/SiO_2-Al_2O_3	Triolein	7 wt.% catalyst loading, 60 min, 340 ^{o}C under partial vacuum condition	74	56
	NiO-5CaO/SiO_2-Al_2O_3	Triolein JCO PFAD WCO	7 wt.% catalyst loading, 60 min, 350 ^{o}C under inert N_2 flow condition	92 74 81 86	61 74 73 53
	Co-CaO W-CaO	Triolein	5 wt.% catalyst loading, 60 min, 350 ^{o}C under partial vacuum condition	32 23	< 25 <40
	Ni-CaO Co-CaO Zn-CaO Fe-CaO	Triolein	5 wt.% catalyst loading, 60 min, 350 ^{o}C under inert N_2 flow condition	54 52 51 44	48 41 28 38
Base catalyst	Nano-$Ca(OH)_2$	Triolein	5 wt.% catalyst loading, 45 min, 350 ^{o}C under partial vacuum condition	47	<11
	CaO	Triolein		35	5

10.1 Recommendations for future works

Though this work has articulately reported a compelling advancement of knowledge on the performance of deCOx reaction via observation of product distribution analyzed by GC-FID and GC-MS, it is nonetheless imperative to pre-empt inevitable critiques on some recommendations worthy of further investigation. These include:

I. Utilization of gas chromatography thermal conducting detector (GC-TCD) online gas analysis to observe the type of gases released during the reaction.

II. Study of turn over frequency (TOF) calculations for base and acid-base catalysts in deoxygenation reaction.

III. Integration of HDO reaction system is necessary as this system in order to enhance the production of saturated hydrocarbon via hydrogenation mechanism.

IV. Study the fuel properties (flash point, viscosity test, cloud point, poor point) of the pure green gasoline and green diesel liquid product.

V. Further studies on improving the fuel properties of the catalyst by enhancing the present of large isomer compound in the green fuel.

Future studies will undoubtedly lead to a better understanding of deoxygenation reaction via deCOx reaction and improve the production of high quality green fuel.

REFERENCES

Aasberg-Petersen, K., Nielsen, C. S., Dybkjær, I., & Perregaard, J. (2008). Large scale methanol production from natural gas. *Haldor Topsoe*, 22.

Aatola, H., Larmi, M., Sarjovaara, T., & Mikkonen, S. (2008). Hydrotreated Vegetable Oil (HVO) as a Renewable Diesel Fuel: Trade-off between NOx, Particulate Emission, and Fuel Consumption of a Heavy Duty Engine. *SAE Technical Papers*, (724), 12.

Abdulkareem-Alsultan, G., Asikin-Mijan, N., Lee, H. V., & Taufiq-Yap, Y. H. (2016a). A new route for the synthesis of La-Ca oxide supported on nano activated carbon via vacuum impregnation method for one pot esterification- transesterification reaction. *Chemical Engineering Journal*, *304*, 61–71.

Abdulkareem-Alsultan, G., Asikin-Mijan, N., & Taufiq-Yap, Y. H. (2016b). Effective Catalytic Deoxygenation of Waste Cooking Oil over Nanorods Activated Carbon Supported CaO. *Key Engineering Materials*, *707*, 175–181.

Abelló, S., Medina, F., Tichit, D., Pérez-Ramírez, J., Groen, J. C., Sueiras, J. E., & Cesteros, Y. (2005). Aldol condensations over reconstructed Mg-Al hydrotalcites: Structure-activity relationships related to the rehydration method. *Chemistry - A European Journal*, *11*(2), 728–739.

Absi-Halabi, M., Stanislaus, a., & Trimm, D. L. (1991). Coke formation on catalysts during the hydroprocessing of heavy oils. *Applied Catalysis*, *72*(2), 193–215.

Ahmad, J., Yusup, S., Bokhari, A., & Kamil, R. N. M. (2014). Study of fuel properties of rubber seed oil based biodiesel. *Energy Conversion and Management*, *78*, 266–275.

Ahmed, S., Hassan, M. H., Kalam, M. A., Ashrafur Rahman, S. M., Abedin, M. J., & Shahir, A. (2014). An experimental investigation of biodiesel production, characterization, engine performance, emission and noise of Brassica juncea methyl ester and its blends. *Journal of Cleaner Production*, *79*, 74–81.

Akalework, N. G., Pan, C.-J., Su, W.-N., Rick, J., Tsai, M.-C., Lee, J.-F., & Hwang, B.-J. (2012). Ultrathin TiO_2-coated MWCNTs with excellent conductivity and SMSI nature as Pt catalyst support for oxygen reduction reaction in PEMFCs. *Journal of Materials Chemistry*, *22*(39), 20977.

Akgsornpeak, A., Witoon, T., Mungcharoen, T., & Limtrakul, J. (2014). Development of synthetic CaO sorbents via CTAB-assisted sol-gel method for CO_2 capture at high temperature. *Chemical Engineering Journal*, *237*, 189–198.

Alavi, M. A., & Morsali, A. (2010). Ultrasonic-assisted synthesis of $Ca(OH)_2$ and CaO nanostructures. *Journal of Experimental Nanoscience*, *5*(2), 93–105.

Al-Hamamre, Z., & Al-Salaymeh, A. (2014). Physical properties of (jojoba oil+biodiesel), (jojoba oil+diesel) and (biodiesel+diesel) blends. *Fuel*, *123*, 175–188.

Al-Sabawi, M., Chen, J., & Ng, S. (2012). Fluid catalytic cracking of biomass-derived oils and their blends with petroleum feedstocks: A review. *Energy and Fuels*, *26*(9), 5355–5372.

Dos Anjos, J. S.; De Araujo Gonzalez, W.; Lam, Y. L. & Frety, R (1983). Catalytic Decomposition of Vegetable Oil. *Applied Catalysis*, *5*, 299–308.

Arend, M., Nonnen, T., Hoelderich, W. F., Fischer, J., & Groos, J. (2011). Catalytic deoxygenation of oleic acid in continuous gas flow for the production of diesel-like hydrocarbons. *Applied Catalysis A: General*, *399*(1-2), 198–204.

Arun, N., Sharma, R. V, & Dalai, A. K. (2015). Green diesel synthesis by hydrodeoxygenation of bio-based feedstocks : Strategies for catalyst design and development. *Renewable and Sustainable Energy Reviews*, *48*, 240–255.

Asikin-Mijan, N.; Lee, H. V., Y.H., Taufiq-Yap, Juan, J. C. & Rahman, N.A. (2015a) Pyrolytic-Deoxygenation of Triglyceride via Natural Waste Shell Derived $Ca(OH)_2$ Nanocatalyst. *Journal Analytical Applied Pyrolysis*, *117*, 46–55.

Asikin-Mijan, N., Lee, H. V. & Taufiq-Yap, Y. H.(2015b) Synthesis and Catalytic Activity of Hydration–dehydration Treated Clamshell Derived CaO for Biodiesel Production. *Chemistry Engineering Research Design*, *102*, 368–377.

Asikin-Mijan, N., Taufiq-Yap, Y. H., & Lee, H. V. (2015c) Synthesis of Clamshell Derived $Ca(OH)_2$ Nano-Particles via Simple Surfactant-Hydration Treatment. *Chemical Engineering Journal, 262*, 1043–1051.

Asikin-Mijan, N., Lee, H. V.,Taufiq-Yap, Y. H., Abdulkrem-Alsultan, G., Mastuli, M. S., & Ong, H. C. (2016a) Optimization Study of SiO_2-Al_2O_3 Supported Bifunctional Acid-Base NiO-CaO for Renewable Fuel Production Using Response Surface Methodology. *Energy Conversion Management, 141(1),*325-338.

Asikin-Mijan, N., Lee, H. V.,Taufiq-Yap, Y. H., Abdulkrem-Alsultan, G., Mastuli, M. S., & Ong, H. C. (2016b) Optimization Study of SiO_2-Al_2O_3 Supported Bifunctional Acid-Base NiO-CaO for Renewable Fuel Production Using Response Surface Methodology. *Energy Conversion Management,141(1)*,325-338.

Asikin-mijan, N., Lee, H. V, Abdulkareem-alsultan, G.,Afandi, A. & Taufiq-Yap, Y. H (2016c). Production of Green Diesel via Cleaner Catalytic Deoxygenation of Jatropha Curcas Oil. *Journal Cleaner Production*, 1–12.

Asikin-Mijan, N., Lee, H. V.,Juan, J. C., Noorsaadah, A. R., Abdulkareem-Alsultan, G., Arumugam, M. & Taufiq-Yap, Y. H. (2016d) Waste Clamshell-Derived CaO Supported Co and W Catalysts for Renewable Fuels Production Via Cracking-Deoxygenation of Triolein. *Journal Analytical Applied Pyrolysis*, 120, 110–120.

Asikin-Mijan, N., Lee, H. V., Juan, J. C., Noorsaadah, A. R., Abdulkareem-Alsultan, G.; Arumugam, M. & Taufiq-Yap, Y. H.(2016e) Waste Clamshell-Derived CaO Supported Co and W Catalysts for Renewable Fuels Production via Cracking-Deoxygenation of Triolein. *Journal Analytical Applied Pyrolysis*, 120.

Asikin-Mijan, N. , Lee, H. V., Alsultan, G. A., & Taufiq-Yap, Y.H. (2016). Synthesis and Characterization of Silica-Alumina Supported Ca and Ni Catalyst for Deoxygenation of Vegetable oil into Diesel. *Materials Science Forum*, *840*, 353–358.

Asikin-Mijan, N., Lee, H.V., Juan, J.C., Noorsaadah, A.R. & Taufiq-Yap, Y.H. (2017). Catalytic Deoxygenation of Triglycerides to Green Diesel over Modified CaO-Based Catalysts. *RSC Adv.* 7(73):46445–60.

Asomaning, J., Mussone, P., & Bressler, D. C. (2014). Thermal deoxygenation and pyrolysis of oleic acid. *Journal of Analytical and Applied Pyrolysis*, *105*, 1–7.

Avhad, M. R., & Marchetti, J. M. (2015). A review on recent advancement in catalytic materials for biodiesel production. *Renewable and Sustainable Energy Reviews*, *50*, 696–718.

Ayodele, O. B., Abbas, H. F., & Daud, W. M. A. W. (2014a). Catalytic upgrading of oleic acid into biofuel using Mo modified zeolite supported Ni oxalate catalyst functionalized with fluoride ion. *Energy Conversion and Management*, *88*, 1111–1119.

Ayodele, O. B., Togunwa, O. S., Abbas, H. F., & Daud, W. M. A. W. (2014b). Preparation and characterization of alumina supported nickel-oxalate catalyst for the

hydrodeoxygenation of oleic acid into normal and iso-octadecane biofuel. *Energy Conversion and Management*.

Aziz, M. A.A., Jalil, A. A., Triwahyono, S., & Ahmad, A. (2015). CO_2 methanation over heterogeneous catalysts: recent progress and future prospects. *Green Chem.*, *17*(5), 2647–2663.

Bacha, J., Freel, J., Gibbs, A., Gibbs, L., Hemighaus, G., Hoekman, K., & Mills, J. (2007). Diesel Fuels Technical Review. *Chevron Global Marketing*, 1–116.

Barrón C., A. E., Melo-Banda, J. A., Dominguez E., J. M., Hernández M., E., Silva R., R., Reyes T., a. I., & Meraz M., M. a. (2011). Catalytic hydrocracking of vegetable oil for agrofuels production using Ni-Mo, Ni-W, Pt and TFA catalysts supported on SBA-15. *Catalysis Today*, *166*(1), 102–110.

Baş, D., & Boyacı, İ. H. (2007). Modeling and optimization I: Usability of response surface methodology. *Journal of Food Engineering*, *78*(3), 836–845.

Benson, T. J., Hernandez, R., French, W. T., Alley, E. G., & Holmes, W. E. (2009). Elucidation of the catalytic cracking pathway for unsaturated mono-, di-, and triacylglycerides on solid acid catalysts. *Journal of Molecular Catalysis A: Chemical*, *303*(1-2), 117–123.

Berenblyum, A. S., Podoplelova, T. A., Shamsiev, R. S., Katsman, E. A., & Danyushevsky, V.Y. (2011). On the mechanism of catalytic conversion of fatty acids into hydrocarbons in the presence of palladium catalysts on alumina. *Petroleum Chemistry*, *51*(5), 336–341.

Bernas, H., Eränen, K., Simakova, I., Leino, A. R., Kordás, K., Myllyoja, J., & Murzin, D. Y. (2010). Deoxygenation of dodecanoic acid under inert atmosphere. *Fuel*, *89*(8), 2033–2039.

Bezergianni, S., Voutetakis, S., & Kalogianni, A. (2009). Catalytic hydrocracking of fresh and used cooking oil. *Industrial and Engineering Chemistry Research*, *48*(18), 8402–8406.

Bezerra, M. A., Santelli, R. E., Oliveira, E. P., Villar, L. S., & Escaleira, L. A. (2008). Response surface methodology (RSM) as a tool for optimization in analytical chemistry. *Talanta*, *76*(5), 965–977.

Botas, J. A., Serrano, D. P., García, A., & Ramos, R. (2014). Catalytic conversion of rapeseed oil for the production of raw chemicals, fuels and carbon nanotubes over

Ni-modified nanocrystalline and hierarchical ZSM-5. *Applied Catalysis B: Environmental*, *145*, 205–215.

Botas, J. A., Serrano, D. P., García, A., De Vicente, J., & Ramos, R. (2012). Catalytic conversion of rapeseed oil into raw chemicals and fuels over Ni- and Mo-modified nanocrystalline ZSM-5 zeolite. *Catalysis Today*, *195*(1), 59–70.

Boullosa-Eiras, S., Lødeng, R., Bergem, H., Stöcker, M., Hannevold, L., & Blekkan, E. A. (2014). Catalytic hydrodeoxygenation (HDO) of phenol over supported molybdenum carbide, nitride, phosphide and oxide catalysts. *Catalysis Today*, *223*, 44–53.

Bui, V. N., Laurenti, D., Afanasiev, P., & Geantet, C. (2011). Hydrodeoxygenation of guaiacol with CoMo catalysts. Part I: Promoting effect of cobalt on HDO selectivity and activity. *Applied Catalysis B: Environmental*, *101*(3-4), 239–245.

BP Statistical Review of World Energy. (n.d.). http://doi.org/10.2307/3324639

Calemma, V., Peratello, S., & Perego, C. (2000). Hydroisomerization and hydrocracking of long chain n-alkanes on Pt/amorphous SiO_2-Al_2O_3 catalyst. *Applied Catalysis A: General*, *190*(1-2), 207–218.

Castaño, P., Pawelec, B., Fierro, J. L. G., Arandes, J. M., & Bilbao, J. (2007). Enhancement of pyrolysis gasoline hydrogenation over Pd-promoted Ni/SiO_2-Al_2O_3 catalysts. *Fuel*, *86*(15), 2262–2274.

Centeno, A., Laurent, E., & Delmon, B. (1995). Influence of the Support of CoMo Sulfide Catalysts and of the Addition of Potassium and Platinum on the Catalytic Performances for the Hydrodeoxygenation of Carbonyl, Carboxyl, and Guaiacol-Type Molecules. *Journal of Catalysis*.

Chandra Mouli, K., Soni, K., Dalai, A., & Adjaye, J. (2011). Effect of pore diameter of Ni-Mo/Al-SBA-15 catalysts on the hydrotreating of heavy gas oil. *Applied Catalysis A: General*, *404*(1-2), 21–29.

Chang, J.-S., Cheng, J.-C., Ling, T.-R., Chern, J.-M., Wang, G.-B., Chou, T.-C., & Kuo, C.-T. (2016). Low acid value bio-gasoline and bio-diesel made from waste cooking oils using a fast pyrolysis process. *Journal of the Taiwan Institute of Chemical Engineers*, *0*, 1–11.

Chen, J., Shi, H., Li, L., & Li, K. (2014a). Environmental Deoxygenation of methyl laurate as a model compound to hydrocarbons on transition metal phosphide catalysts. *Applied Catalysis B*, *144*, 870–884.

Chen, J., Yang, Y., Shi, H., Li, M., Chu, Y., Pan, Z., & Yu, X. (2014b). Regulating product distribution in deoxygenation of methyl laurate on silica-supported Ni-Mo phosphides: Effect of Ni/Mo ratio. *Fuel*, *129*, 1–10.

Chen, L., Zhu, Y., Zheng, H., Zhang, C., & Li, Y. (2012). Aqueous-phase hydrodeoxygenation of propanoic acid over the Ru/ZrO_2 and $Ru–Mo/ZrO_2$ catalysts. *Applied Catalysis A: General*, *411-412*, 95–104.

Chen, N., Gong, S., Shirai, H., Watanabe, T., & Qian, E. W. (2013). Effects of Si/Al ratio and Pt loading on Pt/SAPO-11 catalysts in hydroconversion of Jatropha oil. *Applied Catalysis A: General*, *466*, 105–115.

Cheryl-Low, Y. L., Theam, K. L., & Lee, H. V. (2015). Alginate-derived solid acid catalyst for esterification of low-cost palm fatty acid distillate. *Energy Conversion and Management*, *106*, 932–940.

Chiam, L. T., & Tye, C. T. (2013). Deoxygenation of plant fatty acid using $NiSnK/SiO_2$-Al_2O_3 as catalyst. *The Malaysian Journal of Analytical Sciences*, *17*(1), 129–138.

.Colchester, M., Chao, S., Dallinger, J., Sokhannaro, H. E. ., Vo Thai, D., & Villanueva, J. (2011). *Oil Palm Expansion in South East Asia: Trends and implications for local communities and indigenous peoples*.

Di Cosimo, J. I. & Apesteguía, C. R. (1998). Study of the Catalyst Deactivation in the Base-Catalyzed Oligomerization of Acetone. *Journal Molecular Catalysis A Chemistry*. *130* (1-2), 177–185.

Crossley, A., Heyes, T. D., & Hudson, B. J. F. (1962). The effect of heat on pure triglycerides. *Journal of the American Oil Chemists Society*, *39*(1), 9–14.

Danuthai, T., Sooknoi, T., Jongpatiwut, S., Rirksomboon, T., Osuwan, S., & Resasco, D. E. (2011). Effect of extra-framework cesium on the deoxygenation of methylester over CsNaX zeolites. *Applied Catalysis A: General*, *409-410*, 74–81.

Dawes, G.J.S., Scott, E. L., Le Notre, J., Sanders, J. P. M., & Bitter, J. H. (2015). Deoxygenation of biobased molecules by decarboxylation and decarbonylation - a review on the role of heterogeneous and homogeneous bio-catalysis. *Green Chem.*, 17, 3231-3250.

De, S., & Luque, R. (2014). Upgrading of Waste Oils into Transportation Fuels Using Hydrotreating Technologies. *Biofuel Research Journal*, *4*, 107–109.

Deepak S. Thakur,Thomas, G. (1985). Catalyst deactivation in heavy petroleum and synthetic crude processing: A review. *Applied Catalysis*, *15*, 197–225.

Demirbas, A. (2007). Progress and recent trends in biofuels. *Progress in Energy and Combustion Science*, *33*(1), 1–18.

Demirbas, A. (2008). Biofuels sources, biofuel policy, biofuel economy and global biofuel projections. *Energy Conversion and Management*, *49*(8), 2106–2116.

Demirbas, A. (2011). Competitive liquid biofuels from biomass. *Applied Energy*, *88*(1), 17–28.

Dhar, G. M., Srinivas, B. N., Rana, M. S., Kumar, M., & Maity, S. K. (2003). Mixed oxide supported hydrodesulfurization catalysts — a review, *86*, 45–60.

Dietrich, P. J., Sollberger, F. G., Akatay, M. C., Stach, E. A., Delgass, W. N., Miller, J. T., & Ribeiro, F. H. (2014). Structural and catalytic differences in the effect of Co and Mo as promoters for Pt-based aqueous phase reforming catalysts. *Applied Catalysis B: Environmental*, *156-157*, 236–248.

Diesel Prices and Outlook – Basics. (2016).

Ding, L., Rahimi, P., Hawkins, R., Bhatt, S., & Shi, Y. (2009). Naphthenic acid removal from heavy oils on alkaline earth-metal oxides and ZnO catalysts. *Applied Catalysis A: General*, *371*(1-2), 121–130.

Ding, R., Wu, Y., Chen, Y., Liang, J., Liu, J., & Yang, M. (2014). Effective hydrodeoxygenation of palmitic acid to diesel-like hydrocarbons over MoO_2/CNTs catalyst. *Chemical Engineering Science*, *135*,517-525.

Dorozhkin, S. V. (2009). Nanodimensional and nanocrystalline apatites and other calcium orthophosphates in biomedical engineering, biology and medicine. *Materials*, *2*(4), 1975–2045.

Dovì, V. G., Friedler, F., Huisingh, D., & Klemeš, J. J. (2009). Cleaner energy for sustainable future. *Journal of Cleaner Production*, *17*(10), 889–895.

Duan, P., Bai, X., Xu, Y., Zhang, A., Wang, F., Zhang, L., & Miao, J. (2013). Catalytic upgrading of crude algal oil using platinum/gamma alumina in supercritical water. *Fuel*, *109*, 225–233.

Dupain, X., Costa, D. J., Schaverien, C. J., Makkee, M., & Moulijn, J. A. (2007). Cracking of a rapeseed vegetable oil under realistic FCC conditions. *Applied Catalysis B: Environmental*, *72*(1-2), 44–61.

Echeandia, S., Pawelec, B., Barrio, V. L., Arias, P. L., Cambra, J. F., Loricera, C. V., & Fierro, J. L. G. (2014). Enhancement of phenol hydrodeoxygenation over Pd catalysts supported on mixed HY zeolite and Al_2O_3. An approach to O-removal from bio-oils. *Fuel*, *117*(PARTB), 1061–1073.

Elkasabi, Y., Mullen, C.A., Pighinelli, A.L. M.T., & Boateng, A.A. (2014). Hydrodeoxygenation of fast-pyrolysis bio-oils from various feedstocks using carbon-supported catalysts. *Fuel Processing Technology*, *123*, 11–18.

Escobar, J. C., Lora, E. S., Venturini, O.J., Yáñez, E.E., Castillo, E.F., & Almazan, O. (2009). Biofuels: Environment, technology and food security. *Renewable and Sustainable Energy Reviews*, *13*(6-7), 1275–1287.

Evans, W. L., Marling, P. E., & Lower, S. E. (1926). Relationship during Drying between the Acid Value of Linseed Oil and the Concentration Relationship during Drying between the Acid Value of Linseed Oil and the Concentration of Cobalt Acetate'. *Industrial and Engineering Chemistry*, 1229–1230.

Fernández, Y., Arenillas, A., Bermúdez, J. M., & Menéndez, J. A. (2010). Comparative study of conventional and microwave-assisted pyrolysis, steam and dry reforming of glycerol for syngas production, using a carbonaceous catalyst. *Journal of Analytical and Applied Pyrolysis*, *88*(2), 155–159.

Fernández, Y., Arenillas, A., Díez, M. A., Pis, J. J., & Menéndez, J. A. (2009). Pyrolysis of glycerol over activated carbons for syngas production. *Journal of Analytical and Applied Pyrolysis*, *84*(2), 145–150.

Frey, A. M., Karmee, S. K., de Jong, K. P., Bitter, J. H., & Hanefeld, U. (2013). Supported La_2O_3 and MgO Nanoparticles as Solid Base Catalysts for Aldol Reactions While Suppressing Dehydration at Room Temperature. *ChemCatChem*, *5*(2), 594–600.

G, P.Y., Gopal, V. & Kaviarasan, L. (2012). Promising pharmaceutical prospective of Java olive sterculia foetida linn (sterculiaceae). *Internation Journal of Pharmacy Review & Research*, *2*(2), 93–96.

Gan, J., & Yuan, W. (2013). Operating condition optimization of corncob hydrothermal conversion for bio-oil production. *Applied Energy*, *103*, 350–357.

Gao, L., Yoo, E., Nakamura, J., Zhang, W., & Chua, H. T. (2010). Hydrogen storage in Pd–Ni doped defective carbon nanotubes through the formation of CHx (x=1, 2). *Carbon*, *48*(11), 3250–3255.

Gómez, J. M., Romero, M. D., & Callejo, V. (2013). Heterogeneous basic catalysis for upgrading of biofuels. *Catalysis Today*, *218-219*, 143–147.

Gosselink, R. W., Hollak, S. A W., Chang, S. W., Van Haveren, J., De Jong, K. P., Bitter, J. H., & Van Es, D. S. (2013). Reaction pathways for the deoxygenation of vegetable oils and related model compounds. *ChemSusChem*, *6*(9), 1576–1594.

Grace, W.R.C., C. (1993). *Sodasorb® manual of co 2 absorption* (2nd ed.). 62 Whittemore Avenue, Cambridge.

Gunstone, F. (1996). The major sources of oils, fats, and other lipids. *Fatty Acid and Lipid Chemistry*, Blackie, London: Springer.

Guo, X., Zheng, Y., Zhang, B., & Chen, J. (2009). Analysis of coke precursor on catalyst and study on regeneration of catalyst in upgrading of bio-oil. *Biomass and Bioenergy*, *33*(10), 1469–1473.

Guzman, A., Torres, J. E., Prada, L. P., & Nuñez, M. L. (2010). Hydroprocessing of crude palm oil at pilot plant scale. *Catalysis Today*, *156*(1-2), 38–43.

Halim, S. F. A., Kamaruddin, A. H., & Fernando, W. J. N. (2009). Continuous biosynthesis of biodiesel from waste cooking palm oil in a packed bed reactor: optimization using response surface methodology (RSM) and mass transfer studies. *Bioresource Technology*, *100*(2), 710–716.

Hamze, H., Akia, M., & Yazdani, F. (2015). Optimization of biodiesel production from the waste cooking oil using response surface methodology. *Process Safety and Environmental Protection*, *94*(C), 1–10.

Han, L., Wang, Q., Ma, Q., Yu, C., Luo, Z., & Cen, K. (2010). Influence of CaO additives on wheat-straw pyrolysis as determined by TG-FTIR analysis. *Journal of Analytical and Applied Pyrolysis*, *88*(2), 199–206.

Hanafi, S. A., Elmelawy, M. S., El-Syed, H. A., & Shalaby, N. H. (2015). Hydrocracking of Waste Cooking Oil as Renewable Fuel on NiW/SiO_2-Al_2O_3 Catalyst. *Journal of Advanced Catalysis Science and Technology*, *2*, 27–37.

He, Z., & Wang, X. (2014). Renewable energy and fuel production over transition metal oxides: The role of oxygen defects and acidity. *Catalysis Today*, *240*, 220–228.

Hengst, K., Arend, M., Pfützenreuter, R., & Hoelderich, W. F. (2015). Deoxygenation and cracking of free fatty acids over acidic catalysts by single step conversion for the production of diesel fuel and fuel blends. *Applied Catalysis B: Environmental*, *174-175*, 383–394.

Hermida, L., Abdullah, A. Z., & Mohamed, A. R. (2015). Deoxygenation of fatty acid to produce diesel-like hydrocarbons: A review of process conditions, reaction kinetics and mechanism. *Renewable and Sustainable Energy Reviews*, *42*, 1223–1233.

Huang, J., Long, W., Agrawal, P. K., & Jones, C. W. (2009). Effects of acidity on the conversion of the model bio-oil ketone cyclopentanone on H-Y zeolites. *Journal of Physical Chemistry C*, *113*(38), 16702–16710.

Huang, X.G. & Le Z.P. (2015). Continuous Deoxygenation of Triglycerides to Biofuel over 15Co5Ni/ϒ-Al_2O_3. *Asian Journal of chemistry* 2:679–89.

Huber, G. W., O'Connor, P., & Corma, A. (2007). Processing biomass in conventional oil refineries: Production of high quality diesel by hydrotreating vegetable oils in heavy vacuum oil mixtures. *Applied Catalysis A: General*, *329*, 120–129.

Hussan, M. J., Hassan, M. H., Kalam, M. A., & Memon, L. A. (2013). Tailoring key fuel properties of diesel–biodiesel–ethanol blends for diesel engine. *Journal of Cleaner Production*, *51*, 118–125.

Huynh, T. M., Armbruster, U., Nguyen, L. H., & Nguyen, D. A. (2015). Hydrodeoxygenation of Bio-Oil on Bimetallic Catalysts : From Model Compound to Real Feed, *5*,151–160.

Idem, R. O., Katikaneni, S. P. R., & Bakhshi, N. N. (1996). Thermal cracking of canola oil: reaction products in the presence and absence of steam. *Energy & Fuels*, *10*(6), 1150–1162.

Idem, R. O., Katikaneni, S. P. R., & Bakhshi, N. N. (1997). Catalytic conversion of canola oil to fuels and chemicals: roles of catalyst acidity, basicity and shape selectivity on product distribution. *Fuel Processing Technology*, *51*(1-2), 101–125.

Iijima, S. (1991). Helical microtubules of graphitic carbon. *Nature*, *354*(6348), 56–58.

Iliopoulou, E. F., Stefanidis, S. D., Kalogiannis, K. G., Delimitis, a., Lappas, a. a., & Triantafyllidis, K. S. (2012). Catalytic upgrading of biomass pyrolysis vapors using transition metal-modified ZSM-5 zeolite. *Applied Catalysis B: Environmental*, *127*(September), 281–290.

Immer, J. G., Kelly, M. J., & Lamb, H. H. (2010). Catalytic reaction pathways in liquid-phase deoxygenation of C18 free fatty acids. *Applied Catalysis A: General*, *375*(1), 134–139.

Jacob, J. A., Kapoor, S., Biswas, N., & Mukherjee, T. (2007). Size tunable synthesis of silver nanoparticles in water-ethylene glycol mixtures. *Colloids and Surfaces A: Physicochemical and Engineering Aspects*, *301*(1-3), 329–334.

Jacobson, K., Maheria, K. C., & Kumar, A. (2013). Bio-oil valorization : A review, *23*, 91–106.

Javidan, A., Ziarati, A., & Safaei-ghomi, J. (2014). Ultrasonics Sonochemistry Simultaneous sonication assistance for the synthesis of tetrahydropyridines and its efficient catalyst ZrP_{27} nanoparticles. *Ultrasonics Sonochemistry*, *21*(3), 1150–1154.

Jeon, M.-J., Kim, S.-S., Jeon, J.-K., Park, S. H., Kim, J. M., Sohn, J. M., & Park, Y.-K. (2012). Catalytic pyrolysis of waste rice husk over mesoporous materials. *Nanoscale Research Letters*, *7*(1), 18.

Ji, W., Chen, Y., & Kung, H. H. (1997). Vapor phase aldol condensation of acetaldehyde on metal oxide catalysts. *Applied Catalysis A: General*, *161*(1–2), 93–104.

Jiang, J., Yang, C., Lu, Z., Ding, J., Li, T., Lu, Y., & Cao, F. (2015). Characterization and application of a Pt/ZSM-5/SSMF catalyst for hydrocracking of paraffin wax. *Catalysis Communications*, *60*, 1–4.

Jiang, P., Wu, X., Zhu, L., Jin, F., Liu, J., Xia, T. & Li, Q. (2016). Production of jet fuel range paraffins by low temperature polymerization of gaseous light olefins using ionic liquid. *Energy Conversion and Management*, *120*, 338–345.

John, A., Miranda, M. O., Ding, K., Dereli, B., Ortuno, M. A., Lapointe, A. M., & Tolman, W. B. (2016). Nickel Catalysts for the Dehydrative Decarbonylation of Carboxylic Acids to Alkenes. *Organometallics*, *35*(14), 2391–2400.

John Bacha, Freel, J., Gibbs, A., Gibbs, L., & Hemighaus, G. (2007). Diesel Fuels Technical Review. *Chevron Corporation*, 1–107.

Johnson, M. S., Lehmann, J., & Couto, E. G. (2008). A Simple, Direct Method To Measure Dissolved Co2 Using Soda Lime. *Oecologia Australis*, *12*(Butler 1982), 85–91.

Junming, X., Jianchun, J., Yanju, L., & Jie, C. (2009). Liquid hydrocarbon fuels obtained by the pyrolysis of soybean oils. *Bioresource Technology*, *100*(20), 4867–4870.

Kaewmeesri, R., Srifa, A., Itthibenchapong, V., & Faungnawakij, K. (2015). Deoxygenation of waste chicken fats to green diesel over Ni/Al_2O_3: Effect of water and free fatty acid content. *Energy and Fuels*, *29*(2), 833–840.

Kalnes, T. N., Koers, K. P., Marker, T., & Shonnard, D. R. (2014). A Technoeconomic and Environmental Life Cycle Comparison of Green Diesel to Biodiesel and Syndiesel. *Environmental Progress & Sustainable Energy*, *28*(1), 111–120.

Kamimura, Y., Sato, S., Takahashi, R., Sodesawa, T., & Akashi, T. (2003). Synthesis of 3-pentanone from 1-propanol over CeO_2–Fe_2O_3 catalysts. *Applied Catalysis A: General*, *252*(2), 399–410.

Kandel, K., Anderegg, J. W., Nelson, N. C., Chaudhary, U., & Slowing, I. I. (2014). Supported iron nanoparticles for the hydrodeoxygenation of microalgal oil to green diesel. *Journal of Catalysis*, *314*, 142–148.

Karnjanakom, S., Guan, G., Asep, B., Hao, X., Kongparakul, S., Samart, C., & Abudula, A. (2016). Catalytic Upgrading of Bio-Oil over Cu/MCM-41 and Cu/KIT-6 Prepared by #-Cyclodextrin-Assisted Coimpregnation Method. *Journal of Physical Chemistry C*, *120*(6), 3396–3407.

Karp, G. Boeing conducts first flight using green diesel, Tribune, Chicago (2014).

Keith, H., & Wong, S. C. (2006). Measurement of soil CO_2 efflux using soda lime absorption: both quantitative and reliable. *Soil Biology and Biochemistry*, *38*(5), 1121–1131.

Keller, T. C., Rodrigues, E. G., & Pérez-Ramírez, J. (2014). Generation of basic centers in high-silica zeolites and their application in gas-phase upgrading of bio-oil. *ChemSusChem*, *7*(6), 1729–1738.

Kiatkittipong, W., Phimsen, S., Kiatkittipong, K., Wongsakulphasatch, S., Laosiripojana, N., & Assabumrungrat, S. (2013). Diesel-like hydrocarbon production from hydroprocessing of relevant refining palm oil. *Fuel Processing Technology*, *116*, 16–26.

Kim, S. K., Brand, S., Lee, H. S., Kim, Y., & Kim, J. (2013a). Production of renewable diesel by hydrotreatment of soybean oil: Effect of reaction parameters. *Chemical Engineering Journal*, *228*, 114–123.

Kim, S. K., Brand, S., Lee, H. S., Kim, Y., & Kim, J. (2013b). Production of renewable diesel by hydrotreatment of soybean oil: Effect of reaction parameters. *Chemical Engineering Journal*, *228*, 114–123.

Kleinert, M., Gasson, J. R., & Barth, T. (2009). Optimizing solvolysis conditions for integrated depolymerisation and hydrodeoxygenation of lignin to produce liquid biofuel. *Journal of Analytical and Applied Pyrolysis*, *85*(1-2), 108–117.

Klemeš, J. J., Varbanov, P. S., Pierucci, S., & Huisingh, D. (2010). Minimising emissions and energy wastage by improved industrial processes and integration of renewable energy. *Journal of Cleaner Production*, *18*, 843–847.

Kloprogge, J. T., Duong, L. V., & Frost, R. L. (2005). A review of the synthesis and characterisation of pillared clays and related porous materials for cracking of vegetable oils to produce biofuels. *Environmental Geology*, *47*(7), 967–981.

Knothe, G. (2005). Dependence of biodiesel fuel properties on the structure of fatty acid alkyl esters. *Fuel Processing Technology*, *86*(10), 1059–1070.

Knothe, G. (2010). Biodiesel and renewable diesel: A comparison. *Progress in Energy and Combustion Science*, *36*(3), 364–373.

Ko, C. H., Park, S. H., Jeon, J. K., Suh, D. J., Jeong, K. E., & Park, Y. K. (2012). Upgrading of biofuel by the catalytic deoxygenation of biomass. *Korean Journal of Chemical Engineering*, *29*(12), 1657–1665.

Kordulis, C., Bourikas, K., Gousi, M., Kordouli, E., & Lycourghiotis, A. (2015). Development of nickel based catalysts for the transformation of natural triglycerides and related compounds into green diesel: a critical review. *Applied Catalysis B: Environmental*, *181*, 156-196.

Krár, M., Kovács, S., Kalló, D., & Hancsók, J. (2010). Fuel purpose hydrotreating of sunflower oil on $CoMo/Al_2O_3$ catalyst. *Bioresource Technology*, *101*(23), 9287–9293.

Krivan, E., Tomasek, S., & Hancsok, J. (2016). The oligomerization of high olefin containing hydrocarbon by-products to clean engine fuels. *Journal of Cleaner Production*, *136*, 81–88.

Kubatova, A., Stavova, J., Seames, W. S., Luo, Y., Sadrameli, S. M., Linnen, M. J., & Kozliak, E. I. (2012). Triacylglyceride thermal cracking: Pathways to cyclic hydrocarbons. *Energy and Fuels*, *26*(1), 672–685.

Kubička, D., & Horáček, J. (2011). Deactivation of HDS catalysts in deoxygenation of vegetable oils. *Applied Catalysis A: General*, *394*(1-2), 9–17.

Kubička, D., Horáček, J., Setnička, M., Bulánek, R., Zukal, A., & Kubičková, I. (2014). Effect of support-active phase interactions on the catalyst activity and selectivity in deoxygenation of triglycerides. *Applied Catalysis B: Environmental*, *145*, 101–107.

Kubička, D., & Kaluža, L. (2010). Deoxygenation of vegetable oils over sulfided Ni, Mo and NiMo catalysts. *Applied Catalysis A: General*, *372*(2), 199–208.

Kumar, P., Yenumala, S. R., Maity, S. K., & Shee, D. (2014a). Kinetics of hydrodeoxygenation of stearic acid using supported nickel catalysts: Effects of supports. *Applied Catalysis A: General*, *471*, 28–38.

Kumar, P., Yenumala, S. R., Maity, S. K., & Shee, D. (2014b). Kinetics of hydrodeoxygenation of stearic acid using supported nickel catalysts: Effects of supports. *Applied Catalysis A: General*, *471*, 28–38.

Kwon, K. C., Mayfield, H., Marolla, T., Nichols, B., & Mashburn, M. (2011). Catalytic deoxygenation of liquid biomass for hydrocarbon fuels. *Renewable Energy*, *36*(3), 907–915.

Lam, S. S., Russell, A. D., & Chase, H. a. (2010). Microwave pyrolysis, a novel process for recycling waste automotive engine oil. *Energy*, *35*(7), 2985–2991.

Lam, S. S., Russell, A. D., Lee, C. L., & Chase, H. A. (2012). Microwave-heated pyrolysis of waste automotive engine oil: Influence of operation parameters on the yield, composition, and fuel properties of pyrolysis oil. *Fuel*, *92*(1), 327–339.

De Lange, M. W., Van Ommen, J. G., Lefferts, L. Deoxygenation of Benzoic Acid on Metal Oxides: 1. The Selective Pathway to Benzaldehyde. *Appl. Catal. A Gen.* **2001**, *220* (1-2), 41–49.

Lee, H. V., Juan, J. C., Binti Abdullah, N. F., Nizah Mf, R., & Taufiq-Yap, Y. H. (2014). Heterogeneous base catalysts for edible palm and non-edible Jatropha-based biodiesel production. *Chemistry Central Journal*, *8*(1), 30.

Lee, H. V., Juan, J. C., & Taufiq-Yap, Y. H. (2015a). Preparation and application of binary acid–base CaO–La_2O_3 catalyst for biodiesel production. *Renewable Energy*, *74*, 124–132.

Lee, H. V., Juan, J. C., & Taufiq-Yap, Y. H. (2015b). Preparation and application of binary acid–base CaO–La_2O_3 catalyst for biodiesel production. *Renewable Energy*, *74*, 124–132.

Lee, H. V., Taufiq-Yap, Y. H., Hussein, M. Z., & Yunus, R. (2013). Transesterification of jatropha oil with methanol over Mg-Zn mixed metal oxide catalysts. *Energy*, *49*(1), 12–18.

Lee, H. V., Yunus, R., Juan, J. C., & Taufiq-Yap, Y. H. (2011). Process optimization design for jatropha-based biodiesel production using response surface methodology. *Fuel Processing Technology*, *92*(12), 2420–2428.

Lee, H.; Kim, H., Yu, M. J.; Ko, C. H.; Jeon, J.-K., Jae, J.; Park, S. H., Jung, S.-C., & Park, Y.-K. Catalytic Hydrodeoxygenation of Bio-Oil Model Compounds over Pt/HY Catalyst. *Sci. Rep.* **2016**, *6*, 28765.

Lestari, S., Maaki-Arvela, P., Beltramini, J., Lu, G. Q. M., & Murzin, D. Y. (2009). Transforming triglycerides and fatty acids into biofuels. *ChemSusChem*, *2*(12), 1109–1119.

Lestari, S., Mäki-Arvela, P., Eränen, K., Beltramini, J., Max Lu, G. Q., & Murzin, D. Y. (2010). Diesel-like Hydrocarbons from Catalytic Deoxygenation of Stearic Acid over Supported Pd Nanoparticles on SBA-15 Catalysts. *Catalysis Letters*, *134*(3-4), 250–257.

Leung, D. Y. C., Wu, X., & Leung, M. K. H. (2010). A review on biodiesel production using catalyzed transesterification. *Applied Energy*, *87*(4), 1083–1095.

Lewandowski, M., & Sarbak, Z. (2000). Effect of boron addition on hydrodesulfurization and hydrodenitrogenation activity of NiMo/Al_2O_3 catalysts. *Fuel*, *79*(5), 487–495.

Li, L., Quan, K., Xu, J., Liu, F., Liu, S., Yu, S., & Ge, X. (2013). Liquid hydrocarbon fuels from catalytic cracking of waste cooking oils using basic mesoporous molecular sieves K_2O/Ba-MCM-41 as catalysts. *ACS Sustainable Chemistry and Engineering*, *1*(11),

Lianhua, L., Pengmei, L., Wen, L., Zhongming, W., & Zhenhong, Y. (2010). Esterification of high FFA tung oil with solid acid catalyst in fixed bed reactor. *Biomass and Bioenergy*, *34*(4), 496–499.

Lima, D. G., Soares, V. C. D., Ribeiro, E. B., Carvalho, D. A., Cardoso, É. C. V, Rassi, F. C., & Suarez, P.A. Z. (2004). Diesel-like fuel obtained by pyrolysis of vegetable oils. *Journal of Analytical and Applied Pyrolysis*, *71*(2), 987–996.

Lin, Y., Zhang, C., Zhang, M., & Zhang, J. (2010). Deoxygenation of bio-oil during pyrolysis of biomass in the presence of CaO in a fluidized-bed reactor. *Energy and Fuels*, *24*(10), 5686–5695.

Liu, C., Lan, J., Sun, F., Zhang, Y., Li, J., & Hong, J. (2016). Promotion Effects of Plasma Treatment on Silica Supports and Catalyst Precursors for Cobalt Fischer-Tropsch Catalysts. *Journal RSC Advances*, *6*(62), 57701–57708.

Liu, Q., Bie, Y., Qiu, S., Zhang, Q., Sainio, J., Wang, T., & Lehtonen, J. (2014). Hydrogenolysis of methyl heptanoate over Co based catalysts: Mediation of support property on activity and product distribution. *Applied Catalysis B: Environmental*, *147*, 236–245.

Liu, Y., Sotelo-Boyás, R., Murata, K., Minowa, T., & Sakanishi, K. (2012). Production of Bio-Hydrogenated Diesel by Hydrotreatment of High-Acid-Value Waste Cooking Oil over Ruthenium Catalyst Supported on Al-Polyoxocation-Pillared Montmorillonite. *Catalysts*, *2*(1), 171–190.

Loe, R., Santillan-Jimenez, E., Morgan, T., Sewell, L., Ji, Y., Jones, S., & Crocker, M. (2016). Effect of Cu and Sn promotion on the catalytic deoxygenation of model and algal lipids to fuel-like hydrocarbons over supported Ni catalysts. *Applied Catalysis B: Environmental*, *191*, 147–156.

Lokman, I. M., Rashid, U., & Taufiq-Yap, Y. H. (2015a). Meso- and Macroporous Sulfonated Starch Solid Acid Catalyst for Esterification of Palm Fatty Acid Distillate.*Arab Journal Chemistry*, *9* (2), 179–189.

Lokman, I. M., Rashid, U., & Taufiq-Yap, Y. H. (2015b). Production of Biodiesel from Palm Fatty Acid Distillate using Sulfonated-Glucose Solid Acid Catalyst: Characterization and Optimization. *Chinese Journal of Chemical Engineering*, *23*, 1857–1864.

Lou, Y., He, P., Zhao, L., & Song, H. (2016). Refinery oil upgrading under methane environment over PdOx/H-ZSM-5: Highly selective olefin cyclization. *Fuel*, *183*, 396–404.

Lovás, P., Hudec, P., Hadvinová, M., & Ház, A. (2015). Conversion of rapeseed oil via catalytic cracking: Effect of the ZSM-5 catalyst on the deoxygenation process. *Fuel Processing Technology*, *134*, 223–230.

Lu, Q., Li, W. Z., & Zhu, X. F. (2009). Overview of fuel properties of biomass fast pyrolysis oils. *Energy Conversion and Management*, *50*(5), 1376–1383.

Lu, Q., Zhang, Z. F., Dong, C. Q., & Zhu, X. F. (2010). Catalytic Upgrading of Biomass Fast Pyrolysis Vapors with Pd/SBA-15 Catalysts. *Ind. Eng. Chem. Res*, *49*(11), 2573–2580.

Mahajan, A., Kingon, A., Kukovecz, Á., Konya, Z. & Vilarinho, P. M. (2013). Studies on the Thermal Decomposition of Multiwall Carbon Nanotubes under Different Atmospheres. *Mater. Lett. 90*, 165–168.

Maity, S. K., Blanco, E., Ancheyta, J., Alonso, F., & Fukuyama, H. (2012). Early stage deactivation of heavy crude oil hydroprocessing catalysts. *Fuel*, *100*, 17–23.

Mäki-Arvela, P., Kubickova, I., Snåre, M., Eränen, K., & Murzin, D. Y. (2007). Catalytic deoxygenation of fatty acids and their derivatives. *Energy and Fuels*, *21*(1), 30–41.

Mäki-Arvela, P., Snåre, M., Eränen, K., Myllyoja, J., & Murzin, D. Y. (2008). Continuous decarboxylation of lauric acid over Pd/C catalyst. *Fuel*, *87*(17-18), 3543–3549.

Meller, E., Green, U., Aizenshtat, Z., & Sasson, Y. (2014). Catalytic deoxygenation of castor oil over Pd/C for the production of cost effective biofuel. *Fuel*, *133*, 89–95.

Mello, V. M., Oliveira, F. C. C., Fraga, W. G., Do Nascimento, C. J., & Suareza, P. A. Z. (2008). Determination of the content of fatty acid methyl esters (FAME) in biodiesel samples obtained by esterification using 1H-NMR spectroscopy. *Magnetic Resonance in Chemistry*, *46*(11), 1051–1054.

Miao, C., Marin-Flores, O., Davidson, S. D., Li, T., Dong, T., Gao, D., & Chen, S. (2016). Hydrothermal catalytic deoxygenation of palmitic acid over nickel catalyst. *Fuel*, *166*, 302–308.

Mirghiasi, Z., Bakhtiari, F., Darezereshki, E., & Esmaeilzadeh, E. (2014). Preparation and characterization of CaO nanoparticles from $Ca(OH)_2$ by direct thermal decomposition method. *Journal of Industrial and Engineering Chemistry*, *20*(1), 113–117.

Montgomery, D. (2001). Design and analysis of experiments. Newyork: John Wiley & Son Inc.

Morgan, T., Grubb, D., Santillan-Jimenez, E., & Crocker, M. (2010). Conversion of triglycerides to hydrocarbons over supported metal catalysts. *Topics in Catalysis*, *53*(11-12), 820–829.

Morgan, T., Santillan-Jimenez, E., Harman-Ware, A. E., Ji, Y., Grubb, D., & Crocker, M. (2012). Catalytic deoxygenation of triglycerides to hydrocarbons over supported nickel catalysts. *Chemical Engineering Journal*, *189-190*, 346–355.

Mortensen, P. M., Grunwaldt, J., Jensen, P. A., Knudsen, K. G., & Jensen, A. D. (2011). Applied Catalysis A : General A review of catalytic upgrading of bio-oil to engine fuels. *"Applied Catalysis A, General," 407*(1-2), 1–19.

Moser, B. R. (2009). Biodiesel production, properties, and feedstocks. *In Vitro Cellular & Developmental Biology - Plant*, *45*(3), 229–266.

Mu, W., Ben, H., Du, X., Zhang, X., Hu, F., Liu, W., & Deng, Y. (2014). Noble metal catalyzed aqueous phase hydrogenation and hydrodeoxygenation of lignin-derived pyrolysis oil and related model compounds. *Bioresource Technology*, *173*, 6–10.

Murata, K., Liu, Y., Inaba, M., & Takahara, I. (2010). Production of synthetic diesel by hydrotreatment of jatropha oils using Pt-Re/H-ZSM-5 catalyst. *Energy and Fuels*, *24*(4), 2404–2409.

Na, J. G., Han, J. K., Oh, Y. K., Park, J. H., Jung, T. S., Han, S. S., & Ko, C. H. (2012a). Decarboxylation of microalgal oil without hydrogen into hydrocarbon for the production of transportation fuel. *Catalysis Today*, *185*(1), 313–317.

Na, J. G., Yi, B. E., Han, J. K., Oh, Y. K., Park, J. H., Jung, T. S., & Ko, C. H. (2012b). Deoxygenation of microalgal oil into hydrocarbon with precious metal catalysts: Optimization of reaction conditions and supports. *Energy*, *47*(1), 25–30.

Na, J. G., Yi, B. E., Kim, J. N., Yi, K. B., Park, S. Y., Park, J. H., & Ko, C. H. (2010). Hydrocarbon production from decarboxylation of fatty acid without hydrogen. *Catalysis Today*, *156*(1-2), 44–48.

Nagashima, O., Sato, S., Takahashi, R., & Sodesawa, T. (2005). Ketonization of carboxylic acids over CeO_2-based composite oxides. *Journal of Molecular Catalysis A: Chemical*, *227*(1-2), 231–239.

Nagy, J. B. (1996). Carbon Deposits Analysis of Catalyst. *Fuel*, *75*(12), 1363–1376.

Nair, P., Singh, B., Upadhyay, S. N., & Sharma, Y. C. (2012). Synthesis of biodiesel from low FFA waste frying oil using calcium oxide derived from Mereterix mereterix as a heterogeneous catalyst. *Journal of Cleaner Production*, *29-30*, 82–90.

Nam, S., Parikh, D. V., Condon, B. D., Zhao, Q., & Yoshioka-Tarver, M. (2011). Importance of poly(ethylene glycol) conformation for the synthesis of silver nanoparticles in aqueous solution. *Journal of Nanoparticle Research*, *13*(9), 3755–3764.

National Biodiesel Board (NBB). (2009)

Noordin, M., Venkatesh, V., Sharif, S., Elting, S., & Abdullah, a. (2004). Application of response surface methodology in describing the performance of coated carbide tools when turning AISI 1045 steel. *Journal of Materials Processing Technology*, *145*(1), 46–58.

Nutter, M. K., Lockhart, E. E., & Harris, R. S. (1943). The chemical composition of depot fats in chciken and turkeys, 231-234.

Oasmaa, A., Kuoppala, E., & Elliott, D. C. (2012). Development of the basis for an analytical protocol for feeds and products of bio-oil hydrotreatment. *Energy and Fuels*, *26*(4), 2454–2460.

Oi, L. E., Choo, M.-Y., Lee, H. V., Ong, H. C., Hamid, S. B. A., & Juan, J. C. (2016). Recent advances of titanium dioxide (TiO_2) for green organic synthesis. *RSC Adv.*, *6*(110), 108741–108754.

Ong, H. C., Silitonga, A. S., Masjuki, H. H., Mahlia, T. M. I., Chong, W. T., & Boosroh, M. H. (2013). Production and comparative fuel properties of biodiesel from non-edible oils: Jatropha curcas, Sterculia foetida and Ceiba pentandra. *Energy Conversion and Management*, *73*, 245–255.

Oyama, S. T., Hacarlioglu, P., Gu, Y., & Lee, D. (2012). Dry reforming of methane has no future for hydrogen production: Comparison with steam reforming at high pressure in standard and membrane reactors. *International Journal of Hydrogen Energy*, *37*(13), 10444–10450.

Parida, K., & Das, J. (2000). Mg/Al hydrotalcites: Preparation, characterisation and ketonisation of acetic acid. *Journal of Molecular Catalysis A: Chemical*, *151*(1-2), 185–192.

Park, S.-J., Jeong, H.-J., & Nah, C. (2004). A study of oxyfluorination of multi-walled carbon nanotubes on mechanical interfacial properties of epoxy matrix nanocomposites. *Materials Science and Engineering: A*, *385*(1-2), 13–16.

Pasias, S. A, Barakos, N. K., & Papayannakos, N. G. (2009). Catalytic Effect of Free Fatty Acids on Cotton Seed Oil Thermal, 4266–4273.

Payormhorm, J., Kangvansaichol, K., Reubroycharoen, P., Kuchonthara, P., & Hinchiranan, N. (2013). Pt/Al_2O_3-catalytic deoxygenation for upgrading of Leucaena leucocephala-pyrolysis oil. *Bioresource Technology*, *139*, 128–135.

Peng, B., Zhao, C., Kasakov, S., Foraita, S., & Lercher, J. A. (2013). Manipulating catalytic pathways: Deoxygenation of palmitic acid on multifunctional catalysts. *Chemistry - A European Journal*, *19*(15), 4732–4741.

Popov, A., Kondratieva, E., Goupil, J. M., Mariey, L., Bazin, P., Gilson, J. P., & Maugé, F. (2010). Bio-oils hydrodeoxygenation: Adsorption of phenolic molecules on oxidic catalyst supports. *Journal of Physical Chemistry C*, *114*(37), 15661–15670.

Prado, C. M. R., & Antoniosi Filho, N. R. (2009). Production and characterization of the biofuels obtained by thermal cracking and thermal catalytic cracking of vegetable oils. *Journal of Analytical and Applied Pyrolysis*, *86*(2), 338–347.

Pstrowska, K., Walendziewski, J., Łuzny, R., & Stolarski, M. (2014). Hydroprocessing of rapeseed pyrolysis bio-oil over $NiMo/Al_2O_3$ catalyst. *Catalysis Today*, *223*, 54–65.

Puértolas, B., Keller, T. C., Mitchell, S., & Pérez-Ramírez, J. (2016). Deoxygenation of bio-oil over solid base catalysts: From model to realistic feeds. *Applied Catalysis B: Environmental*, *184*, 77–86.

Qian, E. W., Chen, N., & Gong, S. (2014). Role of support in deoxygenation and isomerization of methyl stearate over nickel-molybdenum catalysts. *Journal of Molecular Catalysis A: Chemical*, *387*, 76–85.

Rabiah Nizah, M. F., Taufiq-Yap, Y. H., Rashid, U., Teo, S. H., Shajaratun Nur, Z. A., & Islam, A. (2014). Production of biodiesel from non-edible Jatropha curcas oil via transesterification using Bi_2O_3-La_2O_3 catalyst. *Energy Conversion and Management*, *88*, 1257–1262.

Rahman, M. M., Hassan, M. H., Kalam, M. A., Atabani, A. E., Memon, L. A., & Rahman, S. M. A. (2014). Performance and emission analysis of Jatropha curcas and

Moringa oleifera methyl ester fuel blends in a multi-cylinder diesel engine. *Journal of Cleaner Production*, *65*, 304–310.

Rana, M. S., Ancheyta, J., Sahoo, S. K., & Rayo, P. (2014). Carbon and metal deposition during the hydroprocessing of Maya crude oil. *Catalysis Today*, *220-222*, 97–105.

Rashid, U., Anwar, F., Ashraf, M., Saleem, M., & Yusup, S. (2011). Application of response surface methodology for optimizing transesterification of Moringa oleifera oil: Biodiesel production. *Energy Conversion and Management*, *52*(8-9), 3034–3042.

Reddy Yenumala, S., Maity, S. K., & Shee, D. (2016). Hydrodeoxygenation of Karanja Oil over Supported Nickel Catalysts: Influence of Support and Nickel Loading. *Catal. Sci. Technol.*, *6*(1), 3156.

Regali, F., Boutonnet, M., & Järås, S. (2013). Hydrocracking of n-hexadecane on noble metal/silica-alumina catalysts. *Catalysis Today*, *214*, 12–18.

Regali, F., Liotta, L. F., Venezia, A. M., Boutonnet, M., & Järås, S. (2014). Hydroconversion of n-hexadecane on Pt/silica-alumina catalysts: Effect of metal loading and support acidity on bifunctional and hydrogenolytic activity. *Applied Catalysis A: General*, *469*, 328–339.

Renz, M. (2005). Ketonization of carboxylic acids by decarboxylation: Mechanism and scope. *European Journal of Organic Chemistry*, (6), 979–988.

Rezgui, Y., & Guemini, M. (2005). Effect of acidity and metal content on the activity and product selectivity for n-decane hydroisomerization and hydrocracking over nickel-tungsten supported on silica-alumina catalysts. *Applied Catalysis A: General*, *282*(1-2), 45–53.

Rodrigues, E. G., Keller, T. C., Mitchell, S., & Pérez-Ramírez, J. (2014). Hydroxyapatite, an exceptional catalyst for the gas-phase deoxygenation of bio-oil by aldol condensation. *Green Chem.*, *16*(12), 4870–4874.

Roh, H.-S., Eum, I.-H., Jeong, D.-W., Yi, B. E., Na, J.-G., & Ko, C. H. (2011). The effect of calcination temperature on the performance of $Ni/MgO–Al_2O_3$ catalysts for decarboxylation of oleic acid. *Catalysis Today*, *164*(1), 457–460.

Romero, M. J.A, Pizzi, A., Toscano, G., Bosio, B., & Arato, E. (2014). Study of an innovative process for the production of biofuels using non-edible vegetable oils. *Chemical Engineering Transactions*, *37*(2013), 883–888.

Romero, M. J.A, Pizzi, A, Toscano, G., Busca, G., Bosio, B., & Arato, E. (2015a). Deoxygenation of waste cooking oil and non-edible oil for the production of liquid hydrocarbon biofuels. *Waste Management (New York, N.Y.)*, *47*, 62–68.

Romero, M. J. A., Pizzi, A., Toscano, G., Busca, G., Bosio, B., & Arato, E. (2015b). Deoxygenation of waste cooking oil and non-edible oil for the production of liquid hydrocarbon biofuels. *Waste Management*, *47*, 62–68.

Romero, M., Pizzi, A., Toscano, G., Casazza, A. A., Busca, G., Bosio, B., & Arato, E. (2015c). Preliminary experimental study on biofuel production by deoxygenation of Jatropha oil. *Fuel Processing Technology*, *137*, 31–37.

Romero, Y., Richard, F., & Brunet, S. (2010). Hydrodeoxygenation of 2-ethylphenol as a model compound of bio-crude over sulfided Mo-based catalysts: Promoting effect and reaction mechanism. *Applied Catalysis B: Environmental*, *98*(3-4), 213–223.

Roussel, M., Norsic, S., Lemberton, J. L., Guisnet, M., Cseri, T., & Benazzi, E. (2005). Hydrocracking of n-decane on a bifunctional sulfided NiW/silica-alumina catalyst: Effect of the operating conditions. *Applied Catalysis A: General*, *279*(1-2), 53–58.

Rout, P. K., Naik, M. K., Naik, S. N., Goud, V. V., Das, L. M., & Dalai, A. K. (2009). Supercritical CO_2 fractionation of bio-oil produced from mixed biomass of wheat and wood sawdust. *Energy and Fuels*, *23*(12), 6181–6188.

Sahoo, S. K., Ray, S. S., & Singh, I. D. (2004). Structural characterization of coke on spent hydroprocessing catalysts used for processing of vacuum gas oils. *Applied Catalysis A: General*, *278*(1), 83–91.

Salimon, J., Mohd Noor, D. A., Nazrizawati, A. T., Mohd Firdaus, M. Y., & Noraishah, A. (2010). Fatty Acid Composition and Physicochemical Properties of Malaysian Castor Bean Ricinus communis L . Seed Oil. *Sains Malaysiana*, *39*(5), 761–764.

Salimon, J., Salih, N., & Abdullah, B. M. (2011). Improvement of physicochemical characteristics of monoepoxide linoleic acid ring opening for biolubricant base oil. *Journal of Biomedicine and Biotechnology*, *2011*.

Sanjid, A., Masjuki, H. H., Kalam, M. A., Rahman, S. M. A., Abedin, M. J., & Palash, S. M. (2014). Production of palm and jatropha based biodiesel and investigation of palm-jatropha combined blend properties, performance, exhaust emission and noise in an unmodified diesel engine. *Journal of Cleaner Production*, *65*, 295–303.

Sannita, E., Aliakbarian, B., Casazza, A.A., Perego, P., & Busca, G. (2012). Medium-temperature conversion of biomass and wastes into liquid products, a review. *Renewable and Sustainable Energy Reviews*, *16*(8), 6455–6475.

Santillan-Jimenez, E., & Crocker, M. (2012a). Catalytic deoxygenation of fatty acids and their derivatives to hydrocarbon fuels via decarboxylation/decarbonylation. *Journal of Chemical Technology and Biotechnology*, *87*(8), 1041–1050.

Santillan-Jimenez, E., & Crocker, M. (2012c). Catalytic Deoxygenation of Fatty Acids and Their Derivatives to Hydrocarbon Fuels via Decarboxylation/Decarbonylation. *Journal of Chemical Technology and Biotechnology, Society of Chemical Industry, Wiley Oline Library*, (January 2016), 1041–1050.

Santillan-Jimenez, E., Morgan, T., Lacny, J., Mohapatra, S., & Crocker, M. (2013). Catalytic deoxygenation of triglycerides and fatty acids to hydrocarbons over carbon-supported nickel. *Fuel*, *103*, 1010–1017.

Santillan-Jimenez, E., Morgan, T., Loe, R., & Crocker, M. (2014). Continuous catalytic deoxygenation of model and algal lipids to fuel-like hydrocarbons over Ni–Al layered double hydroxide. *Catalysis Today*. *258*, 284-293.

Santillan-Jimenez, E., Morgan, T., Shoup, J., Harman-Ware, A. E., & Crocker, M. (2014). Catalytic deoxygenation of triglycerides and fatty acids to hydrocarbons over Ni–Al layered double hydroxide, *237*, 136–144.

Satyarthi, J. K., & Srinivas, D. (2011). Fourier Transform Infrared Spectroscopic Method for Monitoring Hydroprocessing of Vegetable Oils To Produce Hydrocarbon-based Biofuel. *Energy Fuels*, *25*, 3318–3322.

Schwab, A. W., Dykstrab, G. J., Selkeo, E., Sorensonb, S. C., & Prydeo, E. H. (1988). Diesel Fuel from Thermal Decomposition of Soybean Oil. *Journal of the Americal Oil Chemists' Society*, *65*(11), 1781–1786.

Sharma, Y. C., & Singh, B. (2008). Development of biodiesel from karanja, a tree found in rural India. *Fuel*, *87*(8-9), 1740–1742.

Shi, F., Wang, P., Duan, Y., Link, D., & Morreale, B. (2012). Recent developments in the production of liquid fuels via catalytic conversion of microalgae: experiments and simulations. *Journal RSC Advances*, *2*(26), 9727.

Shi, H., Chen, J., Yang, Y., & Tian, S. (2014). Catalytic deoxygenation of methyl laurate as a model compound to hydrocarbons on nickel phosphide catalysts: Remarkable support effect. *Fuel Processing Technology*, *118*, 161–170.

Shim, J. O., Jeong, D. W., Jang, W. J., Jeon, K. W., Jeon, B. H., Cho, S. Y., & Han, S. S. (2014). Deoxygenation of oleic acid over $Ce_{(1-x)}Zr_{(x)}O_2$ catalysts in hydrogen environment. *Renewable Energy*, *65*, 36–40.

Shimada, I., Shin, K., Naoki, H., Yoshitaka, N., Haruhisa, O., Kengo, S., & Toru, T. (2016) Deoxygenation of Triglycerides by Catalytic Cracking with Enhanced Hydrogen Transfer Activity. (2016) *Industrial & Engineering Chemistry Research*. DOI: acs.iecr.6b03514

Siahvashi, A., & Adesina, A. A. (2013). Kinetic study of propane CO_2 reforming over bimetallic Mo-Ni/Al_2O_3 catalyst. *Chemical Engineering Science*, *93*(44), 313–325.

Silitonga, A. S., Atabani, A. E., Mahlia, T. M. I., Masjuki, H. H., Badruddin, I. A., & Mekhilef, S. (2011). A review on prospect of Jatropha curcas for biodiesel in Indonesia. *Renewable and Sustainable Energy Reviews*, *15*(8), 3733–3756.

Silitonga, A. S., Ong, H. C., Masjuki, H. H., Mahlia, T. M. I., Chong, W. T., & Yusaf, T. F. (2013). Production of biodiesel from Sterculia foetida and its process optimization. *Fuel*, *111*, 478–484.

Silva, L. N., Fortes, I. C. P., De Sousa, F. P., & Pasa, V. M. D. (2016). Biokerosene and green diesel from macauba oils via catalytic deoxygenation over Pd/C. *Fuel*, *164*, 329–338.

Šimáček, P., Kubička, D., Kubičková, I., Homola, F., Pospíšil, M., & Chudoba, J. (2011). Premium quality renewable diesel fuel by hydroprocessing of sunflower oil. *Fuel*, *90*(7), 2473–2479.

Simakova, I., Simakova, O., Mäki-Arvela, P., Simakov, A., Estrada, M., & Murzin, D. Y. (2009). Deoxygenation of palmitic and stearic acid over supported Pd catalysts: Effect of metal dispersion. *Applied Catalysis A: General*, *355*(1-2), 100–108.

Sirisomboonchai, S., Abuduwayiti, M., Guan, G., Samart, C., Abliz, S., Hao, X., & Abudula, A. (2015). Biodiesel production from waste cooking oil using calcined scallop shell as catalyst. *Energy Conversion and Management*, *95*, 242–247.

Snare, M., Kubickova, I., Maki-Arvela, P., Eranen, K., & Murzin, D. Y. (2006). Heterogeneous Catalytic Deoxygenation of Stearic Acid for Production of Biodiesel. *Ind. Eng. Chem. Res.*, *45*(16), 5708–5715.

Snåre, M., Kubičková, I., Mäki-Arvela, P., Eränen, K., Wärnå, J., & Murzin, D. Y. (2007). Production of diesel fuel from renewable feeds: Kinetics of ethyl stearate decarboxylation. *Chemical Engineering Journal*, *134*(1-3), 29–34.

Snåre, M., Mäki-Arvela, P., Simakova, I. L., Myllyoja, J., & Murzin, D. Y. (2009). Overview of catalytic methods for production of next generation biodiesel from natural oils and fats. *Russian Journal of Physical Chemistry B*, *3*(7), 1035–1043.

Song, H., Wang, N., Song, H.-L., & Li, F. (2015). La–Ni modified $S_2O_{82}-/ZrO_2$-Al_2O_3 catalyst in n-pentane hydroisomerization. *Catalysis Communications*, *59*, 61–64.

Sooknoi, T., Danuthai, T., Lobban, L. L., Mallinson, R. G., & Resasco, D. E. (2008). Deoxygenation of methylesters over CsNaX. *Journal of Catalysis*, *258*(1), 199–209.

Sotelo-Boyas, R., Trejo-Zarraga, F., & Jesus Hernandez-Loyo, F. De. (2012). Hydroconversion of Triglycerides into Green Liquid Fuels. *Hydrogenation*, 338.

Srifa, A., Faungnawakij, K., Itthibenchapong, V., & Assabumrungrat, S. (2014). Roles of monometallic catalysts in hydrodeoxygenation of palm oil to green diesel. *Chemical Engineering Journal*, 1–10.

Stellwagen, D. R., & Bitter, J. H. (2015). Structure-performance relations of molybdenum- and tungsten carbide catalysts for deoxygenation. *Green Chemistry*, *17*(8), 582–593.

Su, M., Yang, R., & Li, M. (2013). Biodiesel production from hempseed oil using alkaline earth metal oxides supporting copper oxide as bi-functional catalysts for transesterification and selective hydrogenation. *Fuel*, *103*, 398–407.

Sullivan, M. M., Chen, C.-J., & Bhan, A. (2016). Catalytic deoxygenation on transition metal carbide catalysts. *Catal. Sci. Technol.*, *6*, 602-616.

Sundararaman, R., & Song, C. (2013). Catalytic decomposition of benzothiophenic and dibenzothiophenic sulfones over MgO-based catalysts. *Applied Catalysis B: Environmental*, *148-149*, 80–90.

Taguchi, A., & Schüth, F. (2005). *Ordered mesoporous materials in catalysis*. *Microporous and Mesoporous Materials*, *7*, 1-45

Tagusagawa, C., Takagaki, A., Iguchi, A., Takanabe, K., Kondo, J. N., Ebitani, K., & Domen, K. (2010). Highly active mesoporous Nb-W oxide solid-acid catalyst. *Angewandte Chemie - International Edition*, *49*(6), 1128–1132.

Tan, C.-Y., & Tsai, W.-T. (2015). Effects of Ni and Co-decorated MWCNTs addition on the dehydrogenation behavior and stability of $LiAlH_4$. *International Journal of Hydrogen Energy*, *40*(40), 14064–14071.

Tani, H., Hasegawa, T., Shimouchi, M., Asami, K., & Fujimoto, K. (2011). Selective catalytic decarboxy-cracking of triglyceride to middle-distillate hydrocarbon. *Catalysis Today*, *164*(1), 410–414.

Tariq, M., Ali, S., Ahmad, F., Ahmad, M., Zafar, M., Khalid, N., & Khan, M. A. (2011). Identification, FT-IR, NMR (1H and 13C) and GC/MS studies of fatty acid methyl esters in biodiesel from rocket seed oil. *Fuel Processing Technology*, *92*(3), 336–341.

Taufiq-Yap, Y. H., Sivasangar, S., & Salmiaton, A. (2012). Enhancement of hydrogen production by secondary metal oxide dopants on NiO/CaO material for catalytic gasification of empty palm fruit bunches. *Energy*, *47*(1), 158–165.

Taufiq-Yap, Y. H., Teo, S. H., Rashid, U., Islam, A., Hussien, M. Z., & Lee, K. T. (2014). Transesterification of Jatropha curcas crude oil to biodiesel on calcium lanthanum mixed oxide catalyst: Effect of stoichiometric composition. *Energy Conversion and Management*, *88*, 1290–1296.

Toba, M., Abe, Y., Kuramochi, H., Osako, M., Mochizuki, T., & Yoshimura, Y. (2011). Hydrodeoxygenation of waste vegetable oil over sulfide catalysts. *Catalysis Today*, *164*(1), 533–537.

Trinkler, N., Labonne, M., Marin, F., Jolivet, A., Bohn, M., Poulain, C., & Paillard, C. (2010). Clam shell repair from the brown ring disease: A study of the organic matrix using Confocal Raman micro-spectrometry and WDS microprobe. *Analytical and Bioanalytical Chemistry*, *396*(2), 555–567.

Tubino, M., Junior, J. G. R., & Bauerfeldt, G. F. (2016). Biodiesel synthesis: A study of the triglyceride methanolysis reaction with alkaline catalysts. *Catalysis Communications 75 (2016) 6–12*, *75*, 6–12.

Tymchyshyn, M., Yuan, Z., & Xu, C. (2013). Direct conversion of glycerol into bio-oil via hydrotreatment using supported metal catalysts. *Fuel*, *112*(2013), 193–202.

Varma, J. P., Dasgupta, S., Nath, B., & Aggarwal, J. S. (1957). Composition of the seed oil of sterculia foetida, Linn. *Journal of the American Oil Chemists Society*, *34*(9), 452–454.

Varma, M. N., & Madras, G. (2007). Synthesis of biodiesel from castor oil and linseed oil in supercritical fluids. *Industrial and Engineering Chemistry Research*, *46*(1), 1–6.

Venderbosch, R. H., Ardiyanti, A. R., Wildschut, J., Oasmaa, A., & Heeres, H. J. (2010). Stabilization of biomass-derived pyrolysis oils. *Journal of Chemical Technology and Biotechnology*, *85*(5), 674–686.

Venderbosch, R., & Prins, W. (2010). Fast pyrolysis technology development. *Biofuels, Bioproducts and Biorefining*, *4*(178-208), 178–208.

Veses, A., Puértolas, B., López, J. M., Callén, M. S., Solsona, B., & García, T. (2016). Promoting Deoxygenation of Bio-Oil by Metal-Loaded Hierarchical ZSM-5 Zeolites. *ACS Sustainable Chemistry and Engineering*, *4*(3), 1653–1660.

Viriya-empikul, N., Krasae, P., Puttasawat, B., Yoosuk, B., Chollacoop, N., & Faungnawakij, K. (2010). Waste shells of mollusk and egg as biodiesel production catalysts. *Bioresource Technology*, *101*(10), 3765-3767.

Vitolo, S., Seggiani, M., Frediani, P., Ambrosini, G., & Politi, L. (1999). Catalytic upgrading of pyrolytic oils to fuel over different zeolites. *Fuel*, *78*(10), 1147–1159.

Vyas, A. P., Verma, J. L., & Subrahmanyam, N. (2010). A review on FAME production processes. *Fuel*, *89*(1), 1–9.

Wang, A., He, P., Yung, M., Zeng, H., Qian, H., & Song, H. (2016). Catalytic co-aromatization of ethanol and methane. *Applied Catalysis B: Environmental*, *198*, 480–492.

Wang, D., Xiao, R., Zhang, H., & He, G. (2010). Comparison of catalytic pyrolysis of biomass with MCM-41 and CaO catalysts by using TGA-FTIR analysis. *Journal of Analytical and Applied Pyrolysis*, *89*(2), 171–177.

Wang, W., Qiao, Z., Zhang, K., Liu, P., Yang, Y., & Wu, K. (2014). Highly selective catalytic hydrodeoxygenation of C aromatic –OH in bio-oil to cycloalkanes on a Ce–Ni–W–B amorphous catalyst. *Journal RSC Advances*, *4*(70), 37288.

Wildschut, J., Iqbal, M., Mahfud, F. H., Cabrera, I. M., Venderbosch, R. H., & Heeres, H. J. (2010). Insights in the hydrotreatment of fast pyrolysis oil using a ruthenium on carbon catalyst. *Energy & Environmental Science*, *3*, 962.

Wildschut, J., Mahfud, F. H., Venderbosch, R. H., & Heeres, H. J. (2009). Hydrotreatment of fast pyrolysis oil using heterogeneous noble-metal catalysts. *Industrial & Engineering Chemistry Research*, *48*(23), 10324–10334.

Wu, J., Xia, Q., Wang, H., & Li, Z. (2014). Catalytic performance of plasma catalysis system with nickel oxide catalysts on different supports for toluene removal: Effect of water vapor. *Applied Catalysis B: Environmental*, *156-157*, 265–272.

Xiu, S., & Shahbazi, A. (2012). Bio-oil production and upgrading research : A review. *Renewable and Sustainable Energy Reviews*, *16*(7), 4406–4414.

Xu, J., Jiang, J., Sun, Y., & Chen, J. (2010). Production of hydrocarbon fuels from pyrolysis of soybean oils using a basic catalyst. *Bioresource Technology*, *101*(24), 9803–9806.

Yang, C., Nie, R., Fu, J., Hou, Z., & Lu, X. (2013). Production of aviation fuel via catalytic hydrothermal decarboxylation of fatty acids in microalgae oil. *Bioresource Technology*, *146*, 569–73.

Yang, Y., Gilbert, A., & Xu, C. (Charles). (2009). Hydrodeoxygenation of bio-crude in supercritical hexane with sulfided CoMo and CoMoP catalysts supported on MgO: A model compound study using phenol. *Applied Catalysis A: General*, *360*(2), 242–249.

Yang, Y., Wang, Q., Zhang, X., Wang, L., & Li, G. (2013a). Hydrotreating of C18 fatty acids to hydrocarbons on sulphided NiW/SiO_2-Al_2O_3. *Fuel Processing Technology*, *116*, 165–174.

Yang, Yan, Jixiang Chen, and H. S. (2013b). "Deoxygenation of methyl laurate as a model compound to hydrocarbons on Ni_2P/SiO_2, Ni_2P/MCM-41, and Ni_2P/SBA-15 catalysts with different dispersions." *Energy & Fuels*, *27*(6), 3400–3409.

Yigezu, Z. D., & Muthukumar, K. (2014). Catalytic cracking of vegetable oil with metal oxides for biofuel production. *Energy Conversion and Management*, *84*, 326–333.

Yoosuk, B., Udomsap, P., & Puttasawat, B. (2011). Hydration-dehydration technique for property and activity improvement of calcined natural dolomite in heterogeneous biodiesel production: Structural transformation aspect. *Applied Catalysis A: General*, *395*(1-2), 87–94.

Yoosuk, B., Udomsap, P., Puttasawat, B., & Krasae, P. (2010). Improving transesterification acitvity of CaO with hydration technique. *Bioresource Technology*, *101*(10), 3784–3786.

Yoshida, H., Matsushita, N., Kato, Y., & Hattori, T. (2002). Active sites in sol–gel prepared silica-alumina for photoinduced non-oxidative methane coupling. *Physical Chemistry Chemical Physics*, *4*(11), 2459–2465.

Yu, X., Chen, J., & Ren, T. (2014). Promotional effect of Fe on performance of Ni/SiO2 for deoxygenation of methyl laurate as a model compound to hydrocarbons. *RSC Adv.*, *4*(87), 46427–46436.

Yu, X.-H., Rawat, R., & Shanklin, J. (2011). Characterization and analysis of the cotton cyclopropane fatty acid synthase family and their contribution to cyclopropane fatty acid synthesis. *BMC Plant Biology*, *11*(1), 97.

Zhang, H., Linang, H., & Zheng, Y. (2014). The role of cobalt and nickel in deoxygenation of vegetable oils. *Applied Catalysis B: Environmental*, *160-161*, 415–422.

Zhang, J., Choi, Y. S., & Shanks, B. H. (2016). Catalytic deoxygenation during cellulose fast pyrolysis using acid–base bifunctional catalysis. *Catal. Sci. Technol.*, *6*(20), 7468–7476.

Zhang, J., Wang, K., Nolte, M. W., Choi, Y. S., Brown, R. C., & Shanks, B. H. (2016). Catalytic Deoxygenation of Bio-Oil Model Compounds over Acid-Base Bifunctional Catalysts. *ACS Catalysis*, *6*(4), 2608–2621.

Zhang, X., Cheng, D., Chen, F., & Zhan, X. (2017). n-Heptane catalytic cracking on hierarchical ZSM-5 zeolite: The effect of mesopores. *Chemical Engineering Science*, *168*, 352–359.

Zhang, X., Zhang, Q., Wang, T., Ma, L., Yu, Y., & Chen, L. (2013). Hydrodeoxygenation of lignin-derived phenolic compounds to hydrocarbons over Ni/SiO_2-ZrO_2 catalysts. *Bioresource Technology*, *134*, 73–80.

Zhang, Z., Tang, M., & Chen, J. (2016). e hydrodeoxygenation pathway. *Applied Surface Science*, *360*, 353–364.

Zhao, C., Brück, T., & Lercher, J. a. (2013). Catalytic deoxygenation of microalgae oil to green hydrocarbons. *Green Chemistry*, *15*(7), 1720.

Zhao, J., Wang, G., Qin, L., Li, H., Chen, Y., & Liu, B. (2016). Synthesis and catalytic cracking performance of mesoporous zeolite Y. *Catalysis Communications*, *73*, 98–102.

Zhao, X., Wei, L., Julson, J., Qiao, Q., Dubey, A., & Anderson, G. (2015). Catalytic cracking of non-edible sunflower oil over ZSM-5 for hydrocarbon bio-jet fuel. *New Biotechnology*, *32*(2), 300–312.

Zhu, Y., Wu, S., & Wang, X. (2011). Nano CaO grain characteristics and growth model under calcination. *Chemical Engineering Journal*, *175*(1), 512–518.

LIST OF PUBLICATIONS AND PAPERS PRESENTED

Chapter In Book

Taufiq-Yap, Y.H. Arumugan**,** M., Asikin-Mijan, N., Lee, H.V. & Juan, J.C. (2015), Catalytic Hydrodeoxygenation Vegetable Oil to Green Diesel, Chapter 5 p.p. 107-146, In: A.K. Agarwal, S.K. Aggarwal, A.K. Gupta, A. Kushari, and A. Pandey (Eds.) Energy, *Combustion & Propulsion: New Perspectives, Ane Books, India.*

Papers Published In Refereed Journals

Asikin-Mijan N., Lee, H.V., Taufiq-Yap, Y.H., Juan, J.C. & Noorsaadah A.R.(2015). Pyrolytic-Deoxygenation of Triglyceride via Natural Waste Shell Derived $Ca(OH)_2$ Nanocatalyst. *Journal Analytical Applied Pyrolysis, 117*: 46–55.

Asikin-Mijan, N., Lee, H.V., Juan, J.C., Noorsaadah, A.R., Abdulkareem-Alsultan, G., Arumugam, M. & Taufiq-Yap, Y.H. (2016). Waste Clamshell-Derived CaO Supported Co and W catalysts for Renewable Fuels Production Via Cracking-Deoxygenation of Triolein. *Journal Analytical Applied Pyrolysis, 120*:110–20.

Asikin-Mijan, N., Lee, H.V., Taufiq-Yap, Y.H., Abdulkrem-Alsultan, G., Mastuli, M. & Ong, H.C. (2016). Optimization study of SiO_2-Al_2O_3 supported bifunctional acid–base NiO-CaO for renewable fuel production using response surface methodology. *Energy Conversion Management, 141*: 325–338.

Asikin-Mijan, N., Lee, H.V., Abdulkrem-Alsultan, G., Afandi G., & Taufiq-Yap Y.H.(2016) Production of green diesel via cleaner catalytic deoxygenation of Jatropha curcas oil. *Cleaner production,* 1-12.

Asikin-Mijan N, Lee, H.V., Abdulkreem-Alsultan, G., & Taufiq-Yap Y.H. (2016). Synthesis and Characterization of Silica-Alumina Supported Ca and Ni Catalyst for Deoxygenation of Vegetable oil into Diesel, *Materials Science Forum*, *840:* 353-358.

Asikin-Mijan, N., Lee, H.V., Marliza, T.S. & Taufiq-Yap, Y.H., Pyrolytic-deoxygenation of triglycerides model compound and non-Edible Oil to hydrocarbons over over SiO_2-Al_2O_3 supported NiO-CaO catalysts, *Journal Analytical Applied Pyrolysis* (accepted).

Asikin-Mijan, N., Lee, H.V., Juan, J.C., Noorsaadah, A.R.& Taufiq-Yap, Y.H (2018), Catalytic deoxygenation of triglycerides into renewable diesel over modified CaO-based catalysts, *Journal RSC Advances, 7:* 46445-46460.

Asikin-Mijan, N., Lee, H.V., Juan, J.C., Noorsaadah, A.R., Ong, H.C. & Taufiq-Yap, Y.H, (2018), Promoting deoxygenation of triglycerides by Co and Ca loaded SiO_2-Al_2O_3 catalyst, *Journal of Applied Catalysis A: General, 552:* 38-48.

International conferences

1. Asikin-Mijan, N., Lee, H.V., & Taufiq-Yap, Y.H. Facile synthesis method for nano-waste shell derived CaO production. Seminar on Advanced Materials Characterization Techniques in Research, Industry and Nuclear Applications, (AMCT), Putra World Trade Centre(PWTC), Kuala Lumpur (13^{th}-16^{th} May 2014).

2. Asikin-Mijan, N., Lee, H.V., Taufiq-Yap, Y.H. & Syazwani O.N. (2014). Synthesis of $Ca(OH)_2$ Nanoparticle Via Sonochemical Method for Biomaterial Production, N., EnCon 7th Engineering Conference," Advances in Process Engineering & Green Energy, Kuching Sarawak (8th-9th Dicember 2014).

3. Asikin-Mijan, N., Lee, H.V., Juan, J.C, Taufiq-Yap, Y.H., Suraya Z., Shajaratun Nur, Z.A.(2014). Development of Calcium-Based Catalyst for Biofuel Production Proceeding of the 2nd International Conference on Green Technology & Ecosystem for Global Sustainable Development(ICGTEC), Palm Garden Hotel, IOI resort, Putrajaya (24th-25th November 2014).

4. Asikin-Mijan, N., Lee, H.V. & Taufiq-Yap, Y.H. (2014). Synthesis of clamshell-derived $Ca(OH)_2$ nanoparticles, International journal of Institute of Material Malaysia (IJMM),(5th-6th November 2014).

5. Asikin-Mijan, N., Lee, H.V., Abdulkreem-Alsultan, G. & Taufiq-Yap, Y.H. Synthesis and Characterization of Silica-Alumina Supported Ca and Ni Catalyst for Deoxygenation of Vegetable oil into Diesel, Seminar on Advanced Materials Characterization Techniques in Research, Industry and Nuclear Applications, Palace of The Golden Horses (AMCT), (9th-10th June 2015).

6. Asikin-Mijan, N., Lee, H.V., Taufiq-Yap, Y.H., Juan, J.C. & Noorsaadah A.R. (2015). Synthesis of transportation fuels from biomass: Co-CaO and W-CaO catalyzed deoxygenation reaction, 2nd International Conference on Waste Management & Environment (ICMWE), University of Malaysa, Kuala Lumpur, (20th-22nd 2015).

7. Abdulkreem-Alsultan G, Asikin- Mijan N. & Taufiq-Yap Y.H. (2015). Preparation of Activated Carbon from walnut shell doped La and Ca Catalyst for biodiesel production from waste cooking oil, Seminar on Advanced Materials characterization Techniques in Research, Industry and Nuclear Applications, Palace of The Golden Horses (AMCT), (9^{th}-10^{th} June 2015).

8. Asikin-Mijan, N., Lee, HV., ABD Hamid, S.B., Juan, J.C. & Taufiq-Yap, Y.H. Sonochemically treated waste shell-derived nanoparticles for catalytic deoxygenation of triglycerides, 5^{th} International conference on environment (ICENV), Penang (18^{th}-19^{th} August 2015).

9. Asikin-Mijan, N., Abdulkrem-Alsultan, G., Afandi, M.A, Lee, H.V., & Taufiq-Yap, Y.H. (2015). Cleaner production of Green-Fuel via Deoxygenation of Bio-based Feedstocks by using Co/Ni supported on Carbon Nanotube Catalyst, The 5^{th} international conference on Green and Sustainable Innovation, (ICGSI), Pattaya, Thailand (8^{th}-10^{th} November 2015).

10. Asikin-Mijan, N. Lee, H.V. & Taufiq-Yap, Y.H. Optimization of Cleaner Production for Green fuel via Response Surface Methodology (RSM) for from triglycerides, The 5^{th} international conference on Green and Sustainable Innovation, (ICGSI), Pattaya, Thailand (8^{th}-10^{th} November 2015).

11. Asikin-Mijan, N. Lee, HV. & Taufiq-Yap, Y.H. Deoxygenation of triglycerides for diesel production over mesoporous catalyst, 5^{th} International conference on the advancement of materials and technology (ICAMN), Bayview Hotel, Langkawi (9^{th}-11^{th} November 2016).

12. Asikin-Mijan, N. Lee, H.V., Juan, J.C., Mei O.J., Aldulkareem-Ghassan A., Phoon, B.L & Taufiq-Yap, Y.H. Catalytic Deoxygenation of Jatropha Curcas Oil to Green Diesel over Cocoa Pod Husk derived Carbon-supported Ni-Ag Catalyst, 4th Postgraduate Colloquium for Environmental Research (POCER), Malacca (25th – 27th July 201).

List of other related publications

Asikin-Mijan, N., Taufiq-Yap, Y.H. & Lee, H.V. (2015). Synthesis of clamshell derived $Ca(OH)_2$ nano-particles via simple surfactant-hydration treatment, *Chemical Engineering Journal, 262*:1043–1051.

Asikin-Mijan, N., Lee, H.V., & Taufiq-Yap, Y.H. (2015). Synthesis and catalytic activity of hydration–dehydration treated clamshell derived CaO for biodiesel production, *Chemical Engineering Research and Design, 102*:368–377.

Alsultan, G Abdulkareem, **Asikin-Mijan, N**., Lee, H.V., Albazzaz, Ahmed S. & Taufiq-Yap, Y.H. (2017). Deoxygenation of waste cooking to renewable diesel over walnut shell- derived nanorode activated carbon supported $CaO\text{-}La_2O_3$ catalyst. *Energy Conversion Management, 151:*311-323.

Abdulkareem-Alsultan, G., **Asikin-Mijan, N**., Lee, H.V., & Taufiq-Yap, Y.H. (2016). A new route for the synthesis of La-Ca oxide supported on nano activated carbon via vacuum impregnation method for one pot esterification-transesterification reaction. *Chemical Engineering Journal, 304*:61-71.

Abdulkareem-Alsultan, G., **Asikin-Mijan, N.** & Taufiq-Yap, Y.H. (2016). Effective catalytic deoxygenation of waste cooking Oil over nanorods activated carbon supported CaO. *Key Engineering Materials, 707*:175-181.

Abdulkareem-Alsultan, G. **Asikin-Mijan, N.** & Taufiq-Yap, Y.H. (2015). Preparation of Activated Carbon from Walnut Shell Doped La and Ca Catalyst for Biodiesel Production from Waste Cooking Oil, *Materials Science Forum, 840*: 348-352.